An exploration into the proteins that regulate skeletal muscle lipid metabolism

Katie L Whytock

A thesis submitted in partial fulfilment of the requirements of Liverpool John Moores University for the degree of Doctor of Philosophy

November 2018

Abstract

Dysregulation of intramuscular triglyceride (IMTG) turnover in human skeletal muscle in sedentary and obese states leads to accumulation of lipid metabolites that contribute to skeletal muscle insulin resistance and ultimately progression to type 2 diabetes (T2D). People with T2D display low levels of IMTG turnover in comparison to insulin sensitive and trained individuals. IMTG stores are used as an energy substrate during 1 h of moderate-intensity exercise in trained individuals only and can be increased by consumption of a high fat, high calorie (HFHC) diet in sedentary and trained states. This thesis explores the metabolic and molecular regulation of proteins that regulate IMTG turnover, specifically focusing on the effects of 1) a HFHC diet and 2) a moderate-intensity exercise bout and 3) IMTG stores in different diseases states (lean, obese and T2D). Chapter 2 determined there were no sex-specific differences or main effects in functional outcomes of cardiovascular (arterial stiffness) and metabolic health (glucose tolerance and metabolic flexibility) in response to 7 days HFHC diet. Chapter 3 provides novel evidence that 7 days HFHC diet induces fibre type specific increases in IMTG stores primarily underpinned by an increase in perilipin-3 (PLIN3) protein expression and a redistribution of perilipin-2 (PLIN2) to lipid droplets (LD) storing IMTG. This occurred with no impairments in skeletal muscle insulin signalling and it is therefore proposed that increases in IMTG content assisted by PLIN2 and PLIN3 minimise the accumulation of lipid metabolites known to disrupt the insulin signalling cascade. Chapter 4 revealed that hormone sensitive lipase (HSL) preferentially redistributes to LD associated with perilipin-5 (PLIN5) following 1 h of moderate-intensity exercise. Chapter 5 developed a PLIN5 immunoprecipitation mass spectrometry protocol which identified phospholipase A_2- group II, subgroup A (PA2GA) as a novel protein associated to PLIN5 in muscle from lean sedentary humans. In conclusion, this thesis presents novel data on key proteins that regulate IMTG turnover in human skeletal muscle.

Acknowledgements

There are a number of people that I wish to acknowledge and thank for their involvement in the completion of this PhD thesis.

Firstly, I would like to say a sincere thank you to all members of Team Anton. I have been extremely fortunate enough to do my doctoral studies in such a prestigious and supportive group. In particular thank you to my supervisors Dr Juliette Strauss, Dr Sam Shepherd and Professor Anton Wagenmakers and advisor Dr Matt Cocks for the having the faith in me to complete this PhD, for your amazing support and guidance over the last 3 years, for introducing me to the wonderful world of disco muscle and most importantly for shaping me into the scientist I am today.

I would also like to thank the collaborators of the work included in this thesis. To Professor Jatin Burniston for graciously taking me under his proteomic wing and patiently imparting his wisdom for my last PhD study. To Dr Carl Hulston and colleagues for collaborating on high fat high calorie diet research and sharing the important muscle samples used in chapter 3.

Importantly I would like to thank all the support staff at RISES. To the sport science technicians in particular, Gemma, Dean and George whose work ensured that every one of my studies ran as smoothly as possible and for solving all of my problems so effortlessly. To Louise, Rachel and Zoe for all their fantastic organisational support throughout my PhD.

To all the inhabitants, colleagues and reprobates of the PGR office including; Áine, Lucy, Katie, Sam Scott, Joe, Ben, Sam Thomas, Maddie, Andrea, Carts, Holds, Phil, Craig, Temps, Thijs and anyone who I may have missed off! Thank you for the nerdy stats discussions, for the copious coffees, for the bake-off and most importantly for the Friday after-work beers.

A big thank you to all the participants who loved the idea of overeating fat food for 7-days and grew to hate me by day 3. Your angry messages comforted me in the knowledge that you were indeed adhering to the diet. To everyone who has kindly donated muscle for any of my studies, my research really would not be possible without it!

For my friends; to Ash, Kirsty and Kelsie thank you for all the radgie adventures and being my constant rock away from Liverpool. A big thank you to the Liverpool girls (Megan, Madden, Helen, Kate, Becca, Hannah) for reminding me that life is better sunny side up and for often encouraging me to burn the candle at both ends.

I am appreciative to all the educators that have supported me through academia however, a special mention must go to my PE teacher Miss Lawson. Without inspiring me to pursue a career in sport and exercise, I would have never ended up here and I am eternally grateful for that.

Most importantly a special thank you to my Mum, Dad, Simon, Hayley and Dexter for everything you have done. Mum and Dad your constant support, encouragement and belief has been fundamental in all my achievements. I hope I can continue to make you proud.

Conference communications and publications

During the completion of this PhD at Liverpool John Moores University, data from this thesis resulted in the following abstracts and conference communications:

Whytock KL, Parry SA, Turner M, James LJ, Ferguson RA, Hulston CJ, Strauss JA, Cocks M, Wagenmakers AJM and Shepherd SO. (2018). Seven days high-fat overfeeding induces fibre-specific increases in intramuscular triglyceride content and perilipin protein expression in human skeletal muscle. Oral presentation, The International Biochemistry of Exercise Conference, Beijing, China.

Whytock KL, Parry SA, Turner M, James LJ, Ferguson RA, Hulston CJ, Strauss JA, Cocks M, Wagenmakers AJM and Shepherd SO. (2018). Seven days high-fat overfeeding induces fibre-specific increases in intramuscular triglyceride content and perilipin protein expression in human skeletal muscle. Oral presentation, European College of Sport and Exercise Sciences, Dublin, Ireland.

Whytock KL, Shepherd SO, Wagenmakers AJM & Strauss JA. (2017). Hormone sensitive lipase preferentially redistributes to perilipin-5 associated lipid droplets during moderate-intensity exercise in human skeletal muscle. Selected Oral Communication, Young Life Scientists' Symposium: Frontiers in Musculoskeletal Health and Ageing, Nottingham, UK.

Whytock KL, Shepherd SO, Wagenmakers AJM & Strauss JA. (2017). Hormone sensitive lipase preferentially translocates to perilipin-5 associated lipid droplets during moderate-intensity exercise in human skeletal muscle. Poster Presentation, Future Physiology, Leeds, UK.

Whytock KL, Parry SA, Turner M, James LJ, Ferguson RA, Hulston CJ, Strauss JA, Cocks M, Wagenmakers AJM and Shepherd SO. (2017). Intramuscular triglycerides and perilipin proteins show fibre type specific increases in human skeletal muscle following 7 days high-fat, high-calorie diet. Selected Oral Communication, Biochemical Society Insulin and Exercise Signalling for Glucose Homeostasis and Metabolic Health, University of Bath, UK.

Whytock KL, Shepherd SO, Wagenmakers AJM & Strauss JA (2016). Hormone-sensitive lipase preferentially redistributes to perilipin-5 associated lipid droplets during moderate-intensity exercise in human skeletal muscle. Poster Communication, Physiology 2016, Dublin, Ireland.

The following papers were published during the period of postgraduate study:

Whytock KL, Shepherd SO, Wagenmakers AJM & Strauss JA. (2018). Hormone-sensitive lipase preferentially redistributes to lipid droplets associated with perilipin-5 in human skeletal muscle during moderate-intensity exercise**.** J Physiol. 596, 2077-2090.

Whytock KL, Jevons EFP, Strauss JA & Shepherd SO. (2017). Under the microscope: insights into limb-specific lipid droplet metabolism. *J Physiol.* 595, 6229-6230.

Table of Contents

List of Figures

List of Tables

Abbreviations

AGPAT	1-acyl-glycerol-3-phosphate-O-acyltransferase
ALT	alanine transaminase
AML12	alpha mouse liver 12
AMPK	AMP-activated protein kinase
ARF	ADP ribosylation factor
AS160	Akt substrate of 160 kDa
AST	aspartate transaminase
ATGL	adipose triglyceride lipase
AUC	area under the curve
BMI	body mass index
cAMP	3',5'-cyclic adenosine monophosphate
CAP	Cbl-associated protein)
CGI-58	comparative gene-identification-58
CHO	Chinese hamster ovary
COPI	coatomer protein complex I
COX IV	cytochrome oxidase IV
DAG	diacylglycerol
DEXA	dual-energy X-ray absorptiometry
DGAT	diacylglycerol acyltransferase
ER	endoplasmic reticulum
ETC	electron transport chain
FA	fatty acids
FABPm	plasma membrane fatty-acid binding protein
FAT/CD36	fatty acid translocase
FATP1	fatty acid transport protein-1
FFA	free fatty acids
FFM	fat free mass
FRAP	fluorescence recovery after photobleaching
G0S2	G(0)/G(1) switch gene 2
G6P	glucose-6-phosphate
GAP	GTPase-activating protein
GFP	green fluorescent protein
GGT	gamma-glutamyltransferase
GLUT-4	glucose transporter-4
GPAT	glycerol-3- phosphate acyltransferase
GS	glycogen synthase
GSK-3	glycogen synthase kinase-3
HE	hyperinsulineamic euglycemic
HFHC	high-fat high-calorie
HSL	hormone sensitive lipase

Ig	immunoglobulin
IKKβ	IκBα kinaseβ
IMTG	intramuscular triglyceride
IP	immunoprecipitation
IPAQ	international physical activity questionnaire
IRS	insulin receptor substrate
ISI	insulin sensitivity index
JNK	c-Jun NH2-terminal kinase
LC	liquid chromatography
LD	lipid droplets
LPL	lipoprotein lipase
MGAT	monoacylglycerol acyltransferase
MHC	myosin heavy chain
MS/MS	tandem mass spectrometry
NAFLD	non-alcoholic fatty liver disease
NEFA	non-esterified fatty-acids
NSF	N-ethylmaleimide sensitive factor
OGTT	oral glucose tolerance test
PA	physical activity
PA2GA	phospholipase A_2 group II, subgroup A
PAP	Phosphatidate
PBS	phosphate buffer solution
PCC	Pearson correlation coefficient
PDH	pyruvate dehydrogenase
PDK1	phosphoinositide-dependent kinase 1
PFK	phosphofructokinase
PI3-K	phosphoinositide 3-kinase
PIP3	phosphatidylinositol 3,4,5-triphosphate
PKA	cAMP-dependent protein kinase
PKC	protein kinase c
PLIN	perilipin
PPAR	peroxisome proliferator receptor
PWV	pulse wave velocity
REE	resting energy expenditure
RER	respiratory exchange ratio
RQ	respiratory quotient
SILAC	stable isotope labelling with amino acids
SNAP	soluble NSF associated protein
SNARE	soluble N-ethylmaleimide sensitive factor attachment protein receptor
SoHo	sorbin homology
T2D	type 2 diabetes
TAG	triglyceride
TBCD1D4	TBC 1 domain family, member 4
TEE	total energy expenditure

TEMED	N, N, N',N' –tetramethylethylenediamine
VAMP2	v-SNARE vesicle associated membrane protein-2
WGA	wheat germ agglutinin

Chapter 1. General Introduction

1.1 Defining the normal human phenotype

In the late-Palaeolithic era (50,000 – 10,000 BC) food sources were not always readily available and food consumption would rely on the capacity to perform high levels of physical activity to hunt and gather food (Diamond, 2003). Due to seasonal changes and often a low abundance of food sources, humans would cycle between periods of famine and feast. In 1962, Neel (1962) proposed that these environmental pressures would have led to the evolution of a 'thrifty' human genotype, making humans exceptionally efficient at storing and utilising energy sources. In particular, humans are capable of digesting, storing and utilising two main fuel sources, carbohydrates and fats (glycogen and triglyceride), and switching between these two sources depending on energy intake and energy expenditure (Chakravarthy & Booth, 2004). Furthermore, the 'thrifty' human genotype is better equipped to tolerate fluctuating periods of feast and famine and physical activity and rest (Neel, 1999; Booth *et al.*, 2002). The human genotype has remained largely the same for the past 10,000 years (Eaton *et al.*, 1988). However, unlike our hunter-gatherer ancestors, humans in modern day western civilization are now confronted with readily available poor quality, energy-dense food sources mirrored by increasingly sedentary daily living, and this has had catastrophic metabolic consequences. In the UK, 60% of people's total waking hours is occupied by sedentary behaviour (Townsend *et al.*, 2012) and 39% of the UK population do not meet current physical activity guidelines of 150 min/week of moderate intensity exercise (British Heart Foundation, 2017), thus minimising habitual energy expenditure. If this is not matched with a decrease in energy intake, positive energy balance and weight gain will ensue. It is proposed that high-fat foods often contribute to this positive energy balance due to being palatable yet very energy dense (Rolls, 2000).

This westernised lifestyle has led to an increase of the prevalence of obesity and type 2 diabetes (T2D). In 2016, the World Health Organisation estimated that 1.9 billion

adults, equivalent to 39% of the adult population worldwide, were overweight (body mass index (BMI) ≥ 25 kg.m^{-2}). Of these, 650 million adults, equivalent to 13% of the world adult population were classified as obese (BMI ≥ kg.m^{-2}). These most recent estimates imply that worldwide obesity prevalence has almost tripled since 1975 (World Health Organisation, 2017). In 2017 nearly 3.7 million people were diagnosed with diabetes in the UK (Diabetes UK, 2017). However, the actual number of people living with diabetes in the UK is expected to be considerably larger due to undiagnosed cases. Of the diagnosed cases, approximately 90% had T2D and about 10% type I diabetes.

This introduction will first outline the regulation of healthy glucose and lipid metabolism in human skeletal muscle. This will be followed by perturbations in lipid metabolism that are seen in sedentary and obese individuals and that can lead to the development of skeletal muscle insulin resistance and, therefore, loss of glucose homeostasis contributing to the development of T2D.

1.1.1 Insulin Sensitivity

Fasting blood glucose concentration is typically <5.5 mmol.L^{-1} in healthy insulin sensitive individuals (American Diabetes, 2015). Following meal ingestion carbohydrates are digested in the gut and released into circulation as glucose. Post-prandial elevations in plasma glucose are followed by secretion of insulin from the pancreas into circulation (Wilcox, 2005). Meal-induced increases in plasma insulin accelerate the arterial blood supply to skeletal muscle (Keske *et al.*, 2016) due to an increased recruitment of microvascular units. This allows an increase in the delivery of insulin, glucose, fatty acids, lipids and amino acids (Wagenmakers *et al.*, 2016). Insulin-sensitive tissues such as skeletal muscle, adipose tissue and liver have insulin receptors to which insulin binds to in order to stimulate glucose uptake from the blood (Wilcox, 2005). During this post-prandial period, there is concomitant suppression of

hepatic glucose production, thus synergistically minimising large elevations in blood glucose levels (Edgerton *et al.*, 2017).

1.1.1.1 Skeletal Muscle Insulin Sensitivity

Various tissues have the ability to uptake glucose from the circulation including; adipose, skeletal muscle, liver and brain. Skeletal muscle is the largest of these tissues and is estimated to account for 80% of glucose removal during a hyperinsulinaemic euglycemic (HE) clamp in lean healthy individuals (DeFronzo *et al.*, 1981) and up to 50% of glucose uptake following a mixed meal in older individuals (Capaldo *et al.*, 1999). Of the tissues linked to T2D, skeletal muscle is recognised for its high plasticity to adapt or mal-adapt to increased or decreased physical activity and different nutritional challenges (Brook *et al.*, 2016; Hoppeler, 2016), which can impact skeletal muscle insulin sensitivity. Due to its capacity to store and/or oxidise glucose, maintaining skeletal muscle insulin sensitivity is paramount in preventing the development of T2D (Petersen *et al.*, 2007; DeFronzo & Tripathy, 2009). Whilst it is accepted that control of the microvascular system is important in mediating insulin-stimulated glucose uptake at the muscle, this thesis will primarily focus on the intramuscular factors that regulate and impact insulin-stimulated muscle glucose uptake.

1.1.1.2 Metabolic Flexibility

Metabolic flexibility is defined as the capacity to switch from lipid oxidation in fasting conditions to increased glucose uptake, oxidation and/or storage with supressed lipid oxidation following insulin-stimulated conditions such as a HE clamp (Kelley & Mandarino, 2000). An ability for muscle to prioritise lipid oxidation during an overnight fast or when fatty acid supply to the muscle is increased such as during high-fat diets or exercise is also an important facet of metabolic flexibility (Galgani *et al.*, 2008b; Corpeleijn *et al.*, 2009). Metabolic flexibility is important to meet the varying demands of nutrient availability and energy expenditure throughout habitual living. The ability

to prioritise fat oxidation during fasting conditions serves as an inherent mechanism to preserve glucose for glucose-dependent organs such as the brain. During fasted conditions, fatty acids (FA) constitute the primary fuel source resulting in a low respiratory quotient (RQ). Fasting RQ is often elevated in skeletal muscle of obese insulin-resistant individuals (0.90 vs 0.83 in lean individuals) (Kelley *et al.*, 1999) or T2D adults (0.85 vs 0.77 in non T2D subjects) (Kelley & Simoneau, 1994) resulting in persistently high rates of carbohydrate oxidation. Individuals with visceral obesity display a reduced fasting fatty acid uptake into skeletal muscle (Colberg *et al.*, 1995). During fasting conditions and during exercise, obese T2D individuals show reduced oxidation of plasma-derived fatty acids compared to obese controls (Blaak *et al.*, 2000). A decreased capacity for mitochondrial beta-oxidation and impaired oxidative activity are also believed to contribute to impairments in fatty acid oxidation during fasting, allowing glucose oxidation to take precedent (reviewed more thoroughly by Corpeleijn (2009)). Elevated fasting RQ in metabolically inflexible individuals may therefore be a consequence of an impaired ability to uptake and oxidise fatty acids, in addition to the chronic hyperglycaemia. However, it is important to note that a study has also reported a higher fasting RQ in lean subjects compared to obese individuals (Blaak *et al.*, 2006). Given these equivocal findings, more research needs to be conducted to address whether a low fasting RQ or an elevated fasting RQ is indicative of impaired metabolic health.

Whilst the amount of fat that can be stored in adipose tissue is extremely large, glucose storage as glycogen in the liver and muscle is comparatively limited. Following carbohydrate ingestion, it is not only essential to take up glucose from the blood to maintain euglycaemia but to also increase carbohydrate oxidation, particularly when glycogen stores are full. To prioritise glucose oxidation there needs to be concomitant suppression of fatty acid uptake and oxidation during insulin-stimulated conditions. Metabolic flexibility to insulin-stimulated conditions is

traditionally measured during a HE clamp, where the difference from fasting RQ to peak RQ during the clamp is denoted as ΔRQ. During the clamp, various studies have shown a positive association between insulin sensitivity and ΔRQ (Kelley *et al.*, 1999; Wohl *et al.*, 2004; Ukropcova *et al.*, 2007). Obese subjects show a diminished capacity to suppress fat oxidation during a HE clamp compared to lean controls (Kelley *et al.*, 1999). Impairments in ΔRQ during a HE clamp in T2D individuals compared to non-diabetic subjects were no longer observed after adjusting for glucose disposal rates (Galgani *et al.*, 2008a) suggesting glucose entering the cells is likely to be directed towards oxidation rather than storage. Similar findings of impaired substrate switching have also been observed in response to a meal in individuals with T2D and in individuals with impaired glucose tolerance (Kelley & Simoneau, 1994; Corpeleijn *et al.*, 2008). Impairments in substrate oxidation are believed to be linked to impairments in substrate uptake, however, these two aberrations do not always occur in parallel and can be independently impeded (Corpeleijn *et al.*, 2009). Importantly impairments in metabolic flexibility can exist in people with a pre-diabetic state of impaired glucose tolerance (Mensink *et al.*, 2001; Faerch & Vaag, 2011) suggesting impairments in substrate switching may have an early role in the development of T2D.

1.1.2 Sex differences in metabolic flexibility and insulin sensitivity

Prevalence rates of T2D is higher in males compared to females (Wild *et al.*, 2004) and pre-menopausal females have a lower cardiovascular risk compared to males (Groban *et al.*, 2016). Large cross-sectional studies have confirmed that males have a higher prevalence of impaired fasting glucose in comparison to females (Kuhl *et al.*, 2005; Munguia-Miranda *et al.*, 2009) and a reduced blood glucose clearance capacity following an intravenous glucose tolerance test (Clausen *et al.*, 1996). Smaller clinical trials ($n \sim 30$) investigating insulin sensitivity in BMI and age-matched males and females using a HE clamp have established that females exhibit a similar or higher

glucose infusion rate per kilogram of body mass when compared to males (Yki-Jarvinen, 1984; Nuutila *et al.*, 1995; Donahue *et al.*, 1996; Rattarasarn *et al.*, 2004; Borissova *et al.*, 2005), and a markedly higher glucose infusion rate when adjusted per kilogram of lean mass (Yki-Jarvinen, 1984; Donahue *et al.*, 1996). In the post-prandial state females have shown greater metabolic flexibility by favouring carbohydrate oxidation (Uranga *et al.*, 2005), which may be indicative of increased glucose uptake and subsequent oxidation in insulin sensitive tissue. Despite females displaying a lower risk of metabolic and cardiovascular complications, they have notably higher adipose tissue mass (a known risk factor for T2D), in comparison to BMI-matched males yet also display greater insulin sensitivity (Clausen *et al.*, 1996). This may be partly due to females favouring deposition of fat in the lower regions of the body which has a lower risk of metabolic complications (Janjic, 1996).

Differences in insulin sensitivity between sexes appear to be largely influenced by sex hormones. A longitudinal study using a HE clamp examined insulin sensitivity (expressed relative to lean body mass) in adolescents between the ages of 11 and 19 years and showed divergent changes in insulin sensitivity between the sexes through puberty (Moran *et al.*, 2008). Males displayed a reduction in insulin sensitivity whereas females increased insulin sensitivity culminating in a significantly higher insulin sensitivity for females compared to males at the age of 19 (Moran *et al.*, 2008). The cessation of female sex hormone production during menopause results in an increased risk of cardiovascular disease and T2D (Polotsky & Polotsky, 2010), indicating female sex hormones exert a protective effect whilst females are pre-menopausal. When post-menopausal females received a venous 2.5mg estrogen bolus during a HE clamp, plasma estradiol levels increased acutely by ~200% and insulin action on glucose disposal rate increased by 20% compared to the saline control (Van Pelt *et al.*, 2003). Female sex hormones undergo large fluctuations during each menstrual cycle however there has been confounding data on how this

impacts insulin sensitivity. When estradiol and progesterone levels are higher in the luteal phase some studies have shown a reduction in insulin sensitivity in healthy eumenorrheic females (Valdes & Elkind-Hirsch, 1991; Escalante Pulido & Alpizar Salazar, 1999), whereas other have shown no changes between different phases of the menstrual cycle or between menstrual cycles (Bingley *et al.*, 2008). Despite the known reduced risk of T2D and cardiovascular disease in pre-menopausal females compared to males there is surprisingly little research investigating the mechanisms underpinning this protection. Furthermore, the pathology of insulin resistance and T2D is largely understudied in females with very few studies directly comparing sexes.

1.2 Insulin-mediated skeletal muscle glucose uptake

Transendothelial transport of glucose from the lumen of skeletal muscle capillaries into the interstitial fluid surrounding the skeletal muscle fibres is mediated by the insulin independent glucose transporter-1 (GLUT-1). Transendothelial transport of glucose occurs via facilitated diffusion and depends on the existence of a downward glucose concentration gradient between the lumen of the capillaries and the muscle interstitium (Wagenmakers *et al.*, 2016). Insulin-stimulated glucose uptake in skeletal muscle occurs through activation of the insulin signalling cascade resulting in the translocation of glucose transporter-4 (GLUT-4) from intracellular storage vesicles in the muscle fibres into the plasma membrane (Watson *et al.*, 2004; Bradley *et al.*, 2015). Glucose uptake in skeletal muscle also occurs via facilitated diffusion and depends on the existence of a downward glucose concentration gradient between the interstitial fluid and the cytosol of the muscle fibres.

The initiation of the insulin signalling cascade in skeletal muscle commences when insulin binds to domains on the extracellular α- subunit of the insulin receptor. This causes a conformational change in the insulin receptor resulting in trans-autophosphorylation of the tyrosine kinase domain in the transmembrane β-subunit. Insulin receptor tyrosine phosphorylation results in recruitment and tyrosine

phosphorylation of the insulin receptor substrate proteins (IRS1-4) and the Shc adapter protein isoforms, signal regulatory protein family members, Gab-1, Cbl, and adaptor protein with pleckstrin homology and Src homology (APS) (Pessin & Saltiel, 2000). Activation of the insulin receptor results in activation of two divergent yet complimentary insulin signalling pathways that both appear crucial in regulating glucose uptake from the blood. The first, and more well-established pathway, is the IRS-PI3-K signalling cascade. The second pathway is the APS/CAP/Cbl pathway. Highlighting the importance of the IRS-PI3-K pathway is the finding that inhibition of phosphoinositide 3-kinase (PI3-K) with wortmannin, or overexpression of a dominant interfering mutant of the p85 regulatory subunit of PI3-K, reduces GLUT-4 translocation and glucose uptake (Cheatham *et al.*, 1994; Okada *et al.*, 1994). Pharmacological activation of intermediates of the IRS-PI3-K pathway, however, does not completely account for GLUT-4 translocation to the plasma membrane and glucose uptake (Egawa *et al.*, 2002; Konrad *et al.*, 2002) suggesting the secondary pathway also needs to function in concert with the IRS-PI3-K pathway (Figure 1.1)

1.2.1 IRS-PI3-K Insulin signalling pathway

Several tyrosine phosphorylation sites exist on IRS-1 (White & Kahn, 1994b), but specific phosphorylation of Tyr612 and Tyr632 are considered pivotal for downstream PI3-K activation and GLUT-4 translocation (Esposito *et al.*, 2001). These phosphorylation sites reside on the C-terminus of IRS-1, which when phosphorylated reveals *Src* homology (SH2)-domain binding sites (White & Kahn, 1994b). PI3-K is a hetero-dimer consisting of a p85 regulatory subunit containing two SH2 domains that bind to the tyrosine phosphorylation sites of IRS-1 (Myers *et al.*, 1992) and a p110 catalytic subunit. Upon activation, PI3-K is then targeted to the inositol ring where it phosphorylates PI to produce phosphatidylinositol-3-phosphates. The formation of phosphatidylinositol-3,4,5-triphosphate (PIP_3) is particularly important because it attracts downstream targets phosphoinositide-dependent kinase 1 (PDK1) and Akt

(also known as protein kinase B) to the plasma membrane via their pleckstrin homology (PH) domain. Once PDK1 and Akt are colocalised, PDK1 phosphorylates Akt at Thr308 and Ser473 resulting in complete kinase activity (Alessi *et al.*, 1996). Downstream Akt targets include glycogen synthase kinase-3 (GSK-3) and Akt substrate of 160 kDa (AS160), also known as TBC 1 domain family, member 4 (TBC1D4). Akt phosphorylates and inactivates GSK-3 at Ser9 which reduces inhibition of glycogen synthase thus increasing its activity and promoting glycogen synthesis. AS160 contains a Rab-GAP (GTPase-activating protein) domain and several Akt phospho-motifs (Miinea *et al.*, 2005). Rab proteins are small G proteins implicated in vesicle trafficking and exocytosis of glucose transporters. Under basal conditions Rab-GAP retains Rab proteins in a GDP-loaded state. Upon AS160 phosphorylation by Akt on the Akt phospo-motifs, Rab-GAP is inhibited, allowing GTP loading which subsequently enables the translocation of GLUT-4 to the plasma membrane (Figure 1.1).

1.2.2 APS/CAP/Cbl complex pathway

The APS/CAP/Cbl pathway is proposed to originate from lipid raft microdomains located at the plasma membrane that are enriched with cholesterol. Caveolin binds to cholesterol in a subset of these microdomains forming caveolae which are small invaginations of the plasma membrane enriched in signalling proteins including the insulin receptor (Gustavsson *et al.*, 1999). Another substrate for insulin receptor kinase is APS, an adaptor protein with a PH and SH2 domain. The SH2 domain of APS forms a homodimer which binds to different subunits of the insulin receptor heterodimer. Association and phosphorylation of APS with the insulin receptor provides a binding site for the SH2 domain of Cbl. Cbl has multiple tyrosine residues which can be phosphorylated by the insulin receptor but requires the association of Cbl adaptor proteins, mainly CAP (Cbl-associated protein) (Baumann *et al.*, 2000). The SH3 domains in the C-terminus of CAP bind to the proline rich domain of Cbl

whereas the Sorbin homology (SoHo) domain in the N-terminus of CAP binds to flotillin which recruits and incorporates CAP/Cbl complex into the lipid raft. Tyrosine phosphorylation of Cbl further recruits the adaptor protein CrkII and guanine nucleotide exchange factor CG3 to the lipid rafts activating TC10, a Rho family small GTP-binding protein (Kanzaki, 2006), that has been implicated in GLUT-4 tethering (Figure 1.1).

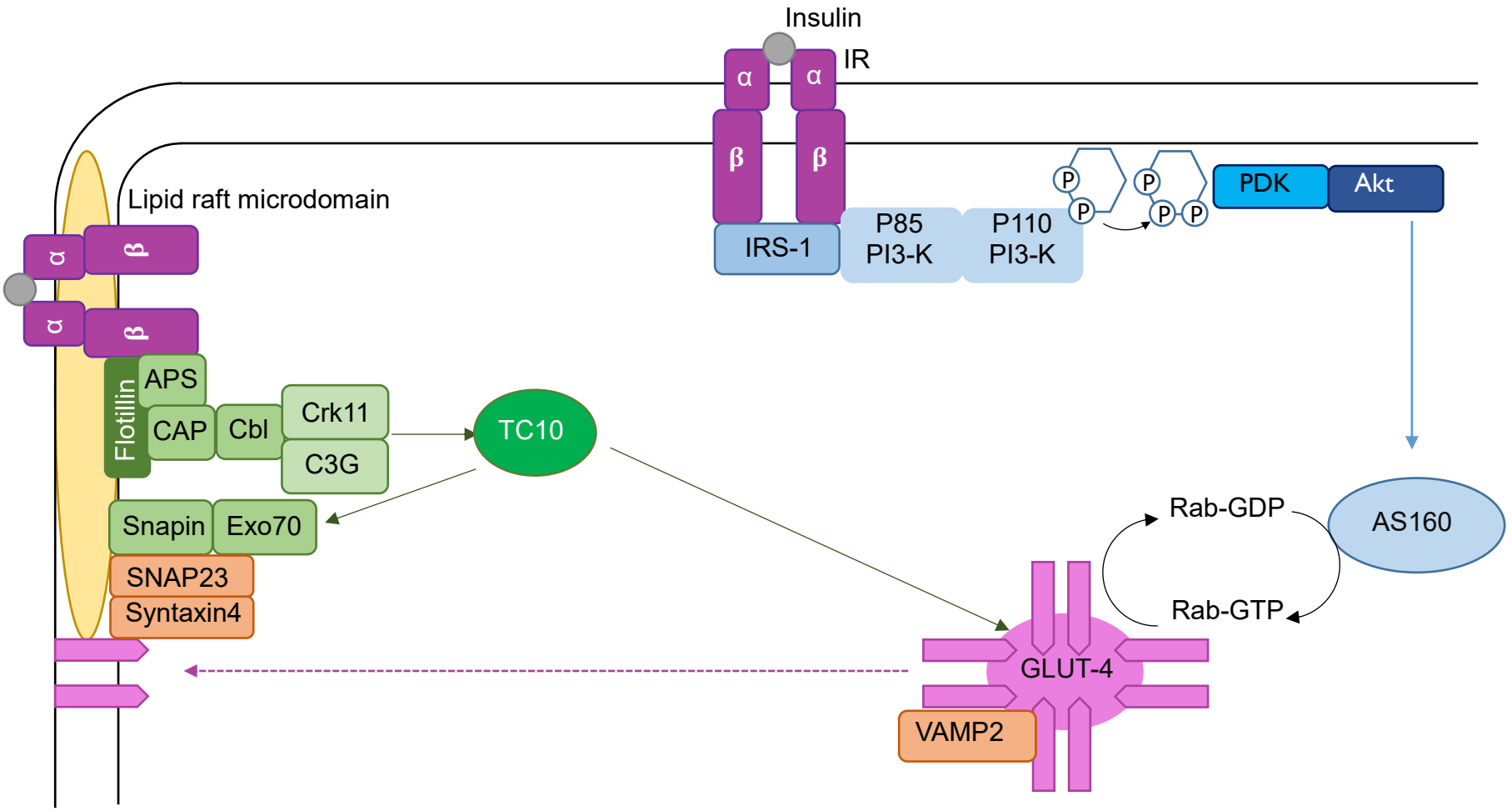

Figure 1.1. Insulin-mediated glucose uptake into skeletal muscle. APS, adaptor protein with a PH and SH2 domain; AS160, Akt substrate of 160 kD; CAP, Cbl-associated proteain; GLUT4, glucose transporter 4; IR, insulin receptor; IRS-1, insulin receptor substrate-1; PDK, phosphoinositide-dependent kinase 1; PI3-K phosphoinositide 3-kinase; Rab-GDP, Rab guanosine disphosphate; Rab-GDP, Rab guanosine triphosphate; SNAP23, synaptosomal associated protein; VAMP2, v-SNARE vesicle associated membrane protein-2.

1.2.3 GLUT-4 translocation

GLUT-4 translocation to the plasma membrane can occur by either polymerized microtubules or actin cytoskeleton pathways (Fletcher *et al.*, 2000; Lopez *et al.*, 2009). Actin polymerization is likely mediated by PI3-K and atypical protein kinase C (PKC) isoforms following insulin stimulation (Liu *et al.*, 2006b). The quantity of GLUT-4 at the cell surface is a balance between endocytosis to intracellular storage vesicles and exocytosis embedment into the plasma membrane. Invagination of the plasma membrane forms t-tubules protruding into the cell, which can increase surface area for GLUT-4 exocytosis and glucose diffusion into the cell. Evidence from cell culture studies suggests that under basal conditions approximately 2-5% of GLUT-4 is located at the cell surface (Kanzaki, 2006). Following insulin stimulation GLUT-4 exocytosis to the plasma membrane at the cell surface and at t-tubules increases allowing for larger uptake of glucose to the cell (Cushman & Wardzala, 1980; Lauritzen *et al.*, 2006; Fazakerley *et al.*, 2010). More recently, the increase in GLUT-4 at the plasma membrane has been confirmed in human skeletal muscle following glucose feeding (75g) with the use of confocal immunofluorescence microscopy (Bradley *et al.*, 2015).

1.2.4 GLUT-4 tethering and fusion

Once translocated to the plasma membrane, GLUT-4 requires tethering and fusion to the plasma membrane facilitated by soluble N-ethylmaleimide sensitive factor (NSF) attachment protein receptor (SNARE) proteins. Target SNAREs (tSNAREs) located on the plasma membrane interact with vesicle SNAREs (vSNAREs) on the GLUT-4 vesicle. SNARE proteins facilitate numerous exocytosis processes however the SNARE proteins implicated primarily in GLUT-4 docking are the v-SNARE vesicle associated membrane protein-2 (VAMP2) and t-SNAREs; synaptosomal associated protein 23 (SNAP23) and syntaxin 4 (Figure 1.1). For SNARE proteins to become activated and form a SNARE complex they require a conformational change in shape

fuelled by NSF and alpha SNAP (soluble NSF associated protein) (Sollner *et al.*, 1993). Formation of a SNARE complex brings together the plasma membrane and GLUT-4 into close proximity allowing their lipid bilayers to fuse. APS/CAP/Cbl mediated activation of TC10 results in translocation and activation of Exo70 to lipid raft microdomains where it binds to Snapin (Figure 1.1). The binding of Snapin with Exo70 activates SNAP23 (Bao et al., 2008), a SNARE protein that appears crucial in GLUT-4 tethering and insulin-stimulated glucose uptake. In vitro studies that have transfected adipocytes with an inactive mutant of SNAP23 or microinjected an antibody to SNAP23 have shown reduced GLUT-4 translocation and docking to the plasma membrane (Foster et al., 1999; Kawanishi et al., 2000) and reduced glucose transport (Foster *et al.*, 1999). In addition to this important role SNAP23 has more recently been implicated in fusion of lipid droplets (LD) (discussed in section 1.6.3.3).

The formation of a SNARE complex is also initiated by insulin-mediated phosphorylation of the insulin receptor leading to Munc18c phosphorylation. This reduces Munc18c association to t-SNARE syntaxin 4, thus increasing syntaxin 4 availability to form SNARE-complexes (Jewell *et al.*, 2011). v-SNARE VAMP2 on the GLUT-4 vesicle binds with syntaxin 4 at the plasma membrane (Watson *et al.*, 2004). Once GLUT-4 is tethered and fused to the plasma membrane glucose is able to enter the muscle via a diffusion gradient.

1.2.5 Carbohydrate metabolism

Once glucose is transported into the muscle, it is phosphorylated to glucose-6-phosphate (G6P) by hexokinase (Ureta, 1982). This reaction is important in keeping intracellular glucose levels low and maintaining a diffusion gradient for glucose uptake into the muscle. G6P is subsequently converted to fructose-6-phosphate before being phosphorylated to fructose-1, 6 bisphosphate by the key glycolytic enzyme phosphofructokinase (PFK) (Wegener & Krause, 2002). Following several subsequent catalytic reactions two 3 carbon pyruvate molecules are formed leading

to the next important step in glycolysis. Pyruvate is converted to acetyl-CoA by pyruvate dehydrogenase (PDH) which requires the inactivation of PDH kinase, which is regulated by intrinsic factors within the muscle and substrate availability (Bhagavan & Ha, 2011). Acetyl-CoA then enters the tricarboxylic acid cycle in the mitochondria.

Instead of being converted to pyruvate, G6P can undergo glycogen synthesis by the action of the enzyme glycogen synthase (GS). Glycogen synthase activity can be increased by insulin and allosteric activation by G6P (reviewed in (Jensen & Lai, 2009)). Dephosphorylation of glycogen synthase occurs via insulin-stimulated Akt-mediated phosphorylation of GSK3 (Cohen, 1999). The phosphorylation of GSK3 decreases its kinase activity thus decreasing phosphorylation of GS and therefore increasing GS fractional activity (Jensen & Lai, 2009). An accumulation of G6P through glycolytic flux can also increase GS activity independent of phosphorylation status (Jensen & Lai, 2009). During post-prandial periods when insulin levels are elevated there is an increase in glucose uptake and an increase in glucose oxidation and/or glycogen storage.

During increased energetic demands of skeletal muscle such as high intensity exercise, glycogenolysis occurs to release glucose-1-phosphate via the phosphorylation of glycogen which can be converted to G6P and continue down the glycolytic pathway towards the mitochondria (Blanco & Blanco, 2017). Glycogen phosphorylase is responsible for glycogenolysis and is regulated by muscle contraction, substrate availability and hormonal regulation (Blanco & Blanco, 2017).

1.3 Skeletal muscle lipid metabolism

1.3.1 Adipose tissue storage

Adipose tissue is the principal organ responsible for buffering the flux of FA in the circulation during the postprandial period. Most FA are packaged and stored as triglyceride (TAG) in adipose tissue equating to total fat mass of ~18kg for males and

~25kg for females when BMI is approximately 25 $kg.m^{-2}$ (Heymsfield *et al.*, 2002). Following ingestion of a mixed meal, digested fat is directed to chylomicron-TAG synthesis in the small intestine. Increases in insulin following carbohydrate or mixed meal ingestion suppresses hormone sensitive lipase (HSL) activity in adipose tissue therefore reducing FA release into the circulation. Insulin also activates lipoprotein lipase (LPL) on the capillaries of adipose tissue, stimulating the hydrolysis of chylomicron-TAG into FA for subsequent uptake into adipocytes for storage as TAG. Although adipose tissue is the primary site for TAG storage, ectopic lipid accumulation can occur in the cells of many tissues including skeletal muscle, liver and heart (Ryysy *et al.*, 2000; Goodpaster *et al.*, 2001; Schulze, 2009). The focus of this thesis will be on how TAG is stored and used in skeletal muscle.

1.3.2 IMTG metabolism

Muscle has the capability to oxidise both carbohydrates and lipids (see 1.1.1.2). In addition to glucose uptake, healthy skeletal muscle is capable of trafficking FA from the circulation into the muscle facilitated by various FA transporter proteins. Once transported into the muscle FA are converted to fatty acyl-CoA by fatty acyl-CoA synthetase (Coleman *et al.*, 2000) and consequently are either esterified into intramuscular triglyceride (IMTG) stores or directed to the mitochondria for β-oxidation. Although most FA are packaged and stored as triglyceride in adipose tissue in the body, a small (~200g) (van Loon, 2004) yet significant proportion is capable of being stored in skeletal muscle as IMTG (1-2% of total fat stores). Furthermore, IMTG is now recognised as an important source of ATP production during moderate-intensity exercise. During moderate-intensity exercise IMTG contribute to ~50% to total fat oxidation with the remaining ~50% attributable to plasma FA (van Loon *et al.*, 2001). Tracer studies in human skeletal muscle have demonstrated that a significant proportion of plasma derived-FA are trafficked into the IMTG stores (Kanaley *et al.*, 2009). Pharmacological blockers of lipases with radiolabelled FA in cultured

myotubes showed increase radioactivity in the IMTG pool further demonstrating that a large proportion of plasma derived FA are first trafficked towards IMTG before being oxidised (Meex *et al.*, 2015). The quantity of IMTG within the muscle reflects the balance between the rate of IMTG synthesis and IMTG lipolysis

1.3.2.1 IMTG synthesis

In healthy individuals at rest IMTG synthesis rates are ~3.4%/h resulting in complete IMTG turnover in 29 h (Capaldo *et al.*, 1999). If fatty-acyl CoA are directed to IMTG synthesis via acyl-CoA synthetase isotypes (Teodoro *et al.*, 2017), they undertake acylation to a glycerol-3-phosphate in a stepwise progression (Figure 1.2). The acylation of the first fatty-acyl CoA generates lysophosphatidic acid which is catalysed by glycerol-3- phosphate acyltransferase (GPAT). An additional fatty acyl-CoA is acylated to lysophosphatidic acid to form phosphatidic acid by 1-acyl-glycerol-3-phosphate-O-acyltransferase (AGPAT). Following removal of a phosphate group by phosphatidate phosphatase-1, lipin-1 diacylglycerol (DAG) is formed. DAG can also be produced by acylation of fatty acyl-CoA to MAG by monoacylglycerol acyltransferase (MGAT). An additional FA-CoA is acylated to DAG by diacylglycerol acyltransferase (DGAT) forming IMTG.

(i) Glycerol-3-Phosphate Acyltransferase (GPAT)

GPAT is considered the rate-limiting enzyme in the IMTG synthesis pathway because it exhibits the lowest enzyme activity (Coleman & Lee, 2004). There are 4 known GPAT isoforms; GPAT1 and 2 are located at the mitochondria whereas GPAT3 and 4 are located at the endoplasmic reticulum (ER) membrane (microsomal) (Gimeno & Cao, 2008). Approximately 10% of total GPAT activity is attributable to mitochondrial GPAT in most tissues (Takeuchi & Reue, 2009). Despite this, mitochondrial GPAT1 is the most-extensively studied of all the isoforms. Biochemical assays reveal that GPAT1 has a two-fold higher preference for saturated compared to unsaturated fatty-acyl CoAs (Vancura & Haldar, 1994). GPAT1 is regulated both transcriptionally and

post-transcriptionally. For example, GPAT1 mRNA levels in mouse liver increase by 20-fold upon high-carbohydrate diet after fasting, which stimulates hepatic lipogenesis (Shin *et al.*, 1991). The increase in GPAT1 mRNA is reduced by 70% when rats were also supplemented with dibutyryl 3', 5'-cyclic adenonsine monophosphate (cAMP), identifying adenylate cyclase and increased cAMP levels as a negative regulator of GPAT1 gene expression (Shin *et al.*, 1991). Contrastingly GPAT1 protein and activity decreases by more than 30% following 48 h fasting in liver and adipose tissue in rats (Lewin *et al.*, 2001). The importance of GPAT1 in TAG synthesis has been exemplified in mice through GPAT1 overexpression by adenovirus resulting in increased TAG and DAG content by 12-fold and 7-fold, respectively (Linden *et al.*, 2006). GPAT1-KO mice exhibit lower, but not completely diminished, hepatic TAG and lower plasma TAG and VLDL-TAG concentrations (Hammond *et al.*, 2002), thus indicating other GPAT isoforms may serve a functional role upon ablation of GPAT1. GPAT1 content has been identified in human skeletal muscle by western blot (Schenk & Horowitz, 2007; Newsom *et al.*, 2011), but the understanding of the regulation of GPAT1 in this tissue is limited. If lysophosphatidic acid is produced at the mitochondria by GPAT it may require transportation to the ER where the majority of other IMTG-synthesising enzymes are located. In the liver this occurs by liver-fatty acid binding protein (Gonzalez-Baro *et al.*, 2007), but how this process occurs in skeletal muscle is still unknown. Elevations in DAG and TAG synthesis occur in soleus muscle *in vitro* in response to insulin (Dyck *et al.*, 2001) suggesting that both GPAT and DGAT activity is increased by feeding. Inhibition of PI3-K reduces FA esterification, further indicating insulin-stimulated IMTG synthesis occurs via a PI3-K pathway (Muoio *et al.*, 1999; Dyck *et al.*, 2001).

(ii) 1-acyl-glycerol-3-phosphate-O-acylytransferase (AGAPT)

Phosphatidic acid is produced from the acylation of a fatty acyl-CoA to lysophosphatidic acid catalysed by AGPAT. There are 10 AGPAT isoforms reported

thus far in the literature, with AGPAT1 and AGPAT2 being the most well-established (Takeuchi & Reue, 2009). Expression of AGPAT1 and AGPAT2 is more pronounced in adipose tissue, but they are also expressed in skeletal muscle (Yamashita *et al.*, 2014). The location and activity of AGPAT is largely at the ER (Takeuchi & Reue, 2009) but also at the mitochondria (Bursten *et al.*, 1991). AGPAT1 plays a key role in TAG synthesis because in 3T3-L1 adipocytes and C2C12 myotubes overexpression of AGPAT1 increased [3H]oleate incorporation into TAG (Ruan & Pownall, 2001). The importance of AGPAT2 in adipocyte TAG synthesis has been illustrated by studies showing defects in the AGPAT2 gene resulting in congenital generalized lipodystrophy, which results in a lack of adipose tissue (Agarwal *et al.*, 2002).

(iii) Phosphatidate phosphatase (PAP)/ Lipin-1

Phosphatidate phosphatases (PAP) are Mg^{2+}-dependent and inactivated by N-ethylmaleimide (Martin *et al.*, 1987). Lipin-1, -2 and -3 have been identified as the proteins responsible for PAP activity during the process of TAG synthesis and lipin-1 accounts for all the PAP activity in skeletal muscle (Donkor *et al.*, 2007). PAP activity levels are present both in the cytosol and at the ER where it catalyses the dephosphorylation of phosphatidic acid into DAG (Takeuchi & Reue, 2009). Lipin-1 is phosphorylated by insulin and dephosphorylated by epinephrine (Harris *et al.*, 2007). Paradoxically the increased phosphorylation by insulin results in a decreased fraction of lipin-1 at the ER where target substrate phosphatidic acid is produced (Harris *et al.*, 2007). This unusual finding may be partly explained by lipin-1 having divergent roles in muscle cell cycle differentiation and autophagy (Zhang *et al.*, 2014; Jiang *et al.*, 2015), requiring different localisation and regulation. Importantly, overexpression of lipin-1 in mouse skeletal muscle reduces energy expenditure and fatty acid utilisation (Phan *et al.*, 2004) highlighting its importance in TAG synthesis.

(iv) Diacylglycerol Acyltransferase (DGAT)

DGAT is responsible for the final acylation of DAG with fatty acyl-CoA to form IMTG (Choi *et al.*, 2007). DGAT1 and DGAT2 are the two isoforms that have been identified in human adipose tissue (Cases *et al.*, 1998; Cases *et al.*, 2001) and mouse skeletal muscle (Levin *et al.*, 2007; Yu *et al.*, 2015), however limited research has been conducted in human skeletal muscle. Overexpression of DGAT1 in mouse skeletal muscle increases DGAT1 content 50% and triglyceride content 4-fold (Yang *et al.*, 2013). Furthermore, overexpression of DGAT1 by recombinant adenovirus in C2C12 myotubes increased DGAT activity 4-fold and increased TAG content by 6-fold (Liu *et al.*, 2007). DGAT-1 KO mice have reduced fat pads and are resistant to weight gain compared to wild type mice, yet were still capable of producing TAG in adipose tissue (Smith *et al.*, 2000), suggesting a compensatory role for DGAT2. DGAT activity increases 60-fold in differentiating adipocytes (Dircks & Sul, 1997), but mRNA expression for DGAT1 and DGAT2 only increases 8-fold and 30-fold, respectively, suggesting DGAT is regulated by post-transcriptional mechanisms (Coleman & Lee, 2004). An early study concluded DGAT activity is a function of steady state DGAT1 protein levels in differentiated 3T3-L1 adipocytes (Yu *et al.*, 2002b). Despite this, multiple phosphorylation sites have been discovered for DGAT1 and the use of glutamate mutation as a phosphorylation mimetic on Ser83, Ser86 and Ser89 increased DGAT1 activity in C2C12 cells (Yu *et al.*, 2015), therefore suggesting it's activity can be regulated post-translationally.

(v) Monoacylglycerol acyltransferase pathway (MGAT)

Monoacylglycerol (a substrate of DAG lipolysis) can also be re-synthesised back into DAG in a reaction catalysed by MGAT. Research from this pathway primarily exists from the small intestine where it is estimated that 75% of the TAG synthesis occurs via this route following ingestion of a meal (Johnston, 1977). As such, activity levels have been recorded higher in the small intestine and to a lesser extent in skeletal

muscle (Yen & Farese, 2003). There are 3 MGAT isoforms, MGAT1 and MGAT2 which acylate both *sn*-2 and *sn*-1(3)- monoacylglycerols whereas MGAT3 has a higher specificity for *sn*-2-monoaclyglycerol (Coleman & Lee, 2004). Information regarding the importance and regulation of the MGAT pathway in TAG synthesis in skeletal muscle is limited and warrants further investigation.

1.3.2.2 IMTG lipolysis

In trained individuals fat oxidation rates increase approximately 10-fold when exercising at moderate-intensity compared to resting values (Romijn *et al.*, 1993; van Loon *et al.*, 2001). Adipose tissue has the largest TAG stores in the body and it is therefore unsurprising that adipose tissue derived TAG provides the largest contribution to fat oxidation. However, studies employing stable isotope methodology and indirect calorimetry have demonstrated that other fat sources (IMTG and lipoprotein-TAG) also provide a substantial contribution (~30-50%) to total fat oxidation particularly during moderate-intensity exercise (40-65% $VO_{2\,max}$) (Romijn *et al.*, 1993; van Loon *et al.*, 2001). These findings are complemented by non-invasive ^{1}H magnetic resonance spectroscopy (^{1}HMRS) technology showing that IMTG concentrations are consistently reduced (~20-40%) during moderate-intensity exercise lasting between 1-3 hours (van Loon, 2004). More recently, using immunofluorescence microscopy studies have shown that IMTG stores are 2-4 fold higher in type I fibres compared to type II (van Loon *et al.*, 2003a; Shepherd *et al.*, 2013) and IMTG utilisation is specific to type I fibres during moderate-intensity exercise (van Loon *et al.*, 2003a; Van Proeyen *et al.*, 2011a; Shepherd *et al.*, 2013). This is unsurprising considering type I fibres are characterised by a greater mitochondrial content and oxidative capacity (Essen *et al.*, 1975).

IMTG hydrolysis occurs from 3 sequential cleavages of a FA from the glycerol backbone and is catalysed by 3 lipases; adipose triglyceride lipase (ATGL), hormone sensitive lipase (HSL) and monoacylgycerol lipase (MGL) (Figure 1.2). Historically,

HSL was considered to be the rate-limiting enzyme in lipolysis. At rest, HSL accounts for ~60% of total neutral hydrolase activity and the exercise-induced increase in skeletal muscle lipase activity was attributable to HSL (Watt *et al.*, 2004). Immuno-inhibition of HSL with an anti-HSL antibody has also been shown to eradicate contraction-induced increase in TAG lipase activity (Langfort *et al.*, 2000). However, the existence of other important lipases became apparent in an experiment where an antiserum against HSL was applied to an assay medium measuring TAG hydrolysis in human skeletal muscle, and this only reduced neutral lipase activity by ~25% (Roepstorff *et al.*, 2004). Additionally, only 50% of TAG hydrolase activity was reduced in adipose tissue in HSL-deficient mice compared to wild type mice (Haemmerle *et al.*, 2002b), adding to the suggestion that other lipases are present. A lipase with high-affinity for TAG named ATGL was subsequently discovered, predominantly expressed in adipose tissue and to a lesser extent in skeletal muscle (Villena *et al.*, 2004; Zimmermann *et al.*, 2004). Overexpression of ATGL in human primary myotubes resulted in reduced TAG content and increased FA release and oxidation (Badin *et al.*, 2011), whilst ATGL-KO mice accumulate excessive TAG in skeletal muscle (Haemmerle *et al.*, 2006). On the other hand *in vitro* assay systems have demonstrated that HSL has a higher specificity for substrate DAG in comparison to TAG (Fredrikson *et al.*, 1981b), and HSL-KO mice accumulate DAG in skeletal muscle (Haemmerle *et al.*, 2002a). The existing evidence therefore suggests that ATGL and HSL preferentially hydrolyse IMTG in a sequential process (Figure 1.2) whereby ATGL cleaves the initial FA from IMTG to produce DAG. HSL is likely to then be crucial for DAG hydrolysis to monoacylglycerol (Figure 1.2). Evidence from adipose tissue suggests the final FA liberation is conducted by MGL (Taschler *et al.*, 2011). Considering ATGL and HSL collectively account for at least 98% of contraction-induced TAG lipase activity in rat skeletal muscle (Alsted *et al.*, 2013), little research has been conducted exploring the regulation and activation of MGL.

(i) Hormone Sensitive Lipase

Similar to IMTG, HSL also appears to have a higher abundance in type I fibres compared to type II fibres (Langfort *et al.*, 1999). HSL activity during exercise is regulated allosterically, by multiple contraction and adrenergic phosphorylation sites. Under lipolytic stimuli such as exercise, rising catecholamine levels activate HSL by cAMP-dependent protein kinase (PKA) phosphorylation on Ser563 and Ser660 (Watt *et al.*, 2003c; Watt *et al.*, 2006). Conversely, postprandial increases in insulin exert an inhibitory effect on skeletal muscle HSL activity by activating a phosphodiesterase which converts cAMP to inactive 5'-AMP so that less HSL is phosphorylated (Enoksson *et al.*, 1998). Muscle contraction observed during exercise also activates HSL via protein kinase C and extracellular signal-related kinase (Donsmark *et al.*, 2003), most probably through phosphorylation at Ser600 (Greenberg *et al.*, 2001). Due to the increase in AMP-activated protein kinase (AMPK) activity seen during higher intensities of exercise, phosphorylation and inhibition of HSL on Ser565 results in an anti-lipolytic effect (Watt *et al.*, 2004; Watt *et al.*, 2006). Additionally, accumulation of fatty acyl-CoA also exhibited at higher exercise intensities (Kiens *et al.*, 1999) may allosterically inhibit HSL activity. HSL activity is therefore upregulated for longer at lower (30% and 60% $\dot{V}o_{2peak}$) in comparison to higher (90% $\dot{V}o_{2peak}$) exercise intensities (Watt *et al.*, 2003b). In agreement, Achten and Jeukendrup (2003) established that maximal fat oxidation rates in males occurs at ~63% $\dot{V}o_{2\ max.}$ In addition to the regulation of HSL via phosphorylation, an insightful study by Prats et al. (2006) demonstrated that HSL translocates to LD in isolated rat skeletal muscle following adrenaline or electrical stimulation. The translocation of HSL from the cytosol to the LD was already well established in adipocytes following adrenergic stimulation (Brasaemle *et al.*, 2000), but this was the first study in skeletal muscle to demonstrate this effect. Transmission electron microscopy also confirmed that HSL penetrated the phospholipid monolayer of the LD thus enabling access to the substrates within the LD core (Prats *et al.*, 2006). The use of isolated rat skeletal

muscle in the study elegantly eliminated the interference of plasma-derived FA on substrate use and IMTG synthesis allowing for IMTG hydrolysis to be studied in isolation. Substrate and hormone levels can however influence lipolytic rates and contraction of muscle during exercise induces a host of regulatory mechanisms that are not observed *in vitro* or *ex vivo*. Whether HSL redistribution to LDs occurs in human skeletal muscle *in vivo* still needs to be investigated.

(ii) Adipose Triglyceride Lipase

As ATGL is a comparatively new lipase, research examining its regulation particularly in skeletal muscle is relatively limited. Similar to HSL, ATGL is found in a higher abundance in type I compared to type II muscle fibres (Jocken *et al.*, 2008). ATGL interacts with its co-activator, comparative gene-identification-58 (CGI-58), to increase lipase activity up to 20-fold in cultured kidney cells (Lass *et al.*, 2006). CGI-58 appears particularly important because individuals with a CGI-58 mutation have increased IMTG content (Lass *et al.*, 2006) likely due to diminished IMTG hydrolysis capabilities. ATGL activity is inhibited and ATGL-mediated lipolysis is reduced if the patatin-like domain of ATGL interacts with the hydrophobic domain of the G(0)/G(1) switch gene 2 (G0S2) protein (Yang *et al.*, 2010). In adipocytes, under resting conditions CGI-58 is prevented from activating ATGL because it is associated with the LD protein perilipin 1 (PLIN1) (Yamaguchi *et al.*, 2004). Upon beta-adrenergic stimulation, PKA phosphorylates PLIN1 thus releasing CGI-58 so it can bind to and activate ATGL (Granneman *et al.*, 2009). PLIN1 however, is not expressed in skeletal muscle (Greenberg *et al.*, 1991) and research regarding ATGL regulation in skeletal muscle is limited. It has been demonstrated however, that following contraction there is an increase in CGI-58/ATGL protein interaction in rat soleus muscle (MacPherson *et al.*, 2012), suggesting a similar mechanism may exist in skeletal muscle.

In humans, subcutaneous adipose tissue phosphorylation of Ser404 on ATGL is increased by β-adrenergic stimulation and is correlated with increased lipolysis rates

(Pagnon *et al.*, 2012). ATGL phosphorylation on Ser404 in human skeletal muscle is not however altered following moderate-intensity exercise (Mason *et al.*, 2012), suggesting it is not vital for ATGL activation. Phosphorylation of the Thr372 residue on the hydrophobic region in the C-terminus of ATGL prevents LD colocalisation to ATGL and ATGL mediated TAG hydrolysis (Xie *et al.*, 2014). This mechanism would serve to reduce lipolysis under non-stimulated basal conditions. Several other phosphorylation sites of ATGL have been identified including Ser87 and Thr210 in the NH_2- terminus patatin-like domain, and Ser430, Thr372, Tyr378 and Ser393 in the C-terminus (Xie *et al.*, 2014), but their function and regulation still requires further investigation. In contrast to HSL which translocates to the LD, it is suggested that ATGL is already localised to LD in skeletal muscle under basal conditions and its positioning is unaltered following moderate-intensity exercise (Mason *et al.*, 2014a). This was investigated using wide-field microscopy, which does not permit a detailed assessment of ATGL distribution and location relative to IMTG stores due to the limitations resulting from the refraction of light (compared to a laser) and the resolving power of the microscope. The use of higher resolution confocal microscopy is warranted to investigate in greater detail the location of ATGL before and after exercise in human skeletal muscle.

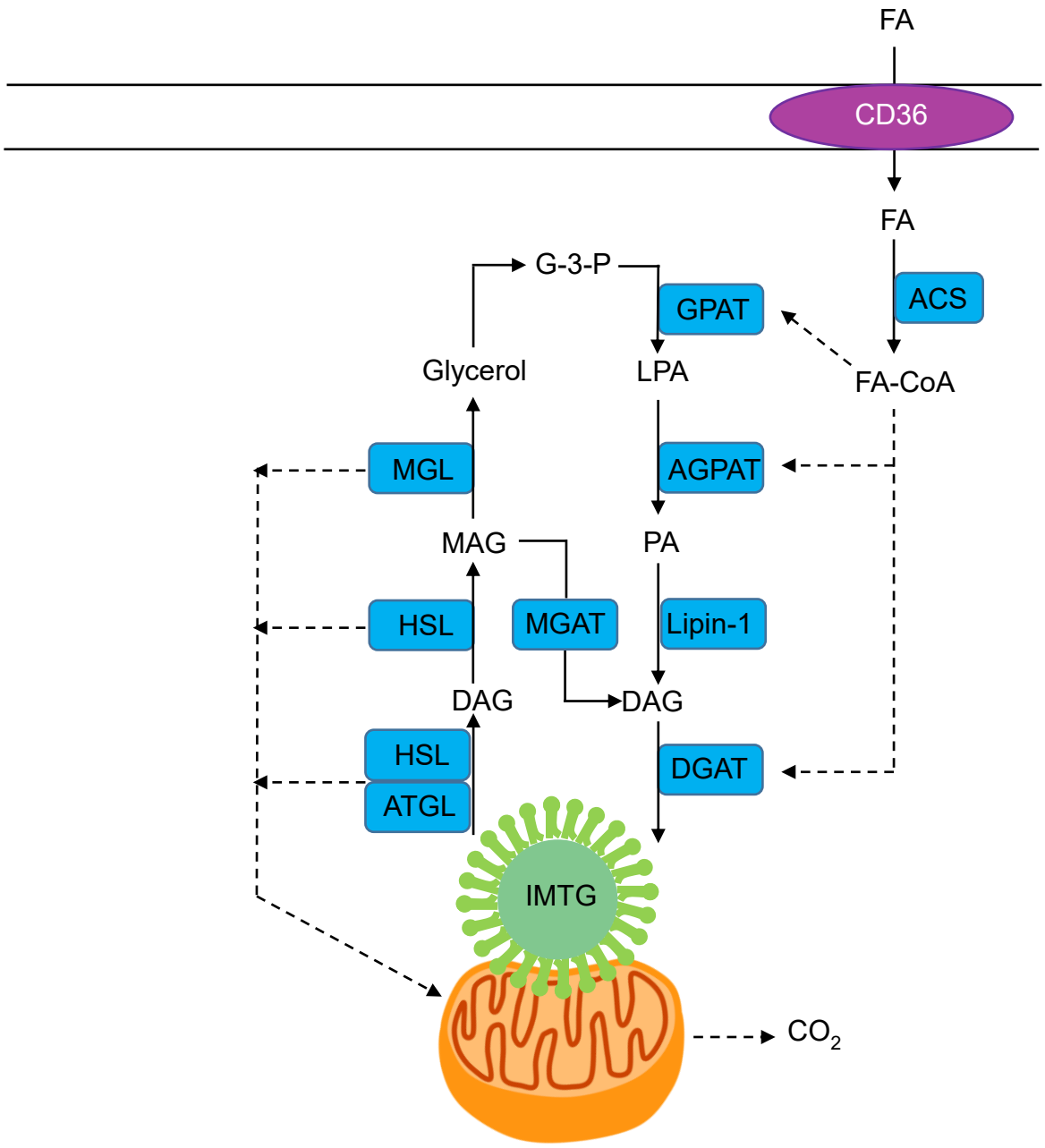

Figure 1.2. IMTG synthesis and hydrolysis in skeletal muscle. AGPAT, 1-acylglycerol-3-phosphate acyltransferase; ATGL adipose triglyceride lipase, ACS, acyl-CoA synthetase; DAG, diacylglycerol; DGAT, diacylglycerol transferase; FA, fatty acid; FA-CoA, fatty acyl-CoA; CD36, cluster of differentiation 36; G-3-P, glycerol-3- phosphate; GPAT, glycerol-3-phosphate acyltransferase; HSL, hormone sensitive lipase; IMTG, intramuscular triglyceride; LPA, lysophosphatidic acid; MAG monoacylglycerol; MGAT, monoacylglycerol transferase; PA, phosphatidic acid.

1.4 Lipid Droplets

Previously considered an inert storage depot, LD are now recognised as functional and dynamic organelles implicated in various biological processes (Walther & Farese, 2009). Having a core of neutral lipids (TAG and cholesterol esters) and surrounded by a phospholipid monolayer, LD are primarily abundant in adipocytes however they are also present in myocytes, hepatocytes and other cells to a lesser extent. As the primary role of LD is to store TAG, dysregulation of LD homeostasis is proposed to be implicated in the pathogenesis of insulin resistance and T2D (Greenberg *et al.*, 2011).

1.4.1 LD formation and growth

It is extensively accepted that LD are formed by or in close proximity to the ER, but the exact mechanism is still under debate. It is commonly proposed that TAG and cholesterol esters accumulate between the leaflets of the ER bilayer forming a lens type structure before the LD buds off towards the cytoplasm (Bersuker & Olzmann, 2017). Evidence from cultured human macrophages analysed using freeze-fracture high resolution electron microscopy showed that ER membranes lie external to and follow the LD contour similar to an egg held by an egg cup (Robenek *et al.*, 2006). Furthermore immunogold labelling indicated that protein perilipin-2 enriched domains of the cytoplasmic leaflet of the ER are where LD are located, suggesting this protein is important for LD biogenesis (Robenek *et al.*, 2006). Data from yeast cells also indicate new LD may form from fission of pre-existing LDs (Long *et al.*, 2012). Newly-synthesised LD are typically small in diameter (0.5 < μm) and referred to as primordial droplets.

LD can increase in size by a number of mechanisms; 1) coalescence of fusion of two LDs via pores in the phospholipid monolayer, 2) ripening of one LD through transfer of molecules from a LD decreasing in size and 3) expansion of LD due to increased synthesis of IMTG from FA (Gemmink *et al.*, 2017b). Experiments in NIH 3T3 cells

demonstrated that LD growth through fusion was independent of TAG synthesis but required the presence of microtubules and motor protein dynein (Bostrom *et al.*, 2005). Freeze-fracture electron microscopy images of macrophages show close contact between LDs and amalgamation of smaller LD in a larger LD, indicative of homotypic fusion (Robenek *et al.*, 2006). Microtubules provide a pathway in cells for LD to move to different organelles or to other LD (Welte, 2009). Interestingly, knockdown of SNARE fusion machinery; SNAP23, synataxin-5 and VAMP4, reduced the rate of fusion and LD size in NIH-3T3 cells (Bostrom *et al.*, 2007).

LD can decrease in size through a fission or fragmentation process. ADP ribosylation factor (ARF) – COPI, which coats Golgi vesicles and endosomal membranes, has been implicated in this process. RNAi knockdown of ARF1-COPI results in larger and more dispersed LD in Drosophila S2 cells (Guo *et al.*, 2008). Lipolysis of IMTG in the central core of LD by ATGL and HSL is also expected to reduce LD size, but whether fission of LD and TAG lipolysis occur in sequence or independent of one another is still unknown. It is generally accepted that a large number of small-sized LD is metabolically advantageous as this will provide a greater surface area for lipases to access and may increase phospholipid availability for regulatory proteins to associate with.

1.4.2 LD proteome

Decorating the phospholipid monolayer of LD are various proteins. The composition of this LD coat can impact the function and biological fate of each LD. The hydrophobic core of LD is an unfavourable environment for hydrophilic protein domains and therefore proteins are normally attached to or overspanning the outer membrane sometimes with multiple hydrophilic and hydrophobic protein domains. It has been proposed that the two primary ways that LD proteins associate with the phospholipid monolayer are; by hydrophobic domains (Class I) or amphipathic helices (Class II) (Kory *et al.*, 2016). Class I proteins such as DGAT2 (Stone *et al.*, 2006) and

GPAT4 (Wilfling *et al.*, 2013) possess a hydrophobic segment embedded in the LD membrane and a cytosolic hydrophilic N- and C- terminus. Dually found in the ER and LD, class I proteins are believed to be initially inserted into the ER before being trafficked to nascent LD. Class II proteins, such as perilipin (PLIN) proteins (Kory *et al.*, 2016), are proposed to sense physiochemical properties of the LD membrane and insert their amphipathic helix into the LD membrane (Rowe *et al.*, 2016). There is evidence to suggest that PLINs compete with each other for LD localisation, suggesting sites for amphipathic helix insertion may be limited (Rowe *et al.*, 2016). Some PLINs also contain a C-terminal helical bundle which contains a hydrophobic cleft capable of binding to lipids (Rowe *et al.*, 2016) which may provide another avenue of PLIN binding to LD. SNAP23 is neither a class I or II protein and instead is anchored to LD through a palmitate group (Bostrom *et al.*, 2007). ATGL co-activator CGI-58 also binds to LD unusually by a unique membrane embedded motif which forms a hydrophobic core allowing it to anchor to the LD (Boeszoermenyi *et al.*, 2015). Class I and II proteins bound to LD are also capable of recruiting other proteins to the LD, classically exemplified by HSL translocation to the phosphorylated N-terminus of PLIN1 (Wang *et al.*, 2009). Similar to other skeletal muscle proteomes, LD proteins are also subject to degradation processes to aptly remove damaged and dysfunctional proteins. Several LD associated proteins are degraded by the ubiquitin-proteasome system (Bersuker & Olzmann, 2017), however the regulation of this is still relatively unknown. The constant flux of class I proteins associating to nascent LD, attachment of class II proteins, further recruitment of other proteins to the LD and degradation of proteins is suggestive that a proteome of a singular LD is dynamic and likely influenced by location, maturity and metabolic state. The fact LD are heterogeneous in size, characteristic and function amongst different tissues and cell types further complicates the understanding of the LD proteome.

The discovery of proteins on the LD surface or within the LD has prompted various studies aiming to determine the LD proteome. Due to LD having a close association to mitochondria (Hoppeler *et al.*, 1999) and the endoplasmic reticulum (Jacquier *et al.*, 2011), it is unsurprising that proteomic analysis of the LD fraction has yielded proteins from both of these organelles. It may be argued that the purity of the LD sub-fraction is compromised in this instance, as it does not reflect a completely isolated LD proteome. Given that class I LD proteins are inserted at the ER and LD can form LD-mitochondrial complexes, this finding should not be overlooked and may be indicative of the current metabolic state of the LD within the muscle homogenate at a particular time. For example, an abundance of mitochondrial protein found in the LD proteome (Zhang *et al*., 2011) may suggest a significant portion of LD are metabolically linked to mitochondria. This can often be classified as a metabolic advantage as it would allow FA sequestered from IMTG hydrolysis to be shuttled to mitochondria more efficiently (Aon *et al.*, 2014). Indeed, endurance training has shown to increase the spatial interaction between LD and mitochondria (Tarnopolsky *et al.*, 2007) which likely underpins the increased IMTG utilisation during an acute exercise bout (Shepherd *et al*., 2013). Alternatively, a high abundance of ER proteins from the LD fraction may indicate that a substantial portion of LD within a muscle homogenate are newly-formed at the ER. Nevertheless, there is still a desire by many researchers to identify the proteome of an isolated LD fraction. Very stringent studies to this effect have used quantitative protein correlation profiling to identify high confidence LD proteins (111) in *Drosphila* S2 cells (Krahmer *et al.*, 2013) and in yeast cells (35) (Currie *et al.*, 2014).

Amongst the various LD proteome studies, several groups of proteins are commonly identified including; PLIN proteins (section 1.5) TAG biosynthetic enzymes (section 1.3.1) TAG lipolytic machinery (section 1.3.2), ubiquitination factors and Ras-related proteins (Bersuker & Olzmann, 2017). Rab GTPases identified in the LD proteome of

Chinese hamster ovary (CHO) cells (Liu *et al.*, 2004) may be responsible for mediating reactions with endosomes or with the ER. Most of these findings originate from non-myocyte cell lines or from tissues other than skeletal muscle. Zhang and colleagues (2011) identified 324 LD-associated proteins following ultracentrifugation of mouse skeletal muscle. An abundance of these proteins was associated to the mitochondria and the majority was part of the electron transport chain within the inner mitochondrial membrane. This shows that there is a tight association of LD with the mitochondria and an inability to separate the two organelles through ultracentrifugation. Although there were over 300 proteins identified, it still needs to be investigated how these proteins work together to regulate LD homeostasis and if there is a heterogeneity to LD proteome composition which may be related to the metabolic state and determine the regulation of each LD.

1.5 Perilipin proteins regulating IMTG turnover

Of the proteins associated with the LD, PAT/perilipin (PLIN) proteins have been the most extensively researched. Perilipin 1 was the first to be identified and its regulation in adipocytes is well characterised, but it is exclusively expressed in adipose tissue and steroidogenic cells (Londos *et al.*, 1995). Consequently, research in skeletal muscle has focused on the four remaining perilipin proteins namely; adipose differentiation related protein/adipophilin (PLIN2), tail interacting protein of 47kDA (PLIN3), S3-12 (PLIN4) and OXPAT (PLIN5). The following section will focus on the role of each perilipin protein on IMTG turnover and LD regulation.

1.5.1 Perilipin 2

PLIN2 was the second perilipin protein to be identified and was originally implicated in LD biosynthesis because it was present in 3T3-L1 adipocytes and in early differentiated adipocytes, but absent from maturing adipocytes (Brasaemle *et al.*, 1997). Cultured cells exposed to oleic acid demonstrate increased PLIN2 protein expression concomitant to an increase in TAG stores, studied in CHO fibroblast cells

(Xu *et al.*, 2005) and in J774 murine macrophages (Masuda *et al.*, 2006). In COS-7 cells, oleate treatment results in PLIN2 and DGAT2 colocalising at the LD surface (Stone *et al.*, 2009). Knockdown of PLIN2 *in vitro* in C2C12 cells results in reduced formation of LD following oleate treatment (Bosma *et al.*, 2012a). Together the data from cell culture studies suggests PLIN2 is important for expanding intracellular TAG stores following exposure to lipids.

Cross-sectionally, in humans where IMTG content is elevated such as in; endurance trained individuals, females or specifically in type I skeletal muscle fibres, PLIN2 protein expression is also elevated (Shaw *et al.*, 2009; Peters *et al.*, 2012; Shepherd *et al.*, 2013). Furthermore, endurance training increases IMTG content concomitant with an increase of PLIN2 protein expression (Shaw *et al.*, 2012; Shepherd *et al.*, 2013). Immunohistochemistry analyses in human skeletal muscle has revealed that approximately 60% of LD are colocalised with PLIN2 (Shaw *et al.*, 2009; Shepherd *et al.*, 2013) which has allowed the identification of LD associated with PLIN2 (PLIN2+ LD) and LD without PLIN2 association (PLIN2- LD) and demonstrates a heterogeneous LD pool. When IMTG content increases following 6 h lipid infusion during a HE clamp, the amount of PLIN2+ LD increases without any changes in PLIN2 protein expression (Shepherd *et al.*, 2017b), indicating PLIN2 has the capacity to be redistributed when the LD pool expands. Together, the research suggests PLIN2 is important for the formation of new LD which would support an increase in IMTG storage.

PLIN2 co-immunoprecipitates with ATGL in isolated rat skeletal muscle at rest but this interaction is decreased by 21% following electrically-stimulated muscle contraction (MacPherson *et al.*, 2013a). It has therefore been proposed that PLIN2 promotes lipid accumulation by sequestering ATGL and preventing lipolysis in basal conditions but releases ATGL so it can interact with its co-activator CGI-58 following lipolytic stimulation (MacPherson *et al.*, 2013a). Researchers from the same lab,

however, were unable to identify serine phosphorylation of PLIN2 following adrenaline or electrically stimulated muscle contraction of isolated rat muscle (Macpherson *et al.*, 2013b) and therefore how PLIN2 is regulated to assist in IMTG lipolysis still needs further investigation. In isolated rat skeletal muscle, both adrenaline and electrically-stimulated muscle contraction results in an increase in HSL colocalisation to PLIN2 (Prats *et al.*, 2006), illustrating one mechanism by which PLIN2 may directly support IMTG hydrolysis. In human skeletal muscle, PLIN2+ LD are preferentially utilised during 1 hour of moderate–intensity exercise in lean untrained men (Shepherd *et al.*, 2012). Interestingly though, following endurance or sprint interval training there are no differences in the use of PLIN2+ LD or PLIN2- LD utilised during 1 hour of moderate-intensity exercise (Shepherd *et al.*, 2013). This indicates that other perilipins may be more important in regulating IMTG lipolysis following endurance training.

1.5.2 Perilipin 3

Perilipin 3 was the third perilipin family member to be identified and research from non-skeletal muscle cell lines has implicated PLIN3 to play a role in lipid synthesis. Following oleate treatment, PLIN3 associates with smaller nascent peripherally located LD in 3T3-L1 adipocytes and resulted in an increase of PLIN3 in the LD fraction compared to cytosolic fraction (Wolins *et al.*, 2005). In HeLa cells suppression of PLIN3 reduced LD maturation and decreased incorporation of TAG into LD (Bulankina *et al.*, 2009). Together these studies suggest that PLIN3 plays a supportive role in the formation and maturation of LD.

Although it is not known if PLIN3 plays a similar role in skeletal muscle, pharmacological activation of AMPK in mouse skeletal muscle is reported to increase PLIN3 gene expression resulting in elevated IMTG content (Kleinert *et al.*, 2016). In human skeletal muscle PLIN3 protein expression is higher in type I fibres (Shepherd *et al.*, 2017b) and in females (Peters *et al.*, 2012) where IMTG content is elevated. At

present there is confounding data if PLIN3 increases following endurance training. PLIN3 protein expression does not increase following either 12 weeks of endurance training in lean or obese males and females (Peters *et al.*, 2012) or 12 weeks of combined strength and endurance training in T2D individuals (Daemen *et al.*, 2018). PLIN3 protein expression however does increase after 4 weeks of endurance training in sedentary obese males (Shepherd *et al.*, 2017a). Cross-sectionally endurance-trained in comparison to lean sedentary individuals show higher PLIN3 protein expression (Shepherd *et al.*, 2017b) or comparative levels (Daemen *et al.*, 2018). Following 6 h lipid infusion during a HE clamp, IMTG content increases with a concomitant increase in PLIN3+ LD in type I fibres without alterations in PLIN3 protein expression (Shepherd et al., 2017). Together the data suggests PLIN3 could play a role in increasing IMTG stores but the exact role requires much more investigation.

Until recently, little evidence existed to suggest that PLIN3 assisted in IMTG lipolysis. Lipolytic stimulation (palmitate, forskolin, and ionomycin treatment) of myotubes from lean individuals increased PLIN3 protein expression, whilst knockdown of PLIN3 in these myotubes reduced lipid oxidation (Covington *et al.*, 2015). A prolonged acute exercise bout at 50% VO_{2max} results in an increase in PLIN3 protein expression in human skeletal muscle (Covington *et al.*, 2014), but how this is related to IMTG lipolysis is unknown. Co-immunoprecipitation confirms that PLIN3 also interacts with lipases ATGL and HSL in rat skeletal muscle however this interaction is unchanged following lipolytic stimulation (Macpherson *et al.*, 2013b). At present the evidence indicates PLIN3 may support the expansion of IMTG stores, but there is still little evidence to suggest PLIN3 has a functional role in IMTG lipolysis.

1.5.3 Perilipin 4

PLIN4 is apparently the most abundant PLIN in skeletal muscle (Deshmukh *et al.*, 2015a) and has the highest mRNA expression (Pourteymour *et al.*, 2015), yet is the least researched. This is partly due to the importance of PLIN4 in regulating IMTG

being questioned by the finding that PLIN4-KO mice show no major alterations in skeletal muscle lipid levels (Chen *et al.*, 2013). Adding to this PLIN4 mRNA expression and protein content remains the same or are reduced following endurance training (Peters *et al.*, 2012; Pourteymour *et al.*, 2015). Nevertheless, new evidence has emerged that trained individuals tend to have a higher PLIN4 protein expression compared to sedentary individuals (Shepherd *et al.*, 2017b). In a similar fashion to PLIN3, PLIN4 was also found to coat smaller peripherally located LD in 3T3-L1 adipocytes following oleate treatment (Wolins *et al.*, 2005). Incubation of cultured myotubes with oleic acid increases PLIN4 mRNA expression whereas *in vivo* a low fat diet reduces PLIN4 mRNA expression in human skeletal muscle (Gjelstad *et al.*, 2012). Although PLIN4 is the most abundant PLIN in skeletal muscle there is still limited and confounding data on the importance of PLIN4 in regulating IMTG stores.

1.5.4 Perilipin 5

PLIN5 was the last perilipin discovered and is highly expressed in oxidative tissues that exhibit high rates of lipolysis and β-oxidation (Wolins *et al.*, 2006; Peters *et al.*, 2012; Shepherd *et al.*, 2013). PLIN5 is present at the LD surface, within the cytosol and at the mitochondria in skeletal muscle (Bosma *et al.*, 2012b; Shepherd *et al.*, 2013). Similar to PLIN2, PLIN5 protein expression is positively correlated in cases with elevated IMTG stores, for example in females (Peters *et al.*, 2012), in type I fibres (Shepherd *et al.*, 2013; Shepherd *et al.*, 2017b), in endurance trained individuals (Shepherd *et al.*, 2017b; Daemen *et al.*, 2018) or following endurance training (Peters *et al.*, 2012; Shepherd *et al.*, 2013). When PLIN5 is overexpressed there is an increase in TAG stores in CHO cells (Dalen *et al.*, 2007), COS-7 cells (Wolins *et al.*, 2006) and rat skeletal muscle (Bosma *et al.*, 2013). In human skeletal muscle when IMTG increases following 6 h lipid infusion with HE clamp, PLIN5+ LD also increased in type I fibres (Shepherd *et al.*, 2017b). Following a longer exposure to lipid excess with a 5-day high-fat high calorie diet PLIN5 protein expression of whole muscle

homogenate increases (Gemmink *et al.*, 2017a). The increase in IMTG observed following acute elevation of FFA from prolonged fasting, is completely attributable to PLIN5+ LD (Gemmink *et al.*, 2016).

Although PLIN5 protein expression is upregulated or PLIN5 colocalisation to LD increases in cases of augmented IMTG content, there is more evidence to suggest PLIN5 has a more functional role of a scaffold protein regulating levels of lipolysis rather than regulating IMTG synthesis. PLIN5 has a conserved N-terminus sequence that can bind to HSL (Anthonsen *et al.*, 1998) and a C-terminus region that can bind to either ATGL or CGI-58 (Granneman *et al.*, 2011; Wang *et al.*, 2011a). PLIN5 binds to either CGI-58 or ATGL in CHO cells reducing TAG hydrolysis in basal conditions (Wang *et al.*, 2011a). CGI-58 is the known co-activator of ATGL evidenced by an increased lipolysis rate when there is increased interaction of ATGL with CGI-58 (Wang *et al.*, 2011a). PKA stimulation results in PLIN5 phosphorylation and when PKA activation occurs with ectopic overexpression of PLIN5 and ATGL, lipolysis increases (Wang *et al.*, 2011a). These data have generated the hypothesis that PLIN5 serves to limit lipolysis in basal conditions by preventing the interaction of ATGL with CGI-58, and promotes lipolysis by releasing and allowing the interaction of ATGL and CGI-58 following lipolytic stimuli. In rat skeletal muscle PLIN5 co-immunoprecipitates with both ATGL and CGI-58 however this interaction remains unchanged following electrical or epinephrine stimulation (MacPherson *et al.*, 2013a). The importance of PLIN5 in regulating IMTG lipolysis has been highlighted by the finding that following endurance training PLIN5+ LD are preferentially used during 1 h of moderate-intensity exercise in human skeletal muscle compared to PLIN5- LD (Shepherd *et al.*, 2013). Despite PLIN5's proposed role of regulating IMTG, there has been limited research investigating PLIN5's interaction with HSL and ATGL in human skeletal muscle during moderate-intensity exercise. PLIN5 was shown to colocalise with ATGL in human skeletal muscle using wide-field microscopy and this did not

change with 60 min of moderate-intensity exercise. (Mason *et al.*, 2014a). As previously explained (section 1.3.2.2 (ii)) the use of wide-field microscopy does not permit a detailed assessment of distribution and colocalisation of IMTG stores and lipolytic proteins. The use of higher resolution confocal microscopy is therefore needed to investigate PLIN5 colocalisation with ATGL and HSL in human skeletal muscle.

Immunogold electron microscopy and western blot of isolated mitochondria revealed that PLIN5 has a strong association to mitochondria (Bosma *et al.*, 2012b). Overexpression of PLIN5 enhances the interaction of LDs and mitochondria (Bosma *et al.*, 2012b) and increases fatty acid oxidation (Wolins *et al.*, 2006; Bosma *et al.*, 2012b). The metabolic linkage between PLIN5 and mitochondria may assist in directing IMTG-derived FA to the mitochondria for subsequent β-oxidation. PLIN5-KO mice results in decreased whole body fatty acid oxidation however the interaction between LDs and mitochondria is unaltered when PLIN5 is absent (Mason *et al.*, 2014b). The role of PLIN5 in enhanced IMTG-derived fatty-acid oxidation therefore still warrants further investigation.

1.6 Insulin resistance and Type 2 Diabetes

In contrast to our predecessors, we expose our genotype to energy-dense western diets and reduced levels of physical activity. As such, an increased amount of time is spent in the postprandial period exposing the human tissues to excessive surplus of FA and glucose. The following sections explain the mechanisms by which chronic intake of energy-dense foods and low activity levels contribute to the development of insulin resistance with specific focus on skeletal muscle insulin resistance.

Insulin sensitive tissues can mal-adapt due to different stressors such are reduced physical activity, increased sedentary time and overfeeding. This results in tissues becoming less responsive to the effects of insulin, a condition termed insulin resistance. Reduced insulin sensitivity in peripheral tissues (adipose tissue and

skeletal muscle) can result in reduced uptake of glucose from the blood for a given concentration of insulin. Whereas, hepatic insulin resistance is characterised as impaired suppression of hepatic glucose production. In the face of insulin resistance, normal glucose tolerance can be maintained by an increased secretion of insulin by pancreatic beta *β*-cells (Festa *et al.*, 2006). A failure to increase insulin secretion results in impaired glucose tolerance (Festa *et al.*, 2006). T2D ensues with a decline in *β*-cell function, resulting in reduced insulin secretion, leading to chronic hyperglycaemia (Kasuga, 2006). Reduced insulin sensitivity of tissues is therefore a primary aberration in the progression of T2D. As discussed in section 1.1.1.1 skeletal muscle is one of the largest blood glucose disposal sites post-prandial (Capaldo *et al.*, 1999). Results from a HE clamp comparing T2D to controls determined that peripheral rather than splanchnic tissues were the predominant site of insulin resistance (DeFronzo *et al.*, 1985), with skeletal muscle considered the primary tissue accounting for peripheral tissues. Maintaining skeletal muscle insulin sensitivity is therefore important in preserving whole body insulin sensitivity and preventing T2D.

Clinically, T2D is categorised as fasting blood glucose levels above 7 $mmol.L^{-1}$, an inability to reduce blood glucose levels below 11.1 $mmol.L^{-1}$ following a 2 h 75g oral glucose tolerance test (OGTT), or a glycated haemoglobin (HbA1c) level above 6.5% (American Diabetes, 2015). T2D is associated with an increased risk of cardiovascular complications (Laakso, 2010). Persistent hyperglycaemia can cause endothelial dysfunction at the microvasculature leading to complications such as retinopathy or neuropathy (Remuzzi *et al.*, 2002; Watkins, 2003). Microvascular dysfunction at the skeletal muscle can further exacerbate reductions in insulin and glucose delivery to skeletal muscle furthering reducing glucose uptake (Stehouwer, 2018). Importantly, hyperglycaemia at the macrovasculature level can increase a person's risk of heart attack, stroke or peripheral vascular disease (Fowler, 2008).

1.6.1 Lipid induced insulin resistance

1.6.1.2 FFA storage and lipid overflow hypothesis

This postprandial clearance of chylomicron-TAG into adipose tissue (explained in section 1.3.1) serves as an important mechanism to protect the vascular wall from exposure to FA and TAG which can impair endothelial function and increase risk of atherosclerotic plaques. If this lipid buffering mechanism becomes impaired, there is a 'spill over' of FA and TAG in the circulation. The excess lipids are then deposited in non-adipose tissues such as liver, pancreatic beta cells and skeletal muscle (Frayn, 2002). Accumulation of TAG in insulin-responsive tissues such as skeletal muscle (Goodpaster *et al.*, 1997; Forouhi *et al.*, 1999) and liver (Goto *et al.*, 1995; Ryysy *et al.*, 2000) is associated with insulin resistance. Furthermore, prolonged exposure of FA to human pancreatic islets results in impaired insulin secretion (Paolisso *et al.*, 1995; Zhou & Grill, 1995). Accumulation of FA and TAG in non-adipose tissues is, therefore, detrimental to insulin sensitivity.

The importance of adipose tissue as a buffer for FA flux is exemplified by the condition of lipodystrophy or lipoatrophy which is characterised by partial or complete loss of adipose tissue, presented with exacerbated insulin resistance (Ganda, 2000). Mice without adipose tissue (A-ZIP/F-1) have been created to mimic lipodystrophy or lipoatrophy (Kim *et al.*, 2000a). These mice develop accumulation of TAG in skeletal muscle and liver which are associated with defects in insulin signalling in both tissues (Kim *et al.*, 2000a). Interestingly fat transplantation from WT mice into A-ZIP/F-1 mice results in reversal of hyperglycaemia, hyperinsulinemia and insulin resistance with modest reductions of TAG content in liver and skeletal muscle (Gavrilova *et al.*, 2000; Kim *et al.*, 2000a). Additional evidence of the importance of buffering adipose tissue stems from treatment with thiazolidinedione in obese Zucker rats which results in adipocyte differentiation from the activation of peroxisome proliferator receptors (PPARγ) (Hallakou *et al.*, 1997). This increase in adipocytes results in an enhanced

capacity to store TAG in adipose tissue resulting in a reduction in liver and skeletal muscle TAG concomitant to an improvement in insulin sensitivity (Hallakou *et al.*, 1997). Adipose tissue's ability to buffer FA flux therefore proves important in reducing ectopic lipid accumulation in liver and skeletal muscle and maintaining insulin sensitivity and euglycaemia.

The size of adipocytes in adipose tissue appears to be an important factor in adipose tissue buffering. Historical evidence has shown that larger adipocytes are less responsive to insulin stimulation (Olefsky, 1977). Furthermore, the accumulation of larger adipocytes in the subcutaneous area is a risk for developing T2D (Weyer *et al.*, 2000). Thiazolidinedione stimulates adipocyte differentiation via nuclear receptor PPARγ resulting in smaller adipocytes and alleviated insulin resistance (Okuno *et al.*, 1998). It is therefore hypothesised that smaller adipocytes are more efficient at buffering FA flux in the post-prandial period and an inability to differentiate new adipocytes required for excess TAG storage may result in ectopic lipid accumulation and subsequent insulin resistance. Adipocytes from different regions in the body also display different properties. For example visceral adipose tissue (VAT) are characterised by high rates of lipolysis (Ostman *et al.*, 1979) which to maintain levels must be matched by high rates of fat deposition (Frayn, 2000). Enlargement of VAT is associated with insulin resistance (Kelley *et al.*, 2000) and is more commonly associated with males than females (Janjic, 1996). VAT is unique in being the only adipose tissue depot which has an anatomical position capable of draining FA to the liver via the portal vein (Bjorndal *et al.*, 2011). Impairments of FA buffering in VAT may therefore augment ectopic lipid accumulation to the liver. However, it has been demonstrated that VAT only contributes a small proportion of total FA release, and VAT lipolysis directed to the portal vein is only elevated when there are increases in VAT stores (Nielsen *et al.*, 2004).

Fasting FA concentrations are unchanged with increasing fat mass (Karpe *et al.*, 2011), suggesting that basal lipolysis per kilogram of fat mass is reduced in obesity. This is supported by adipocytes from obese people showing reduced lipolysis *in vitro* and reduced expression of the key lipolytic enzyme HSL (Large *et al.*, 1999). This downregulation of basal lipolysis per kg of mass normalises FA appearance in the face of elevated adipose tissue. Reduced basal lipolysis of expanding adipose stores however will ultimately increases adipose tissue accumulation, which may impact overall adipose buffering capability. The obese state is characterised by an impaired insulin-mediated suppression of adipose tissue lipolysis resulting in greater appearance of FA from adipocytes into the circulation (Coppack *et al.*, 1992; Hickner *et al.*, 1999). This relationship does not exist however when FA appearance is normalised to total fat mass (Bickerton *et al.*, 2008; McQuaid *et al.*, 2011). Hyperinsulinemia observed in insulin resistant states therefore may be sufficient to suppress FA release following meal ingestion when normalised to total adipose tissue mass. Exacerbation of reduced lipid flux and consequent lipid spill over is therefore likely to be due to a reduced capacity of adipose tissue to hydrolyse and store plasma-derived TAG (McQuaid *et al.*, 2011).

In lean individuals it is estimated that LPL activity measured in adipose tissue biopsies increases by 124% following a meal, but it only increases by 27% in obese subjects (Ong & Kern, 1989). Another study demonstrated that whilst LPL activity increased in obese subjects following insulin stimulation this increase was delayed (6 h compared to 3 h) in comparison to lean subjects (Sadur *et al.*, 1984). This could lead to prolonged exposure of elevated plasma TAG levels, which is more closely related to insulin resistance in comparison to plasma FA (Bickerton *et al.*, 2008). It is postulated that to maintain lipid homeostasis, plasma TAG will remain in the circulation until it has been hydrolysed on the capillary bed and transported into nearby tissue. The

longer plasma TAG remains in circulation the increased likelihood that this will be a non-adipose tissue such as skeletal muscle or liver.

1.6.2 Athlete's Paradox

Accumulation of TAG in skeletal muscle was previously associated with reduced insulin sensitivity particularly in obese, sedentary and type 2 diabetic individuals (Pan *et al.*, 1997; Kelley *et al.*, 2001; van Loon, 2004) . Paradoxically, endurance trained athletes also display high levels of IMTG content yet remain very insulin sensitive (Goodpaster *et al.*, 2001; van Loon *et al.*, 2004). This phenomenon is termed the athletes paradox and has resulted in important research investigating why endurance trained individuals can remain insulin sensitive whilst having elevated IMTG stores. IMTG has no mechanistic link towards skeletal muscle insulin resistance per se; however, accumulation of lipid metabolites including fatty-acyl CoA, ceramides and certain DAG species in the muscle have been shown to contribute to skeletal muscle insulin resistance (Yu *et al.*, 2002a; Gual *et al.*, 2005; Samuel *et al.*, 2010). As such lipid metabolites are often elevated in obese or type 2 diabetic individuals compared to lean or endurance trained controls (Hulver *et al.*, 2003; Adams *et al.*, 2004; Straczkowski *et al.*, 2007; Coen *et al.*, 2010; Bergman *et al.*, 2012). The lipid metabolite species and mechanisms underpinning lipid metabolite-induced skeletal muscle insulin resistance are discussed in more detail in the following section (section 1.6.3). Work from Jensen and colleagues has established that healthy individuals have high IMTG turnover at rest (Kanaley *et al.*, 2009) and during submaximal exercise (Guo *et al.*, 2000). Conversely, obese pre-diabetic individuals showed impaired IMTG turnover leading to subsequent IMTG accumulation (Perreault *et al.*, 2010). The efficient regulation of FA uptake, esterification, hydrolysis and oxidation appears paramount in minimising the accumulation of lipid metabolites. This section will discuss differences in the size and turnover of IMTG stores between endurance

trained individuals and sedentary people, who are more susceptible to develop insulin resistance that is likely to result in the accumulation of lipid metabolites.

1.6.2.1 Dysregulation of FA transporters

In addition to delivery of FA to skeletal muscle, FA uptake is regulated by FA transporters namely fatty acid translocase (FAT/CD36), fatty acid transport protein1-5 (FATP1-5) and plasma membrane fatty-acid binding protein (FABPm). These FA transporters are located in skeletal muscle and/or capillary endothelial cells. Whilst this section focuses on dysregulation of FA transporters in skeletal muscle, it is important to note that endothelial cells on skeletal muscle microvasculature present the first main barrier to transport of FA into the muscle (Wagenmakers *et al.*, 2016). In whole muscle homogenates CD36 and FATP1 protein content is similar between obese/ type 2 diabetic groups in comparison to lean or endurance trained controls (Bonen *et al.*, 2004; Holloway *et al.*, 2007; Pelsers *et al.*, 2007; Aguer *et al.*, 2010). FABPm mRNA expression and protein content was higher in endurance trained individuals compared to individuals with T2D and sedentary controls, likely reflecting greater FA uptake and oxidation rates during increased energy expenditure of exercise bouts (Pelsers *et al.*, 2007). Although protein content of CD36 and FATP1 is not altered in insulin resistant states, evidence is accumulating that the location of these proteins has an influence on FA uptake. In particular, CD36 was shown to permanently relocate from the intracellular compartment to the sarcolemma region to increase FA uptake in the face of elevated plasma FA observed in obese populations (Bonen *et al.*, 2004; Aguer *et al.*, 2010). The increase uptake of FA transport proteins and uptake of FA observed in endurance trained individuals appears to be an adaptation to allow greater utilisation of adipose tissue derived fatty acids during exercise bouts. Comparatively in insulin-resistant states, a permanent relocation of CD36 to the plasma membrane can increase the flux of FA entering the muscle from

elevated plasma FA level. If FA entering the muscle is not directed to IMTG for storage or mitochondria for β-oxidation, it could contribute to an increase lipid metabolites.

1.6.2.2 Dysregulation of IMTG synthesis

Long chain acyl-CoA synthases are responsible for activation and partitioning of FA in skeletal muscle to synthesis into IMTG or to the mitochondria for β-oxidation. Studies using stable isotope tracers have confirmed that a significant portion of FA entering skeletal muscle are directed to IMTG storage prior to entering long-chain acyl-carnitine oxidative pools (Sacchetti *et al.*, 2004; Kanaley *et al.*, 2009). Fractional synthesis rates of IMTG tend to be lower in obese people with pre-diabetes (0.21/h) compared to obese people with normal glucose tolerance (0.42/h) (Perreault *et al.,* 2010). Compared to sedentary individuals (0.61/h), endurance trained cyclists display greater (1.56/h) IMTG fractional synthesis rates (Bergman *et al.*, 2018). Endurance cyclists are also capable of fully replenishing IMTG stores 48 hours after a 3 hour moderate-intensity (55% W_{max}) cycling protocol whilst consuming a normal fat diet (39% energy) (van Loon *et al.*, 2003b). Following moderate-intensity exercise, the content of TAG synthesis enzymes DGAT1 and GPAT1 (Schenk & Horowitz, 2007) or GPAT1 activity (Newsom *et al.*, 2011) increase, which likely aids in the replenishment of IMTG stores. The increase in DGAT1 and GPAT1 content prevented lipid-induced insulin resistance following lipid-heparin infusion by reducing the content of DAG, ceramides and FA metabolites (Schenk & Horowitz, 2007). Overexpression of DGAT1 by recombinant adenovirus in C2C12 myotubes increases TAG content and reduces DAG content (Liu *et al.*, 2007). Cross-sectionally there are no differences in expression of GPAT1 or DGAT1 between obese and lean individuals (Thrush *et al.*, 2009; Li *et al.*, 2011) or DGAT1 mRNA or protein expression between trained athletes and sedentary controls (Schmitt *et al.*, 2003; Bergman *et al.*, 2010; Amati *et al.*, 2011). Furthermore, 8-16 weeks of endurance training does not alter DGAT1 protein expression in lean (Alsted *et al.*, 2009) or obese individuals (Dube *et al.*,

2011). It is therefore evident that whilst DGAT and GPAT are vital for IMTG synthesis, there is little evidence to show that DGAT or GPAT protein expression or activity is impaired in insulin resistant states. A recent study has confirmed that greater IMTG synthesis rates observed in endurance-trained athletes compared to obese controls and people with T2D was not due to alterations in FA delivery, DGAT1 mRNA expression or protein content (Bergman *et al.*, 2018). Basal IMTG synthesis rates were greater in athletes and were positively correlated to insulin sensitivity and also cytosolic DAG accumulation whilst being inversely correlated to C18:0 ceramide and glucosylceramide (Bergman *et al.*, 2018). Clearly, IMTG synthesis rates are important, but the differences between endurance trained in comparison to insulin resistant individuals is likely due to the favourable partitioning of incoming FA away from ceramides and glucosylceramide and towards IMTG.

1.6.2.3 LD size and location

Although IMTG content has no mechanistic link towards insulin resistance recent advances in microscopy techniques have added to our current understanding of how the location and size of LD storing IMTG may impact skeletal muscle insulin sensitivity. Transmission electron microscopy (TEM) can be used to accurately decipher between the intermyofibrillar (nearer to contractile elements) and subsarcolemmal region (near vicinity of plasma membrane) in skeletal muscle cells. Using TEM, Nielsen and colleagues (2017) found the diameter but not the number of individual subsarcolemmal LD was negatively associated with insulin sensitivity, as measured by HE clamp in healthy young untrained males. Despite having similar IMTG content, older individuals that have reduced insulin sensitivity have larger LD and a higher IMTG content in the subsarcolemmal region in comparison to BMI matched younger individuals (Crane *et al.*, 2010). Using confocal immunofluorescence microscopy it was demonstrated that T2D individuals primarily store larger LD in the subsarcolemmal region of type II fibres whereas endurance

trained individuals stored smaller LD in the intermyofibrillar region of type I fibres (Daemen *et al.*, 2018). Increase in LD size rather than total LD content following 8 weeks of a high-fat high-calorie diet in sedentary males is related to reduced insulin sensitivity (Covington *et al.*, 2017) whilst a decrease in LD size following weight loss or exercise training was associated with improved insulin sensitivity (He *et al.*, 2004). TEM and confocal immunofluorescence microscopy have confirmed that LDs are located in close proximity to mitochondria in skeletal muscle (Hoppeler *et al.*, 1999; Shaw *et al.*, 2008). Younger more insulin sensitive individuals have a greater fraction of LD in contact to mitochondria (Crane *et al.*, 2010). The preferential location of LD to the mitochondria would assist in trafficking IMTG-derived FA from the LD to the mitochondria for subsequent *β*-oxidation. The evidence thus far suggests that LD that are smaller, located in the intermyofibrillar region and in contact to mitochondria are more metabolically advantageous and are associated with the healthy insulin-sensitive phenotype. Larger LD observed in insulin-resistant states, that have a lower surface area to volume ratio, are proposed to result in lower IMTG turnover and subsequent accumulation of lipid metabolites. The accumulation of these lipid metabolites in subsarcolemmal region near to insulin signalling cascades are proposed to contribute to skeletal muscle insulin resistance.

1.6.2.3 Impairments in IMTG lipolysis and substrate use

A key discrepancy between endurance trained athletes and sedentary, obese individuals or individuals with T2D is their capability to utilise IMTG as a fuel source during exercise. Longitudinal exercise training interventions (Phillips *et al.*, 1996; Schrauwen *et al.*, 2002; De Bock *et al.*, 2008; Van Proeyen *et al.*, 2011b) and cross-sectional comparisons between trained and untrained individuals (Klein *et al.*, 1994; Coggan *et al.*, 2000) have demonstrated that endurance training leads to an increased use of IMTG as a substrate during exercise. In contrast sedentary, obese individuals or individuals with T2D display little or no IMTG use during exercise

(Schrauwen *et al.*, 2002; van Loon, 2004). This may be a consequence of elevated plasma FA observed in obese/ type 2 diabetic individuals taking precedence over IMTG as substrate to minimise circulatory FA (van Loon *et al.*, 2005b). Indeed, when adipose tissue lipolysis and FA release is inhibited with administration of Acipimox, IMTG utilisation during exercise increases in both lean and T2D individuals (van Loon *et al.*, 2005a).

The reduced capacity to utilise IMTG stores may also be the result of impaired IMTG lipolysis and the location of IMTG substrates within the muscle. In obese individuals there is impaired β_2-adrenergic-mediated stimulation of muscle lipolysis compared to lean participants (Blaak *et al.*, 2004). *In vitro* assays in conjunction with ATGL or HSL knockout mice models have suggested that ATGL and HSL have a higher specificity for TAG and DAG, respectively (Fredrikson *et al.*, 1981a; Haemmerle *et al.*, 2002b; Haemmerle *et al.*, 2006). An undesirable DAG to TAG hydrolysis activity stemming from an imbalance between HSL and ATGL protein content and activity may lead to accumulation of DAG. Males diagnosed with T2D have lower skeletal muscle HSL protein content in comparison to normal glucose tolerant controls, and HSL activity in people with T2D shows signs of dysregulation at rest and following insulin stimulation (Jocken *et al.*, 2013). ATGL protein content increases following endurance training (Alsted *et al.*, 2009) whereas HSL protein remains unchanged following endurance training in rats (Enevoldsen *et al.*, 2001) and is not different between untrained and trained skeletal muscle (Helge *et al.*, 2006). Rats with low intrinsic exercise capacity have a decreased ability to activate HSL by epinephrine stimulated phosphorylation of Ser660 (Lessard *et al.*, 2009). Contrasting data has shown that there is no difference in HSL activity and IMTG net hydrolysis before and after 180 min of exercise at 60% $VO_{2\ max}$ between trained and untrained participants (Helge *et al.*, 2006). Although the imbalance between ATGL and HSL hydrolysis gives an appealing explanation for the accumulation of DAG and subsequent skeletal muscle insulin

resistance, there is controversy whether ATGL-derived DAG can contribute to insulin resistance. For example, ATGL cannot produce signalling *sn*-1, 2-DAG capable of activating PKC and disrupting the insulin signalling cascade (Eichmann *et al.*, 2012).

The ability to oxidise FA in skeletal muscle can also limit the use of IMTG as a substrate. It has been reported that skeletal muscle from obese and T2D individuals have lower fatty acid oxidation in post-absorptive conditions (Kim *et al.*, 2000b; Blaak & Wagenmakers, 2002). Decreases in fatty acid oxidation may be explained by reduced mitochondrial content and increased mitochondrial dysfunction observed in muscle from obese and type 2 diabetic populations. Muscle from obese and type 2 diabetic individuals have smaller, less dense mitochondria in the intermyofibrillar and subsarcolemmal region (Kelley *et al.*, 2002) and lower electron transport chain (ETC) activity (Ritov *et al.*, 2005). Greater spatial contact between LD and mitochondria is proposed to be physiologically advantageous by reducing the distance IMTG-derived FA have to travel to undergo β-oxidation. Confocal immunofluorescence microscopy have confirmed that in lean physically active individuals LD stores are mainly located in spaces between mitochondria (Shaw *et al.*, 2008). When comparing lean and obese insulin-resistant females however there are no differences in the amount of contact between LD and mitochondria (Devries *et al.*, 2013). Endurance training which is associated with improvements in insulin sensitivity has been shown to improve mitochondrial function and contact to LD. For example, Sixteen weeks of combined weight loss and endurance training in obese individuals resulted in an increase in ETC activity in the intermyofibrillar and subsarcolemmal regions, with increases in subsarcolemmal ETC correlated to improvements in insulin sensitivity even when adjusted for changes in aerobic capacity (Menshikova *et al.*, 2005). Importantly following 7-weeks of endurance training in previously sedentary individuals there is an increase in IMTG and mitochondria content concurrent to an increase in the number of LD in contact with mitochondria (Tarnopolsky *et al.*, 2007).

Similarly 12-weeks of endurance training increases mitochondrial oxidative and β-oxidation capacity with an increase contact between LD and mitochondrial in both obese and lean females (Devries *et al.*, 2013). Mitochondrial oxidative capacity and location to LD are important factors in enabling IMTG to be substrate and therefore preventing the accumulation of lipid metabolites known to contribute to skeletal muscle insulin resistance.

1.6.2.4 Difference in proteins regulating IMTG turnover

As discussed more thoroughly in section 1.5, PLINs are likely to play a regulatory role in IMTG turnover and therefore maintaining skeletal muscle insulin sensitivity. PLIN2-5 protein expression is higher in endurance trained compared to sedentary individuals (Shepherd *et al.*, 2017b). Furthermore PLIN2, PLIN3 and PLIN5 protein expression have all been shown to be upregulated following endurance training (Peters *et al.*, 2012; Shaw *et al.*, 2012; Shepherd *et al.*, 2013; Shepherd *et al.*, 2017a; Daemen *et al.*, 2018) which is typically associated with improvements in insulin sensitivity.

Previous studies have reported PLIN2 protein expression is correlated positively with insulin sensitivity (Phillips *et al.*, 2005; Coen *et al.*, 2010). Additionally, overexpression of PLIN2 in rat skeletal muscle increases IMTG content and improves insulin sensitivity (Bosma *et al.*, 2012a). Recently however PLIN2 was elevated more in obese and T2D in comparison to endurance-trained individuals resulting in a negative correlation with insulin sensitivity (Daemen *et al.*, 2018). The reason for this discrepancy is unknown and clearly shows that the influence of PLIN2 on regulating IMTG turnover and maintaining insulin sensitivity requires further investigation.

Overexpression of PLIN5 in rat skeletal muscle also increases also IMTG content without compromising insulin sensitivity (Bosma *et al.*, 2013). PLIN5 overexpression in human primary myotubes also been shown to protect against lipid-induced lipotoxicity (Laurens *et al.*, 2016). Deletion of PLIN5 in mice decreases TAG stores, increases lipid metabolites and leads to the development of skeletal muscle insulin

resistance (Mason *et al.*, 2014b). The accumulating evidence therefore suggests PLIN5 is important in regulating IMTG turnover and maintaining skeletal muscle insulin sensitivity. Gemmink et al., (2018) explored therefore whether the fraction of PLIN5+ LD was a determinant of skeletal muscle insulin sensitivity when IMTG content was matched in; endurance trained athletes, untrained controls, obese and T2D individuals. It was discovered that whilst PLIN5 protein expression was almost double in endurance trained athletes compared to T2D, PLIN5 protein content or PLIN5+ LD did not correlate with insulin sensitivity (Gemmink *et al.*, 2018). PLIN5 protein expression and PLIN5+ LD was correlated with $VO_{2\ max}$ indicating its importance in oxidative capacity. PLIN proteins have been widely implicated in regulation of IMTG stores and lipolysis (section 1.5), however how this directly impacts skeletal muscle insulin sensitivity is still unknown.

The SNARE protein SNAP23 may also assist in regulating IMTG turnover. Ablation of SNAP23 in fibroblasts reduces the formation of LD-mitochondria complexes and results in a decreased mitochondrial β-oxidation (Jagerstrom *et al.*, 2009). This has led to the suggestion that SNAP23 also aids the formation of LD-mitochondria complexes and assists in the shuttling of IMTG-derived FA to the mitochondria. This is important because incomplete oxidation of IMTG-derived FA can also be a source of lipid metabolites disruptive to the insulin signalling cascade (Koves *et al.*, 2008). To date however, no research has been conducted to investigate differences in SNAP23 content and localisation in endurance trained insulin sensitive individuals compared to insulin resistant individuals who show impaired IMTG turnover.

Together the evidence presented suggests reduced oxidative capacity mirrored with impaired IMTG turnover can generate lipid metabolites; ceramides and DAG which can impair the insulin signalling cascade (Moro *et al.*, 2008).

1.6.3 Skeletal muscle insulin resistance

1.6.3.1 The Randle cycle

Accumulation of certain lipid metabolites in skeletal muscle is critical in the aetiology of insulin resistance. Initially Randle and colleagues (1963) proposed that increased FA availability within cardiac and diaphragm muscle would result in increased acetyl-CoA and citrate. Acetyl-CoA was thought to inhibit PDH by activating PDH kinase which phosphorylates PDH to its less active form. *In vitro* work established that citrate was an inhibitor of PFK. Together it was proposed that these lead to an accumulation of G6P which inhibits hexokinase activity thus resulting in a rise in intracellular glucose concentrations causing a negative feedback for glucose uptake from the blood. In 1996, Roden and colleagues (1996) combined lipid infusion with HE clamp in healthy individuals to show that muscle G6P levels were actually reduced. Furthermore a HE clamp with glycerol infusion protocol resulted in a four-fold increase in PI3-K activity from basal levels whereas this increase was completely abolished during a HE clamp with lipid infusion protocol suggesting elevations in intracellular FA negatively impacts insulin signalling (Dresner *et al.*, 1999). The evidence therefore suggests that accumulating lipid metabolites can impair glucose uptake but this is likely due to interferences with the insulin signalling cascade rather than the Randle cycle

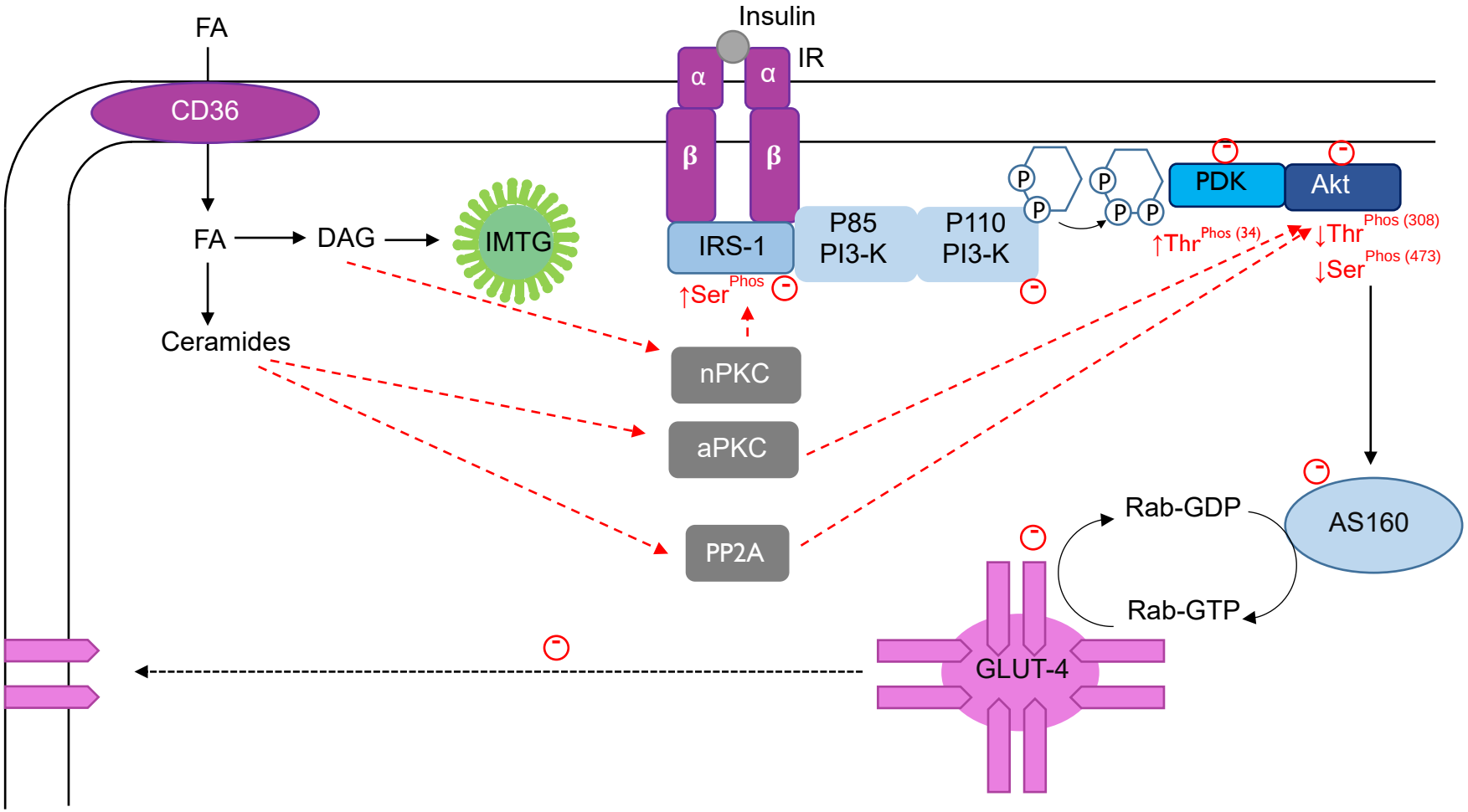

Figure 1.3. Lipid induced skeletal muscle insulin resistance. aPKC, atypical protein kinase C; AS160, Akt substrate of 160 kD; DAG, diacylglycerol; FA, fatty acid; fatty acyl-CoA; GLUT4, glucose transporter-4; IMTG, intramuscular triglyceride; IR, insulin receptor; IRS-1, insulin receptor substrate-1; nPKC, novel protein kinase C, PDK, phosphoinositide-dependent kinase 1; PI3-K phosphoinositide 3-kinase; Rab-GDP, Rab guanosine disphosphate; Rab-GTP, Rab guanosine triphosphate.

1.6.3.2 Lipid metabolites

Accumulations in fatty acyl-CoA, ceramides and certain DAG species have all been linked to skeletal muscle insulin resistance (Yu *et al.*, 2002a; Gual *et al.*, 2005; Samuel *et al.*, 2010). Primarily lipid metabolites can impair skeletal muscle insulin signalling through increased serine phosphorylation of IRS-1 or through reduced serine phosphorylation of Akt (Summers & Nelson, 2005; Morino *et al.*, 2006) (Figure 1.3). Amati et al. (2011) highlighted the complexity of DAG's role in contributing to skeletal muscle insulin resistance when they demonstrated elevated DAG content was observed in endurance trained insulin sensitive athletes compared to sedentary insulin resistant controls. It has been proposed that subcellular location, saturation and FA positioning on the glycerol backbone are all influential factors in DAGs contribution to insulin resistance, however controversy still exists in this area. Athletes with higher insulin sensitivity had lower saturated DAG levels in muscle compared to sedentary subjects (Bergman *et al.*, 2010). In addition to lower saturated DAG an endurance trained athletic group also displayed lower membrane fraction of DAG compared to obese and type 2 diabetic individuals (Bergman *et al.*, 2012). A more thorough examination of DAG species revealed however that DAG containing two unsaturated FA was higher in obese muscle compared to lean athletic and sedentary controls (Amati *et al.*, 2011). Historical work has also suggested that the *sn*-1, 2 stereoisomer is the only DAG stereoisomer capable of being an active signalling molecule (Rando & Young, 1984) thus suggesting that positioning of FA on the glycerol backbone is important for activating PKC. It is clear future research is needed to identify which DAG specific species are directly linked to skeletal muscle insulin resistance and at what quantities they have a lipotoxic effect.

It appears that when DAG does contribute to skeletal muscle insulin resistance it is via the activation of novel protein kinase c (nPKCs) isoforms (δ, ε, η, and θ). The nPKCs have two tandem C1 domains that have a high affinity for DAG-containing

membranes and unlike other PKCs are able to be activated by DAG alone (Dries *et al.*, 2007). The translocation of a PKC to the plasma membrane is a mark of its activation. Elevated DAG concentrations following high-fat feeding or lipid infusion is associated with increased PKC translocation to the plasma membrane and reduced glucose disposal rate (Schmitz-Peiffer *et al.*, 1997; Itani *et al.*, 2002). Increased PKC-θ is observed in the muscle plasma membrane fraction of obese individuals (Itani *et al.*, 2000) and type 2 diabetic patients (Itani *et al.*, 2001). PKC-θ-KO mice are protected from lipid infusion induced insulin resistance (Kim *et al.*, 2004). PKC-ε activation is positively associated with membrane DAG and insulin resistance (Bergman *et al.*, 2012). The translocation of novel PKC isoforms to the plasma membrane is likely to be a detrimental factor by increasing its proximity to intermediates of the insulin signalling cascade. Here, it is proposed that PKC targets IRS-1 directly or indirectly through upstream activation of stress kinases IκBα kinaseβ (IKKβ) and c-Jun NN-terminus kinase (JNK). In addition to tyrosine phosphorylation sites, multiple serine/threonine phosphorylation sites have been identified on IRS-1 (White & Kahn, 1994a). It is now well established that nPKCs or the aforementioned stress kinases are capable of phosphorylating IRS-1 on serine residues 307, 636/639 and 1101 (Gual *et al.*, 2005; Boura-Halfon & Zick, 2009). Recently it was shown that increased DAG species (C16:0, C18:0, C18:1, C18:2, and C20:4) following lipid infusion was temporally associated with PKC-θ activation, increased Ser^{1101} and impairments in PI3-K activation and Akt phosphorylation in healthy, obese and type 2 diabetic individuals which occurred without increases in ceramide (Szendroedi *et al.*, 2014). Increased serine phosphorylation of IRS-1 via PKC-θ activation is associated with reduced tyrosine phosphorylation (Yu *et al.*, 2002a). Reduced insulin stimulated tyrosine phosphorylation will result in decreased subsequent activation of PI3-K and Akt/PKB therefore reducing activation and translocation of GLUT-4 and glucose uptake (Figure 1.3).

Ceramides are composed of a sphingosine base and a fatty acid moiety. It is evident that ceramides are elevated in obese insulin resistant individuals compared to lean insulin sensitive controls (Adams *et al.*, 2004) and this appears apparent across saturated and unsaturated ceramide species in addition to ceramides of varying FA chain length (Amati *et al.*, 2011). When a HE clamp was performed with intralipid/heparin infusion in normal glucose tolerant males, ceramide content increased and was negatively associated with decreases in insulin sensitivity (Straczkowski *et al.*, 2004). There are two proposed mechanisms by which ceramides can disrupt the insulin signalling pathway which are both centred around the inhibition of Akt. Ceramides have been shown to activate atypical PKCζ which can phosphorylate Akt on a Thr34 located on the enzyme's PH domain lowering affinity to PIP_3 (Powell *et al.*, 2003). Ceramides can also activate protein phosphatase 2A (PP2A) which is a serine/threonine phosphatase capable of dephosphorylating Akt on its active Ser473 and Thr308 residues thus blocking recruitment of Akt to the plasma membrane by PIP_3 (Stratford *et al.*, 2004). Both of these mechanisms have been expertly reviewed in more detail (Lipina & Hundal, 2011; Chavez & Summers, 2012). Ultimately, both mechanisms can reduce necessary recruitment of Akt to the plasma membrane by PIP_3, which is required for downstream activation of AS160 and GLUT4 activation and translocation to the plasma membrane (Fig 1.3).

Prior to storage or oxidation FA entering the muscle requires activation to fatty acyl-CoA. Elevations in fatty acyl-CoA skeletal muscle content have also been have also been inversely correlated to whole body insulin action (Ellis *et al.*, 2000). High-fat high-calorie diets induce insulin resistance with rats and is positively correlated with fatty acyl-CoA (Oakes *et al.*, 1997a; Oakes *et al.*, 1997b; Ellis *et al.*, 2000). Elevations in fatty acyl-CoA are associated with increased PKC activity and reduced insulin sensitivity (Yu *et al.*, 2002a) however this is likely a result of increased ceramide and DAG formation from increased fatty acyl-CoA substrate availability. To date, there

has been no evidence to show that fatty acyl-CoA directly activate PKCs known to disrupt insulin signalling. Fatty acyl-CoA also has a regulatory role in inhibiting enzymes necessary to maintaining normal glucose and lipid homeostasis. There is evidence to suggest that fatty acyl-CoA can inhibit hexokinase in rat and human skeletal muscle which was additive to its inhibition by glucose-6-phosphate (discussed earlier in the Randle cycle, section 1.6.1.3) (Thompson & Cooney, 2000) thus reducing glycolytic flux into the muscle. Fatty acyl-CoA can also downregulate hormone sensitive lipase (Jepson & Yeaman, 1992) and reduce IMTG utilisation (Watt *et al.*, 2003a). Without this regular turnover of IMTG stores, it is likely that less FA will be directed to IMTG stores resulting in even higher concentration of fatty acyl-CoA. This elevation is likely to disrupt the insulin signalling pathway indirectly by providing more substrate for DAG and ceramide formation.

Lipid induced skeletal muscle insulin resistance may also occur via lipid peroxidation and lipid-induced inflammation. When the IMTG turnover is reduced as observed in sedentary populations, the IMTG pool is prone to more oxidative stress which can generate lipid peroxidation products with the potential to inhibit insulin signalling (Russell *et al.*, 2003; Russell, 2004). In particular, formation of TNFα can increase suppression of suppressor of cytokine signalling proteins (SOCS) which can increase tyrosine phosphorylation of IRS-1. Additionally disruptions in lipid homeostasis can activate inflammation and ER stress pathways which can disrupt IRS-1 and Akt activation (reviewed in Ye et al., 2007).

1.6.3.3 SNAP23 role in lipid induced insulin resistance

SNAP23 is a t-SNARE found in non-neural tissues that shares a similar homology and function to neural exclusive tissue SNAP25 (Ravichandran *et al.*, 1996). SNAP23 binds to multiple syntaxins and VAMPs to assist in membrane fusion (exocytosis). Most notably found at the plasma membrane (Jahn & Scheller, 2006) the primary function of SNAP23 was to mediate the docking of GLUT-4 to the plasma membrane

during insulin stimulated conditions (Foster *et al.*, 1999; Kawanishi *et al.*, 2000) (section 1.2.4). There is accumulating evidence that SNAP23 also aids in the formation of LD-mitochondrial complexes (section 1.6.2.4) and assists in LD fusion Knockdown of the SNAP23 gene in NIH-3T3 fibroblast cells decreased the rate of fusion and size of LD (Bostrom *et al.*, 2007). Treatment of cardiomyocytes with oleic acid increased intracellular LD volume resulting in an increase in LD associated pool of SNAP23 and a simultaneous reduction in plasma membrane SNAP23 pool (Bostrom *et al.*, 2007). This resulted in a decrease in insulin-stimulated uptake of glucose through reduced SNAP23 mediated GLUT-4 vesicle exocytosis. Transfection of SNAP23 in cardiomyocytes incubated in oleic acid restored insulin-stimulated glucose uptake (Bostrom *et al.*, 2007), most likely from restoration of SNAP23 content at the plasma membrane. The findings from this paper lead to the SNAP23 highjacking hypothesis (Sollner, 2007). In response to lipid excess SNAP23 is sequestered away from the plasma membrane to cytosolic compartments to assist with the demand for fusion of LD. Whilst this will assist in minimising the accumulation of lipid metabolites, a reduction of SNAP23 at the plasma membrane may reduce the fusion and docking of GLUT-4 storage vesicles which can lead to a decreased insulin-stimulated glucose uptake (Figure 1.4).

Ablation of SNAP23 in fibroblasts reduces the formation of LD-mitochondria complexes (Jagerstrom *et al.*, 2009). SNAP23s putative role in the formation of LD-mitochondria complexes may serve as an additional means to minimise skeletal muscle lipid metabolites however this may again occur at the expense of reduced plasma membrane SNAP23 pool. Our current knowledge of SNAP23 is largely restricted to adipocytes or *in vitro* systems. More recently, our lab has established a validated confocal immunofluorescence microscopy technique to confirm that SNAP23 has a high colocalisation to the plasma membrane and mitochondria and a weaker colocalisation to LD in lean healthy trained males (Strauss *et al.*, 2016). There

is a now a need to investigate whether LD acutely hijack SNAP23 in human skeletal muscle following lipid excess.

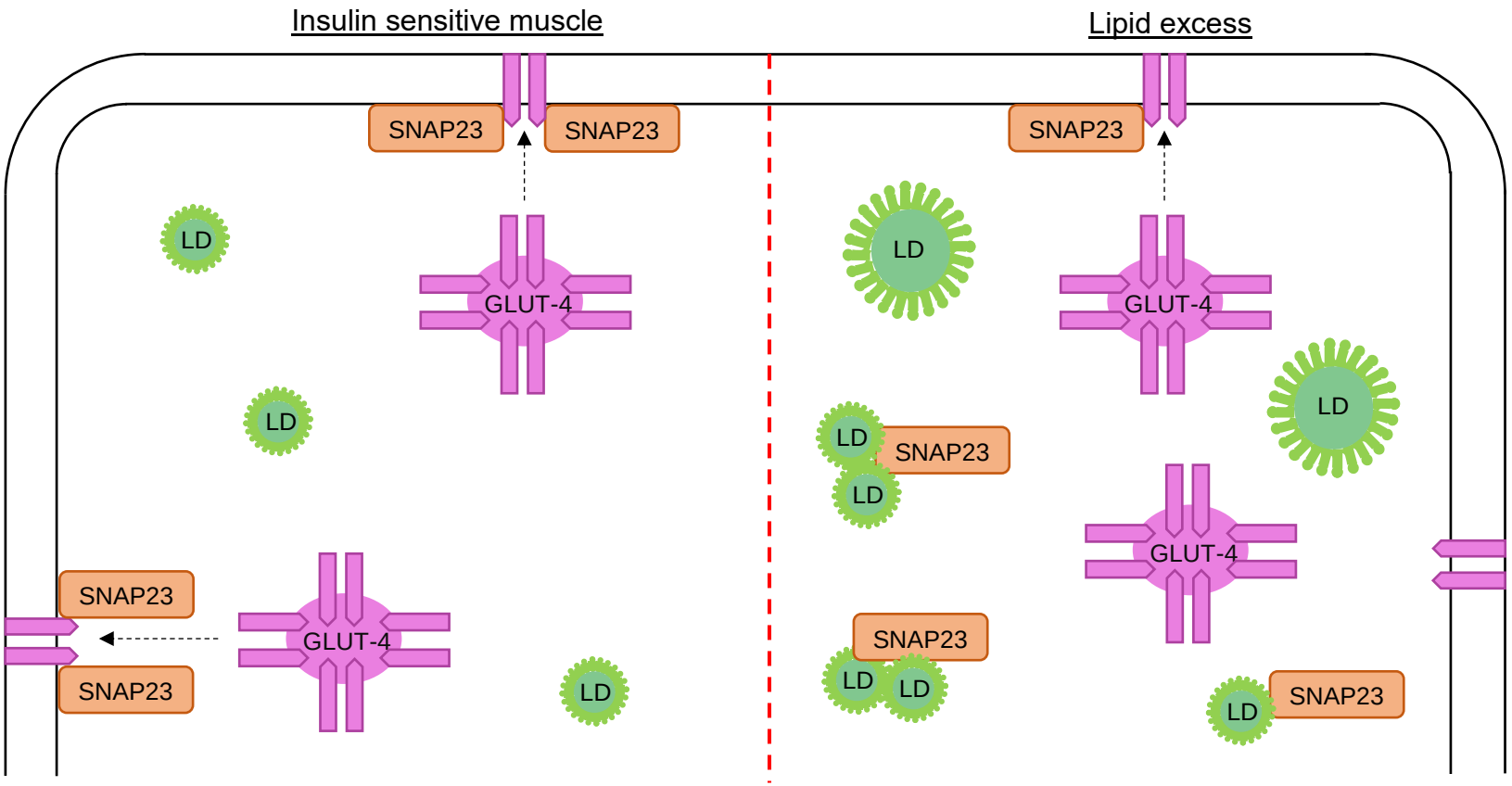

Figure 1.4. LD hijacking SNAP23 hypothesis. In insulin sensitive muscle, GLUT-4 translocates to the plasma membrane following insulin stimulation. SNAP23 assists in the docking of GLUT-4 to the plasma membrane allowing glucose uptake into muscle. During lipid excess, lipid droplets hijack SNAP23 to assist in LD fusion reducing the amount of SNAP23 at the plasma membrane and therefore minimising GLUT-4 docking and glucose uptake. Image adapted from Sollner (2007).

1.7 Investigating lipid-induced skeletal muscle insulin resistance

1.7.1 Lipid infusion

Due to the low solubility of NEFA, lipid (TAG) with heparin infusion protocols have been established to elucidate the mechanisms underpinning the relationship between short-term increases in FA availability and insulin resistance. Heparin is important because it releases LPL from its endothelial binding sites and increases the activity of LPL thus stimulating plasma TAG hydrolysis and an elevation of FA concentrations. Lipid infusion studies are effective in reducing peripheral glucose uptake (Boden *et al.*, 1994; Shah *et al.*, 2002) and increasing hepatic gluconeogenesis (Roden *et al.*, 2000). Importantly as discussed in section 1.6.3.2, lipid infusion studies have been paramount in elucidating the mechanisms by which increased FA availability results in increased lipid signalling metabolites known to activate PKC isoforms that disrupt insulin signalling (Itani *et al.*, 2002; Yu *et al.*, 2002a; Szendroedi *et al.*, 2014).

IMTG content also increases with lipid infusion and is associated with insulin resistance (Bachmann *et al.*, 2001). It is now established that IMTG per se is not causative of insulin resistance and therefore lipid infusion-induced insulin resistance is more likely due to an increase in lipid metabolites with benign simultaneous increase in IMTG. Recently Chow et al. (2014) demonstrated that both trained and untrained individuals have similar reductions in insulin sensitivity following 6 h of lipid infusion during a HE clamp. Interestingly, trained individuals showed a preferential accumulation of IMTG whereas the untrained controls accumulated both IMTG and DAG (Chow *et al.*, 2014). Immunohistochemistry analysis on the same muscle samples from this study revealed that trained individuals increased the number of LD associated with PLIN2, PLIN3 and PLIN5 whereas untrained individuals only increased LD not associated with any PLIN protein (Shepherd *et al.*, 2017b). As both populations experienced similar reductions in insulin sensitivity yet clearly divergent lipid storage pathways, it is important to employ more chronic lipid excess models to

reveal how manifestations of lipid accumulation contribute to skeletal muscle insulin resistance.

1.7.2 High-fat diets

The high palatability and energy density of high-fat foods observed in western countries has prompted a rise in studies using high-fat and often high-calorie diets as a method to induce whole-body insulin resistance and mimic the metabolic effects observed in obesity and T2D. The following section will review the effects of high-fat diets on parameters of insulin sensitivity and lipid metabolism.

1.7.2.1 Insulin sensitivity

In healthy lean individuals short-term high-fat high-calorie (HFHC) diets of only 5-14 days are able to reduce hepatic insulin sensitivity (Brons *et al.*, 2009) or peripheral insulin sensitivity (Bakker *et al.*, 2014) measured with HE clamp, or whole-body insulin sensitivity measured with an oral glucose or mixed meal tolerance test (Hulston *et al.*, 2015; Parry *et al.*, 2017). Peripheral insulin sensitivity measured from HE clamp becomes more impaired in low birth weight individuals who have a higher pre-disposed risk of T2D compared to normal birth weight controls following a five day HFHC diet (Brons *et al.*, 2012). There were similar reductions however in insulin sensitivity measured with oral glucose sensitivity index in Caucasian and south-Asian populations following a four day HFHC diet (Wulan *et al.*, 2014). Following 5 days of high-fat (40%) high calorie (40%+ energy) diet there were no decrements in insulin sensitivity measured with HE clamp in healthy lean individuals however muscle biopsies revealed impairments in skeletal muscle insulin signalling (Adochio *et al.*, 2009). Namely there was an increased serine phosphorylation of IRS-1 and increased content of P85α which expression is inversely correlated with PI3-K activity (Adochio *et al.*, 2009). Interestingly when the same participants were fed a high-carbohydrate high-calorie diet, insulin signalling intermediates IRS-1 and PI3-K were upregulated (Adochio *et al.*, 2009).

Together the data suggests that high-fat high-calorie diets can impair aspects of insulin sensitivity however, this is not homogenous amongst all participant cohorts. Despite the known sex differences in insulin sensitivity and prevalence of T2D (section 1.1.2) no studies have investigated whether males are more susceptible to high-fat high-calorie diet induced insulin resistance and metabolic complications in comparison to females.

1.7.2.2 IMTG content

Very short-term (48 hr) high-fat (60%) diet increases IMTG content by 36% in endurance-trained cyclists when measured by biochemical extraction (Zderic *et al.*, 2004). Similar increases (45%) were observed following 60 h of isocaloric high saturated fat diet (45% energy of fat, 60% saturated fat) measured in healthy male participants by ^{1}HMRS (Stettler *et al.*, 2005). When high-fat (60%) feeding was administered for 7 days there was an increase in IMTG content by 54% measured by ^{1}HMRS in young healthy males (Schrauwen-Hinderling *et al.*, 2005). When high-fat (53%- 62% energy) feeding is extended to longer period of 5-7 weeks IMTG content increases are more elevated (Helge *et al.*, 2001; Vogt *et al.*, 2003). Both of these longer duration high-fat diets were done in conjunction with regular endurance exercise training and therefore indicative of regular IMTG turnover which may have affected the results. Bachmann *et al.,* (2001) aimed to decipher changes in IMTG content in different muscle types (soleus and tibilias anterior) using ^{1}HMRS following a 3 day high-fat (55-60% energy) high-calorie (~80%) diet. The more oxidative soleus muscle displayed a greater increase in IMTG content (50%) in comparison to the tibilias anterior (14%) (Bachmann *et al.*, 2001) indicating increase in IMTG stores may be dependent on fibre type. Most of the studies investigating the effects of high-fat diets on IMTG content have been isocaloric. Recently Gemmink *et al.,* (2017a) showed IMTG content measured by biochemical extraction increased by 30% following 5 days high-fat high-calorie diet (normal diet plus 1275 kcal/day of 94% fat

surplus) in Caucasian and south Asian populations. Notable this study was the first to measure markers of lipid metabolism (ATGL, CGI-58, PLIN2, PLIN3 and PLIN5) following the high-fat high-calorie diet and showed that PLIN5 increased with a more profound increase in the south Asian group that is more prone to decrements in insulin sensitivity (Gemmink *et al.*, 2017a). Considering type I fibres are capable of storing 2-4 fold greater IMTG than type II fibres (van Loon *et al.*, 2003a; Shepherd *et al.*, 2013), there is a need to decipher fibre-type specific changes in IMTG and perilipin stores following high-fat high-calorie diets.

1.8 Thesis overview

Chapter 1 has established normal regulation of insulin-dependent glucose uptake and IMTG metabolism in healthy insulin-sensitive individuals. It identified that impairments in IMTG metabolism and lipid excess following dietary interventions can lead to accumulations in lipid metabolites known to disrupt the insulin-signalling cascade. The introductory chapter also identified several gaps in our knowledge regarding the regulation of IMTG metabolism and the effects of high-fat high-calorie diets on measurements of metabolic health. Consequently, studies in this thesis were designed to further our knowledge and understanding in these areas.

Section 1.7.2.1 highlighted that short-term a high-fat high-calorie diets can impair components of insulin sensitivity in healthy individuals, however to date no studies have compared sex-differences. In **Chapter 2** a pilot study was conducted to investigate sex-differences in metabolic and cardiovascular responses to a 7 day HFHC diet in young healthy males and females matched for age, BMI, cardio-respiratory fitness and habitual activity levels.

Chapter 3 was designed to gain further insight to the molecular consequences of 7 days of high-fat, high-calorie diets. The athlete's paradox (section 1.6.3) established that IMTG does not directly contribute to skeletal muscle insulin resistance and directing FA to IMTG stores might minimise the accumulation of lipid metabolites

known to contribute to skeletal muscle insulin resistance. **Chapter 3** aimed to test the hypothesis that increases in IMTG stores following 7-days of high-fat, high-calorie in lean healthy individuals would minimise disruptions in skeletal muscle insulin signalling. Section (1.5) highlighted that PLINs promote TAG storage in cell culture models following lipid excess however how PLINs regulate IMTG synthesis in skeletal muscle is still understudied. **Chapter 3** used novel confocal immunofluorescence microscopy techniques to investigate; fibre-type and region-specific changes on IMTG content (LD number and morphology), PLIN protein expression and the colocalisation of these PLIN to LD following a 7- day HFHC diet . Section 1.6.3.3 explained the hypothesis that SNAP23 may be hijacked by LD from the plasma membrane following lipid excess. **Chapter 3** also investigated whether there are fibre-type specific changes in SNAP23 distribution within muscle fibres following a 7- day HFHC diet.

Section 1.3.2.2 explained that HSL translocates to LD in isolated rat skeletal muscle and LD associated with PLIN2 and PLIN5 are utilised during an hour of moderate intensity exercise in human skeletal muscle. On the other hand, ATGL distribution appears to be unchanged following exercise. **Chapter 4** used novel confocal immunofluorescence microscopy techniques to test the hypothesis that HSL redistributes in human skeletal muscle in response to moderate-intensity exercise and investigated the preferential colocalisation of HSL and ATGL to LD associated with either PLIN2 or PLIN5.

Chapter 3 and 4 established novel mechanisms by which PLINs regulate IMTG metabolism. Section 1.4.2 highlighted that over 300 proteins are associated to LD in mouse skeletal muscle however how these proteins interact together on the LD surface still needs much further investigation. **Chapter 5** aimed to develop a new immunoprecipitation- mass spectrometry method to identify proteins associated to

PLIN5 in human skeletal muscle that would generate new hypotheses to investigate how proteins regulate IMTG metabolism.

Chapter 2. A pilot study investigating sex differences in the effects of a 7-day high-fat high-calorie diet on metabolic and cardiovascular functional outcomes.

2.1 Abstract

High-fat high-calorie diets (HFHC) diets have been used as a model to investigate lipid-induced insulin resistance. Acute HFHC diets reduce insulin sensitivity in young healthy males, but to date no study has directly compared males and females to elucidate sex-specific differences in the effects of a HFHC diet on measurements of cardio-metabolic health. Eleven males (24 ± 4 years; BMI 23 ± 2 $kg.m^{-2}$; $\dot{V}O2$ peak 62.3 ± 8.7 $ml.min^{-1}.kg^{-1}$FFM) were matched to 10 females (25 ± 4 years; BMI 25 ± 4 $kg.m^{-2}$; $\dot{V}O2$ peak 58.2 ± 8.2 $ml.min^{-1}.kg^{-1}$FFM). Insulin sensitivity from an oral glucose tolerance test, metabolic flexibility, arterial stiffness, body composition and blood lipid and liver enzymes were measured before and after 7 days of a high-fat (65%) high-calorie (+50%) diet. The HFHC diet did not have an effect on measures of insulin sensitivity, metabolic flexibility or arterial stiffness in either sex. There was a trend towards increased total body fat (kg) after the HFHC diet (P = 0.056) (+1.8% and +2.3% for males and females respectively; *P* = 0.056). In contrast to females, males had a significant increase in trunk to leg fat mass ratio (+5.1%; P = 0.005). Lean, healthy young males and females appear to be protected from the negative cardio-metabolic effects of a 7 day HFHC diet. Future research should aim to determine whether low levels of cardiorespiratory fitness or ageing exacerbates the detrimental effects of a 7 day HFHC diet observed in other studies but not in this current study.

2.2. Introduction

A western lifestyle is characterised by regular consumption of readily available energy-dense foods (Kearney, 2010), often paired with sedentary behaviour throughout the day (Townsend *et al.*, 2012) and minimal exercise (British Heart Foundation, 2017). These western behavioural patterns are associated with increased risk of obesity, type 2 diabetes (T2D) and cardiovascular disease (Tuomilehto *et al.*, 2001; Katzmarzyk, 2010; Naja *et al.*, 2015). At present, cardiovascular disease is established as the leading cause of mortality in western countries (Groban *et al.*, 2016) and T2D vastly increases the risk of cardiovascular complications (Laakso, 2010).

T2D is characterised by hyperglycaemia which often manifests as a result of insulin resistance. Insulin resistance can be defined as impaired insulin-stimulated glucose uptake in skeletal muscle and adipose tissue stores and/or impaired insulin-induced suppression of hepatic glucose production. Skeletal muscle is the largest disposal site of blood glucose following insulin stimulation (DeFronzo *et al.*, 1981), and therefore skeletal muscle insulin resistance is a primary aberration in the progression of T2D (DeFronzo, 2004). Metabolic flexibility is closely linked with skeletal muscle insulin sensitivity (Galgani *et al.*, 2008a), and is defined as the capacity to switch from high rates of lipid oxidation in the fasted state to an increased rate of carbohydrate oxidation under insulin-stimulated conditions (Kelley & Mandarino, 2000). Metabolic flexibility is therefore diminished in obese insulin-resistant individuals in comparison to the lean insulin-sensitive state (Kelley *et al.*, 1999).

Hepatic insulin resistance is also crucially important in the development of T2D (Perry *et al.*, 2014) and is closely associated with non-alcoholic fatty liver disease (NAFLD) (Sanyal *et al.*, 2015; Brouwers *et al.*, 2017). Both of these metabolic impairments are associated with ectopic lipid accumulation in the liver, which is proposed to manifest from adipose tissue lipolysis (Perry *et al.*, 2014). Visceral fat and in particular

mesenteric fat depots are expected to be the primary sources leading to lipid accumulation in the liver (Liu *et al.*, 2006a), due to the full drainage of these depots reaching the liver via the portal vein (Montague & O'Rahilly, 2000). In addition, the release of free fatty acids FA from these abdominal fat depots is higher than from the subcutaneous depots (Wajchenberg *et al.*, 2002). Although obesity has been linked to T2D and cardiovascular disease (Abdullah *et al.*, 2010), increases in subcutaneous fat away from visceral stores initially serve as a protective mechanism to store FFA, reducing daily lipid flux and therefore preventing ectopic lipid accumulation (Frayn, 2002). Abdominal adiposity is characterised by both abdominal subcutaneous fat depots and visceral fat and is commonly measured with waist circumference or waist-to-hip ratios. Although this is not a direct measure of visceral fat and mesenteric fat depots, studies have shown a strong association of abdominal obesity with insulin resistance and T2D (Racette *et al.*, 2006; Huang *et al.*, 2015). Abdominal adiposity is a primary feature of male rather than female fat accumulation, with females generally observing any increases in adipose tissue to lower body (femoral and gluteal) subcutaneous depots (Janjic, 1996).

In addition to differential adipose tissue storage, sex differences are also apparent in the risk of developing metabolic diseases. For example epidemiological studies have shown that the incidence of T2D, NAFLD and cardiovascular disease is lower in females compared to males (Montague & O'Rahilly, 2000; Wild *et al.*, 2004; Pan & Fallon, 2014; Groban *et al.*, 2016). Large cross-sectional studies have also shown that males (35-65 years) have a higher prevalence (+1.3-1.9%) of elevated fasting glucose in comparison to females (Kuhl *et al.*, 2005; Munguia-Miranda *et al.*, 2009). In another cross-sectional study, males (18-32 years) also showed reduced blood glucose clearance capacity (-15%) following an intravenous glucose tolerance test compared to females (Clausen *et al.*, 1996). Smaller clinical trials investigating insulin sensitivity in BMI and age-matched males and pre-menopausal females (20-45 years)

using a hyperinsulinaemic euglycaemic (HE) clamp have established that females exhibit a similar or higher glucose infusion rate per kilogram of body weight (+36-47%) when compared to males (Yki-Jarvinen, 1984; Nuutila *et al.*, 1995; Donahue *et al.*, 1996; Rattarasarn *et al.*, 2004; Borissova *et al.*, 2005), and a markedly higher glucose infusion rate when adjusted per kilogram of lean mass (45-98%) (Yki-Jarvinen, 1984; Donahue *et al.*, 1996). Aerobic capacity and habitual activity levels are also positively related to insulin sensitivity (Balkau *et al.*, 2008; Nojima *et al.*, 2017). However, of the studies comparing insulin sensitivity between sexes only two studies matched for VO_2 peak levels (Yki-Jarvinen, 1984; Nuutila *et al.*, 1995) and none measured habitual activity levels.

Despite females being at a reduced risk of developing insulin resistance and cardio-metabolic disease, there is little research investigating the differences in the progression of insulin resistance between the sexes. One approach to investigate this is to provide excess lipid through an acute lipid infusion during a HE clamp, and it has been shown that a 7 h lipid infusion caused less reduction in glucose infusion in females (26%) in comparison to males (38%) (Hoeg et al., 2011). Excess lipid exposure from infusion studies may only illustrate acute physiological responses, whereas more prolonged HFHC diets provide a chronic stimulus to investigate the influence of increased energy intake (creating a positive energy balance) on adipose tissue stores and early abnormalities in metabolic and cardiovascular regulation. In healthy individuals short-term HFHC diets of 5-7 days have been demonstrated to reduce HE clamp derived indices of hepatic insulin sensitivity (-65%) (Brons et al., 2009) and peripheral insulin sensitivity (-20%) (Bakker et al., 2014), or whole-body insulin sensitivity (-27%) measured with an oral glucose tolerance test (Hulston *et al.*, 2015) or glucose tolerance (-11%) measured with a mixed meal (112g carbohydrate in a 771 kcal meal) tolerance test (Parry *et al.*, 2017). Although some of these studies have included female participants (Cornford *et al.*, 2013; Hulston *et al.*, 2015; Parry

et al., 2017), to date no study has directly compared sexes to clarify the sex-specific cardiovascular and metabolic responses to a short-term HFHC diet. This is a considerable oversight considering pre-menopausal women with normal levels of the female hormones (oestrogen and progesterone) appear to be better protected against metabolic diseases compared to males. Establishing whether females are better equipped to handle lipid overload from a 7 day HFHC diet will be beneficial in underpinning the pathology of T2D in this understudied cohort.

The aim of this study was to identify the sex-specific differences in metabolic and cardiovascular responses to a 7 day HFHC diet in young healthy males and females matched for age, BMI, cardio-respiratory fitness and habitual activity levels.

2.3 Methods

2.3.1 Subjects and ethical approval

A cohort of young healthy males (n=11) and females (n=11) were matched for BMI ($kg.m^{-2}$), age and cardiorespiratory fitness ($ml.min^{-1}.kg\ (FFM)^{-1}$) (see Table 2.1 for characteristics). The sample size for this experiment was estimated based on previous literature that showed a reduction in glucose tolerance or insulin sensitivity following 7-days of high-fat (65% energy) high-calorie diet (+50%) (Hulston *et al.*, 2015; Parry *et al.*, 2017). Written informed consent was obtained from all participants. The study protocol adhered to the Declaration of Helsinki and was approved by NHS West Midlands, Black Country Research Ethics Committee. All participants were free from cardiovascular or metabolic disorders, physically active (exercising at least 3 times per week for more than 30 minutes at a time) and non-smokers. Additionally, females were required to have a regular menstrual cycle, not be pregnant or breast-feeding during the study and only using the following contraceptive methods; condoms, diaphragm, IUD (intrauterine device), combined pill. Due to the nature of the dietary intervention, vegetarians and vegans were excluded from participation.

Table 2.1 Participants characteristics		
	Males	Females
N	11	10
Age (years)	24 ± 4	25 ± 4
Body mass (kg)*	72.6 ± 5.3	63.9 ± 9.5
BMI (kg m^{-2})	23 ± 2	23.1 ± 2
$\dot{V}O_{2peak}$ ($L.min^{-1}$)*	3.60 ± 0.59	2.51 ± 0.48
$\dot{V}O_{2\,peak}$ ($ml.min^{-1}.kgFFM^{-1}$)	62.3 ± 8.7	58.2 ± 8.2
Matsuda ISI	11.6 ± 10.5	9.22 ± 3.38

Data provided as means ± SD. BMI, body mass index; FM, fat mass; FFM, fat free mass; ISI, insulin sensitivity index. * Significant difference between sexes $P < 0.05$.

2.3.2 Pre-experimental procedures

Prior to the start of the study participants attended the laboratory following an overnight fast (≥10 h) for baseline assessments of body composition, resting energy expenditure (REE) and $VO_{2\,peak}$. Body composition was measured using whole-body fan beam dual-energy X-ray absorptiometry (DEXA) (Hologic QDR Series, Discovery A, Bedford, MA, USA). Following removal of jewellery and metal objects participants were scanned (~180 seconds) in a supine position. Each scan was automatically analysed with the QDR software; however, the operator manually corrected the trunk and limb regions and an area identifying visceral adipose tissue (VAT). Percentage body fat (%), total body fat (kg) and lean body mass (kg) are presented as subtotal values excluding head measurements in order to reduce measurement error.

Following the DEXA scan, participants REE was measured using a Moxus Modular Metabolic system (AEI Technologies, IL, USA). Participants were required to lay in a supine position in dark room for 10 minutes before the Moxus ventilation hood was placed over their head and shoulders for a further 20 minutes. Volume flow rate was maintained above 25 $L.min^{-1}$. The first five minutes of data was discarded according to best practice methods (Compher *et al.*, 2006). REE was calculated towards the end of the 20 minute period, averaged over a 5 minute stable period where coefficient

of variation for VO_2 and VCO_2 was ≤ 10 %. REE (kcal/min) was calculated using the Weir equation where REE (kcal/min) = (3.94 x VO_2 ($L.min^{-1}$)) +(1.11 x VCO_2 ($L.min^{-1}$)) (Weir, 1949). This number was then used to calculate REE (Kcal/day) over an entire day.

Participants also performed a progressive exercise test to exhaustion on an electronically-braked cycle ergometer (Lode Corival, Lode B.V, Groningen, Holland) in order to determine $VO_{2\ peak}$ using the Moxus Modular Metabolic system (AEI Technologies, IL, USA). The test consisted of cycling initially at 60W, followed by sequential increments of 35 W every 3 minutes until cadence was reduced to <50 rpm, at which point the test was terminated. $VO_{2\ peak}$ ($L.min^{-1}$) was taken as the highest value obtained in the last 30 seconds of the test. This value was then expressed relative to fat free mass (FFM) (kg) obtained from the DEXA scan to give a $VO_{2\ peak}$ ($ml.min^{-1}$. kg $(FFM)^{-1}$) normalised for fat free mass body weight allowing sexes to be compared directly.

Following pre-experimental testing, participants were provided with a 3-axis activity monitor (wGT3X-BT, ActiGraph, Pensacola, FL, USA) and a food diary to record habitual activity levels and food intake, respectively. Participants were advised to continue habitual activity levels whilst wearing the activity monitor on their right waist for a duration of 3 days (2 weekdays and 1 weekend day). Participants were provided with detailed written and verbal instructions on how to complete the 3-day food diary (2 weekdays and 1 weekend day), including information on quantity, food preparation, brand information and cooking methods. Habitual diets were later analysed manually for total daily intake (kcal) and macronutrient breakdown (Table 2.2)

2.3.3 Experimental design

Participants were advised to consume their habitual diet 7 days prior to pre-testing. Experimental testing was conducted pre and post 7-days HFHC diet. Pre-testing for female participants occurred between days 1-6 of the follicular phase of the menstrual

cycle to minimise the impact of fluctuations of sex hormones on the results. Participants attended the laboratory following an overnight fast (≥10 h) after abstaining from caffeine, alcohol and vigorous exercise the day before testing. The following measurements were conducted pre and post-HFHC diet intervention in addition to a DEXA scan, as previously described.

2.3.3.1 Arterial stiffness

Participants rested in a supine position for 15 minutes before 3 brachial artery blood pressure measurements were conducted using an automated sphygmomanometer (GE CARESCAPE V100-1 Patient monitor, GE Healthcare, Chicago, USA). Arterial stiffness was measured using central (carotid- femoral) pulse wave velocity (PWV) using a semi-automated device and software (SphygmoCor, AtCor Medical, Sydney, Australia) as previously described (Cocks *et al.*, 2013). Systemic wave reflection was investigated using pulse wave analysis to produce an augmentation index with the semi-automated device and software (SphymoCor; (Cocks *et al.*, 2013)). The augmentation index was normalised to a heart rate of 75bpm (AI_x@75bpm) to account for confounding influence of heart rate. All measurements were made in triplicate.

2.3.3.2 Oral Glucose Tolerance Test

A 20G cannula (BD Venflon^{TM}, BD, Oxford, England) was inserted into an antecubital vein to allow for repeated blood sampling during the oral glucose tolerance test (OGTT). A 10 ml blood sample was obtained at baseline before participants consumed a 75g glucose drink made with 225ml of water. Subsequent blood samples (10 ml) were obtained at 15, 30, 45, 60, 90 and 120 min following glucose ingestion. Blood samples were divided equally between vacutainers containing EDTA or a clotting agent (BD, Oxford, England) to allow for the separation of plasma and serum, respectively. Prior to centrifugation EDTA tubes were stored on ice, whereas serum tubes were left at room temperature until clotting had occurred. Blood tubes were

centrifuged at 1000g for 10 min at 4°C before being stored at -80 °C for subsequent analysis.

2.3.3.3 Metabolic Flexibility

Prior to the OGTT, participants rested in a supine position for 20 minutes in a dark room with a ventilation hood placed over their head and shoulders (Moxus Modular Metabolic System, AEI Technologies, IL, USA). VO_2 and VCO_2 was measured from the collected expired air and used to calculate the respiratory exchange ratio (RER). The first five minutes of data was discarded according to best practice methods (Compher *et al.*, 2006). Fasting RER was averaged over a 5 minute stable period where coefficient of variation for VO_2 and VCO_2 was ≤ 10 %. The Moxus ventilation hood was removed for a brief period (≤ 2 min) to allow participants to consume the glucose beverage before being returned over their head and shoulders for the remainder of the OGTT. The Moxus volume flow rate was maintained at >25 $L.min^{-1}$. For the remaining OGTT, RER was averaged over 5 minute intervals. Peak RER following glucose ingestion was identified as the maximum RER obtained at any 5 minute interval during the 120 min OGTT. The time that peak RER was obtained was recorded and used in the following equation to calculate metabolic flexibility.

$$\text{Metabolic flexibility} = \frac{\text{Peak RER} - \text{Fasting RER}}{\text{Time to reach peak RER}}$$

2.3.4 Blood Analyses

Serum samples were analysed for glucose (all time points during OGTT) and fasting; Non-esterified fatty-acids (NEFA), triglycerides, cholesterol, AST, ALT and GGT concentrations using a commercially available spectrophotometric assays (Randox) with a semi-automatic analyser (Randox Daytona RX, Randox, Crumlin, UK). Plasma samples from the OGTT were analysed for insulin concentrations with a commercially available direct insulin ELISA kit (Fisher Scientific, Loughborough, UK).

2.3.5 Calculations

Glucose area under the curve (AUC) and insulin AUC during the OGTT was calculated using the trapezoidal rule with zero as baseline.

Whole-body insulin sensitivity was calculated using the Matsuda insulin sensitivity index (ISI) (Matsuda & DeFronzo, 1999) with the following equation.

$$\text{Matsuda ISI} = \frac{10{,}000}{\sqrt{(\text{FPG x FPI}) \text{ x } (\text{MPG x MPI})}}$$

Hepatic and muscle insulin resistance indexes were estimated using the following equations from Abdul-Ghani et al. (2007);

$$\text{Hepatic insulin resistance} = \text{PG AUC}_{0-30\text{ min}} \text{ x PI AUC}_{0-30\text{ min}}$$

$$\text{Muscle insulin resistance} = \text{dG/dt} \div \text{MPI}$$

Where FGP is fasting plasma glucose, FPI is fasting plasma insulin, MPG is mean plasma glucose during the OGTT, MPI is mean plasma insulin during the OGTT, PG $AUC_{0-30\text{ min}}$ is plasma glucose area under the curve from 0 to 30 min, PI $AUC_{0-30\text{ min}}$ is plasma insulin area under the curve from 0 to 30 min and dG/ dt is rate of change in plasma glucose from its peak to its nadir.

2.3.6 Seven day high-fat high-calorie diet

Although habitual dietary intake was assessed (Table 2.2), there are known issues with participants under-reporting food intake, and therefore the energy value of the HFHC was determined based on REE. The participants were highly active, as measured objectively by accelerometry and subjectively by the International Physical Activity Questionnaire (IPAQ) (Craig *et al.*, 2003). As fitness and activity levels were similar between sexes, the same activity factor of 1.7 was multiplied by REE for both males and females to calculate total energy expenditure (TEE), before being multiplied by 1.5 to calculate each individual's energy intake required during the HFHC diet (Table 2.2). The diets were designed so that fat contributed 65% of total

energy intake, with approximately 37% of fat intake derived from saturated fat. The remaining energy was provided from carbohydrate (~17%) and protein (~18%). All food was purchased and provided by the research team, in addition to a set of scales provided to the participants so all food items could be weighed correctly. Food for the diet was selected such that it would require minimal preparation and cooking by each participant. Where cooking was required, participants were given strict instructions on how to cook the food and were provided with the quantity of cooking oil/butter where necessary.

To increase compliance to the diet, all participants were provided with a HFHC diet plan prior to the intervention to ensure palatability with all foods. Participants were instructed of the importance to consume all food on their HFHC dietary plan and to not consume any other food products. Participants were advised to report and return any food items that they could not consume during the diet so that energy intake and macronutrient percentage could be adjusted as necessary. All participants were required to record the food items and note the time they consumed them in an individual food diary. Each participant was instructed to continue their habitual physical activity (PA) levels and wore the 3-axis activity monitor (wGT3X-BT, ActiGraph, Pensacola, FL, USA) to ensure habitual PA levels remained constant.

Table 2.2 Estimated energy requirements and actual HFHC energy intakes

	Males	Females
Self-reported habitual intake (kcal)	2639 ± 453	2193 ± 407
Self-reported diet fat intake (%)	33 ± 2	34 ± 7
Estimated TEE (kcal)	2653 ± 407	2259 ± 349
Required HFHC intake (kcal)	3979 ± 610	3389 ± 523
Actual HFHC intake (kcal)	4063 ± 669	3464 ± 357
HFHC diet fat intake (%)	65 ± 1	65 ± 1
HFHC diet saturated fat intake (% of overall fat)	37 ± 3	37 ± 2

Data provided as means ± SD. TEE, total energy expenditure.

2.3.7 Statistics

An independent t-test was used to confirm equal matching of male and female participants for age, BMI and $VO_{2\ peak}$ (ml min^{-1} kg $(FFM)^{-1}$). All metabolic and cardiovascular parameters were analysed using a two-factor repeated measures ANOVA, with the between subjects factor 'sex' (males vs. females) and within-subjects factor 'HFHC diet' (pre- vs. post-diet). Significant main effects and interactions were assessed post-hoc using Bonferroni adjustment analysis.

2.4 Results

2.4.1 Subject Characteristics

At baseline there was no significant difference between males and females for age, BMI and $VO_{2\ peak}$ ($ml.min^{-1}.kgFFM^{-1}$) ($P > 0.05$; Table 2.1). Of the females who completed the HFHC diet, 4 were using the combined pill contraceptive method. During the dietary intervention one female participant withdrew from participation due to gastro-intestinal discomfort and therefore her data was withdrawn from the analyses. Withdrawal of this participant did not affect the group matching of sexes.

2.4.2 Energy Intake and macronutrient composition during the HFHC diet

All participants returned their HFHC diet plan with confirmation of times that they had consumed the food throughout the 7 days. Any food that was not consumed by the participants was notified to the researchers and returned to the lab to allow HFHC diet calculations to be adjusted. All participants adhered to the HFHC diet and consumed 153 $\pm$ 8 % and 155 $\pm$ 19% of their habitual energy intake for males and females, respectively, following adjustment for any food that was returned. Both sexes consumed an equal proportion of dietary fat as saturated fat (Table 2.2). Average daily physical activity energy expenditure calculated from the 3-axis activity monitor (wGT3X-BT, ActiGraph, Pensacola, FL, USA) revealed no significant differences between habitual levels (535 ± 224 kcal) and during the HFHC (510 ± 229 kcal) for either sex ($P = 0.552$).

2.4.3 Body Composition

At baseline males had significantly higher body mass than females ($P < 0.009$), but there was no effect of the HFHC diet for either sex ($P = 0.121$). Although matched for BMI, at baseline females had a significantly higher body fat percentage ($P < 0.001$) and total fat mass ($P = 0.003$; Table 2.3). Conversely at baseline, males had significantly higher FFM ($P < 0.001$), visceral fat ($P < 0.001$) and a higher trunk to leg fat mass ratio ($P < 0.001$), whereas trunk fat mass was not different between sexes ($P = 0.101$; Table 2.3). Following the HFHC diet, body mass did not increase ($P = 0.121$), but there was a trend towards an increase in total fat mass ($P = 0.056$) which was similar for males (+1.8%) and females (+2.3%; Table 2.3). Following the HFHC diet there was a significant increase in trunk to leg fat mass ratio in males only (+5.1%; HFHC diet x sex interaction, $P = 0.039$, Table 2.3). After the HFHC there were no alterations in FFM, body fat percentage, visceral fat or trunk fat mass in either sex.

2.4.4 OGTT

At baseline, fasting glucose levels were similar between males (4.3 ± 0.6 mmol.L^{-1}) and females (4.2 ± 0.4 mmol.L^{-1} L; $P = 0.766$) and after the HFHC diet fasting glucose did not change in either sex. There were no differences between fasting insulin levels between males (7.1 ± 3.9 μl U.mL^{-1}) and females (7.5 ± 4 μl U.mL^{-1}; $P > 0.05$) and this did not change following the HFHC diet in either sex. Serum glucose AUC and plasma insulin AUC during the OGTT were not significantly different between sexes ($P > 0.05$) and not altered following the HFHC diet in either sex ($P > 0.05$; Figure 2.1).

2.4.4.1 Insulin Sensitivity

In an attempt to decipher changes in insulin sensitivity dependent on origin (liver or muscle), glucose and insulin values from the OGTT were also used to predict hepatic and muscle insulin resistance using the calculations proposed by Abdul-Ghani et al. (2007), in addition to the Matsuda ISI measure of whole-body insulin sensitivity. At

baseline there were no significant differences between sexes for the Matsuda ISI (P = 0.844), hepatic insulin resistance (P = 0.211) or muscle insulin resistance (P = 0.584; Figure 2.2). After the HFHC diet there were no significant changes in any of the aforementioned measures of insulin sensitivity in males or females (Figure 2.2).

2.4.4.2 Metabolic Flexibility

At baseline there was no significant differences in fasting RER between males (0.81 ± 0.07) and females (0.76 ± 0.08; P = 0.189). Following the HFHC diet there was a trend towards a reduction in fasting RER, which was reduced similarly between males and females (0.78 ± 0.08 and 0.74 ± 0.07 post-HFHC diet for males and females, respectively; P = 0.052). At baseline, peak RER during OGTT was similar between males (0.94 ± 0.07) and females (0.91 ± 0.16; P = 0.629). Following the HFHC diet there was a trend towards a reduction in peak RER for males (0.91 ± 0.07) and females (0.86 ± 0.08; P = 0.070). The time it took to reach peak RER during the OGTT was similar between males (88 ± 6 min) and females (90 ± 7 min; P = 0.644) and this did not change after the HFHC diet.

Metabolic flexibility was determined as the rate of change from fasting RER to peak RER during the OGTT. At baseline there was no significant difference between males and females for metabolic flexibility (P = 0.877) and this was unaltered following the HFHC diet in both sexes (P > 0.05; Figure 2.3A).

2.4.5 Arterial Stiffness

AI_x@75bpm was not significantly different at baseline between sexes (P = 0.162) and was unaltered following the HFHC diet (P = 0.318; Figure 2.3B). PWV was also not significantly different at baseline between sexes (P = 0.826) and was unaltered after the HFHC diet (P = 0.307; Figure 2.3C).

2.4.6 Lipid and Liver Blood Profile

At baseline, there was no significant differences between sexes for NEFA ($P = 0.912$), cholesterol ($P = 0.878$) and triglycerides ($P = 0.315$; Table 2.4). After the HFHC diet there was a significant increase in cholesterol ($P = 0.049$) which was similar between males (+8.1%) and females (+6.3%; Table 2.4). Triglyceride levels and NEFA levels remained unchanged following the HFHC diet for both sexes ($P = 0.685$; Table 2.4).

At baseline, there was no significant difference in AST level between sexes ($P = 0.152$), however males had significantly higher ALT levels ($P = 0.006$) and a trend towards higher GGT levels ($P = 0.059$; Table 2.4). After the HFHC diet there was no significant changes in levels of AST, ALT or GGT in either sex ($P > 0.05$; Table 2.4).

Table 2.3. Effect of 7-days HFHC diet on body composition

	Males		Females	
	Pre	Post	Pre	Post
Body mass (kg)	72.9 ± 4.9*	73.2 ± 5.2	63.7 ± 9.3	63.9 ± 2.9
BMI (kg m^{-2})	23.2 ± 1.4	23.3 ± 1.4	22.7 ± 2.3	22.8 ± 2.4
FM (kg)	11.7 ± 3.1*	11.9 ± 3	17.3 ± 4.1	17.7 ± 4
FFM (kg)	58.6 ± 5.5*	57.9 ± 1.2	43.2 ± 5.9	40.3 ± 10.0
Body fat (%)	16.8 ± 4.0*	16.9 ± 3.8	28.4 ± 3.6	29 ± 3.3
Trunk fat mass (kg)	5.4 ± 1.4	5.6 ± 1.4	6.7 ± 2.0	6.6 ± 2.0
Trunk/leg fat ratio † ‡	0.87 ± 0.13*	0.92 ± 0.17	0.63 ± 0.09	0.63 ± 0.09
VAT (g)	308 ± 45*	295 ± 47	174 ± 71	177 ± 22

Data are provided as means ± SD. BMI, body mass index; FM, fat mass; FFM, fat free mass; VAT, visceral adipose tissue. * Significant difference *vs* females at baseline $P < 0.05$. † Significant main effect for the HFHC diet $P < 0.05$. ‡ Significant interaction effect $P < 0.05$.

Table 2.4 . Effect of 7-days HFHC diet on lipid and liver blood profile

	Males		Females	
	Pre	Post	Pre	Post
Lipid profile				
NEFA (mmol.L^{-1})	1.16 ± 0.43	1.05 ± 0.25	1.17 ± 0.26	1.37 ± 0.46
Cholesterol (mmol.L^{-1}) †	3.56 ± 0.86	3.85 ± 0.63	3.95 ± 0.59	4.20 ± 0.58
Triglycerides (mmol.L^{-1})	0.81 ± 0.92	0.70 ± 0.45	0.51 ± 0.17	0.59 ± 0.25
Liver profile				
AST (U/L^{-1})	35.82 ± 7.86	34.64 ± 13.66	28.10 ± 4.52	28.25 ± 17.77
ALT (U/L^{-1})	35.36 ± 19.80*	35.05 ± 16.77	16.15 ± 7.35	16.80 ± 7.30
GGT (U/L^{-1})	21.65 ± 11.87	21.13 ± 8.41	15.28 ± 12.15	11.56 ± 5.39

Data are provided as means ± SD. ALT, alanine aminotransferase; AST, aspartate aminotransferase; GGT Gamma-glutamyltransferase. * Significant difference *vs* females at baseline $P < 0.05$. † Significant main effect for the HFHC diet $P < 0.05$.

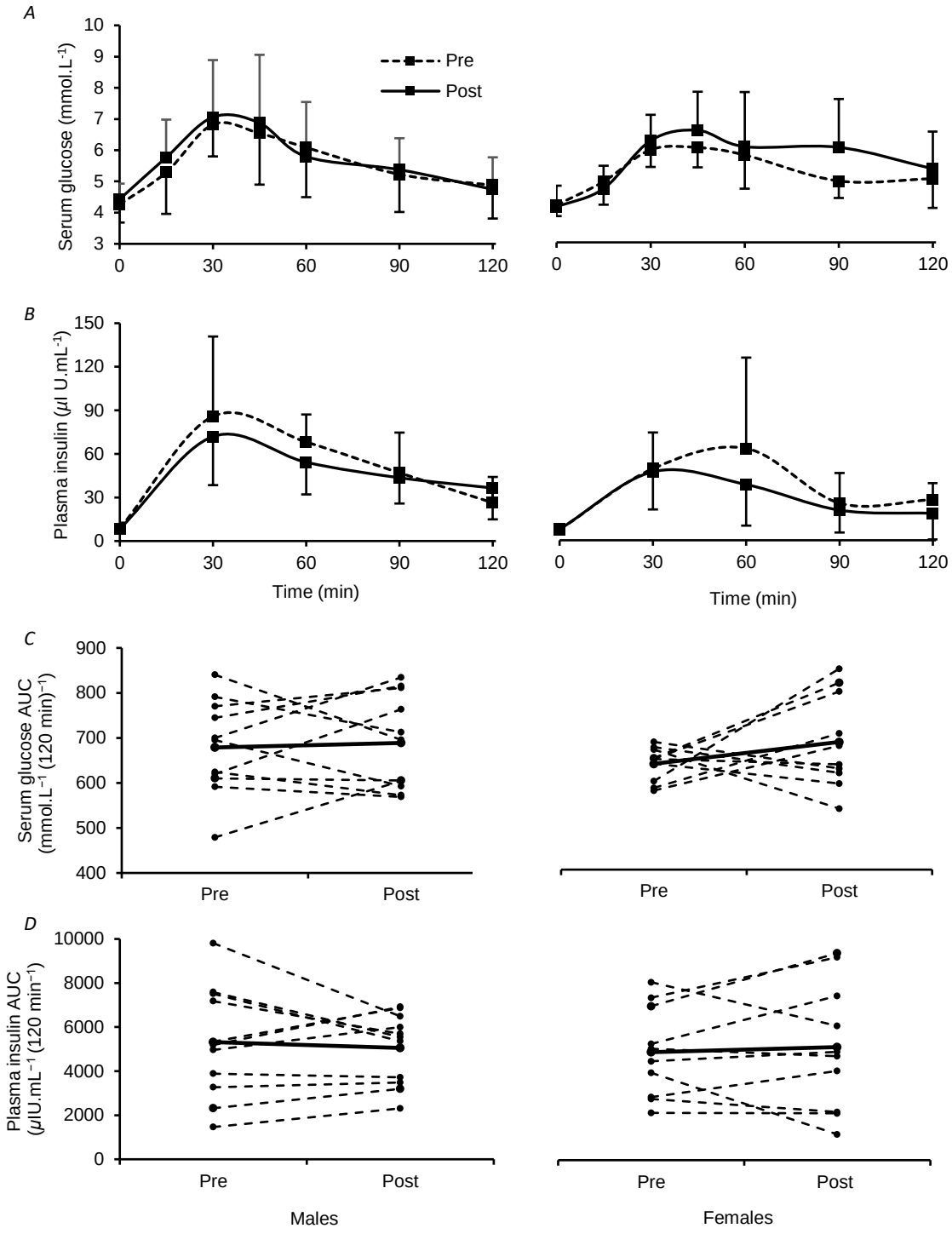

Figure 2.1. Effect of 7-days HFHC diet on glucose and insulin values during an OGTT in males and females. No sex differences or effects of HFHC diet on OGTT serum glucose levels (A) or plasma insulin values (B). OGTT AUC shows no differences between sexes or effects of the HFHC diet for glucose (C) or insulin (D). Solid black line in graphs C & D represents mean value whereas dashed lines show individual responses.

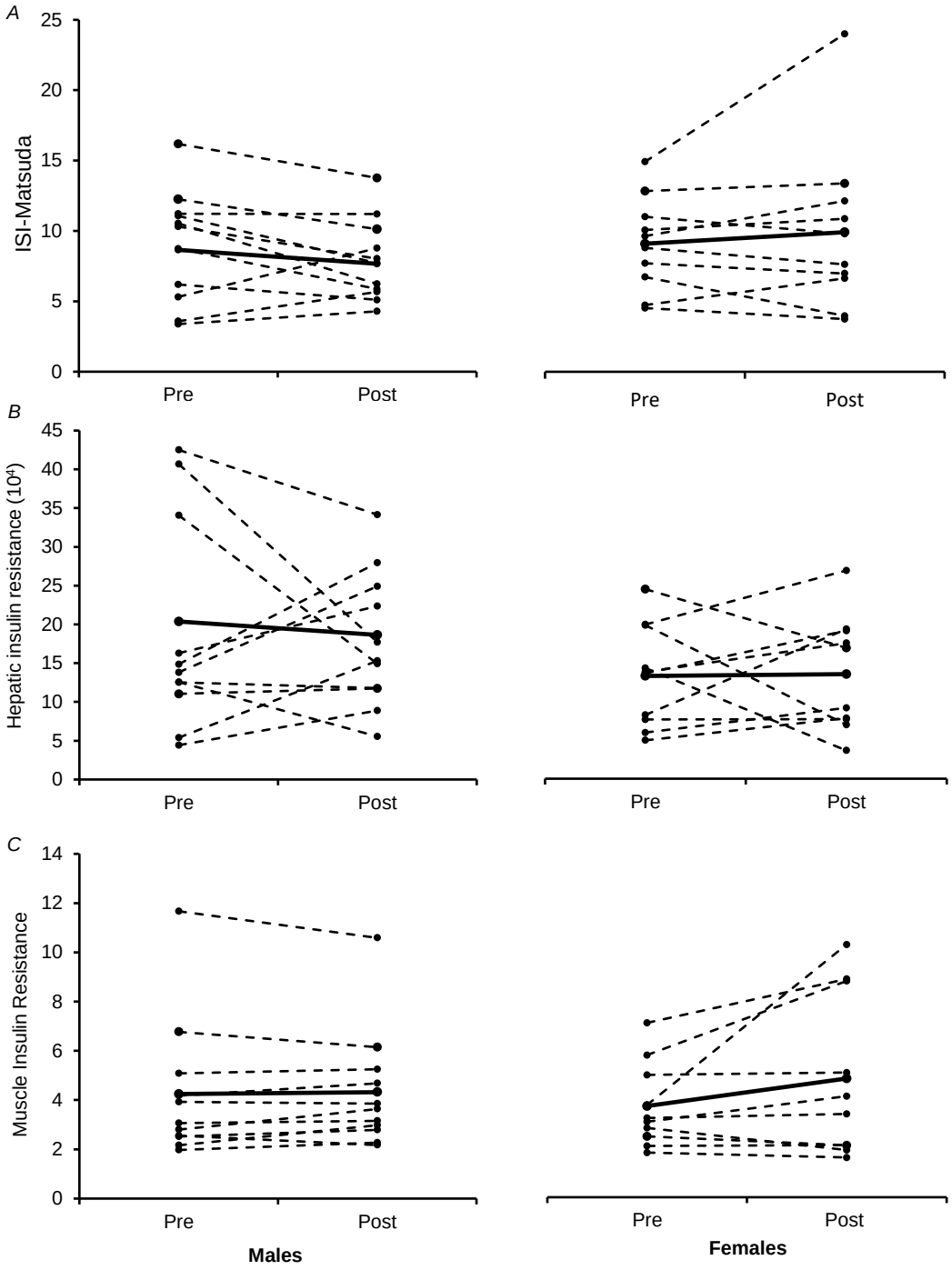

Figure 2.2. Effect of 7-days HFHC diet on parameters of insulin sensitivity measured with OGTT. No sex differences or effects of the HFHC diet on the Matsuda index (A), hepatic insulin resistance (B) and muscle insulin resistance (C) in males and females, however results show varied individual responses for both males and females. Solid black line represents mean value whereas dashed lines show individual responses. Matsuda index was derived from Matsuda & DeFronzo (1999) whilst hepatic and muscle insulin resistance values were derived from Abdul-Ghani et al. (2007).

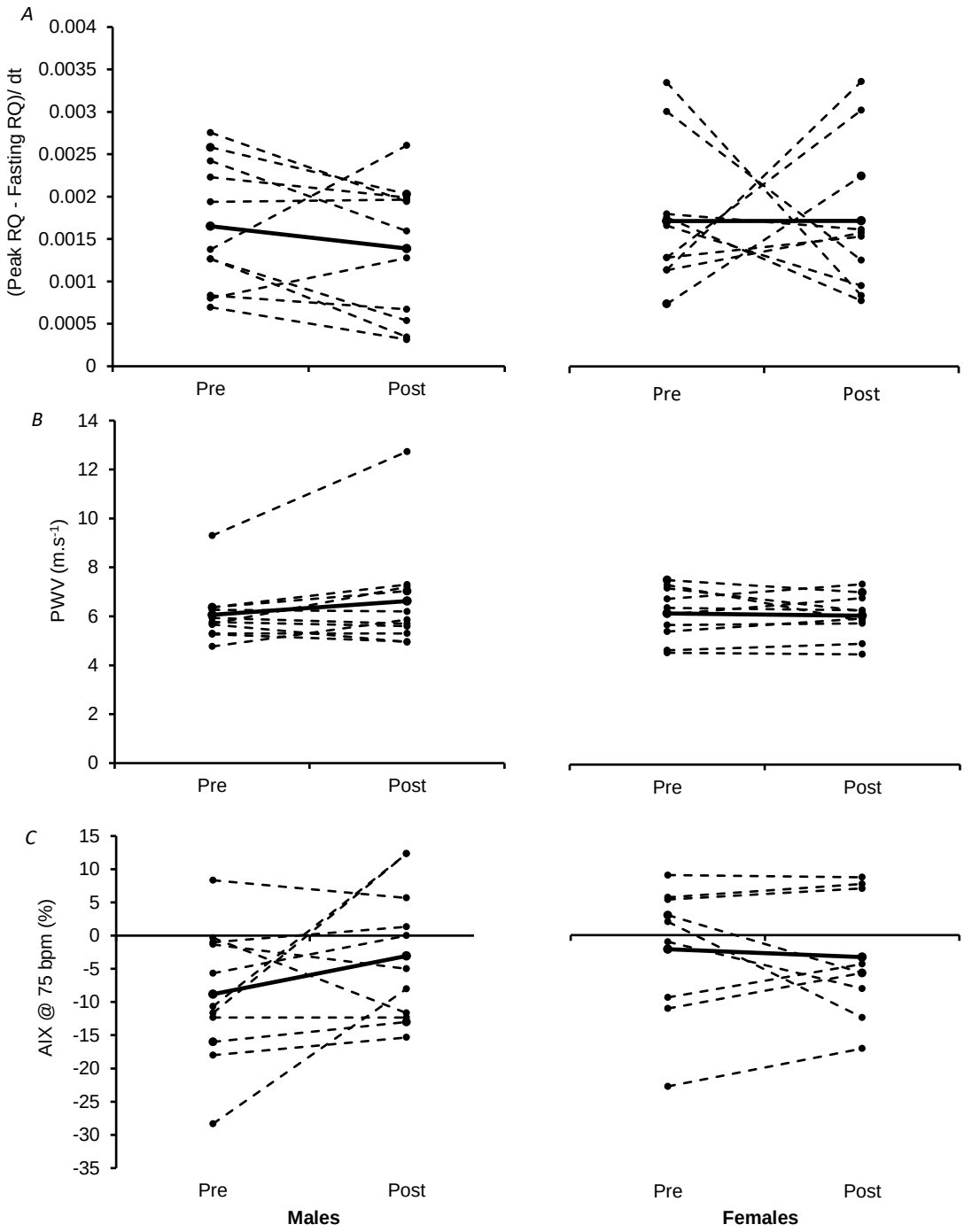

Figure 2.3. Effect of 7-days HFHC diet on metabolic and cardiovascular parameters of health. No sex differences or effects of HFHC diet on metabolic flexibility (A), arterial stiffness (B) and augmentation index (@ 75bpm) (C) in males and females, however results show varied individual responses for both males and females. Solid black line represents mean value whereas dashed lines show individual responses.

2.5 Discussion

The was the first study to investigate sex differences in measurements of metabolic and cardiovascular health in response to a 7 day HFHC diet. Our results show there was no effect of the HFHC diet on outcomes related to metabolic and cardiovascular health in either sex, highlighting that a HFHC diet does not always impede aspects of health in a young, physically active cohort who have good levels of cardio-respiratory fitness.

Overall, 7 days of HFHC diet did not induce changes in whole-body insulin sensitivity (Matsuda ISI), or indices of hepatic or muscle insulin resistance. This was a surprising finding considering previous studies have reported a reduction in Matsuda ISI in young lean, healthy individuals (males and females combined) using the same 7-day HFHC diet protocol (65% energy from fat, +50% calories) as the current study (Hulston *et al.*, 2015; Parry *et al.*, 2017). However, consistent with our finding, there are also studies that report no effect of a HFHC diet on lean healthy individuals on indices of insulin sensitivity (Adochio *et al.*, 2009; Brons *et al.*, 2009), however only one of these studies included female participants (Adochio et al., 2009). Specifically, when peripheral insulin sensitivity quantified by glucose disposal rate and M-value during a hyperinsulinaemic clamp was not altered in studies using a similar HFHC diet protocol for five days in lean healthy individuals (Adochio *et al.*, 2009; Brons *et al.*, 2009). However, it should be noted that Brons (2009) did observe reductions in hepatic insulin sensitivity. These findings were later extended to demonstrate that reductions in peripheral insulin sensitivity following a HFHC diet only existed in low birth weight individuals (males only) who have a predisposed risk of developing T2D in comparison to matched normal birth weight individuals (Brons *et al.*, 2012). It is apparent from this study and others that short-term HFHC diets do not always induce insulin resistance in lean healthy individuals of both sexes. Importantly this current

study was unique in comparing sexes and measuring cardio-respiratory fitness and physical activity levels of participants.

There was a trend towards a decrease in fasting RER by 0.03 following the HFHC diet with no differences between sexes. There was a large variability between participants and given the large reduction observed in RER, significance would have likely been observed if a larger cohort was studied. A decrease in RER has also been observed following 3-days eucaloric high-fat (50%) diet in young males when measured using a 24 h metabolic chamber (Ukropcova *et al.*, 2007). Obese insulin-resistant individuals exhibit lower metabolic flexibility in comparison to lean insulin sensitive individuals (Kelley *et al.*, 1999). In the current study, metabolic flexibility was measured as the rate of change from fasting RER to peak RER during the OGTT and this was not altered following the HFHC diet in either sex. This current study is the only study to investigate sex differences in metabolic flexibility following a HFHC diet in young healthy active individuals. Similar findings have however been observed following 28-days of HFHC diet in older (~ 37 years) participants (males and females) with and without a family history of type 2 diabetes (Samocha-Bonet *et al.*, 2010). Impairments in metabolic flexibility have been observed in the presence of normal peripheral insulin sensitivity in older individuals (Faerch & Vaag, 2011) suggesting metabolic inflexibility is an early aberration in the progression of insulin resistance and T2D. However, we and others (Samocha-Bonet *et al.*, 2010) have been unable to detect changes in metabolic flexibility without changes in peripheral insulin sensitivity.

There was a small but significant increase in body fat following the HFHC diet in both sexes which is comparable to previous studies showing an increase in body mass following HFHC diet over 7-days (Hulston *et al.*, 2015; Parry *et al.*, 2017). Abdominal adiposity, and in particular elevated visceral fat are more closely associated with insulin resistance and T2D (Montague & O'Rahilly, 2000; Huang *et al.*, 2015). This is

due to visceral fat contributing excess FFA to the liver via the portal vein (Liu *et al.*, 2006a) and as a consequence of visceral fat being a source of systemic inflammation through increased adipocytokines that can contribute to insulin resistance (Yudkin, 2007). In line with previous findings (Ludescher *et al.*, 2007; Haupt *et al.*, 2010; Staiano & Katzmarzyk, 2012) at baseline visceral fat stores were higher in males compared to females, but this did not change following the HFHC diet. Trunk fat measured by the DEXA scan represents overall abdominal adiposity rather than specific visceral fat. There were no differences between males and females at baseline for trunk fat and following the HFHC diet trunk fat was not changed, but there was an increase in trunk to leg fat mass ratio which increased only in males. This change in unfavourable fat accumulation ratio occurred after only 7 days of a HFHC diet. It is likely that more chronic overfeeding would exacerbate this fat accumulation and start to contribute to the development of metabolic disorders.

An obesogenic environment is often associated with reduced PA levels in addition to HFHC diets. A recent systematic review concluded that HFHC diet studies can often influence participant's PA levels, which may impact changes in weight gain (Giroux *et al.*, 2018). In the current study, all participants exhibited high habitual PA levels as measured by the IPAQ and this was largely due to participants participating in regular structured exercise. During the HFHC diet period participants were instructed to maintain their PA and exercise regimes. This was confirmed by examining energy expenditure predicted by the accelerometer and revealing that it remained the same during habitual measures and the HFHC diet period. Although this minimised the influence of activity levels on the effects of the HFHC diet, the pre-existing high PA levels may have helped compensate for the negative effects of a HFHC diet in some participants. Indeed, increased PA levels through daily vigorous-intensity exercise has been shown to counteract the detrimental metabolic effects of a HFHC diet and reduced habitual PA in healthy young males (Walhin *et al.*, 2013). Reduced PA is

therefore likely to be a more potent stimulus to reduce insulin sensitivity. The combination of both reduced PA and HFHC have shown more clear reductions in insulin sensitivity in healthy young males (Knudsen *et al.*, 2012).

In this study self-reported habitual energy intake closely matched estimates of TEE derived from measurements of RMR with indirect calorimetry and physical activity levels with IPAQ. These values were also very close to the recommended energy intakes for males (2500 kcal) and females (2000kcal). It was therefore assumed that the HFHC diet did indeed provide a 50% energy surplus of relative to habitual energy levels although there was no distinct change in any metabolic parameters. Although PA maintenance was confirmed with accelerometer a limitation of this measurement is it might not always accurately measure high-intensity exercise bouts particularly if performed by modes other than running e.g. cycling or swimming. Future research would benefit from controlling participant's physical activity levels or quantifying them more accurately with the use of combined heart rate/accelerometry measures.

Longitudinal studies have shown that high cardio-respiratory fitness can reduce the risk of T2D (Nojima *et al.*, 2017) and all-cause mortality (Blair *et al.*, 1989). A further analysis of the Aerobic Centre Longitudinal Study involving over 20,000 males between the ages of 30-83 years were assessed for cardio-respiratory fitness in different BMI categories (19.0 to <25.0, 25.0 to <27.8, ≥27.8) and followed for 8 years (Lee *et al.*, 1998). The results from this analysis showed that the group with the lowest cardio-respiratory fitness had a higher risk of all-cause mortality than their higher fitness level counterparts. Interestingly, males who were in the highest two BMI categories but had high cardio-respiratory fitness were at a lower risk of all-cause mortality than normal BMI but low fit counterparts (Lee *et al.*, 1998). When a more diverse longitudinal study (2,506 females and 2,860 males) was conducted with different ethnicities and socio-economic status, high BMI and low cardio-respiratory fitness both presented as risk factors for cardiovascular disease and all-cause

mortality (Stevens *et al.*, 2002). When a female only cohort (116,564 females) were followed for 24 years, both obesity and low activity levels were strong and independent risk factors for all-cause mortality (Hu *et al.*, 2004), however in this study there was no direct measurement of cardiorespiratory fitness. Together, the evidence suggests that low cardio-respiratory fitness is an independent risk factor for cardiovascular disease and all-cause mortality and in certain populations is a stronger risk factor than increased adiposity. The male and female groups in the current study displayed high cardio-respiratory fitness associated with a reduced risk of all-cause mortality (Blair *et al.*, 1989). It is possible, therefore, that the benefits of having a high cardio-respiratory fitness leading to a lower risk of all-cause mortality may have also counteracted the negative effects imposed from a HFHC diet in this study. Future research should compare low and high cardio-respiratory fitness individuals to determine if cardio-respiratory fitness can protect against short-term HFHC diets.

In summary, this study aimed to determine sex differences in the response to a short-term HFHC diet. Although no sex differences were observed we now highlight that there are large inter-individual responses to a HFHC diet in both sexes. Although there is a reduced prevalence of T2D in women, the pathophysiology of this metabolic disorder in this sex is still understudied and not understood. There is a very clear need to explore and understand the mechanisms of how lipid induced insulin resistance manifests in females, particularly if these are exacerbated following menopause.

Chapter 3. A 7 day high-fat high-calorie diet induces fibre-specific increases in intramuscular triglyceride content and perilipin protein expression in human skeletal muscle.

3.1 Abstract

High-fat high-calorie (HFHC) diets can induce whole body insulin resistance (IR) whilst increasing stores of intramuscular triglyceride (IMTG) contained within lipid droplets (LD). Perilipin (PLIN) proteins assist in IMTG storage. Synaptosomal-associated protein (SNAP23) may support LD growth and also direct IMTG-derived fatty acids (FA) to mitochondria for *β*-oxidation. The objectives of this study were: 1) to test the hypothesis that 7 days HFHC diet increases IMTG content to prevent lipid induced impairments in skeletal muscle insulin signalling and 2) identify changes in expression and subcellular distribution of key proteins related to lipid metabolism. Muscle biopsies were obtained from the *vastus lateralis* of thirteen (n=11 male, n=2 female) healthy individuals (age: 23±1 years, body mass index:24.4±0.7 $kg.m^{-2}$) before (0min), during (30min) and at the end (120 min) of an oral glucose challenge, pre and post 7-days consuming a high-fat (65% energy) high-calorie (+50% kcal) diet. IMTG, PLIN2, PLIN3, PLIN5, SNAP23 and mitochondria content were measured using (semi)-quantitative confocal immunofluorescence microscopy. PLIN2, PLIN3 and PLIN5 colocalisation to LD was measured using object based colocalisation analyses. Pearson's correlation coefficient quantified colocalisation between SNAP23 and; plasma membrane, mitochondria and LD. Phosphorylation of intermediates of the insulin-signalling cascade (Akt and AS160) were measured with western blot at 0, 30 and 120 min of an oral glucose challenge pre and post the diet. Following the HFHC diet phosphorylation of Akt and AS160 were not impaired during the oral glucose challenge, however whole body glucose tolerance (P = 0.007) was significantly reduced. IMTG content increased in type I fibres (+100%; $P < 0.001$) after the diet due to both an increase in LD number (+43%; $P < 0.001$) and size (+44%; $P < 0.001$). Of the PLINs investigated, only PLIN3 content increased (+50%; $P < 0.01$) which occurred solely in type I fibres. PLIN2+ LD increased (80%; $P < 0.01$) in type I fibres only whereas PLIN3+ LD and PLIN5+ LD were unaltered. SNAP23 and

mitochondria content did not change with the diet, nor did the colocalisation of SNAP23 with the plasma membrane, mitochondria or LD. Seven days of HFHC diet increased IMTG stores without impairments of the insulin signalling cascade. This increase in IMTG number and size is likely aided by a concurrent increase in PLIN3 content and a redistribution of existing stores of PLIN2 to LD in type I fibres. These adaptations may protect skeletal muscle insulin signalling by channelling meal-derived FA towards IMTG rather than accumulating as lipid metabolites.

3.2 Introduction

The development of insulin resistance and type 2 diabetes is initiated by a reduction in peripheral insulin sensitivity (DeFronzo & Tripathy, 2009). Skeletal muscle serves as a large depot for insulin-stimulated glucose uptake (Katz *et al.*, 1983; Ferrannini *et al.*, 1985) and therefore impairments in skeletal muscle insulin sensitivity are a contributing factor to hyperglycemia. Elevated intramuscular triglyceride (IMTG) stores were initially associated with insulin resistance in sedentary, obese and/or type 2 diabetes individuals (Kelley *et al.*, 1999; Goodpaster *et al.*, 2001). This association disappeared when endurance trained individuals were introduced into the comparison because they also had elevated IMTG stores but combined with high insulin sensitivity in a phenomenon termed 'the athlete's paradox' (Goodpaster *et al.*, 2001; van Loon *et al.*, 2004). IMTG has no mechanistic link to impairments of skeletal muscle insulin signalling. Conversely, acute (4-6h) elevation of lipid metabolites, diacylglycerol (DAG) and ceramides have resulted in skeletal muscle insulin signalling concomitant to a reduction in insulin-stimulated glucose uptake (Itani *et al.*, 2002; Yu *et al.*, 2002a; Straczkowski *et al.*, 2004). Cross-sectionally insulin resistant states have also demonstrated elevated ceramide levels correlated with impairments in insulin signalling and glucose uptake in skeletal muscle (Adams *et al.*, 2004).

Directing an influx of lipid from the diet to IMTG storage would, therefore, be of benefit because this would reduce the risk of generating lipid metabolites. High-fat, high-calorie (HFHC) diets provide a model of dietary lipid excess, comparable to that observed when consuming a typical western diet. Several studies have shown that short-term HFHC diets reduce insulin sensitivity or glucose disposal in healthy individuals (Bakker *et al.*, 2014; Hulston *et al.*, 2015; Gemmink *et al.*, 2017a; Parry *et al.*, 2017). However, the mechanisms underpinning the development of insulin resistance are still not fully understood.

IMTG is stored within lipid droplets (LD) which are coated by a phospholipid monolayer, decorated with numerous proteins. The most extensively studied of these proteins is the perilipin (PLIN) family of proteins. PLIN2 and PLIN5 protein content increases in response to exercise training concomitant with an increase in IMTG content (Shaw *et al.*, 2012; Shepherd *et al.*, 2013; Shepherd *et al.*, 2014), suggesting that PLIN proteins play a role in IMTG storage. In support, myotubes overexpressing PLIN3 accumulate IMTG (Kleinert *et al.*, 2016), and primary human myotubes overexpressing PLIN5 promote IMTG storage by restricting basal lipolysis (Laurens *et al.*, 2016). To date, only one study has investigated the effect of a HFHC diet on PLIN protein expression. Using biochemical extraction to determine IMTG concentration and western blotting of whole muscle homogenates to investigate PLIN protein expression, Gemmink et al., (2017a) were the first to show that a short-term HFHC diet led to increased IMTG concentration and PLIN5 protein content in human skeletal muscle, without alterations in PLIN2 or PLIN3. Type I fibres have an enhanced capacity to store IMTG (Shepherd *et al.*, 2013), and therefore it is important to consider fibre-type specific changes in IMTG content and PLIN protein expression that may not be detected using whole muscle homogenates. Another important consideration is the distribution of PLIN proteins relative to LDs within the muscle. In support, elevating free fatty acid availability in trained individuals through a lipid infusion augments IMTG content in type I fibres and increases the number of LD associated with PLIN2, PLIN3 and PLIN5, without any changes in PLIN protein expression (Shepherd *et al.*, 2017b). Our first aim was therefore to investigate fibre-type and region-specific changes in IMTG content (LD number and morphology) and PLIN protein expression in response to 7 days of HFHC diet. By using our previously validated immunofluorescence microscopy techniques (Shepherd *et al.*, 2012, 2013; Shepherd *et al.*, 2017b), we also aimed to investigate fibre-type and region-specific changes in the redistribution of perilipins with LD.

Synaptosomal-associated protein (SNAP23) is a t-SNARE (target- Soluble N Ethylmaleimide Sensitive Factor Attachment Protein Receptor) found at the plasma membrane (Jahn & Scheller, 2006) that mediates the docking of GLUT-4 to the plasma membrane under insulin-stimulated conditions (Foster *et al.*, 1999; Kawanishi *et al.*, 2000). Notably though, the subcellular distribution of SNAP23 is sensitive to changes in lipid availability. For example, treatment of cardiomyocytes with oleic acid increased intracellular LD volume resulting in an increase in the LD-associated pool of SNAP23, with a concomitant reduction in SNAP23 associated to the plasma membrane (Bostrom *et al.*, 2007). This has led to the hypothesis that in response to lipid excess, LD 'highjack' SNAP23 from the plasma membrane to assist in LD fusion (Sollner, 2007). Although this may assist in minimising the accumulation of lipid metabolites, the removal of SNAP23 from the plasma membrane may reduce GLUT-4 docking, resulting in a reduced capacity for glucose uptake. Ablation of SNAP23 in fibroblasts reduces the formation of LD-mitochondria complexes and results in a decreased mitochondrial β-oxidation (Jagerstrom *et al.*, 2009). This suggests SNAP23 may also have a putative role in minimising accumulation of lipid metabolites by assisting IMTG-derived FA β-oxidation. We have recently confirmed using confocal immunofluorescence microscopy that SNAP23 has a high colocalisation to the plasma membrane and mitochondria and a weaker colocalisation to LD in lean healthy trained males (Strauss *et al.*, 2016). We now aim to extend these findings to determine if SNAP23 colocalisation to the plasma membrane, mitochondria or LD is altered following lipid excess induced by 7 days HFHC diet.

3.3 Methods

3.3.1 Participants and ethical approval

The samples used in this study were collected as part of a larger study investigating the effect of 7 days HFHC on glucose kinetics and insulin sensitivity, in collaboration with Loughborough University. The study adhered to the Declaration of Helsinki and

was approved by Loughborough University Subcommittee Ethical Committee for Human Participants. Fifteen healthy individuals (*n* = 13 males and *n* = 2 females, 24 ± 1 y, body mass index (BMI) 24.8 ± 0.6 kg.m^{-2}) participated in the study following written informed consent. Of these participants, thirteen consented to muscle biopsies, which were used for western blot and immunohistochemistry analysis. All participants were physically active (taking part in at least 3 x 30 min of moderate-intensity physical activity each week), non-smokers, with no diagnosis of cardiovascular or metabolic disease, not taking any medication known to interfere with the study outcomes, and weight stable for at least 3 months.

3.3.2 Pre-testing

Prior to the start of the study, participants attended the laboratory for an initial assessment of their baseline anthropometric characteristics (height, body mass and BMI). This information was then used to estimate resting energy expenditure (REE) (Mifflin *et al.*, 1990). A standard correction for physical activity (1.6 and 1.7 times REE for females and males, respectively) was applied in order to estimate total daily energy requirements. This information was then used to determine individual energy intakes for the experimental diet intervention (Parry *et al.*, 2017).

3.3.3 Experimental protocol

The experimental protocol, as well as the analysis of glycaemic control and skeletal muscle insulin signalling, were conducted at Loughborough University, whilst all immunohistochemical analyses were conducted as part of this PhD experimental chapter. For contextualisation of the immunohistochemical analyses and better scientific understanding of the effects of 7 days HFHC diet, the methodology and results from the oral glucose challenge (whole-body glycaemic control and skeletal muscle insulin signalling) are reported and discussed briefly in this chapter.

Participants consumed a high-fat (65% energy), high-calorie (+50% kcal) diet for 7 days. On experimental days (before and after the HFHC diet) subjects arrived at the

laboratory following an overnight fast (>12 h), to undergo muscle biopsies and an oral glucose challenge (50 g glucose plus 15 g whey protein dissolved in 400 mL plain water). Fasting and postprandial venous blood samples were obtained at 0, 15, 30, 45, 60, 90 and 120 min after beverage ingestion. Plasma and serum samples were used to measure glucose and insulin levels, respectively. These measurements were then use to predict whole-body insulin sensitivity using the Matsuda Index (Matsuda & DeFronzo, 1999).

Muscle biopsies from the *m. vastus lateralis* were obtained at 0, 30 and 120 min time points of the oral glucose challenge under local anaesthesia using the Bergstrom needle biopsy technique with suction (Bergström, 1975). Following removal of excess blood, fat and connective tissue a portion of muscle (10-30 mg) was mounted in Tissue-Tek OCT (Sakura Finetek UK Ltd) and frozen in liquid nitrogen-cooled isopentane for subsequent immunohistochemical analyses. An additional two portions of muscle tissue (30-50 mg each) were snap-frozen in liquid nitrogen. Each biopsy during the oral glucose challenge was obtained from a separate incision on the same leg (~3-4 cm proximal to the initial biopsy site). Following 7 days of HFHC diet, biopsies were obtained from the opposite leg.

3.3.4 Western blot

Commercially available antibodies were used to determine the phosphorylation of key insulin signalling proteins (Akt Ser473 [Cell Signalling #4060], Akt Thr308 [Cell Signalling #13038], AS160 Ser588 [Cell Signalling #8730], AS160 Thr642 [Cell Signalling #8881], by SDS-PAGE and Western blotting as previously described (Hulston *et al.*, 2018).

3.3.5 Immunohistochemistry analysis

Serial cryosections (5 µm) were cut at -30^{o}C onto ethanol-cleaned glass slides. Cryosections of samples obtained pre and post 7 days HFHC diet from one participant were placed on a single slide to account for any variation in staining intensity between

sections. Sections were fixed for 1 h in 3.7% formaldehyde, rinsed 3 x 30 s in doubly distilled water (dd H_2O) and permeabilised in 0.5% Triton X-100 for 5 min, before being washed 3 x 5 min in Phosphate Buffered Saline (PBS, 137mM sodium chloride, 3 mM potassium chloride, 8 mM sodium phosphate dibasic and 3mM potassium phosphate monobasic, pH of 7.4). Slides were incubated for 1 h with primary antibodies, washed 3 x 5 min in PBS, incubated with complementary secondary fluorescence-conjugated antibodies for 30 min, followed by a further 3 x 5 min PBS washes. To visualise IMTG, sections were incubated with BODIPY 493/503 (Invitrogen, Paisley, UK, D3922) for 20 min followed by a single 5 min PBS wash. Coverslips were mounted with Vectashield (H-1000, Vector Laboratories, Burlingame, CA, USA) and sealed with nail varnish.

3.3.5.1 Antibodies and staining combinations

The primary antibodies used were guinea pig anti-adipophilin (PLIN2) and guinea pig anti-OXPAT (PLIN5: both Progen, GP40 & GP31 respectively, Biotechnik, Heidelberg, Germany), rabbit anti-perilipin 3/TIP-47 (PLIN3: NB110-40764 Novus Biologicals, Cambridge, UK), rabbit anti-SNAP23 (SNAP23: 111202, Synaptic Systems, Goettingen, Germany), mouse anti-OxPhos Complex IV subunit I (COX; used as a marker of muscle oxidative capacity: 459600, ThermoFisher Scientific, Paisley, UK), mouse anti-dystrophin (used as a plasma membrane marker: D8168, Sigma-Aldrich, Dorset UK). Cell border visualisation was achieved with either rabbit anti-laminin (L9393, Sigma-Aldrich, Dorset, UK) or with wheat germ agglutinin (WGA) Alexa Fluor 633 conjugate (ThermoFisher Scientific, Paisley, UK). Muscle fibre type was determined using mouse anti-myosin heavy chain I (MHCI) (A4.840c) and mouse anti-myosin heavy chain IIa (MHCIIa) (N2.261c; both DSHB, University of Iowa, USA developed by Dr. Blau). Appropriate Alexa Fluor secondary antibodies were obtained from ThermoFisher Scientific (Paisley, UK).

To determine fibre type-specific protein expression, primary antibodies targeting PLIN2, PLIN3, PLIN5 or COX, or BODIPY 493/503 to stain for IMTG, were used in combination with antibodies targeting MHCI, MHCIIa and the cell border, either laminin or WGA Alexa Fluor 633 conjugate. SNAP23 is also located at the plasma membrane, and therefore SNAP23 protein expression was investigated using antibodies targeting SNAP23 (followed by goat anti-rabbit IgG 488), MHCI and MHCIIA in combination with an antibody targeting dystrophin as previously described (Strauss *et al.*, 2016). To investigate colocalisation between PLIN proteins and LD, PLIN2, PLIN3 or PLIN5 were stained in combination with BODIPY 493/503, and antibodies targeting MHCI and MHCIIa. To investigate the localisation of SNAP23 to the plasma membrane, LD and mitochondria, respectively, SNAP23 was stained in combination with either dystrophin, BODIPY 493/503 or COX, as well as antibodies targeting MHCI and MHCIIa.

3.3.5.2 Image capture, processing and data analysis

All images were captured using an inverted confocal microscope (Zeiss LSM710; Carl Zeiss AG, Oberkochen, Germany) with a 63x 1.4 NA oil immersion objective. A diode laser was used to excite the Alexa Fluor 405 fluorophore, an argon laser for the Alexa Fluor 488 fluorophore and BODIPY 493/503 and a helium-neon laser for the Alexa Fluor 546 and 633 fluorophores.

To assess IMTG content, and the protein expression of the PLIN proteins, COX and SNAP23, cross-sectional images were obtained at 1.1x digital zoom. Type I and type IIa fibres were identified through positive staining, and any fibres without positive staining for either MHCI or MHCIIa were assumed to be type IIx fibres. For type I and IIa fibres 10 images per fibre-type per participant pre and post the HFHC diet for each assay was obtained (equating to a total of 260 images per assay). This was not possible for type IIx fibres due to a low number of these fibres in muscle sections in a number of participants. Type IIx fibres were included in the analyses if it was

possible to obtain 4 or more images of type IIx fibres per time point for a participant. This equated to an average of 71 ± 11 images of type IIx fibres being used in 5 assays that were able to acquire sufficient amount of type IIx fibres to be used in statistical analyses. Image analysis was undertaken using Image-Pro Plus, version 5.1 (Media Cybernetics, Bethesda, MD, USA). To assess IMTG and PLIN protein content within each muscle fibre, the fibre was first separated into a peripheral region (first 5 μm from the cell border) and the central region (remainder of the cell; Figure 3.1). A selected intensity threshold was used to represent a positive signal for IMTG and each PLIN protein. IMTG and PLIN protein content was expressed as the positively stained area fraction relative to the total area of the peripheral region or central region of each muscle fibre. Data was also extracted to examine LD density (number of LDs expressed relative to area) and LD size (mean area of individual LDs) SNAP23 and COX fluorescence intensity was calculated using optical density in the peripheral and central regions of the cell and normalised to each individual peripheral and central area. The peripheral region of the cell does not include the plasma membrane of the muscle fibre. As SNAP23 is also present in the plasma membrane of muscle fibres a dilation mask of 1 μm was set from the inside of the plasma membrane outwards to account for the area occupied by the plasma membrane. This mask was then used to quantify the FI of SNAP23 in the plasma membrane area by measuring optical density and normalised to the area covered by the plasma membrane.

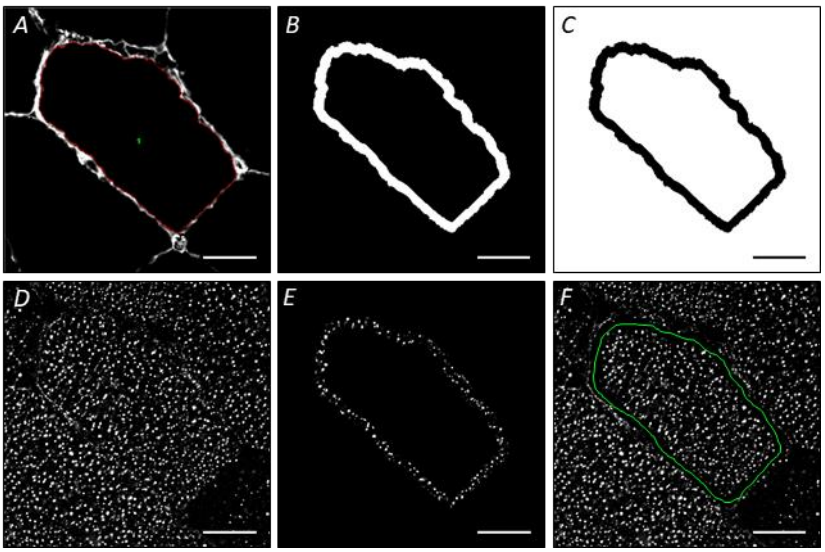

Figure 3.1. Image analysis method for assessing IMTG and protein expression in cross-sectional muscle fibres. Images for content analysis were obtained at 1.1x zoom on a 63x 1.4NA confocal microscope. Grey scale images of the cell border identified with laminin (*A*) and of LD stained with BODIPY 493/503 (*D*). Erosion mask of 5 µm applied from the cell border to produce a peripheral region mask (*B*). Peripheral erosion mask inverted to create a mask for the central region of the cell (*C*). Masks B and C were applied to greyscale image of LD to produce extracted images of LD in the peripheral region of the cell (*E*) and the central region of the cell (*F*). Freehand ROI (green line) was manually drawn around central region of the cell to exclude LD from neighbouring cells (*F*). A selected intensity threshold was then applied to extracted images to represent positive signal for LD or PLIN proteins and the data was extracted to reveal percentage of area stained (IMTG and PLINs) as well as LD density (number of LDs expressed relative to area) and LD size (mean area of individual LDs). White bar = 25µm. For SNAP23 and mitochondria, fluorescence intensity measurement was applied to extracted peripheral and central images of SNAP23 and COX stain.

As previously described (Shepherd *et al.*, 2012, 2013; Strauss *et al.*, 2016), before any colocalisation analysis was undertaken controls were included to confirm absence of 1) bleed through of fluorophores in opposing channels when single staining was performed, 2) non-specific secondary antibody binding, and 3) sample autofluorescence. For colocalisation analysis of PLIN proteins with LD, images were obtained at 4x digital zoom applied to both the centre region and the peripheral region of type I and type IIa muscle fibres pre and post the HFHC diet (n=10 images per region, per fibre-type, pre and post HFHC diet, per participant, equating to a total of 80 images for each participant for each staining protocol; Figure 3.2). Object-based colocalisation analysis was performed separately for PLIN2, PLIN3 and PLIN5 with LD, as previously described (Shepherd *et al.*, 2012, 2013; Shepherd *et al.*, 2017b). Briefly, a selected intensity threshold was used to denote a positive signal for each PLIN protein of interest and LD. These thresholds were used to produce binary images of the PLIN protein and LD used for the colocalisation analysis (Figure 3.2B and C). Binary images were merged to produce a colocalisation map and overlapping regions extracted to a separate image (Figure 3.2D and E). The number of extracted objects was calculated and expressed relative to area to represent the number of PLIN-associated LD (PLIN+ LD). The number of extracted objects was subtracted from the total number of LD and expressed relative to area to represent the number of LD not associated with PLIN (PLIN- LD). Additionally, the number of extracted objects was subtracted from the total number of PLIN objects and expressed relative to area to identify the amount of free PLIN protein not associated with LD. The fraction of PLIN protein colocalising to LD was also reported. When conducting the colocalisation analysis, if there were multiple PLIN objects localised to a single LD this was classified as one colocalisation count, in order to avoid over estimation of PLIN+ LD.

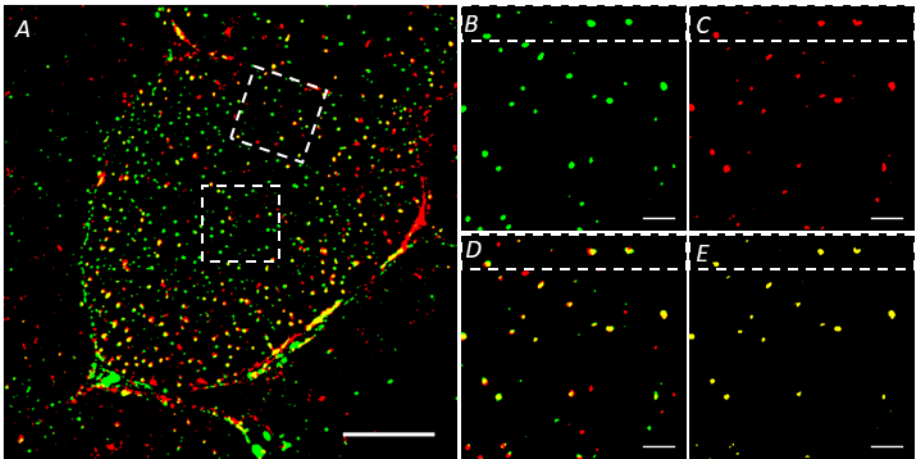

Figure 3.2. Colocalisation analysis between LD and PLIN5. Images for colocalisation analysis were obtained using a 63x 1.4NA confocal microscope at 4x digital zoom at the central and peripheral region of the cell indicated by the two white boxes (*A*). LD were stained with BODIPY 493/503 (green*; B*), PLIN5 was stained red (*C*) and subsequent merged images (*D*) were used to calculate colocalisation. The overlapping area of LD and PLIN5 was extracted (*E*) to calculate the number of PLIN5+ LD and PLIN5- LD relative to the area of interest. White box in images *B-E* represent the peripheral area that was analysed when images at the periphery were obtained. White bar = 25µm (*A*) and 5 µm (*B-E*). The same method was repeated for colocalisation analysis between LD with PLIN2 and PLIN3.

Cross-sectional images at 1.1x digital zoom of type I and type IIa muscle fibres pre and post the HFHC diet were obtained for SNAP23 colocalisation analysis with; plasma membrane, mitochondria and LD (*n*=10 per fibre-type, pre and post diet, per participant, equating to a total of 40 images for each participant for each separate staining protocol; Figure 3.3). For SNAP23 colocalisation analysis, individual type I or type IIa fibres were first isolated from the rest of the image (Figure 3.3) to avoid interference of data from non-type I or non-type IIa fibres respectively. Pearson colocalisation correlation coefficient (PCC) analysis were then performed on SNAP23 with; plasma membrane, mitochondria or LD in a series of separate analysis as previously described (Strauss *et al.*, 2016). At present, it is unclear whether SNAP23 colocalisation to the plasma membrane is homogenous throughout the muscle fibre. PCC analyses allow for proteins of interest to be analysed within the entirety of the cross-sectional area of the imaged muscle fibre. These analyses are consequently more suitable when analysing colocalisation of SNAP23 to the plasma membrane that surrounds the entire cell. The SNAP23 channel was overlapped with either a channel of; plasma membrane, mitochondria or LD and PCC was assessed of the whole cell (Figure 3.3A-C) using Image Pro Plus 5.1 Software (Media Cybernetics). To confirm SNAP23 colocalisation to each of the variables during image analysis SNAP23 stain was paired with non-matched images of either the plasma membrane, LD or mitochondria (Table 3.2) as previously described (Lachmanovich *et al.*, 2003).

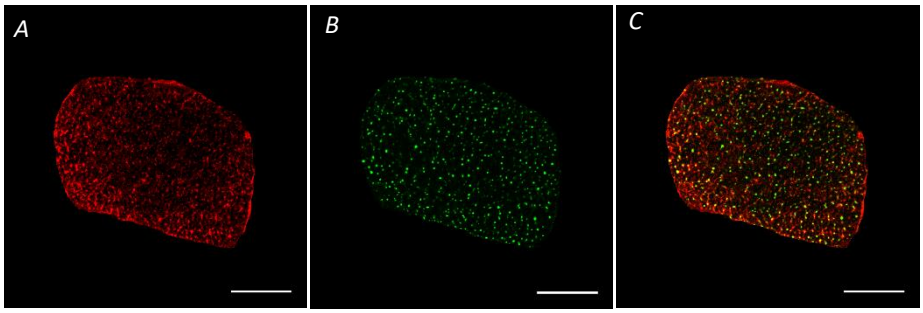

Figure 3.3. Colocalisation analysis between SNAP23 and LD. Images for colocalisation analysis were obtained at 1.1x zoom on a 63x 1.4NA confocal microscope. Cells of interest was isolated so that type I and IIa fibres could be studied separately. SNAP23 stained red (*A*) and LD stained with BODIPY 493/503 (green; *B*). Raw images of SNAP23 and LD were merged (*C*) and Pearson's correlation coefficient was calculated to reveal the degree of colocalisation between SNAP23 and LD. White bar = 25μm. The same process was repeated for SNAP23 with the plasma membrane (dystrophin stain) and mitochondria (COX stain).

3.3.6 Statistics

All data is reported as the mean ± SEM. Significance was set at $P < 0.05$. A linear mixed-effects model with fixed effects for fibre-type (type I vs type IIa vs type IIx), region (central vs peripheral) and time (pre vs post HFHC diet) and random effects to account for repeated measurements within subjects was used. Significant main effects or interaction effects were assessed using Bonferroni adjustment *post hoc* analysis.

3.4 Results

3.4.1 Body Mass

The 7 day HFHC diet caused a significant increase in body mass from pre (76.4 ± 3.3 kg) to post diet (77.7 ± 3.4 kg; $P < 0.001$). Each participant experienced an increase in body weight demonstrating the diet was effective in being hypercaloric.

3.4.2 Insulin sensitivity and insulin signalling

3.4.2.1 Oral glucose challenge

Following 7 days HFHC diet glucose AUC significantly increased (+10%; $P = 0.007$) and there was a trend towards an increased insulin AUC (+17%; $P = 0.086$; Table 3.1). Whole-body insulin sensitivity as measured by the Matsuda index significantly decreased (-23%; $P = 0.006$; Table 3.1).

Table 3.1 Effect of a 7 day high-fat high-calorie diet on an oral glucose challenge

	Pre	Post
Glucose AUC (mmol.L^{-1} (120 min)$^{-1}$)*	648 ± 23	712 ± 24
Insulin AUC (μIU.mL^{-1} (120 min^{-1})	4979 ± 690	5834 ± 17
Matsuda ISI*	6.25 ± 0.75	4.82 ± 2.54

Data provided as means ± SEM. AUC, area under the curve; ISI, insulin sensitivity index. * Significant difference from pre to post diet $P < 0.05$.

3.4.2.2 Insulin signalling

Phosphorylation of AS160 ser588 and thr642, and Akt ser473 and thr308 increased from 0 to 30 minutes during the oral glucose challenge (Figure 3.4) ($P < 0.05$), however this was not impaired following 7 days HFHC diet. Phosphorylation of AS160 thr642 remained elevated 120 minutes into the oral glucose challenge whereas phosphorylation of Akt ser473 and thr308 significantly decreased from 30 to 120 minutes ($P < 0.001$). There was a significant interaction effect for HFHC diet and oral glucose challenge for phosphorylation of AS160 ser588 ($P = 0.035$). Pre HFHC diet phosphorylation of AS160 ser588 remained elevated from 30 to 120 min into the oral glucose challenge whereas after the HFHC diet phosphorylation of AS160 ser588 returned to baseline after 120 min ($P = 0.011$).

3.4.3 IMTG analysis

At baseline, type I fibres had greater IMTG content (expressed as percentage of fibre stained) in comparison to type IIa ($P = 0.006$) and type IIx fibres ($P < 0.001$), although there was no difference between type IIa and type IIx fibres ($P = 0.467$; Figure 3.5A). There was also no significant differences in IMTG content at baseline between the peripheral and central region of the cell ($P = 0.399$). Following HFHC diet there was an increase in IMTG content that was exclusive to type I fibres only (+101%; $P < 0.001$), and this occurred in both the peripheral (+89%; $P < 0.001$) and central regions (+103; $P < 0.001$). Although overall IMTG content did not increase in type IIa or IIx fibres, IMTG content did increase in the peripheral region of both fibres following HFHC diet (type IIa fibres +117%; $P = 0.016$; and type IIx fibres +134%; $P =0.016$). Consequently, following HFHC diet IMTG content was greater in the peripheral region of muscle fibres compared to the central region ($P = 0.022$).

The increase in IMTG content in type I fibres was due to an increase in both LD size (+44%; $P < 0.001$; Figure 3.5B) and LD density (+43%; $P < 0.001$; Figure 3.5C) in

both muscle fibre regions. Although overall IMTG content was not augmented by HFHC diet in type IIa and type IIx fibres, we did observe an increase in LD size in both the peripheral (+36% and +30% for type IIa and IIx respectively; $P < 0.01$) and central region (+47% and +46% for type IIa and IIx fibres respectively; $P < 0.001$) of these fibres. LD density increased in the peripheral region of type IIa fibres (+57%; $P = 0.014$) and there was a trend towards an increase in the peripheral region of type IIx fibres (+48%; $P = 0.074$). There were no changes in LD density in the central region of type IIa fibres ($P = 0.376$) and type IIx fibres ($P = 0.140$) after HFHC diet.

3.4.4 PLIN protein expression

3.4.4.1 PLIN2

At baseline PLIN2 protein expression (expressed as percentage of fibre stained) was significantly greater in type I fibres in comparison to type IIa ($P = 0.048$) and type IIx fibres ($P = 0.019$), however, there was no difference between type IIa and type IIx fibres ($P = 0.112$; Figure 3.6A). There was a trend towards PLIN2 protein expression being greater in the peripheral region compared to the central region at baseline ($P = 0.060$; Figure 3.6A). Following the HFHC diet there was no significant increase in PLIN2 protein expression in any fibre types or any region.

3.4.4.2 PLIN3

In type I fibres PLIN3 protein expression tended to be higher in comparison to type IIa fibres ($P = 0.077$) and was higher compared to type IIx fibres ($P = 0.021$; Figure 3.6B). There were no differences in PLIN3 protein expression between type IIa and IIx fibres ($P = 0.099$). There was a trend towards more PLIN3 in the peripheral region of the muscle fibres compared to the central region ($P = 0.062$; Figure 3.6B). Following HFHC diet there was an increase in PLIN3 protein expression in type I fibres only (+50%; $P = 0.010$), which tended to occur in both the peripheral (+35%; $P = 0.081$) and central region of the muscle fibre (+58%; $P = 0.095$). The increase in type I fibres resulted in a significantly higher PLIN3 protein expression in type I fibres

compared to type IIa (P = 0.001) and IIx (P < 0.001) after the HFHC diet. Although overall PLIN3 protein expression in type IIa fibres did not change there was an increase in PLIN3 protein expression in the peripheral region of type IIa fibres (+58%; P = 0.043).

3.4.4.3 PLIN5

At baseline there was significantly more PLIN5 protein expression in type I fibres compared to type IIa (P = 0.001) and type IIx (P = 0.001), although there were no differences between type IIa and IIx fibres (P = 1.000; Figure 3.6C). PLIN5 protein expression was also greater in the peripheral region of the muscle fibres compared to the central region (P = 0.001). Overall PLIN5 protein expression did not increase with HFHC diet (P = 0.342), although there was a trend towards an increase in type I fibres (+28%; P = 0.099).

3.4.4 Lipid droplet and PLIN protein colocalisation

Colocalisation analysis was only conducted on type I and IIa fibres due to insufficient type IIx fibres being acquired during image capture.

3.4.4.1 PLIN2

At baseline the fraction of PLIN2 colocalising to LD was higher in type I fibres (0.41 ± 0.04) compared to type IIa (0.31 ± 0.04; P = 0.001), with no differences between the central region (0.36 ± 0.04) and the peripheral region (0.36 ± 0.04; P = 0.918). Following the HFHC diet there was an increase in the fraction of PLIN2 colocalising to LD in type I fibres only (+26%; P =0.001), due to increases in both the peripheral (32%; P = 0.006) and central regions (+25%; P = 0.031). At baseline type I fibres had significantly more PLIN2+ LD in comparison to type IIa fibres (P = 0.001) and there was more PLIN2+ LD in the peripheral region of muscle fibres compared to the central region (P < 0.001; Figure 3.7A). Following the HFHC diet there was an increase in PLIN2+ LD in type I fibres only (+80%; P = 0.005; Figure 3.7A), due to increases in both the peripheral (+78%; P = 0.002) and the central regions (+83%; P = 0.017;

Figure 3.6A). There were more PLIN2- LD in type I compared to type IIa fibres (P < 0.001), but no difference in the proportion of PLIN2- LD in the peripheral and central region of muscle fibres at baseline (P = 0.446; Figure 3.7B), and this relationship did not change with the HFHC diet. At baseline the peripheral region of muscle fibres had higher amounts of free PLIN2 (0.065 ± 0.005 μm^{-2}) compared to central (0.041 ± 0.004 μm^{-2}; P < 0.001), however there were no differences between fibre types and this was unaltered after the HFHC diet.

3.4.4.2 PLIN3

At baseline the fraction of PLIN3 colocalising to LD was higher in type I fibres (0.32 ± 0.03) compared to type IIa (0.22 ± 0.04; P < 0.001), with no differences between the central region (0.26 ± 0.04) and the peripheral region (0.28 ± 0.04; P = 0.628). Following the HFHC diet there was an increase in the fraction of PLIN3 colocalising to LD in both type I fibres (+44%; P < 0.001) and type IIa fibres (+39%; P = 0.002). In type I fibres this was due to increases in both the peripheral (60%; P < 0.001) and central regions (29%; P = 0.012). In type IIa fibres however only the central region observed a significant increase (66%; P = 0.001). Type I fibres had significantly more PLIN3+ and PLIN3- LD in comparison to type IIa fibres (P < 0.001), but the proportion of PLIN3+ and PLIN3- LD in the peripheral and central region of muscle fibres was not different (P = 0.219; Figure 3.7C-D). The HFHC diet did not change the number of PLIN3+ LD. However, following the HFHC diet there was a significant increase in PLIN3- LD in both type I (+58%; P < 0.001) and type IIa fibres (+43%; P = 0.017; Figure 3.7D). In type I fibres the increase was observed in both the peripheral (+69%; P < 0.001) and central regions (+47%; P = 0.001), whereas in type IIa fibres there was an increase in the peripheral region (+40%; P = 0.026) and a strong trend towards an increase in the central region (+48%; P = 0.050; Figure 3.7D). There was no difference in free PLIN3 in any fibre type or any region at baseline. The HFHC diet reduced free PLIN3 in type I fibres (0.071 ± 0.006 to 0.050 ± 0.008 μm^{-2}; P = 0.010)

in the peripheral region (-36%; *P* = 0.002), and free PLIN3 tended to be lower in the central region (-23%; *P* = 0.093). There was also a trend towards a decrease in free PLIN3 in type IIa fibres (0.064 ± 0.007 to 0.051 ± 0.008 μm^{-2}; *P* = 0.098).

3.4.4.3 PLIN5

At baseline the fraction of PLIN5 colocalising to LD was similar between type I fibres (0.56 ± 0.04) and type IIa (0.49 ± 0.04; *P* = 0.095), with no differences between the central region (0.54 ± 0.04) and the peripheral region (0.50 ± 0.04; *P* = 0.416). Following the HFHC diet there was an increase in the fraction of PLIN5 colocalising to LD in both type I fibres (+27%; *P* = 0.001) and type IIa fibres (+19%; *P* = 0.027), due to similar increases in central and peripheral region for both fibre types. There was more PLIN5+ LD in type I compared to type IIa fibres (*P* < 0.001) and in the peripheral region compared to the central region (*P* < 0.001), but this relationship was unchanged with the HFHC diet (Figure 3.7E). The number of PLIN5- LD was not different between fibre types, although there was a trend towards more PLIN5- LD in the peripheral compared to the central region of muscle fibres (*P* = 0.097; Figure 3.7F). Following the HFHC diet there was no change in PLIN5- LD however there was a trend towards an interaction effect (*P* = 0.054) due to a trend towards an increase in PLIN5- LD in type I fibres only (+22%; P = 0.069; Figure 3.7F). Free PLIN5 was significantly higher in type I (0.037 ± 0.003 μm^{-2}) in comparison to type IIa fibres (0.028 ± 0.003 μm^{-2}; *P* = 0.003) and in the peripheral region across fibre types (0.040 ± 0.003 μm^{-2}) compared to the central region (0.025 ± 0.003 μm^{-2}; *P* < 0.001) and this was unaltered with the HFHC diet.

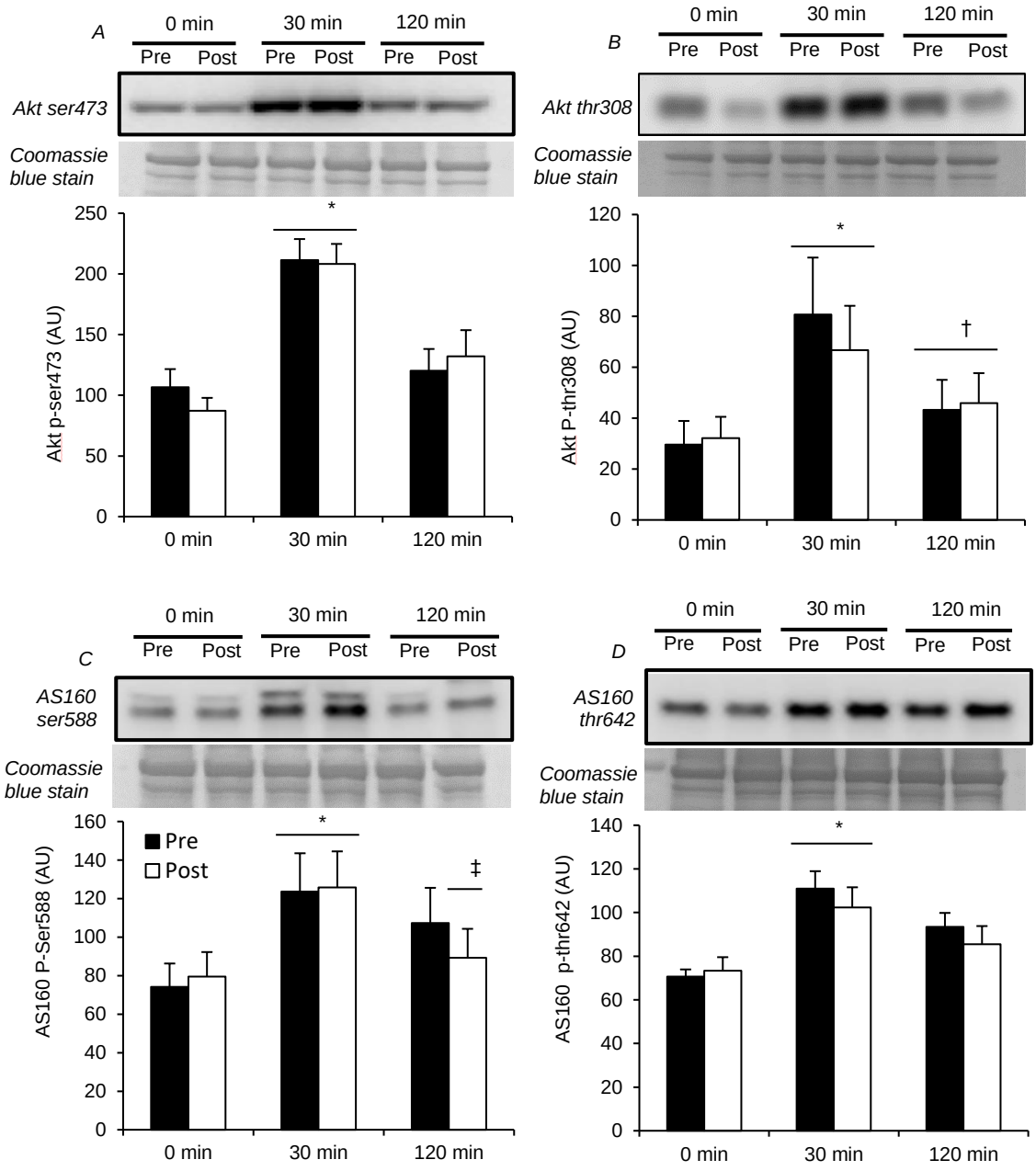

Figure 3.4 Phosphorylation of key insulin signaling intermediates is not impaired following 7 days HFHC diet. Representative western blots of Akt ser473 (A), Akt thr308 (B), AS160 ser588 (C) and AS160 thr642 (D) with coomassie blue stain to show equal loading of proteins. Phosphorylation of Akt ser473 (A), Akt thr308 (B), AS160 ser588 (C) and AS160 thr642 (D) increased from 0 to 30 minutes during the oral glucose challenge and this response was not impaired following 7 days HFHC diet. * Significant increase in phosphorylation from 0 to 30 min ($P < 0.05$). † Significant decrease in phosphorylation from 30 min to 120 min ($P < 0.05$). ‡ Significant interaction effect for HFHC diet and time point 120 min ($P < 0.05$).

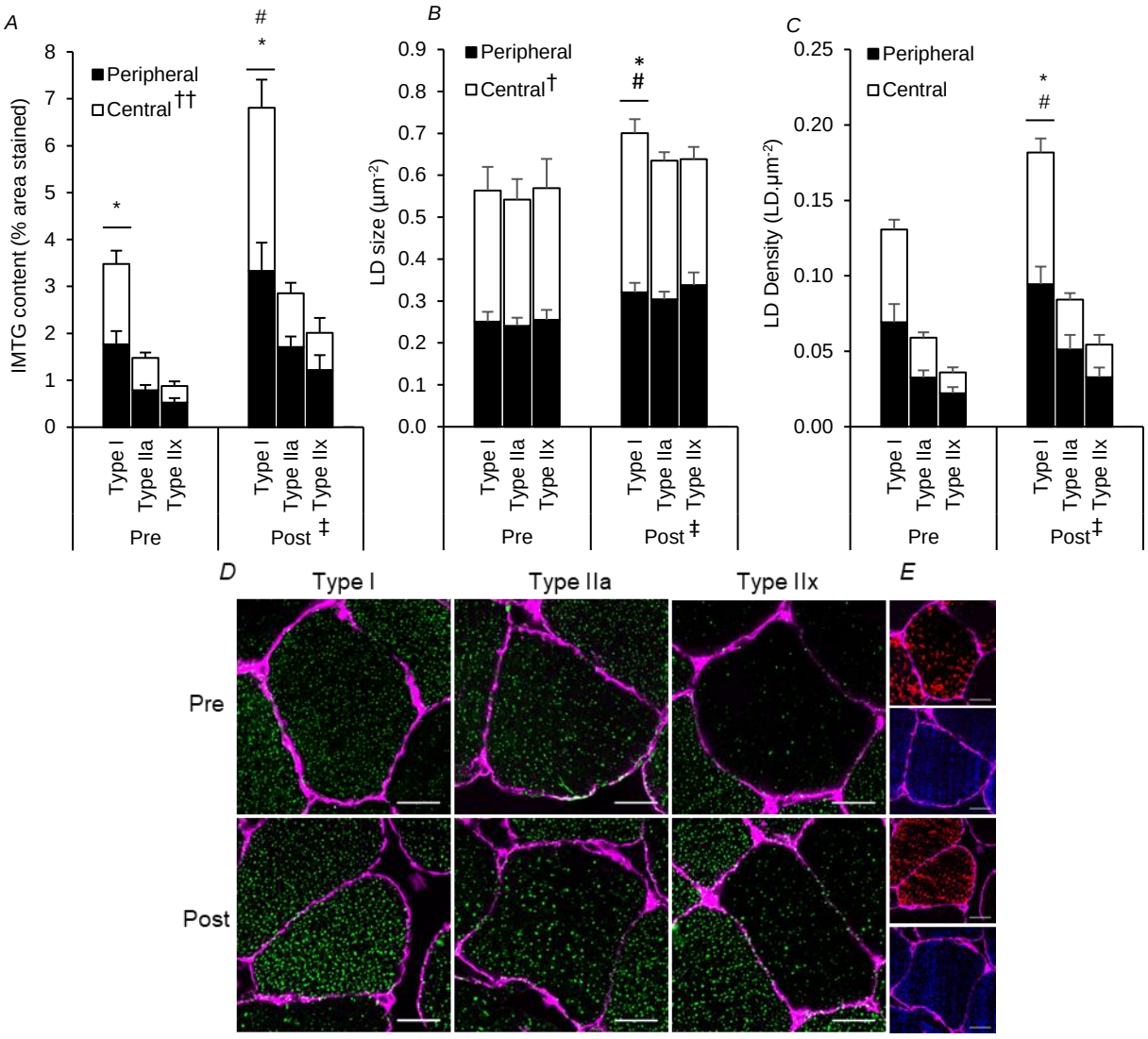

Figure 3.5. 7-days HFHC diet induces increases in IMTG content in type I fibres due to increases in LD density and size. 7 days HFHC diet increases type I fibre IMTG content (*A*), LD density (*B*) and LD size (*C*). Representative images of IMTG content pre and post HFHC diet in different fibre types obtained from confocal microscope with a 63x oil immersion objective and 1.1 digital zoom (*D*). Corresponding images of myosin heavy chain (MHC I) (stained red for type I fibres) and myosin heavy chain (MHC IIa) (stained blue for type IIa fibres), any fibres without a positive red or blue stain were assumed to be type IIx fibres (*E*). White bars represent 25 µm.* Significant difference for type I fibres *vs* type IIa and IIx fibres ($P < 0.001$). ‡ Significant difference for HFHC diet ($P < 0.01$). † Significant difference for central *vs* peripheral region ($P < 0.01$). †† Significant difference for central vs peripheral region after HFHC diet only ($P < 0.05$). # Significant interaction between fibre type and HFHC diet ($P < 0.001$).

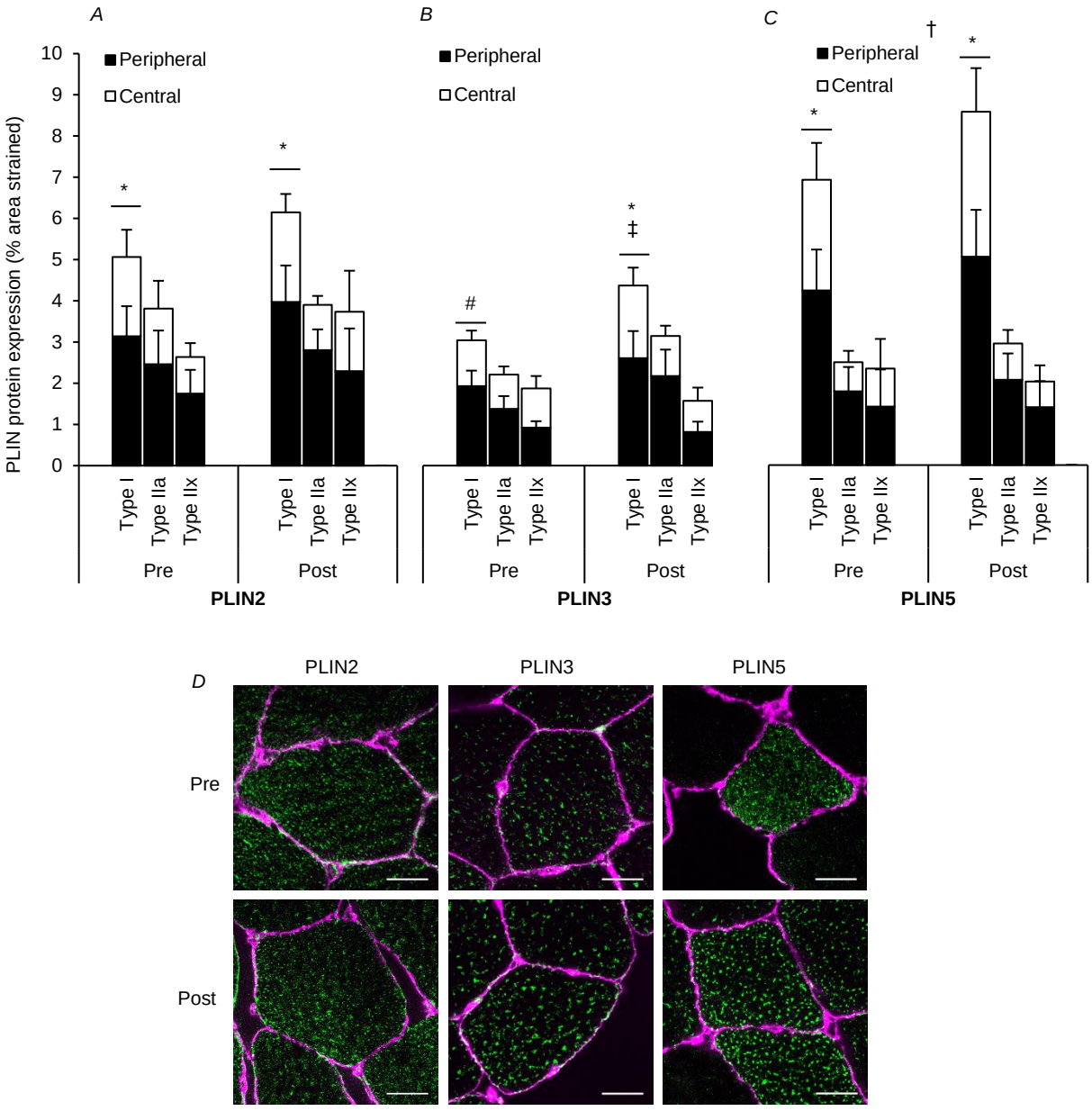

Figure 3.6. PLIN protein expression after pre and post 7 days HFHC diet. 7 days HFHC diet does not alter PLIN2 (*A*) or PLIN5 (*C*) protein expression but increases PLIN3 protein expression in type I fibres only (*B*). Representative images of PLIN2, PLIN3 and PLIN5 protein expression pre and post the HFHC diet in type I fibres obtained from confocal microscope with a 63x oil immersion objective and 1.1 digital zoom (*D*). White bars represent 25 µm. * Significant difference for type I fibres *vs* type IIa and IIx fibres ($P < 0.05$). # Significant difference for type I fibres *vs* IIx fibres ($P < 0.05$). †Significant difference for peripheral region vs central region ($P < 0.01$). ‡ Significant difference for HFHC diet ($P < 0.01$).

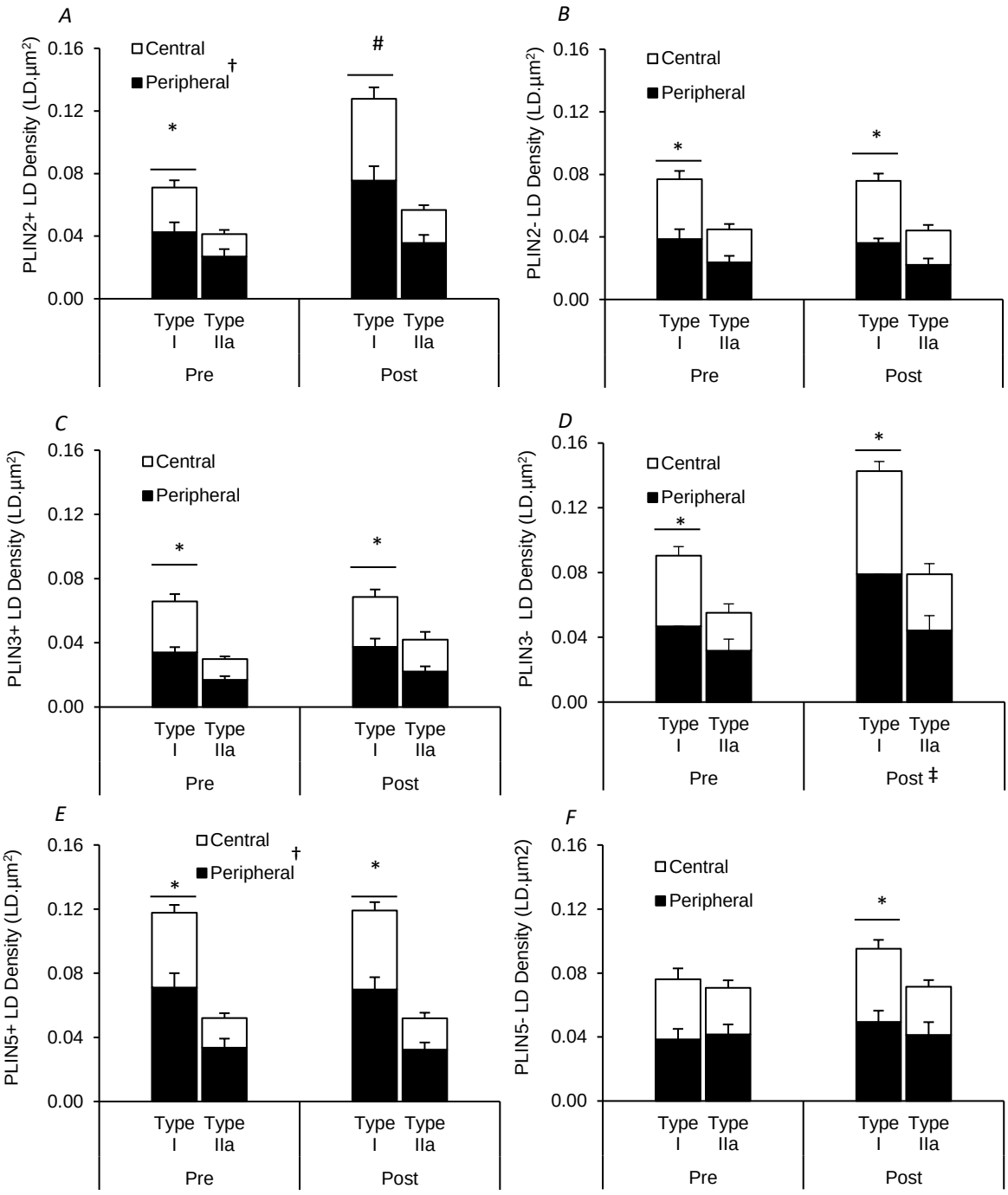

Figure 3.7. HFHC diet increases PLIN2+ LD in type I fibres only. 7 days HFHC diet increased PLIN2+ LD in type I fibres (*A*), whilst there were no changes in PLIN3+ LD (*C*) or PLIN5+ LD (*E*). PLIN2- LD (*B*) and PLIN5- LD (*F*) were not altered with the HFHC diet, whereas PLIN3- LD significant increased (*D*).* Significant difference for type I fibres *vs* type IIa ($P < 0.01$). ‡ Significant difference for peripheral region vs central region ($P < 0.001$). ‡ Significant difference for the HFHC diet ($P < 0.05$). # Significant interaction effect between fibre type and the HFHC diet ($P < 0.001$).

3.4.5 SNAP23 and COX fluorescence intensity

3.4.5.1 Mitochondria

COXIV protein expression, representing mitochondrial density, displayed a hierarchical fibre type distribution such that type I fibres (64 ± 8 AU) was significantly higher in comparison to type IIa (55 ± 7 AU; P = 0.034), and type IIa fibres was significantly higher than type IIx fibres (52 ± 8; P = 0.030). There was also greater COXIV protein expression in the peripheral region (70 ± 4 AU) compared to the central region across fibres (55 ± 3 AU; P < 0.001). Following the HFHC diet there was no change in COXIV protein expression in any fibre type or any region.

3.4.5.2 SNAP23

SNAP23 protein expression was only conducted on type I and IIa fibres due to insufficient type IIx fibres being acquired during image capture. SNAP23 protein expression was similar between type I (24 ± 6 AU) and type IIa fibres (23 ± 5 AU; P = 0.469). There was greater SNAP23 protein expression in the plasma membrane (35 ± 4 AU) region (P < 0.001; in comparison to both peripheral (27 ± 3 AU) and central region (21 ± 2 AU) and in the peripheral compared to the central region (P = 0.004) and this was unaltered after HFHC diet.

3.4.6 SNAP23 colocalisation

Colocalisation data was reported as PCC (the degree of colocalisation between the intensities of images representing SNAP23 and either; plasma membrane LD and mitochondria; Figure 3.8)

3.4.6.1 SNAP23 and the plasma membrane

At baseline there was no significant difference between fibre types for the colocalisation of SNAP23 with the plasma membrane for PCC (P = 0.850; Table 3.2) and this relationship was unchanged after the HFHC diet.

3.4.6.2 SNAP23 and LD

At baseline there was no significant difference between fibre types for the colocalisation of SNAP23 with LD as measured by PCC (P = 0.172; Table 3.2) and this was unaltered after the HFHC diet.

3.4.6.3 SNAP23 and Mitochondria

At baseline type I fibres in comparison to type IIa fibres had significantly more colocalisation between SNAP23 and mitochondria measured by PCC (P = 0.024; Table 3.2) and this did not change following the HFHC diet.

Table 3.2. Pearson's Correlation coefficients of SNAP23 colocalisation to; the plasma membrane, lipid droplets and mitochondria

			PCC
Plasma Membrane	Pre	Type I	0.27 ± 0.01
		Type IIa	0.27 ± 0.02
	Post	Type I	0.26 ± 0.02
		Type IIa	0.25 ± 0.02
	Non-matched pairs		0.08 ± 0.02†
Lipid Droplets	Pre	Type I	0.38 ± 0.02
		Type IIa	0.40 ± 0.03
	Post	Type I	0.36 ± 0.03
		Type IIa	0.38 ± 0.04
	Non-matched pairs		0.21 ± 0.02†
Mitochondria	Pre	Type I	0.66 ± 0.03
		Type IIa	0.62 ± 0.03*
	Post	Type I	0.65 ± 0.03
		Type IIa	0.61 ± 0.03*
	Non-matched pairs		0.14 ± 0.02†

Data provided as means ± SEM (n = 10 per fibre type per time point per participant). PCC, Pearson's correlation coefficient. * indicates difference in fibre type (P < 0.05). † indicates non-matched pairs significantly different from matched pairs.

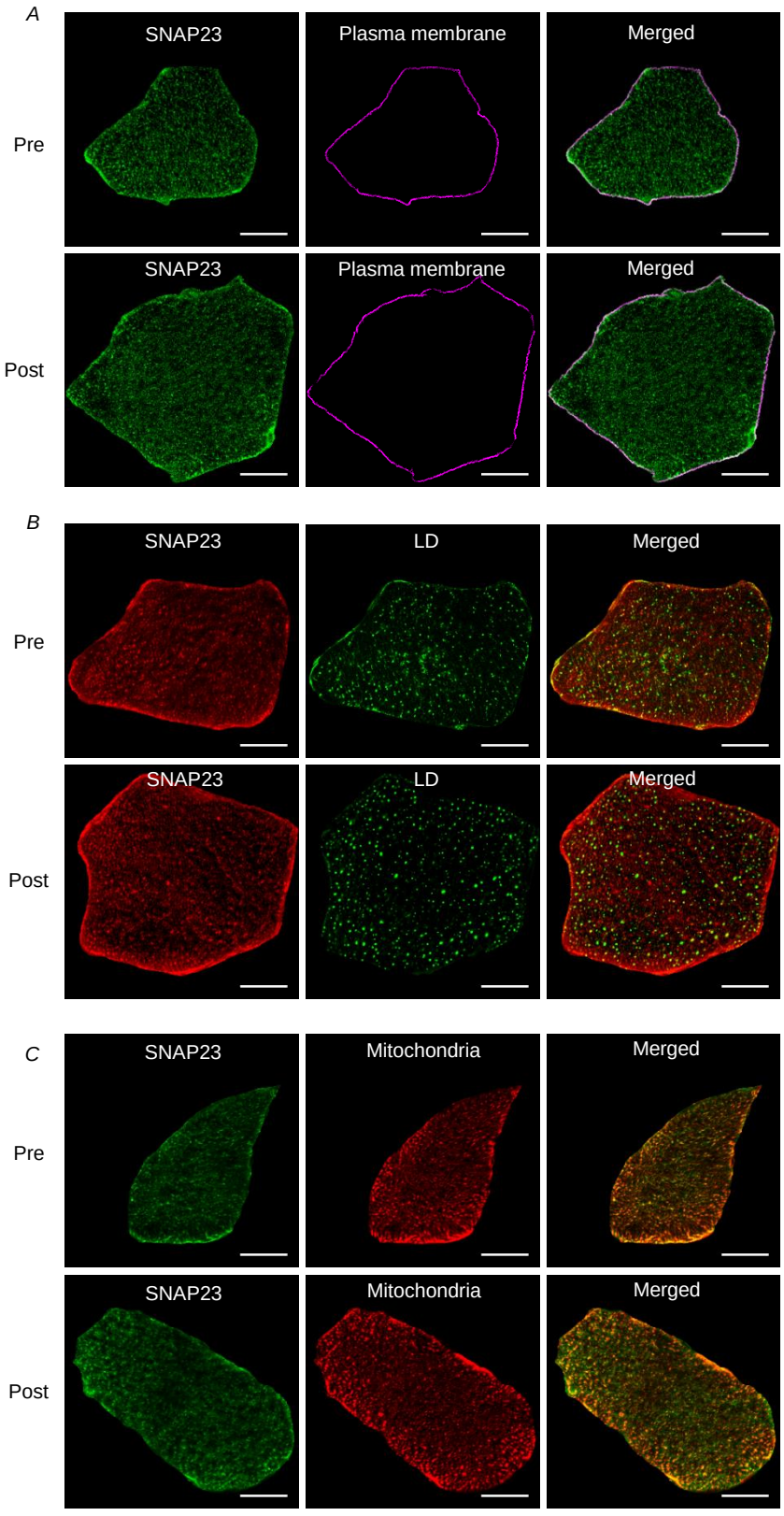

Figure 3.8 Representative images of SNAP23 distribution pre and post 7 days HFHC diet. Representative images of SNAP23 distribution with plasma membrane (*A*), LD (*B*) and mitochondria (*C*) pre and post 7 days HFHC diet in type I fibres obtained from confocal microscope with a 63x oil immersion objective and 1.1 digital zoom. White bars represent 25 µm.

3.5 Discussion

The aim of the present study was to examine the effects of 7 days HFHC diet in healthy individuals on IMTG content (LD number and morphology) and the expression and subcellular distribution of key proteins related to lipid metabolism. To add context to the findings the effects of 7 days HFHC diet on whole body insulin-sensitivity and skeletal muscle insulin resistance are also discussed. The first major finding was that the HFHC diet increased IMTG content exclusively in type I fibres, due to an increase in both LD size and density. PLIN3 was the only PLIN protein to exhibit increased expression after 7 days HFHC diet, but this was not mirrored by an increase in PLIN3+ LD. Rather, we observed an increased number of PLIN2+ LD in type I fibres. SNAP23 colocalisation to LD, mitochondria or the plasma membrane was not altered following 7 days HFHC diet. We examined these adaptations in the context of decreased whole-body insulin sensitivity (as measured by the Matsuda ISI), but this occurred without impairments in the activation of key intermediates of the skeletal muscle insulin signalling cascade. Together, the data shows that following high-fat, high-calorie feeding IMTG storage is enhanced most likely due to increases in PLIN3 protein expression and PLIN2+ LD, and these adaptations may contribute to the maintenance of the skeletal muscle insulin signalling cascade.

Following the HFHC diet glucose tolerance and whole body insulin sensitivity as measured by the Matsuda index was significantly reduced. The Matsuda index was originally designed to be implemented with results derived from a 75g oral glucose tolerance test (Matsuda & DeFronzo, 1999), however in the current study the results were derived from a 50g glucose load with 15 g whey protein. Tracer-derived measurements of insulin sensitivity from the oral glucose challenge analysed in a parallel study (Parry et al., in preparation) shows a reduced metabolic clearance rate (-15%) likely due to reduced uptake in skeletal muscle. These findings of reduced glucose clearance and insulin sensitivity are contradictory to chapter 2 where no

reductions in insulin sensitivity were observed following the same HFHC diet protocol, thus highlighting different a heterogeneous response to the diet protocol. During the current study there were no impairments in phosphorylation of key insulin signalling intermediates (AS160 and Akt) during the oral glucose challenge following the HFHC diet. This suggests that the reduction in insulin sensitivity observed in this current study were not due to lipid metabolite induced disruption of skeletal muscle insulin signalling.

The influx of FA from the diet appear to be instead directed to IMTG stores. The finding that IMTG content increases following high-fat high-calorie feeding is in line with previous studies investigating the short-term effects of a eucaloric or hypercaloric high-fat diet (Schrauwen-Hinderling *et al.*, 2005; Gemmink *et al.*, 2017a). Furthermore, we demonstrate for the first time that IMTG content is augmented exclusively in type I fibres. IMTG accumulation following 6 h lipid infusion during a hyperinsulinaemic-euglycaemic clamp is also specific to type I fibres (Shepherd *et al.*, 2017b), and it is now evident from the current results that this pattern of fibre-type specific accretion continues following more chronic lipid excess (7-days HFHC diet). Type I fibres are characterised by a higher mitochondrial content, higher abundance of lipolytic regulatory proteins and an enhanced ability to utilise IMTG stores during a bout of moderate-intensity exercise (Shepherd *et al.*, 2013; Watt & Cheng, 2017). Therefore, type I fibres are appreciably more equipped to store an influx of dietary FA as IMTG.

We also examined changes in IMTG content on a subcellular-specific basis, as well as exploring adaptations to LD morphology. In this respect, increased IMTG content in type I fibres following the HFHC diet occurred in both the peripheral and central region, and was due to an increase in both LD size and number. Seven days HFHC diet also augmented IMTG content specifically in the peripheral region of type IIa and IIx fibres which was again due to elevations in both LD size and number. Interestingly,

LD size was also greater following the HFHC diet in the central region of type IIa and IIx fibres, although this did not result in increased IMTG content. These distinct patterns of fibre and region-specific IMTG accumulation and changes in LD morphology are the first of their kind in the literature. Moreover, they are indicative of the progression of IMTG accumulation in muscle, whereby lipid accumulates in type I fibres prior to type IIa or IIx fibres, changes in LD size precede an increase in LD density, and this occurs in the peripheral region of the cell before the central region.

Increased IMTG content near the plasma membrane of muscle fibres has been associated with insulin resistance (Chee *et al.*, 2016) particularly if these IMTG stores are characterised by larger LD (Nielsen *et al.*, 2017; Daemen *et al.*, 2018). The accumulation of IMTG near the plasma membrane appears to be of detriment due to the close proximity of insulin signalling cascades. In particular, increases in LD size rather than number near the plasma membrane will be less favourable because larger LD have a lower surface area to volume ratio which is proposed to result in lower IMTG turnover and subsequent accumulation of lipid metabolites. In this study the peripheral region was defined to identify an area within the muscle fibres that was distinct from the central region of the cell but in close proximity to the plasma membrane and therefore near to insulin signalling and trafficking of FA into the myocyte. The predominant increase in IMTG stores occurred in type I fibres and this was accountable to an increase in LD size and number in both the peripheral and central regions. We propose that the beneficial increase in LD number observed in the peripheral region would help to maintain IMTG turnover and minimise the accumulation of lipid metabolites near the insulin signalling cascades located at the plasma membrane.

LD can increase in size by the following mechanisms: 1) coalescence of fusion of two LDs via pores in the phospholipid monolayer, 2) ripening of one LD through transfer of molecules from a LD decreasing in size, and 3) expansion of LD due to increased

synthesis of IMTG from FA (Gemmink *et al.*, 2017b). Increased IMTG synthesis has been hypothesised to increase LD size in such a way that increases distance between phospholipid molecules on the LD membrane thus permitting the binding of regulatory proteins such as PLIN proteins (Hesselink *et al.*, 2017). Recently Gemmink et al., (2016) found that LD size and number increased following acute elevation of FFA from prolonged fasting; however, this was entirely due to an increase in PLIN5+ LD. More importantly, the individuals in this study who had the highest increase in IMTG content also exhibited the smallest reduction in insulin sensitivity (Gemmink *et al.*, 2016). Therefore, larger LDs may not necessarily impede insulin sensitivity if they are decorated with PLINs.

In the present study PLIN3 protein expression increased in type I fibres only. PLIN3 has been linked to formation of new LD following lipid loading in cultured differentiated adipocytes (Wolins *et al.*, 2005). If a similar role exists in skeletal muscle we might have expected to see an increase in PLIN3+ LD following the HFHC diet; however, only an increase in PLIN3- LD was observed. There was however a reduction in free PLIN3 in type I fibres with an increase in the fraction of PLIN3 colocalising to LD. This indicates that PLIN3 is targeted to LD that already have PLIN3 associated and therefore suggests that PLIN3 supports LD growth and stability, rather than increase in LD density in skeletal muscle. PLIN3 has also been observed in the mitochondria in skeletal muscle (Ramos *et al.*, 2014) and PLIN3 knockdown in primary myotubes strongly reduces FA oxidation (Covington *et al.*, 2015). We therefore cannot exclude the possibility that the increase in PLIN3 was related to mitochondrial adaptations.

Despite there not being an increase in PLIN2 protein content there was an increase in PLIN2+ LD in type I fibres. This occurred without a change in free PLIN2 but with an increase in the fraction of PLIN2 colocalising to LD in type I fibres. Together this data suggests that the proportion of PLIN2 that is already localised to LD is redistributed to newly formed LD. Previous research has shown an increase in

PLIN2+ LD without increases in PLIN2 protein expression in trained individuals following lipid infusion (Shepherd *et al.*, 2017b), highlighting that when there is sufficient PLIN2 in muscle fibres it can be redistributed to the expanded LD pool. PLIN2 is associated with LD biogenesis primarily in adipocytes (Wolins *et al.*, 2005) and cell culture studies (Imamura *et al.*, 2002). PLIN2 is localised at clusters in the cytoplasmic leaflet of the endoplasmic reticulum where LD biogenesis occurs (Robenek *et al.*, 2006). Muscle-specific overexpression of PLIN2 increases IMTG storage in rats fed a high-fat diet without accumulation of lipid metabolite DAG (Bosma *et al.*, 2012a). Newly-formed LD may therefore become associated with PLIN2 leading to an increase in PLIN2+ LD, and theoretically this may support IMTG storage rather than accumulation of lipid metabolites such as DAG.

There was a trend towards an increase in PLIN5 protein expression in type I fibres only. This is similar to finding of an increase in PLIN5 protein expression in whole muscle homogenates after 5 days HFHC diet (Gemmink *et al.*, 2017a). This increase in PLIN5 protein expression existed without an increase in PLIN5+ LD but with an increase in the fraction of PLIN5 colocalising to LD in type I fibres. This suggests that any increase in PLIN5 protein expression is directed to LD already associated with PLIN5. PLIN5 has been primarily associated with oxidative capacity (Koves *et al.*, 2013) and IMTG oxidation. For example PLIN5 protein expression is upregulated following endurance training (Louche *et al.*, 2013; Shepherd *et al.*, 2013) and during a moderate-intensity bout of exercise PLIN5+ LD are preferentially used (Shepherd *et al.*, 2013). Recent findings suggest that PLIN5 protein expression and lipid area fraction covered by PLIN5+ LD correlated positively with VO_{2max} and ex vivo fatty acid oxidation but not insulin sensitivity (Gemmink *et al.*, 2018). Increased LD content due to increases in PLIN5+ LD are associated with blunted reductions in insulin sensitivity following acute FFA elevation from prolonged fasting (Gemmink *et al.*, 2016). Given PLIN5's proposed role in regulating IMTG lipolysis, in the current study the increased

faction of PLIN5 to LD may function to support the consistent turnover of PLIN5+ LD pool and thus help to minimise accumulation of lipid metabolites.

The use of previously validated immunofluorescence microscopy techniques (Shepherd *et al.*, 2012, 2013; Shepherd *et al.*, 2017b) to examine fibre-type and region specific changes in IMTG content and perilipin protein expression in addition to colocalisation of PLIN proteins to LD following HFHC diet is a novel strength of this study. A limitation of this method however is that colocalisation analysis could only be conducted on a single PLIN protein with LD. We cannot exclude the possibility therefore that LD have multiple perilipin proteins colocalised to them. The increases observed in PLIN3- LD and PLIN5- LD could be due increases in LD coated with PLIN2. PLIN- LDs may also be newly formed LD that did not have sufficient PLIN associated to them to be detected by the lower detection limit of the microscope. Whether PLIN proteins work together or in isolation in regulating LD dynamics remain an avenue for future research.

Contrary to our hypothesis SNAP23 colocalisation to LD, mitochondria or the plasma membrane did not change with the HFHC diet. Treatment of cardiomyocytes with oleic acid increases the LD associated pool of SNAP23 and reduces SNAP23 content at the plasma membrane (Bostrom *et al.*, 2007), leading to the hypothesis that LD highjack SNAP23 from the plasma membrane to assist in LD fusion following lipid excess (Sollner, 2007). As 7 days of HFHC diet did not alter the distribution or localisation of SNAP23 it is likely that LD highjacking of SNAP23 in skeletal muscle occurs over longer time periods of lipid excess such as in obesity and the development of type 2 diabetes. Nevertheless we did observe an increase in LD size and therefore it is also plausible that there was sufficient SNAP23 within muscle fibres to regulate LD fusion if it occurred without the need to ‘highjack’ SNAP23 from the plasma membrane.

In conclusion, the present study has generated novel evidence that 7 days HFHC diet induces fibre type specific increases in IMTG stores primarily aided by an increase in PLIN3 protein expression and a redistribution of PLIN2 to LD. We propose that these adaptations prevent accumulation of lipid metabolites (FA-CoA, DAG and ceramides) known to disrupt the skeletal muscle insulin-signalling cascade and contribute to the development of skeletal muscle insulin resistance.

Chapter 4. Hormone sensitive lipase preferentially redistributes to lipid droplets associated with perilipin-5 in human skeletal muscle during moderate-intensity exercise.

4.1 Abstract

Hormone-sensitive lipase (HSL) and adipose triglyceride lipase (ATGL) control skeletal muscle lipolysis. ATGL is present on the surface of lipid droplets (LD) containing intramuscular triglyceride (IMTG) in both the basal state and during exercise. HSL translocates to LD in *ex vivo* electrically stimulated rat skeletal muscle. Perilipin-2 and perilipin-5 associated lipid droplets (PLIN2+ and PLIN5+ LD) are preferentially depleted during exercise in humans indicating these PLINs may control muscle lipolysis. We aimed to test the hypothesis that in human skeletal muscle *in vivo* HSL (but not ATGL) is redistributed to PLIN2+ and PLIN5+ LD during moderate-intensity exercise. Muscle biopsies from 8 lean trained males (age 21±1 years, BMI 22.6±1.2 $kg.m^{-2}$ and $\dot{V}o_{2peak}$ 48.2±5.0 $ml.min^{-1}.kg^{-1}$) were obtained before and immediately following 60 min of cycling exercise at ~59% $\dot{V}o_{2peak}$. Cryosections were stained using antibodies targeting ATGL, HSL, PLIN2 and PLIN5. LD were stained using BODIPY 493/503. Images were obtained using confocal immunofluorescence microscopy and object based colocalisation analyses were performed. Following exercise, HSL colocalisation to LD increased (P<0.05), and was significantly larger to PLIN5+LD (+53%) than to PLIN5-LD (+34%) (P<0.05), while the increases in HSL colocalisation to PLIN2+LD (+16%) and PLIN2-LD (+28%) were not significantly different. Following exercise the fraction of LD colocalised with ATGL (0.53 ± 0.04) did not significantly change (P<0.05) and was not affected by PLIN association to the LD. This study presents the first evidence of exercise-induced HSL redistribution to LD in human skeletal muscle and identifies PLIN5 as a facilitator of this mechanism.

4.2 Introduction

Intramuscular triglyceride (IMTG) stores provide a readily available source of energy during moderate-intensity exercise in healthy individuals. IMTG are stored within lipid droplets (LD) which are located in close proximity to mitochondria (Shaw *et al.*, 2008), which is believed to enable fatty acids (FA) liberated from IMTG to be efficiently shuttled to mitochondria to produce energy. Previously there was some debate as to whether IMTG was used during exercise because the presence of extramyocellular lipid deposits in muscle samples confounded measures of net changes in IMTG content in response to exercise (Watt *et al.*, 2002). Recent developments in confocal immunofluorescence microscopy have enabled the exclusion of extramyocellular lipid deposits and also permit fibre type-specific analyses to be performed. Using this approach, it is now well-established that IMTG stores are preferentially used from type I fibres in endurance-trained individuals during moderate-intensity exercise (van Loon *et al.*, 2003a; Shepherd *et al.*, 2013).

Hormone sensitive lipase (HSL) was previously believed to be the only rate-limiting enzyme responsible for triacylglycerol (TAG) lipolysis (Zechner *et al.*, 2009). However, it was shown that mice deficient in HSL accumulated diacylglycerol (DAG) in muscle and other tissues in response to fasting (Haemmerle *et al.*, 2002a), suggesting that other lipases must exist. Adipose triglyceride lipase (ATGL) was subsequently identified as a novel lipase which preferentially hydrolyses TAG (Zimmermann *et al.*, 2004). Moreover, overexpression of ATGL in human primary myotubes results in reduced TAG content and increased FA release and oxidation (Badin *et al.*, 2011), whilst ATGL-KO mice accumulate TAG in skeletal muscle (Haemmerle *et al.*, 2006). A pertinent role for ATGL in IMTG hydrolysis stems from the finding that IMTG breakdown still occurs in electrically stimulated rat muscle following acute pharmacological inhibition of HSL or in muscle of HSL-KO mice (Alsted *et al.*, 2013). Conversely, impairment of IMTG lipolysis during exercise in mice

with muscle specific deletion of ATGL was not profound enough to impact on submaximal or maximal exercise performance which may be due to a compensatory increase in HSL mediated TAG hydrolysis (Dube *et al.*, 2015). Together these data suggest that both ATGL and HSL mediate IMTG hydrolysis and both can compensate functionally when the other is absent. Muscle TAG and DAG accumulate in ATGL-KO and HSL-KO mice respectively (Haemmerle *et al.*, 2002a; Haemmerle *et al.*, 2006). This, in addition to HSL having a higher specificity for DAG as a substrate in comparison to TAG (Fredrikson *et al.*, 1981a), has led to the suggestion that ATGL and HSL hydrolyse IMTG in a sequential process in skeletal muscle. Importantly, ATGL and HSL together account for ~98% of contraction-induced TAG lipase activity in rat skeletal muscle (Alsted *et al.*, 2013).

HSL activity in skeletal muscle is increased during moderate-intensity exercise through protein phosphorylation induced by contraction and adrenergic signalling mechanisms (Watt *et al.*, 2003c; Watt *et al.*, 2006). In addition to regulation of HSL via phosphorylation, Prats et al. (2006) elegantly demonstrated using confocal immunofluorescence microscopy that HSL translocates to LD in rat skeletal muscle *ex vivo* following stimulation with adrenaline or during electrically-induced muscle contractions. Additional examination using immunogold transmission electron microscopy on single rat muscle fibres also generated images evidencing HSL accumulation beneath the LD phospholipid monolayer suggesting that once HSL translocates to the LD it subsequently penetrates the phospholipid monolayer to access IMTG (Prats *et al.*, 2006). Moreover, in this study the colocalisation of HSL to the LD-associated protein perilipin-2 (PLIN2) increased in response to both stimuli, implicating PLIN2 in the regulation of HSL translocation to the LD (Prats *et al.*, 2006). This was the first study to generate evidence of HSL translocation in muscle in response to lipolytic stimuli. It is yet to be determined, however, if a similar mechanism occurs in human skeletal muscle within an *in vivo* environment where the regulation

of HSL activity is under the control of multiple regulatory signalling factors that cannot be replicated *ex vivo*.

Under resting conditions a proportion of ATGL localizes to LDs in human skeletal muscle, and this relationship is unaltered by moderate-intensity exercise (Mason *et al.*, 2014a). It is therefore reasonable to postulate that ATGL is regulated on the LD surface by its co-activator protein, CGI-58 (Lass *et al.*, 2006). Indeed, electrical stimulation of rat skeletal muscle *ex vivo* augments the co-immunoprecipitation of ATGL and CGI-58 (MacPherson *et al.*, 2013a). The PLIN proteins are also believed to play a key regulatory role in controlling IMTG breakdown. Notably, the only member of the PLIN protein family that can bind ATGL is PLIN5, and in cells expressing PLIN5 both ATGL and CGI-58 are recruited to the LD under basal conditions (Wang *et al.*, 2011a) suggesting that PLIN5 plays an important role in determining the activity of ATGL. Although the majority of the available evidence from cell culture studies suggests that PLIN5 (and the other PLIN proteins) facilitate the storage of TAG under basal conditions (Listenberger *et al.*, 2007; Wang *et al.*, 2011a; Laurens *et al.*, 2016), PLIN5 has also been shown to promote TAG hydrolysis under conditions stimulating lipolysis in cultured cells (Wang *et al.*, 2011a). Furthermore, we previously reported that LD associated with PLIN2 or PLIN5 are preferentially utilised during 1 hour of moderate-intensity exercise (Shepherd *et al.*, 2012, 2013). Whether ATGL localises to those LDs with PLIN5 associated and therefore facilitate their preferential use during exercise is yet to be investigated.

Using confocal immunofluorescence microscopy we have previously developed methods to identify LD with (PLIN+ LD) or without PLIN associated (PLIN- LD) (Shepherd *et al.*, 2012, 2013). The aim of the present study was to extend these methods and investigate the localisation of the key lipolytic enzymes ATGL and HSL, with PLIN2 and PLIN5 associated LD under resting conditions and in response to an acute bout of exercise in trained human skeletal muscle. We hypothesised that

exercise would lead to an increase in HSL colocalisation to LDs, and that these LDs would have PLIN2 or PLIN5 associated. We also hypothesised that ATGL would already be colocalised to LD and these LD would be PLIN5 associated.

4.3 Methods

4.3.1 Participants and ethical approval

Archived muscle samples from a prior study of our laboratory comparing the effects of sprint interval and endurance training on IMTG utilisation during exercise (Shepherd *et al.*, 2013) were utilised in the present study. Specifically, muscle samples from 8 lean, healthy male volunteers (see Table 4.1 for brief subject characteristics) were analysed in the present study and the informed consent provided originally covered this subsequent use. The study was approved by the Black Country NHS research ethics committee (West Midlands, UK) and conformed to the standards set by Declaration of Helsinki.

Table 4.1 Subject characteristics	
Age (years)	21 ± 1
Height (m)	1.77 ± 0.03
Body mass (kg)	70.8 ± 4.5
BMI (kg m^{-2})	22.6 ± 1.2
$\dot{V}o_{2peak}$ (l min^{-1})	3.40 ± 0.38
$\dot{V}o_{2peak}$ (l min^{-1} kg^{-1})	48.2 ± 5.0
W_{max} (W)	253 ± 16
FFM (kg)	51.1 ± 2.7
FM (kg)	12.2 ± 1.9
ISI-Matsuda	4.7 ± 0.7

Data provided are means ± SEM (n = 8). BMI, body mass index; FM, fat mass; FFM, fat-free mass; Wmax, maximum workload; ISI, insulin sensitivity index. Data obtained from post endurance training intervention from (Shepherd et al., 2013).

4.3.2 Experimental procedures

Following completion of 6 weeks endurance training (cycling at 65% VO_{2peak} for 40-60 mins 5 days per week; see Shepherd et al., 2013 for further details), participants rested for >72 h and consumed a controlled diet (50%, carbohydrate, 35% fat and 15% protein) matched to habitual caloric intake for 24 h prior to the experimental trial. Following an overnight fast (>10 h), participants performed 60 min cycling on a stationary ergometer at 50 ± 2% W_{max} (equating to ~59% $\dot{V}o_{2peak}$ achieved post-training intervention). Expired air was collected (5 min collection period) at 15 min intervals (t = 15, 30, 45, 60 min), using an online gas system (Oxycon Pro, Jaeger, Germany) in order to calculate rates of carbohydrate and lipid oxidation (Table 4.2). Additionally, heart rate was recorded every 5 min (Table 4.2).

Muscle biopsies were obtained from the *m. vastus lateralis* of one leg before (0 min) and immediately after exercise (60 min). The biopsied leg was randomised to avoid any bias of dominant leg. Initially local anaesthetic (1% lidocaine; B Braun, Sheffield, UK) was injected into the skin and fascia of the muscle before two small incisions were made approximately 2 cm apart. Prior to exercise, a muscle biopsy (~100 mg) was extracted from the distal incision using the Bergström needle technique (Bergström, 1975). The muscle biopsy was first dissected from any fat or connective tissue. A portion (~60mg) of muscle was immediately embedded in Tissue-Tek OCT compound (Sakura Finetek Europe, The Netherlands) and frozen in liquid nitrogen-cooled isopentane for subsequent immunohistochemical analyses. Following exercise, the second muscle biopsy was taken from the proximal incision using the method described above.

4.3.3 Analysis of muscle samples

4.3.3.1 Immunofluorescence staining

Cryosections (5 µm) were cut at -25^{o}C onto ethanol-cleaned glass slides. Cryosections of both pre-and post-exercise samples from one participant were placed

on a single slide to account for any variation in staining intensity between sections. Sections were fixed for 1 h in 3.7% formaldehyde, rinsed 3 x 30 s in doubly distilled water (dd H_2O) and permeabilised in 0.5% Triton X-100 for 5 min, before being washed 3 x 5 min in Phosphate Buffered Saline (PBS, 137mM sodium chloride, 3 mM potassium chloride, 8 mM sodium phosphate dibasic and 3mM potassium phosphate monobasic, pH of 7.4). Subsequently, slides were incubated with primary antibodies (overnight for HSL analysis, 1 hr for ATGL analysis) before being washed again 3 x 5 min in PBS. Sections were then incubated with complementary secondary fluorescence-conjugated antibodies for 30 min, followed by a further 3 x 5 min PBS washes. To visualise LD, sections were incubated with BODIPY 493/503 (Invitrogen, Paisley, UK, D3922, dilution 1:50) for 20 min followed by a further 1 x 5 min PBS wash. After the final wash, coverslips were mounted with Vectashield (H-1000, Vector Laboratories, Burlingame, CA, USA) and sealed. HSL and ATGL visualisation was achieved using rabbit polyclonal anti-HSL (Abcam, Cambridge, UK, ab 63492, dilution 1:50) or rabbit polyclonal anti-ATGL (Abcam, Cambridge, UK, Ab109251, dilution 1:50) respectively, followed by application of Alexa Fluor goat anti-rabbit IgG 546 secondary antibody (Invitrogen, Paisley, UK, A-11035, dilution 1:100). PLIN2 was visualised with mouse monoclonal anti-adipophilin (PLIN2) (American Research Products, MA, USA, Cat. #03-610102, dilution 1:50) and Alexa Fluor goat anti-mouse IgG_1 633 secondary antibody (Invitrogen, Paisley, UK, A-21126, dilution 1:100). PLIN5 was visualised with guinea pig polyclonal anti-OXPAT (PLIN5) (Progen Biotechnik, Germany, GP31, dilution 1:100) and Alexa Fluor goat anti-guinea pig IgG 633 secondary antibody (Invitrogen, Paisley, UK, A-21105, dilution 1:100). All antibodies were previously validated in our lab except the rabbit polyclonal anti-HSL (see supplementary material 1 for validation results). Initially, sections were co-stained for HSL and LD to investigate HSL localisation to LD. HSL and LD were then co-stained with either PLIN2 or PLIN5 in order to determine HSL localisation to LD either associated (PLIN+ LDs) or not associated with each PLIN protein (PLIN- LDs).

This process was then repeated with ATGL and LD being co-stained with either PLIN2 or PLIN5 to establish ATGL localisation to LD either associated (PLIN+ LDs) or not associated with each PLIN protein (PLIN- LDs). As described previously (Shepherd *et al.*, 2012, 2013; Strauss *et al.*, 2016; Shepherd *et al.*, 2017b), before any colocalisation analysis was undertaken controls were included to confirm absence of 1) bleed through of fluorophores in opposing channels when single staining was performed, 2) non-specific secondary antibody binding, and 3) sample autofluorescence.

4.3.3.2 Image capture, processing and data analysis

An inverted confocal microscope (Zeiss LSM710; Oberkochen, Germany) was used to obtain digital images of cross-sectionally orientated muscle sections. An argon laser was used to excite the Alexa Fluor 488 fluorophore whilst a helium-neon laser excited the Alexa Fluor 546 and 633 fluorophores. Images were initially acquired with a 40x 0.7 NA oil immersion objective to examine the cellular distribution of HSL and LDs. The same system was used but with a 16x digital magnification to acquire images that were used to investigate HSL and LD colocalisation. A more powerful oil immersion objective of 63x 1.4 NA combined with 16x digital magnification was then used to identify LD that were coated with PLIN and assess the localisation of HSL to these LD. ATGL appeared punctate and dispersed throughout the cell and to capture its distribution more representatively, images were acquired using the 63X 1.4 NA objective at a wider 8x digital magnification. We were unable to stain for and identify type I fibres during the immunohistochemical analysis in the current study due to limitations on the number of fluorophores that could be used simultaneously. Instead, only muscle fibres that had the highest lipid content were imaged. Type I fibres typically have a high IMTG content alongside a large oxidative capacity (Shaw *et al.*, 2008; Shepherd *et al.*, 2013), and we have previously shown that IMTG utilisation during exercise occurs specifically in type I fibres (Shepherd *et al.*, 2012, 2013).

Results from our previous study also clearly demonstrated that 'in comparison to type IIa fibres, type I fibres had 3-4 fold and 2-3 fold greater IMTG stores pre and post-exercise, respectively (Shepherd *et al.*, 2013). Therefore, by selecting fibres with the highest lipid content we are assuming those fibres would also have the highest oxidative capacity and rates of IMTG utilisation during exercise. We expect that this approach would consequently detect changes in lipase association with LD if they existed. For each participant, images were obtained of pre-exercise muscle fibres (*n*=15) and post-exercise muscle fibres (*n*=15) with the central region of the fibre imaged for each staining combination. Due to insufficient sample being available, ATGL immunohistochemical analysis was only performed on 7 participants.

Image analysis was undertaken using Image-Pro Plus 5.1 software (Media Cybernetics, Bethesda, MD, USA). For colocalisation analysis, an intensity threshold was selected to denote the positive signal for HSL or ATGL, LD (Figure 4.1) and PLIN2 or PLIN5. These thresholds were then used to produce binary images of HSL or ATGL, LD, PLIN2 or PLIN5 that were subsequently used for colocalisation analysis (Figure 4.1). A co-localisation map displaying the merged images was generated, and the overlapping regions extracted to a separate image. Initially colocalisation between LD and HSL was measured by expressing the total number of extracted objects as a proportion of the total number of LDs. To determine HSL colocalisation to LDs with or without PLIN associated the following analysis was conducted. LD that colocalised with PLIN were first characterised as PLIN+ and PLIN- LDs (Shepherd *et al.*, 2013). The number of PLIN+ LDs and PLIN- LDs that overlapped with HSL was then counted per image pre and post-exercise. The number of PLIN+ and PLIN- LDs colocalised with HSL was then expressed relative to area, thereby enabling us to quantify the density of each LD subgroup to be colocalised with HSL. HSL colocalisation to PLIN2 or PLIN5 was also quantified irrespective of LD presence. The same process was then repeated for ATGL instead of HSL. Additional analysis on the size and number

of HSL or ATGL objects per image was conducted to generate a clear understanding of HSL and ATGL distribution pre- and post-exercise.

4.3.4 Statistics

All data are expressed as means ± SEM. Significance was set at $P < 0.05$. A student's paired *t* test was used to measure differences from pre- to post-exercise in variables relating to HSL or ATGL colocalisation to LD. A Wilcoxon signed rank test was used to measure the differences in HSL average area from pre- to post-exercise due to non-normally distributed data. A two-way within-subjects ANOVA was used to measure the differences in HSL colocalisation with LD pre and post-exercise, where within subjects factors were identified as *'time'* (pre vs post-exercise) and *'HSL-colocalisation'* (HSL+ LD *vs.* HSL- LD). A two-way within-subjects ANOVA was also used to measure the differences in HSL or ATGL colocalisation to PLIN+ and PLIN- LDs, pre- and post-exercise. Here, the within-subject factors were identified as *'time'* (pre- *vs.* post-exercise) and *'PLIN-association'* (PLIN+ LD *vs*. PLIN- LD). Significant main effects or interaction effects were assessed using Bonferroni adjustment *post hoc* analysis.

4.4 Results

4.4.1 Substrate utilisation

The RER remained stable during the 60 min of cycling at 59 ± 2% $\dot{V}o_{2peak}$. Fat oxidation rates increased throughout the exercise bout and averaged 45 ± 3% of total substrate oxidation (Table 4.2).

Table 4.2. Substrate utilisation during 60 min cycling at ~60% $\dot{V}o_{2peak}$

	15 min	30 min	45 min	60 min	Overall
Heart rate (beats.min^{-1})	134 ± 3	139 ± 5	139 ± 4	139 ± 6	138 ± 4
% of $\dot{V}o_{2peak}$	58 ± 2	59 ± 2	60 ± 2	58 ± 2	59 ± 2
RER	0.88 ± 0.01	0.86 ± 0.01	0.86 ± 0.01	0.85 ± 0.01	0.86 ± 0.01
CHO oxidation (g.min^{-1})	1.48 ± 0.08	1.38 ± 0.08	1.36 ± 0.1	1.26 ± 0.09	1.37 ± 0.07
(% of total oxidation)	61.7 ± 3.4	57.2 ± 3.6	54.7 ± 3.2	52.8 ± 4.2	56.6 ± 3.1
Fat oxidation (g.min^{-1})	0.43 ± 0.05	0.49 ± 0.06	0.52 ± 0.05	0.54 ± 0.07	0.49 ± 0.05
(% of total oxidation)	40.1 ± 3.3	44.5 ± 3.5	47.0 ± 3.2	48.9 ± 4.1	45.1 ± 3.1

Data provided are means ± SEM (n = 8). CHO, carbohydrate; RER, respiratory exchange ratio. Data obtained from Shepherd et al. (2013).

4.4.2 Increased HSL localisation to LDs following exercise

Images of immunofluorescence staining of HSL showed large storage clusters dispersed throughout the cell (Figure 4.2A). Fibres that exhibited a high lipid content were selected and images of HSL and BODIPY 493/503 were obtained from the central part of each fibre at 16x digital magnification. Using this approach, it became clear that in response to exercise there was a shift in the distribution of HSL from large clusters to a greater number of smaller, discrete clusters (representative images shown in Figure 4.2B). Accordingly, there was a significant increase in the number

of HSL clusters from pre (0.0919 ± 0.0068 μm^{-2}) to post-exercise (0.1250 ± 0.0082 $\mu m^{-}2$; P = 0.001) whilst the size of each HSL cluster significantly decreased from pre (*Mdn* = 44.20) to post-exercise (*Mdn* = 38.04; Z = 2.4; P = 0.025). Importantly, HSL protein content as measured by fluorescence intensity did not change from pre- (39 ± 3 AU) to post-exercise (42 ± 4 AU; P = 0.107). The fraction of LD colocalised with HSL clusters significantly increased (19%; P = 0.014; Figure 4.3A). At baseline, there were significantly more LD that were colocalised to HSL than LD without HSL colocalisation (P = 0.033; Figure 4.3B). Following exercise there was a significant interaction effect (P = 0.014), the number of LD that were colocalised to HSL significantly increased from pre to post-exercise (+21%, P = 0.014) whereas the number of LD without HSL colocalisation showed a trend towards a decrease pre to post-exercise (- 22%, P = 0.063; Figure 4.3B).

4.4.3 ATGL and LD analysis

Immunofluorescence staining of ATGL showed a distinct punctate pattern throughout the cytosol which was unaltered following exercise (Figure 4.4). ATGL protein content as measured by fluorescence intensity was not significantly different from pre (7 ± 1 AU) to post-exercise (8 ± 1 AU; P = 0.354). The average area of each ATGL object per image was unchanged from pre (40.61 ± 8.72 μm^{-2}) to post-exercise (41.35 ± 9.66 μm^{-2}, P = 0.733). The number of ATGL objects was also unchanged from pre (0.044 ± 0.004 μm^{-2}) to post-exercise (0.044 ± 0.002 μm^{-2}; P = 0.925). The fraction of LD colocalised with ATGL was not significant differently from pre (0.53 ± 0.04) to post-exercise (0.43 ± 0.05, P = 0.069). As such, the number of LD colocalised with ATGL was not different from pre (0.0331 ± 0.0035 μm^{-2}) to post-exercise (0.0285 ± 0.0040 μm^{-2}; P = 0.326). Similarly, the number of LD without ATGL colocalisation was not different from pre (0.0304 ± 0.0028 μm^{-2}) to post-exercise (0.0350 ± 0.0021 μm^{-2}; P = 0.253).

4.4.4 Relationship between HSL, PLIN2 or PLIN5 and LD

To quantify colocalisation between HSL and PLIN2+ LD or PLIN2- LD, images of HSL, PLIN2 and LD were acquired pre and post-exercise at 16x magnification using a 63x 1.4 NA objective (Figure 4.5A). This process was then repeated for HSL, PLIN5 and LD (Figure 4.5B). The number of HSL objects colocalised to PLIN2 increased from pre (0.0688 ± 0.0030 μm^{-2}) to post-exercise (0.0773 ± 0.0020 μm^{-2}; $P = 0.049$). However, not all LDs have PLIN2 bound to them, and therefore we investigated the colocalisation of HSL with PLIN2+ and PLIN2- LDs. Pre-exercise, the number of PLIN2+ LD colocalised to HSL was greater (0.0565 ± 0.0043 μm^2) than the number of PLIN2- LD not colocalised with HSL (0.0205 ± 0.0019 μm^{-2}; $P < 0.001$; Figure 4.6A). Exercise led to an increase in HSL colocalisation to both PLIN2+ LD (+16%) and PLIN2- LD (+28%; Fig. 6A, $P = 0.047$) post-exercise. There was however, no interaction effect for exercise and PLIN2 presence on the LD ($P = 0.611$).

The number of HSL objects colocalised to PLIN5 also increased from pre (0.0573 ± 0.0043 μm^{-2}) to post-exercise (0.0772 ± 0.0056 μm^{-2}; $P = 0.002$). Pre-exercise, the number of PLIN5+ LD colocalised with HSL was greater (0.0406 ± 0.0043 μm^{-2}) compared to the number of PLIN5- LD without HSL colocalisation (0.0149 ± 0.0015 μm^{-2}; $P = 0.001$; Figure 4.6B). There was a main effect for exercise on HSL colocalisation to LD ($P < 0.001$; Figure 4.6B), such that HSL colocalisation to LD increased. Moreover, there was a significant interaction effect for exercise and PLIN5 presence on the LD. The increase in HSL colocalisation to PLIN5+ LD (+53%) was greater than the increase to PLIN5- LD (+34%; $P = 0.006$; Figure 4.6B).

4.4.5 Relationship between ATGL, PLIN2 or PLIN5 and LD

To quantify colocalisation between ATGL and PLIN2+ LD or PLIN2- LD, 16x magnification images on a 63x 1.4 NA objective were acquired pre- and post-exercise of ATGL, PLIN2 and LD (Figure 4.4B). This process was then repeated for ATGL, PLIN5 and LD. Pre-exercise, there was greater ATGL colocalised to PLIN2+ LD

(0.0224 ± 0.0029 μm^{-2}) compared to PLIN2- LD (0.0057 ± 0.001 μm^{-2}, $P < 0.001$; Figure 4.7A) and this was unaltered with exercise ($P = 0.187$). Pre-exercise, more ATGL was colocalised to PLIN5+ LD (0.0222 ± 0.0017 μm^{-2}) compared to PLIN5- LD (0.0109 ± 0.0019 μm^{-2}, $P < 0.001$; Figure 4.7B) and this was also not altered with exercise ($P = 0.287$). There was no significant difference in the amount of ATGL colocalised to PLIN2 from pre (0.037 ± 0.0033 μm^{-2}) to post- exercise (0.037 ± 0.0023 μm^{-2}; $P = 0.985$). There was also no significant difference in the amount of ATGL colocalised to PLIN5 from pre (0.0305 ± 0.0018 μm^{-2}) to post-exercise (0.0311 ± 0.0023; $P = 0.877$).

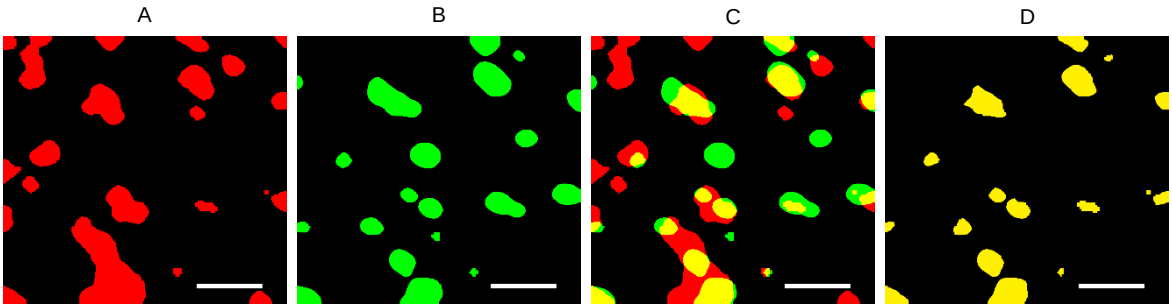

Figure 4.1. Method of colocalisation analysis. Binary images of objects representing HSL (A) and LD (B) identified by a selected intensity threshold to signify a positive signal for HSL or LD, respectively. Colocalisation of HSL objects and LD was investigated by merging the images (C), and the extracted objects (D) represents positive colocalisation between HSL and LD. Any LD that overlapped with a HSL object was counted as colocalisation event. If the same HSL object over-lapped more than once with a LD then this was counted as a dual colocalisation event and omitted from the analysis, allowing for only one colocalisation event to be counted. The same procedure was used to obtain colocalisation analysis for ATGL objects and LD, PLIN2 or PLIN5 and LD. White bars represent 3 μm.

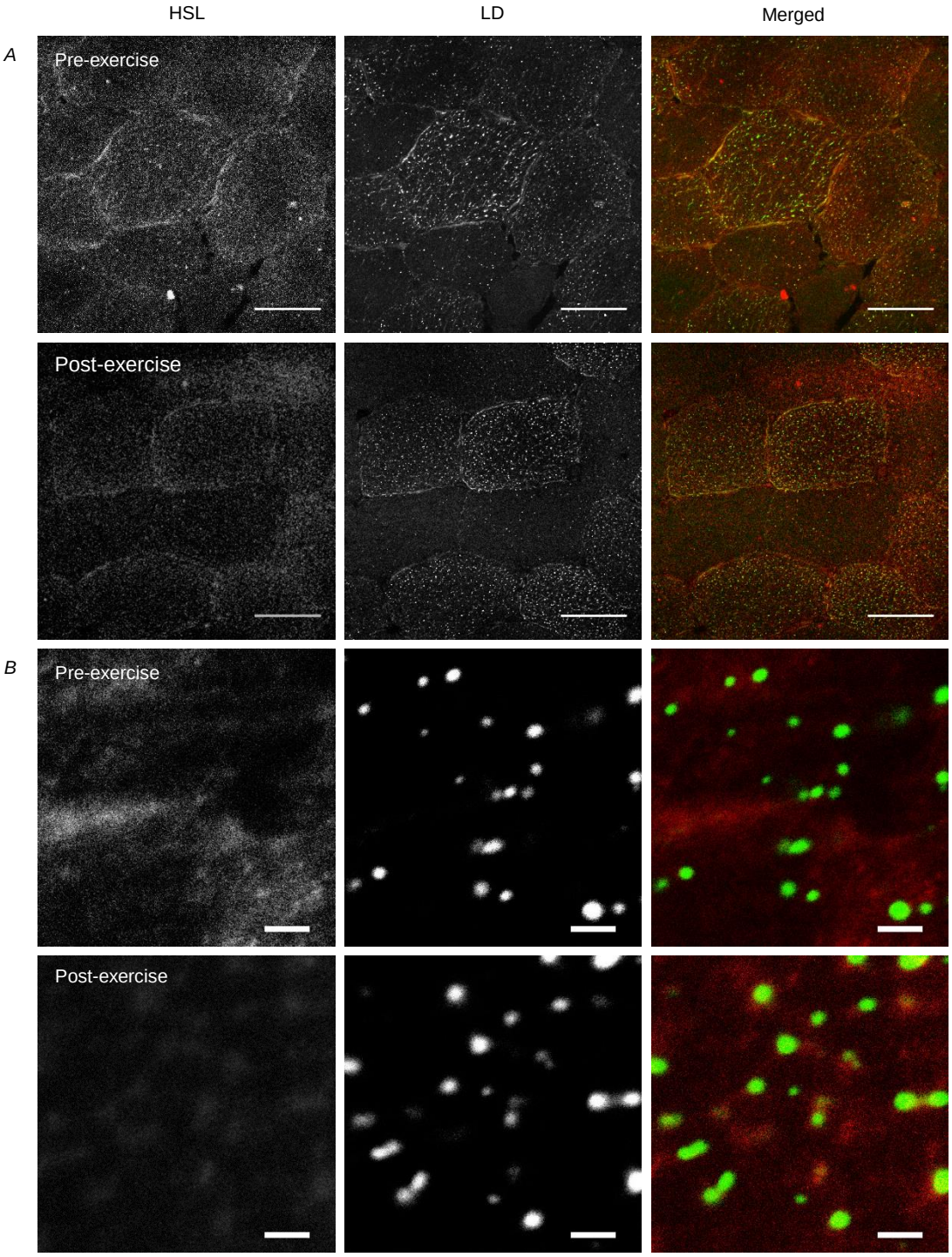

Figure 4.2. HSL redistributes to LD following from pre to post-exercise as visualised through confocal immunofluorescence microscopy. Representative images of HSL and LD pre and post-exercise were initially obtained using a 40x oil objective on a confocal microscope (A). White bars represent 50 µm. LD were visualised using BODIPY 493/503 and represent IMTG stores within the cell. Muscle fibres that had the highest lipid droplet content were selected for analysis. A 16x digital magnification was then applied to the centre of these muscle fibres and images were obtained to identify and quantify distribution and colocalisation between HSL and LD (B). White bars represent 2 µm. Image B shows that in the pre-exercise

state HSL appeared as large storage clusters throughout the cell, whereas post-exercise HSL was visualised as a greater number of smaller, discrete clusters centred on LDs as observed on the merged images.

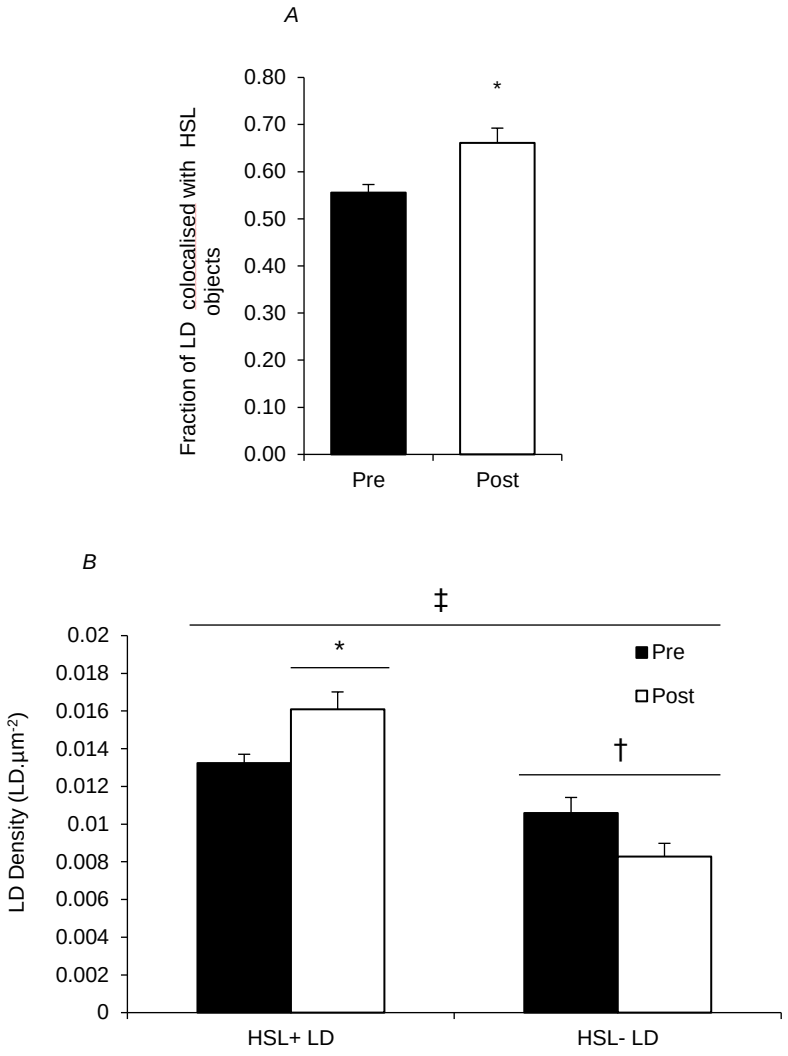

Figure 4.3. HSL redistributes from larger storage clusters to smaller more frequent clusters from pre to post exercise resulting in an increase in LD colocalisation to HSL. Quantification derived from confocal immunofluorescence microscopy images. Colocalisation analysis was performed to determine the fraction of LD overlapping with HSL objects pre- and post-exercise (A). Subsequently, the number of LD colocalised with HSL (HSL+ LD) or not colocalised with HSL (HSL- LD) was calculated and compared from pre to post-exercise (B). Data collected are averages of 15 fibres per participant per time point. Values are given as means ± SEM (n = 8 per group). †Main effect for HSL colocalisation to LD ($P < 0.05$ *vs.* HSL- LD). ‡ Main interaction effect for HSL colocalisation to LD from pre to post-exercise ($P < 0.05$). Post-hoc analysis revealed an increase in HSL+ LD (* $P < 0.05$ *versus* pre-exercise) and a trend towards a decrease in HSL- LD ($P = 0.063$) *versus* pre-exercise.

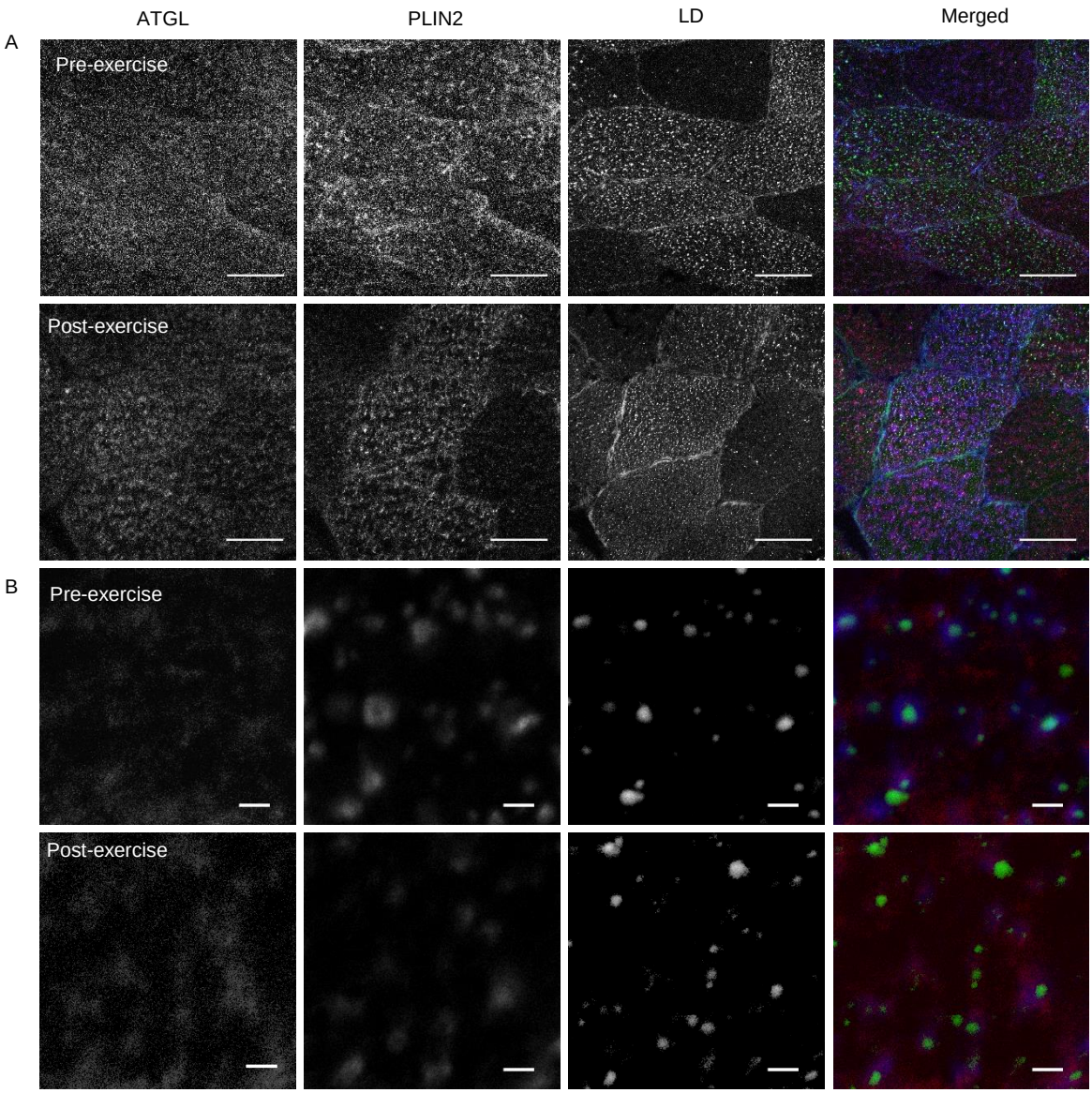

Figure 4.4. ATGL distribution does not change from pre to post-exercise as visualised through immunofluorescence microscopy. Representative images of ATGL, PLIN2 and LD pre and post-exercise obtained using a 63x oil objective of a confocal microscope (A). White bars represent 50 µm. LD were visualised using BODIPY 493/503 and represent IMTG stores within the cell. Muscle fibres that had the highest lipid droplet content were selected and analysed. An 8x digital magnification was then applied to the centre of these muscle fibres and images were obtained to identify and quantify distribution and colocalisation between ATGL and LD associated with either PLIN2 (B) or PLIN5. White bars represent 2 µm. Images A and B show that pre-exercise ATGL had punctate staining throughout the cell and this was unaltered post-exercise.

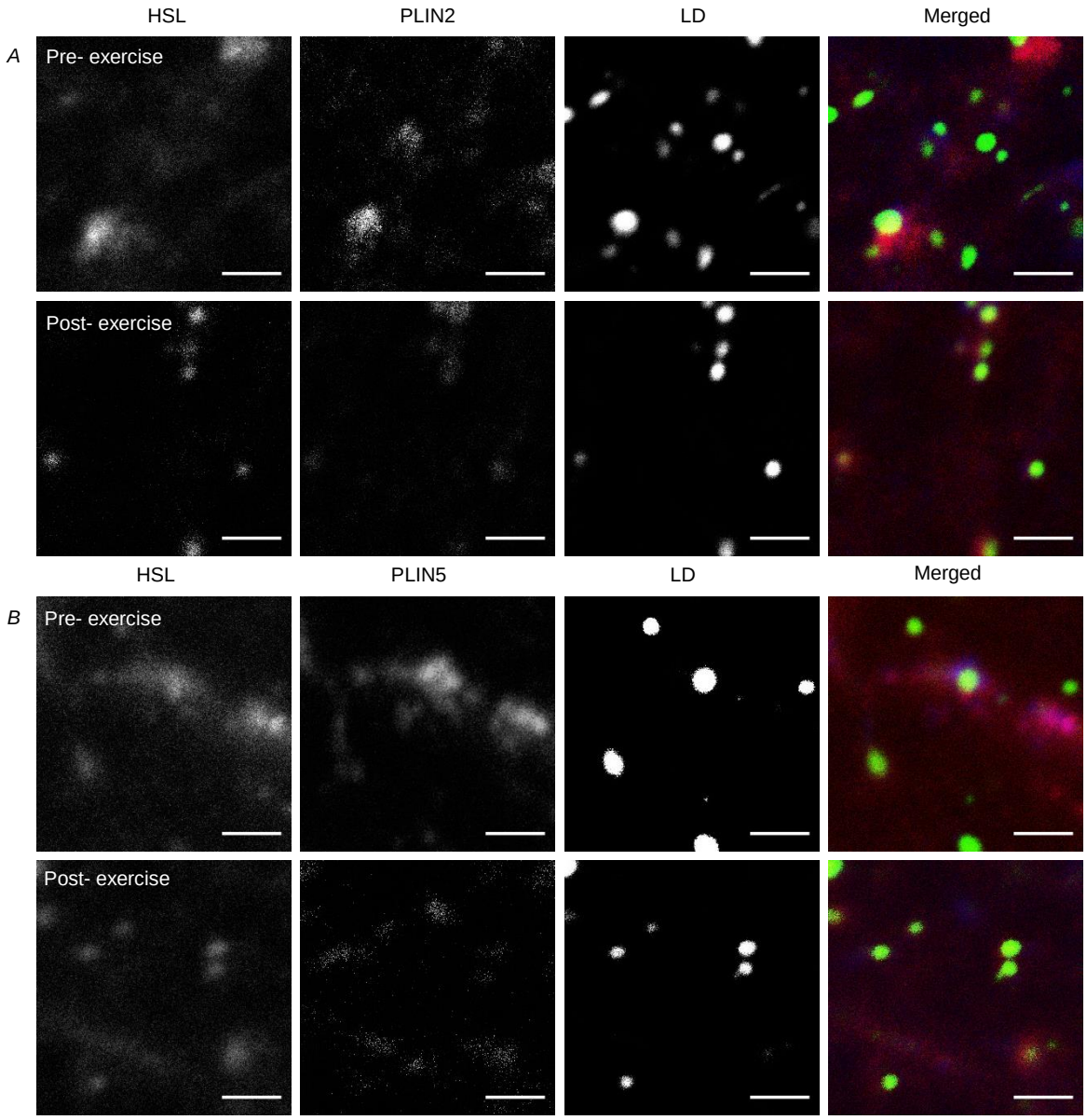

Figure 4.5. Immunofluorescence microscopy images of HSL, PLIN2/PLIN5 and LD pre and post-exercise. Colocalisation between HSL, PLIN2 (A) or PLIN5 (B) and LD as visualised through immunofluorescence microscopy and quantified pre and post exercise. Images captured on a 63x oil objective of a confocal microscope at 16x digital magnification in the central region of fibres that had the highest lipid droplet content. White bars represent 2 µm. PLIN2 (A) and PLIN5 (B) were associated with LD or located in the cytosol. HSL redistributes from larger storage clusters to a greater number of smaller, discrete clusters centred on different subclasses of LD (i.e. PLIN+ or PLIN- LDs).

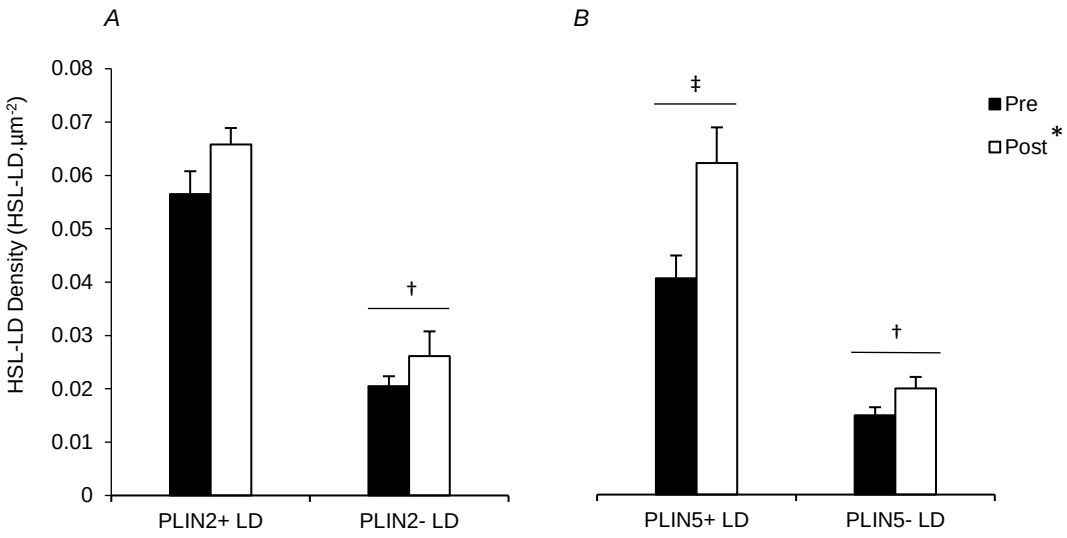

Figure 4.6 HSL preferentially redistributes to PLIN5+ LD from pre to post-exercise. HSL colocalisation with different LD pools (PLIN+ or PLIN- LDs) was quantified from immunofluorescence microscopy images of HSL, LD and PLIN2 (A) or PLIN5 (B) pre and post- exercise. Data were collected as averages of 15 fibres per participant per time point. Values are presented as means ± SEM (n = 8 per group). * Main effect for exercise (P < 0.05 *vs.* pre-exercise). †Main effect for PLIN association to LD (P < 0.05 *vs.* PLIN- LD). ‡ Main interaction effect for PLIN5 association to LD (P < 0.05 *vs.* PLIN5- LD).

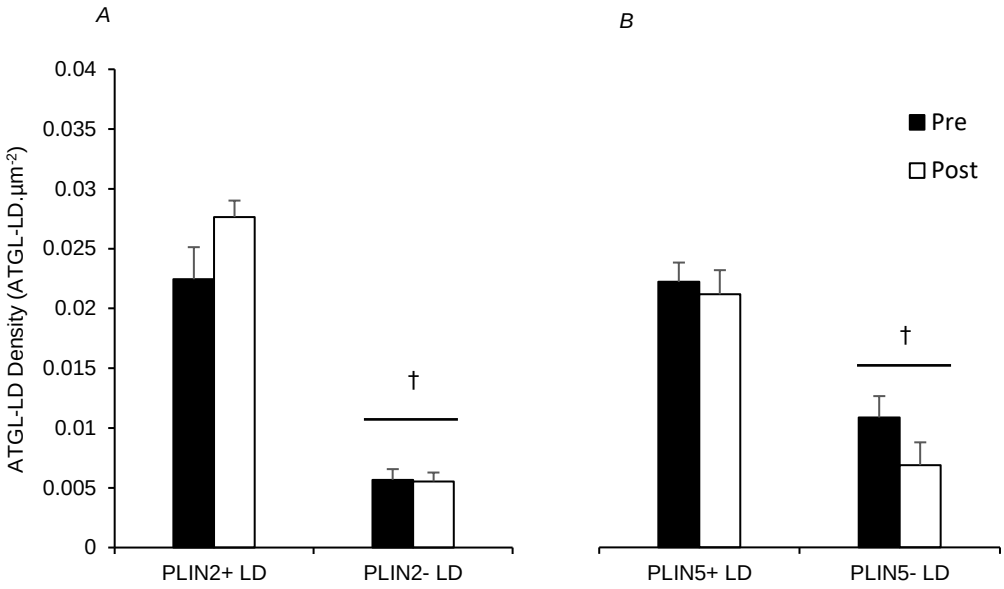

Figure 4.7. ATGL colocalisation with different pools of LD does not change from pre to post-exercise. ATGL colocalisation with different LD pools (PLIN+ or PLIN- LDs) was quantified from immunofluorescence microscopy images of ATGL, LD and PLIN2 (A) or PLIN5 (B) pre and post- exercise. Data were collected as averages of 15 fibres per participant per time point. Values are presented as means ± SEM (n = 7 per group). †Main effect for PLIN association to LD ($P < 0.05$ *vs.* PLIN-LD).

4.5 Discussion

This study examined the localisation of the two key lipases in human skeletal muscle, ATGL and HSL, with LDs and the associated PLIN proteins at rest and in response to moderate-intensity exercise. The major novel observation is that HSL redistributes to LD in human skeletal muscle following 1 h moderate-intensity cycling exercise, with HSL preferentially translocating to LDs with PLIN5 associated. Furthermore, we confirm for the first time that ATGL was colocalised more to PLIN5+ LD in comparison to PLIN5- LD in agreement with our hypothesis. Additionally, the data shows that ATGL is also colocalised more to PLIN2+ LD in comparison to PLIN2- LD and the distribution of ATGL does not alter during the exercise bout. Together, these data demonstrate different distribution patterns of key lipases and their localisation to LD-associated PLIN proteins in skeletal muscle, which may be important in the regulation of IMTG utilisation during moderate-intensity exercise.

In the basal state HSL was observed as large storage clusters throughout the cell, whereas after exercise HSL was visualised as a greater number of smaller, discrete clusters typically centred on LD (Figure 4.2). As a result, we observed an increase in the fraction of LD colocalising with HSL from pre to post-exercise, demonstrating HSL redistributes to LD in response to exercise in human skeletal muscle. A number of studies in cultured adipocytes have demonstrated that HSL translocates from the cytosol to LD in response to lipolytic stimuli (Su *et al.*, 2003; Sztalryd *et al.*, 2003; Wang *et al.*, 2009), whereas studies investigating the localisation of HSL in skeletal muscle are limited. Most notably, Prats et al. (2006) in line with our findings using confocal immunofluorescence microscopy and isolated rat skeletal muscle fibres observed that HSL in the basal state was accumulating either as storage clusters or colocalising with LD, whilst ex vivo electrical or adrenaline stimulation increased the translocation of HSL to LD. In addition transmission electron microscopy using immunogold labelled HSL antibodies was used in the study of Prats et al. (2006) to

show that the HSL translocation led to HSL passing the phospholipid monolayer of the LD into the TAG core (Prats *et al.*, 2006) allowing HSL (the enzyme) greater access to IMTG (the substrate). The *ex vivo* protocol adopted by Prats et al. (2006) elegantly eliminates the interference of plasma-derived FA on substrate use and IMTG synthesis allowing for IMTG hydrolysis to be studied in isolation. We now extend these findings to demonstrate that HSL redistribution occurs in human skeletal muscle in response to moderate-intensity exercise *in vivo*.

Overall we observed an increase in HSL colocalisation to PLIN2 and PLIN5 following exercise. This finding is in agreement with Prats et al. (2006) who demonstrated an increased colocalisation of HSL with PLIN2, but did not investigate PLIN5. In addition, by staining HSL, LD and either PLIN2 or PLIN5, we were able to determine specific colocalisation between HSL and different sub-groups of LD (PLIN2+ LD and PLIN2- LD or PLIN5+ LD and PLIN5- LD). The most important and novel finding of the present study was that HSL preferentially redistributed to LDs with associated PLIN5. Although PLIN5 is implicated in protecting intracellular TAG stores from hydrolysis under basal conditions (Wang *et al.*, 2011a; Laurens *et al.*, 2016), evidence is accumulating that PLIN5 also facilitates TAG breakdown when energy demand increases. PLIN5 is phosphorylated in response to PKA stimulation leading to TAG hydrolysis in cultured cells (Wang *et al.*, 2011a). In addition, we have previously shown that LDs with PLIN5 associated are preferentially used during a bout of moderate-intensity exercise in lean, healthy individuals (Shepherd *et al.*, 2013). We now propose that PLIN5+ LDs are targeted for breakdown during exercise because PLIN5 facilitates the interaction of HSL with the TGs stored in the LD core.

Immunofluorescence staining of ATGL displayed a punctate pattern throughout the cytosol which was not altered in response to moderate-intensity exercise (Figure 4.4). At baseline the fraction of LD colocalising with ATGL was ~0.53 and this was not altered following exercise. Mason et al., (2014a) recently reported no significant

changes in the percentage of ATGL colocalising with LD (stained using Oil Red O) in human skeletal muscle of recreationally active males following moderate-intensity exercise. Together these results suggest that a proportion of LD already is colocalising with ATGL under basal conditions and that the activity of ATGL is instead regulated by its co-activator CGI-58. In line with this suggestion, studies in cultured COS-7 cells have shown that overexpression of GGI-58 led to an increase in ATGL activity (Lass *et al.*, 2006). The fraction of LD colocalising with ATGL showed a trend towards a decrease after exercise, which is likely explained by a decrease in LD number post-exercise (Shepherd *et al.*, 2013). Interestingly the results show there is a substantial fraction of LD (~0.47) that do not have any colocalisation with ATGL. As HSL acts both on TAG and DAG (Lass *et al.*, 2011) it is plausible that LD not colocalised with ATGL are instead subject to HSL-mediated hydrolysis.

Evidence from cultured cells suggests PLIN5 recruits and binds ATGL and CGI-58 at the LD surface under basal conditions but releases ATGL and CGI-58 following PKA induced phosphorylation (Granneman *et al.*, 2011; Wang *et al.*, 2011a). The release of ATGL and CGI-58 from PLIN5 allows ATGL to bind to its co-activator CGI-58 to increase ATGL activity (Granneman *et al.*, 2011; Wang *et al.*, 2011a). In the current study at baseline, ATGL colocalisation was higher to PLIN2+ LD and PLIN5+ LD in comparison to PLIN2- LD and PLIN5- LD respectively. As ATGL distribution did not change during exercise, the amount of ATGL colocalised with PLIN2+ LD and PLIN5+ LD was also not altered after the exercise bout. There was also no change in ATGL colocalisation with PLIN2 or PLIN5 irrespective of LD presence following exercise. In line with our findings, MacPherson et al. (2013a) also reported that PLIN2 and PLIN5 both co-immunoprecipitated with ATGL under basal conditions, but this did not increase in response to lipolytic stimuli (adrenaline, contraction or both) in rat skeletal muscle. Our data therefore suggests that PLIN2 and PLIN5 may support the positioning of ATGL to LD during fasted, non-exercised conditions. Immunogold

labelling of HSL with transmission electron microscopy has confirmed that HSL penetrates the phospholipid monolayer of the LD to access IMTG in response to epinephrine or electrical stimulation in isolated rat skeletal muscle (Prats *et al.*, 2006). Whether PLIN2 or PLIN5 localises ATGL to the outside of the LD phospholipid monolayer during basal conditions but then releases ATGL so it can penetrate the phospholipid monolayer and access IMTG stores clearly warrants further investigation but can only accurately deciphered using immunogold transmission electron microscopy.

IMTG utilisation during 60 min of moderate-intensity cycling exercise in these muscle samples was quantified previously, where it was confirmed that IMTG content decreased from pre to post-exercise (-43 ± 5%) in type I fibres only (Shepherd *et al.*, 2013). Due to constraints with the number of fluorophores that could be used simultaneously we were unable to stain and identify type I fibres as part of the analysis in this study. Instead, fibres with the highest lipid content were selected for analysis. Type I fibres are characterised by high mitochondrial content and elevated IMTG stores (Shaw *et al.*, 2008; Shepherd *et al.*, 2013). It is well documented that IMTG utilisation is strongly associated with pre-exercise IMTG content (van Loon *et al.*, 2003a; van Loon *et al.*, 2003b) and it is therefore likely that the fibres selected in the current study also exhibited net IMTG breakdown. Moreover, despite being unable to identify fibre type in the current study we can conclude that redistribution of HSL occurs in fibres that have a high LD content.

By extending our validated immunofluorescence microscopy techniques, we have been able to generate further insight into the role of the PLIN proteins in the regulation of lipolysis in skeletal muscle during endurance exercise. Our assays, however, only permit the analysis of ATGL or HSL colocalisation with LDs with a single PLIN protein. It is possible, therefore, that PLIN2+ LD or PLIN2- LD may have PLIN5 associated and similarly PLIN5+ LD and PLIN5- LD may have PLIN2 associated. Nevertheless,

the results indicate that whilst there were similar increases in HSL colocalisation to PLIN2+ LD and PLIN2- LD post-exercise, there was a significantly greater increase in HSL colocalisation to PLIN5+ LD in comparison to PLIN5- LD after the exercise bout. It is also possible, that PLIN5 was also present on the surface of PLIN2+ LD or PLIN2- LDs colocalised with ATGL. Despite this limitation we can still conclude that ATGL was present on PLIN5- LDs and therefore PLIN5 is not a prerequisite for ATGL colocalisation to the LD.

In conclusion, this study has generated novel evidence that HSL redistributes to LD in skeletal muscle of endurance-trained men in response to moderate-intensity exercise, whereas ATGL colocalisation with LDs is unaltered by exercise. Furthermore, this is the first study to demonstrate that HSL preferentially redistributes to PLIN5+ LDs following moderate intensity exercise, demonstrating a novel mechanism by which PLIN5 regulates HSL recruitment to LD which could aid in subsequent IMTG utilisation during exercise.

Chapter 5. The development of an immunoprecipitation-mass spectrometry protocol to identify perilipin-5 associated proteins in human skeletal muscle

5.1 Abstract

Perilipin-5 (PLIN5) has emerged as an important protein for regulating intramuscular triglyceride (IMTG) lipolysis and providing metabolic linkage to mitochondria. Dysregulation of IMTG turnover and incomplete fatty acid oxidation is proposed to be a contributing factor to the progression of skeletal muscle insulin resistance. Understanding the proteins that PLIN5 associates with is crucial in gaining a more comprehensive understanding of how IMTG turnover is regulated and how this is altered in insulin-resistant states such as obesity and type 2 diabetes (T2D). The aim of this study was to develop a PLIN5 immunoprecipitation (IP)-mass spectrometry protocol that would identify PLIN5 and its protein-protein interaction partners in human skeletal muscle. The secondary aim was to identify differences in PLIN5-IP associated proteins between the different metabolic environments present in lean sedentary, obese and T2D individuals. Gel electrophoresis prior to ultra-performance liquid chromatography tandem mass spectrometry (GeLC-MS/MS) was used to separate proteins by size (1D SDS-PAGE) and subsequent digested peptides by hydrophobicity (Liquid Chromatography) allowing for a deeper insight into the muscle proteome following IP. A control-IP was used to account for non-specific binding of contaminant proteins. The developed PLIN5-IP protocol successfully and reproducibly immunoprecipitated PLIN5 *vastus lateralis* muscle from lean sedentary individuals. This, however, could not be replicated in *vastus lateralis* muscle from obese and T2D individuals. A list of proteins from the PLIN5-IP obtained from the *vastus lateralis* muscle of lean sedentary individuals muscle, that did not appear in the control-IPs, established phospholipase A2 group II, subgroup A (PA2GA) as a unique protein associated with PLIN5. As phospholipase A2 proteins are found at the lipid droplet surface and have been implicated in lipid metabolism, future research is warranted to investigate how PA2GA interacts with PLIN5. IP of PLIN5 was not consistent in *vastus lateralis* muscle samples from obese and T2D patients. This may

be due to contamination from extramyocellular adipocytes or a lesser content (number and/or size) of type I fibres, thereby reducing PLIN5 expression and availability for immunoprecipitation. Future research could be advanced by using peptide separation by iso-electric focusing combined with using high-definition mass spectrometry which can increase the number of proteins detected in muscle and, therefore, increase the chances of detecting PLIN5 with associated protein(s) in obese and T2D muscle.

5.2 Introduction

Skeletal muscle is essential for maintenance of energy and substrate homeostasis. Within skeletal muscle protein-protein interactions are fundamental for various cellular processes. This is exemplified by the insulin-signalling cascade explained in section 1.2.1, whereby a cascade of proteins interacts in synchronisation to stimulate the activation and translocation of GLUT-4 to the plasma membrane. Identification of further protein interactions and potential disruptions to these interactions is, therefore, crucial in advancing our understanding of molecular physiology and development of diseases (Phizicky & Fields, 1995; Oti *et al.*, 2006). Ectopic lipid accumulation in skeletal muscle has been a major focus in the pathology of skeletal muscle insulin resistance and progression to type 2 diabetes (T2D). Particular emphasis has been placed on underpinning the regulation of proteins involved in intramuscular triglyceride (IMTG) turnover and mitochondrial oxidation. This is due to the working hypothesis that dysregulation of IMTG turnover and/or incomplete fatty acid oxidation results in the accumulation of lipid metabolites known to disrupt the insulin signalling pathway and contribute to skeletal muscle insulin resistance (Moro *et al.*, 2008).

Over the past decade, perilipin-5 (PLIN5) has emerged as an important lipolytic protein that helps to regulate turnover of IMTG stores (Shepherd *et al.*, 2013; Mason *et al.*, 2014b) and provides metabolic linkage to mitochondria (Wang & Sztalryd, 2011). Evidence from different cell lines have demonstrated that PLIN5 can regulate

lipolysis by binding to either; lipolytic enzyme ATGL or its co-activator CGI-58 (but not at the same time) (Granneman *et al.*, 2011; Wang *et al.*, 2011a). PKA stimulation results in PLIN5 phosphorylation and when PKA activation occurs with ectopic overexpression of PLIN5 and ATGL, lipolysis increases (Wang *et al.*, 2011a). These data have generated the hypothesis that PLIN5 serves to limit lipolysis in basal conditions by preventing the interaction of ATGL with CGI-58, and promotes lipolysis by releasing and allowing the interaction of ATGL and CGI-58 following lipolytic stimuli. PLIN5 also has a conserved N-terminal sequence capable of binding to the other key lipase HSL (Anthonsen *et al.*, 1998). Confocal immunofluorescence microscopy has confirmed that ~60% PLIN5 is colocalised to lipid droplets (LD) storing IMTG (Shepherd *et al.*, 2013). Following an acute bout of moderate intensity exercise HSL in human skeletal muscle preferentially redistributes to LD associated with PLIN5 (PLIN5+ LD) (Whytock *et al.*, 2018) and PLIN5+ LD are favourably utilised during the exercise bout compared to LD that are not associated with PLIN5 (Shepherd *et al.*, 2013).

Western blotting in isolated mitochondria and immunogold electron microscopy of rat soleus muscle have revealed that PLIN5 has a strong association to mitochondria (Bosma *et al.*, 2012b). Evidence from heart muscle has demonstrated that PLIN5 is the only perilipin capable of recruiting mitochondria to the LD surface (Wang *et al.*, 2011b). Furthermore, overexpression of PLIN5 enhances the interaction of lipid droplets and mitochondria (Bosma *et al.*, 2012b) and increases fatty acid oxidation (Wolins *et al.*, 2006; Bosma *et al.*, 2012b). The current evidence suggests that PLIN5 supports IMTG hydrolysis following lipolytic stimuli and then assists in the trafficking of FA to the mitochondria for subsequent *β*-oxidation.

This proposed role of PLIN5 in skeletal muscle makes it important to identify the proteins that it works in concert with. Hypothesis-driven techniques such as immunohistochemistry or co-immunoprecipitation followed by immunoblotting of

PLIN5 with suspected lipolytic interacting proteins is commonly used to detect PLIN5 protein interactions. For example co-immunoprecipitation with immunoblotting has identified that PLIN5 binds to HSL (Wang *et al.*, 2009; Macpherson *et al.*, 2013b), ATGL (Wang *et al.*, 2011a; MacPherson *et al.*, 2013a; Macpherson *et al.*, 2013b) and CGI-58 (Wang *et al.*, 2011a; MacPherson *et al.*, 2013a). Protein binding quantified by colocalisation of fluorescent fusion proteins intensities reveals that PLIN5 interacts with both CGI-58 and ATGL (Granneman *et al.*, 2011). More recently in our lab we have identified with colocalisation analysis from confocal immunofluorescence microscopy that PLIN5 colocalises with HSL and ATGL in human skeletal muscle (Whytock *et al.*, 2018). This spatial colocalisation being a pre-requisite for functional protein interaction.

In recent years, the use of immunoprecipitation (IP) combined with mass spectrometry has emerged as a novel avenue to explore non-targeted protein-protein interactions. In contrast to targeted approaches, IP-mass spectrometry provides an unbiased approach so identifying protein interaction partners that would not otherwise be apparent from the current literature. There is currently a wide variation with immunoprecipitation (IP)-mass spectrometry protocols due to differences in tissue, species, target protein abundance, pH and location within the cell. Commonly research has sought to identify protein interactions in cultured cells using stable isotope labelling with amino acids (SILAC) techniques (Kaake *et al.*, 2010) combined with affinity purification with tag proteins such as green fluorescent protein (GFP) or FLAG-tag (Berggard *et al.*, 2007; Trinkle-Mulcahy *et al.*, 2008). Whilst fusion tags such as GFP are benefited by near complete extraction of targeted proteins in cell culture, the use of GFP *in vivo* may not be as efficient. Cytoplasmic *in vivo* fluorescence recovery after photobleaching (FRAP) measurements have shown that photobleaching GFP in live cells results in rapid recovery (Trinkle-Mulcahy *et al.*, 2008) suggesting that GFP diffuses as a free protein *in vivo* which may result in weak

binding of cellular proteins. Fusion tagging can also alter the functionality and expression of the target protein which questions the characteristics of the protein-interactions identified. Whilst cell culture studies utilising fusion tagging with SILAC and mass spectrometry have advanced our knowledge of protein interactions it is now important to develop a technique that can be used to characterise functional protein interactions that exist in human skeletal muscle *in vivo.* Development of such a technique would allow tissues to be extracted and protein interactions to be analysed in different complex metabolic diseases such as T2D that cannot be accurately replicated in cell or animal models.

Due to PLIN5 being a LD associated protein and having a strong association to mitochondria, the IP of PLIN5 may not only yield binding partners but may also harvest other proteins associated to the LD or mitochondrial proteins. An effective non-targeted method to identify PLIN5-associated proteins is therefore of great interest to further characterise its role in skeletal muscle. The primary aim in this experimental chapter was to develop an antibody IP-mass spectrometry protocol that would effectively pull-down a low abundant protein such as PLIN5 in human skeletal muscle. Given the highlighted differences in IMTG turnover between lean, obese and T2D individuals and the proposed link to insulin resistance, the secondary aim was to identify differences in PLIN5-IP associated proteins between the different metabolic environments (lean sedentary, obese and T2D).

5.2.1 Rationale of methodology

Initial fractionation of sarcoplasmic and myofibrillar proteins was performed to assist in removing highly abundant myofibrillar proteins such as myosins, troponins, tropomyosins and other associated proteins from the sarcoplasmic fraction allowing less abundant regulatory proteins to be detected. Immunoprecipitation of PLIN5 was then performed on the sarcoplasmic fraction using a polyclonal guinea-pig anti-PLIN5 antibody (GP31, Progen, Biotechnik, Heidelberg, Germany) raised against the C-

terminal domain (aa 451-463; CPVKHTLMPELDF) of human PLIN5. This antibody has been extensively used and validated for numerous muscle molecular physiology techniques such as immunohistochemistry and immunoblotting (Ramos *et al.*, 2015; Gemmink *et al.*, 2017a; Shepherd *et al.*, 2017a). The use of an antibody for immunoprecipitation is benefited by this specific targeting of the protein of interest in its functional state however this approach is associated with a higher level of contamination compared to protein-tag methods and so control conditions must also be included. A guinea-pig polyclonal antibody for sperm-specific protein calicin (GP-SH3, Progen) which targets synthetic N-terminal domain (aa 1-24; MKLEFTEKNYNSFVLQNLNKQRKR) of bovine calicin coupled to KLH was used as a control IP to provide a background of contaminant proteins that bind non-specifically to guinea-pig immunoglobulins or the Dynabead. Furthermore, a BLAST (Basic Local Alignment Search Tool) search has confirmed the target immunogen for this antibody is not present in any skeletal muscle proteins.

Sarcoplasmic protein fractions contain large quantities of glycolytic enzymes which can overshadow lower abundance proteins when analysed as whole sarcoplasmic fraction (Maughan *et al.*, 2005). The IP sarcoplasmic fraction will therefore be separated by gel electrophoresis prior to high performance liquid chromatography tandem mass spectrometry (GeLC-MS/MS) as previously conducted in our lab (Holloway *et al.*, 2009). This is known to yield large numbers of skeletal muscle proteins (Hojlund *et al.*, 2008), increasing the opportunity for lower abundance proteins to be identified. Following separation by gel electrophoresis, gel lanes are fractionated into equal segments ($n \approx 11$) prior to digestion allowing differentiation of biological samples and the opportunity for less abundant proteins to be recognised from the digested peptides.

Separation of the digested peptides will then be achieved with ultra-performance liquid chromatography. Here the peptide solution from each digested gel fraction is

diluted into an aqueous solution and is carried by a mobile phase which passes through the liquid chromatography column and into the mass spectrometer. As peptides reach the stationary phase of the liquid chromatography column they bind to a matrix of spherical silica non-polar beads (3-5 µm) in a manner proportional to their relative hydrophobicity. A non-linear gradient of organic non-polar solvent elutes the peptides from the matrix, more hydrophilic peptides elute sooner than relatively hydrophobic peptide and therefore the complex peptide mixture is separated in a reproducible manner over the duration of the chromatography gradient (typically 90 min). Electrospray ionization converts peptides to multiple positively charged ions allowing them to be filtered through a quadrupole ion guide before being propelled through the time-of-flight mass detector. The 5 most abundant precursor peptide ions (i.e. MS) of charge 2+ or 3+ detected in the survey scan are fragmented by collision-induced dissociation to produce fragment ions (i.e. MS/MS). When positively charged peptide/fragment ions reach the detector secondary particles including electrons are emitted. These electrons are amplified through a series of dynodes creating a current that is equivalent to a number of peptides/fragment ions that entered the detector allowing for the intensity of each ion to be recorded. The acquired MS/MS data is then searched against the Swiss-Prot protein sequence database to assign peptides to known proteins. By leveraging GeLC-MS/MS it is our aim to produce a replicable PLIN5-IP mass spectrometry protocol that will pull-down PLIN5 and associated proteins in human skeletal muscle.

5.3 Methods

5.3.1 Muscle samples and preparation

5.3.1.1 Lean healthy samples- vastus lateralis

Due to IP-MS/MS protocol requiring a large amount of tissue (500µg of protein), the first step in this method development was to test the protocol on surplus *vastus lateralis* muscle from lean healthy males before applying it to the smaller muscle

samples obtained from lean, obese and T2D sedentary participants. *Vastus lateralis* muscle samples from lean healthy individuals (36.9 ± 1.9 y, body mass index (BMI) 26.9 ± 1 kg.m^{-2}) were acquired from a previous study (Camera *et al.*, 2017), which was approved by the Australian Catholic University Human Research Ethics Committee. All participants provided written informed consent. Under local anaesthesia (2–3 ml of 1% xylocaine), a resting biopsy was obtained from the *m. vastus lateralis* by using a 5-mm Bergstrom needle (Bergstrom, 1975) that has been modified with suction.

5.3.1.2 Lean, obese and T2D sedentary samples- gluteus maximus

Gluteus maximus muscle samples were obtained from 5 lean, sedentary (65 ± 2 y, BMI 25.2 ± 0.7 kg.m^{-2}), 6 obese (61 ± 5 y, BMI 31.6 ± 1.0 kg.m^{-2}) and 8 diagnosed T2D (61 ± 3 y, BMI 35.3 ± 2.0 kg.m^{-2}) males during elective orthopaedic surgery under general anaesthetic. All participants were undergoing surgery at Russells Hall Hospital (Dudley Group of Hospitals) and gave their informed consent for participation in this study. The study was approved by the local NHS Research Ethics Committee. After the initial incisions for the total hip arthroplasty surgery a muscle biopsy (~200 mg) was obtained from the *m. gluteus maximus*.

5.3.1.3 Lean, obese and T2D sedentary samples- vastus lateralis

Vastus lateralis muscle samples were obtained from 2 lean, sedentary (69 ± 7 y, BMI 22.6 ± 1.8 kg.m^{-2}), 4 obese (68 ± 4 y, BMI 37.1 ± 2.7 kg.m^{-2}) and 4 diagnosed T2D (62 ± 6 y, BMI 42.8 ± 3.4 kg.m^{-2}) females during elective orthopaedic surgery under general anaesthetic. All participants were undergoing surgery at Russells Hall Hospital (Dudley Group of Hospitals) and gave their informed consent for participation in this study. The study was approved by the local NHS Research Ethics Committee. After the initial incisions for the total knee arthroplasty surgery a muscle biopsy (~ 200 mg) was obtained from the *m. vastus lateralis.*

5.3.1.4 Muscle preparation

All samples were initially blotted of excess blood and separated from any visible fat and connective tissue. Muscle was homogenised and fractionated as previously described (Malik *et al.*, 2013; Burniston *et al.*, 2014). Briefly, snap frozen muscle samples (~60 mg) were pulverised in liquid nitrogen and homogenized on ice in 10 volume of homogenisation buffer (1% Triton X-100, 50 mM Tris, pH 7.4, 5mM EDTA including phosphatase inhibitor and complete protease inhibitor (Roche Diagnostics, Lewes, United Kingdom) using a PolyTron homogenizer. Samples were incubated on ice for 15 min before being centrifuged at 1000 g at 4^{o}C for 10 min. Following centrifugation the supernatant containing the sarcoplasmic fraction was decanted and stored on ice. Protein concentration of the sarcoplasmic fractions were measured using a Bradford assay (Bradford, 1976). Bovine serum albumin (BSA) standards (0.125. 0.25, 0.5, 0.75 and 1 mg.ml^{-1}) were prepared from a commercial stock solution (1.0 mg.ml^{-1}; Sigma-Aldrich, Poole, Dorset) and pipetted in triplicate (5 µl per well) onto microtitre plate. Muscle supernatants were diluted at 1:20 to bring them within the standard range and pipetted (5 µg per well) in duplicate. Bradford reagent (Sigma-Aldrich, Poole, Dorset, United Kingdom) was added (250 µl per well) and incubated at room temperature for 5 minutes, before reading at a wavelength of 595 nm (Tecan GmbH, Austria). Interpolation from the BSA standard curve was then used to determine the protein concentration of the sarcoplasmic muscle fraction.

5.3.2 Immunoprecipitation

Pooled samples containing 500 µg of protein from sarcoplasmic fractions were used for IP. Magnetised beads (Dynabeads, Invitrogen) were resuspended in phosphate buffer saline (PBS), pH 7.4, with 0.01% Tween-20 and sodium azide. Dynabead slurry (6.7 µl equating to 0.2 mg of protein A Dynabead) was transferred to a clean labelled tube. Dynabeads were magnetised and supernatant was removed. One microgram of PLIN5 antibody (GP31, Progen, Biotechnik, Heidelberg, Germany) or calicin

(control antibody) (GP-SH3, Progen, Biotechnik, Heidelberg, Germany) was diluted in 25 µl in PBS + 0.05 % Tween-20 and added to Dynabeads and left to incubate on a hula shaker for 30 min at room temperature. Following removal of supernatant, Dynabead-antibody solution was washed with PBS- 0.05 % Tween-20. Pooled muscle samples containing 500 µg protein were then added to Dynabead-antibody solution and left to incubate on a hula-shaker for 3 hrs at 4ºC. Dynabeads were magnetised and muscle supernatant was transferred to a clean labelled tube. Dynabead-antibody-PLIN5 was then washed 3 times in PBS- 0.05 % Tween-20. Following the last wash, PBS- 0.05 % Tween-20 was removed and 5 µl of Laemmli sample buffer with DDT was added to Dynabead-antibody-PLIN5 solution and left to incubate at 95 ºC for 4 min. The Dynabeads were then magnetised and sample buffer was transferred to a clean labelled tube (extraction 1) before a further 5 µl sample buffer was added to Dynabead-antibody-PLIN5 solution and incubated for a further 4 min at 95 ºC. Dynabeads were magnetised again and the second sample buffer was added to extraction 1.

5.3.3 1D SDS-PAGE

Proteins from the IP were separated with 12% denaturing SDS-PAGE. Mini-slab gels of the dimensions 11 x 8.5 x 0.75 cm were prepared according to the manufacturers instructions (Mini-VE system, GE Healthcare, Sweden). Initially glass plates (8 x 10.5 cm) were cleaned with 70% ethanol to remove any traces of residue protein, before being separated by spacers (1.0 mm) places at either side. The resolving gel was composed of 12% (v/v) Acrylamide/ Bis-acrylamide RTU solution (Proto-gel) (37.5:1), 1.5 M Tris-HCl (pH 8.8), 0.2 % (w/v) SDS, dd H_20, SDS polymerisation was initiated with 0.06 % (v/v) N, N, N',N' –tetramethylethylenediamine (TEMED) and 0.075 % (v/v) ammonium persulfate (APS). The gel was left to polymerise at room temperature for 1 hr before the stacking gel as added. The stacking gel consisted of 5% (v/v) Acrylamide/ Bis-acrylamide RTU solution (Proto-gel) (37.5:1), 1.0 M Tris-HCl (pH

6.8), 0.2 % (w/v) SDS, dd H_20, SDS polymerisation was initiated with 0.008 % (v/v) TEMED and 0.1 % (v/v) APS. A 12-well comb was inserted into the plates before the stacking gel was added and left to polymerise at room temperature for 1 hr. Combs were removed after polymerisation and wells were washed with running buffer 0.1 % (w/v) SDS, 0.25 M Tris and 0.19 M glycine to remove unpolymerised acrylamide. Eight microliters from each immunoprecipitated sample (protein quantity unknown as it is dependent on quantity of protein immunoprecipitated from initial 500 µg protein sample). Electrophoresis occurred at 100 V for 30 min before being increased to 200 V and left to run until the tracking dye reached the bottom edge of the resolving gel (~ 1 hr 30 min). The gel was then removed from the glass plates and washed 3 times for 5 min in ddH_2O. Following removal of ddH_2O from the last wash, gels were stained in 100 ml of colloidal Coomassie blue (Bio-safe, Bio-rad laboratories, Hercules, USA) for 1 hour before being de-stained overnight in ddH_2O.

5.3.4 In-gel digestion

1D gel lanes from the resolving gel were fractioned in to 11 equal 5 mm x 7 mm segments. Each segment was cut using surgical blades (RS Pro carbon steel scalpel blades, RS Pro, Northants, UK) into $1mm^3$ gel plugs and dispensed into clean labelled lo-bind Eppendorf tubes. Gel plugs were de-stained with 50:50 acetonitrile (ACN)/ 50 mM Ambic for 15 min at 37 ^oC. This process was repeated at least three times or until there was no visible blue stain on the gel plugs. Gel plugs were reduced with 10 mM DDT for 1 hr at 37 ^oC before being alkylated with 50 mM iodoacetamide (IAM) for 1 hr in the dark at 4 ^oC. Gel plugs were then incubated in absolute ACN for 15 min at 37 ^oC. Following removal of the ACN, gel plugs were dehydrated at 60 ^oC for 30 min. Gel plugs were incubated with 0.01 µg/µL of sequence grade trypsin (Promega; V5113) for 15 min at 4 ^oC. After the incubation 50 mM ambic was added to each Eppendorf and digestion was allowed to continue overnight at 37 ^oC. Digestion was stopped the following morning by addition of 10µl 5% (v/v) formic acid for 30 min at

37 ^{o}C. Peptide solutions were cleared by centrifugation at 14,000g for 1 min and removed using a gel loading tip to a clean new labelled Eppendorf (extraction 1). The gel plugs were then incubated with 150µl of 0.5% (v/v) formic acid for a further 30 min at 37 ^{o}C, before being centrifuged again at 14,000g for 1 min. Peptides were removed with a gel loading tip and added to extraction 1. Peptide solutions were de-salted using a C-18 ziptip (Zip-tips; Millipore, Billercia, MA, USA) according to manufacturer's instructions.

5.3.5 Liquid chromatography-mass spectrometry

Label-free liquid chromatography-mass spectrometry analysis was performed by using nanoscale reverse-phase ultra-performance liquid chromatography (NanoAcquity; Waters) and online electrospray ionization quadrupole–time-off light mass spectrometry (Q-TOF Premier; Waters). Samples were loaded in aqueous 0.1 % (v/v) formic acid via a Symmetry C_{18} 5 µm, 2 cm x 180 µm trap column (Waters). Separation was conducted at 35 °C via a BEH C_{18} 1.7 µm, 25 cm x 75 µm analytical reverse-phase column (Waters). Peptides were eluted by using a gradient that rose to 37 % acetonitrile 0.1 % (v/v) formic acid over 90 min at a flow rate of 300 nl/min. Liquid chromatography eluent was sprayed into the mass spectrometer with a glass emitter tip (PictoTip, Waters) using a spray voltage of 3.0 kV in positive-ion mode. Full scan spectra were recorded from m/z 350 to 1600 at a resolution of >10,000 full width at half maximum (FWHM) using mass spectrometry survey scans of 0.45-s durations with an interscan delay of 0.05. Prior to analysis, the time-of-flight analyser was calibrated by using fragment ions of [Glu-1]-fibrinopeptide B from m/z 50 to 1990. MS/MS spectra of collision induced dissociation fragment ions were recorded for the 5 most abundant precursor ions of charge 2+ or 3+ detected in the survey scan. Precursor fragmentation was achieved by collision-induced dissociation at an elevated (20–40 eV) collision energy over a duration of 0.15 s per parent ion with an interscan delay of 0.05 s over 50–2000 m/z. Acquisition was switched from MS to

MS/MS mode when the base peak intensity exceeded a threshold of 30 counts/s and returned to the MS mode when the total ion chromatogram (TIC) in the MS/MS channel exceeded 50,000 counts/s or when 1.0 s (5 scans) were acquired. To avoid repeated selection of peptides for MS/MS, the program used a 30-s dynamic exclusion window. The Lockmass reference (100 fmol/µL Glu-1-fibrinopeptide B) was delivered to the NanoLockSpray source of the mass spectrometer at a flow rate of 200 nL/min, and was sampled at 60 s intervals.

5.3.6 IP Protein identification

Acquired MS/MS data was searched against the Swiss-Prot protein sequence database (2018.1) restricted to 20,333 sequences (human taxology) with Mascot (v2.3.2, Matrix Science) using Mascot Distiller (2.7.0.1) as the data input filter to generate peak lists. Enzyme specificity was trypsin, which allowed 1 missed cleavages, carbamidomethyl modification of cysteine (fixed), deamination of asparagine and glutamine (variable), oxidation of methionine (variable) and an m/z error of ± 0.3 Da. Decoy databases were employed to allow the calculation of identification error rates. Proteins were identified if they had at least one unique peptide with an identity threshold greater than 30 and false discovery rate <5%.

5.4 Results

5.4.1 PLIN5-IP GeLC-MS/MS on *m. vastus lateralis* from lean healthy participants

The PLIN5-IP GeLC-MS/MS protocol was performed twice on 2 (A and B) pooled samples (total of 4) of *vastus lateralis* muscle from lean healthy participants (Figure 5.1). Each replicate successfully immunoprecipitated PLIN5 and overall a total of 364 proteins were identified (Table 5.1). In total 87 proteins were consistently identified in all 4 replicates and a substantial portion of these (32) were immunoglobulins (Ig). Upon removal of known contaminants i.e. keratin, trypsin, filaggrin and all Ig 41

proteins remained (see supplementary Table 1 in appendix for protein list). The positive replication of PLIN5 identification within this IP lead us to apply this technique to muscle samples from obese and T2D participants.

Table 5.1 Number of proteins identified from PLIN5 IP GeLC-MS/MS of *m. vastus lateralis* from lean healthy male participants

	Pooled sample A				Pooled sample B				Combined results	
	A1	A2	Overlap	Total	B1	B2	Overlap	Total	Overlap	Total
Proteins	155	177	115	214	290	172	150	312	87	364
Ig	43	46	41	48	43	41	34	50	32	58

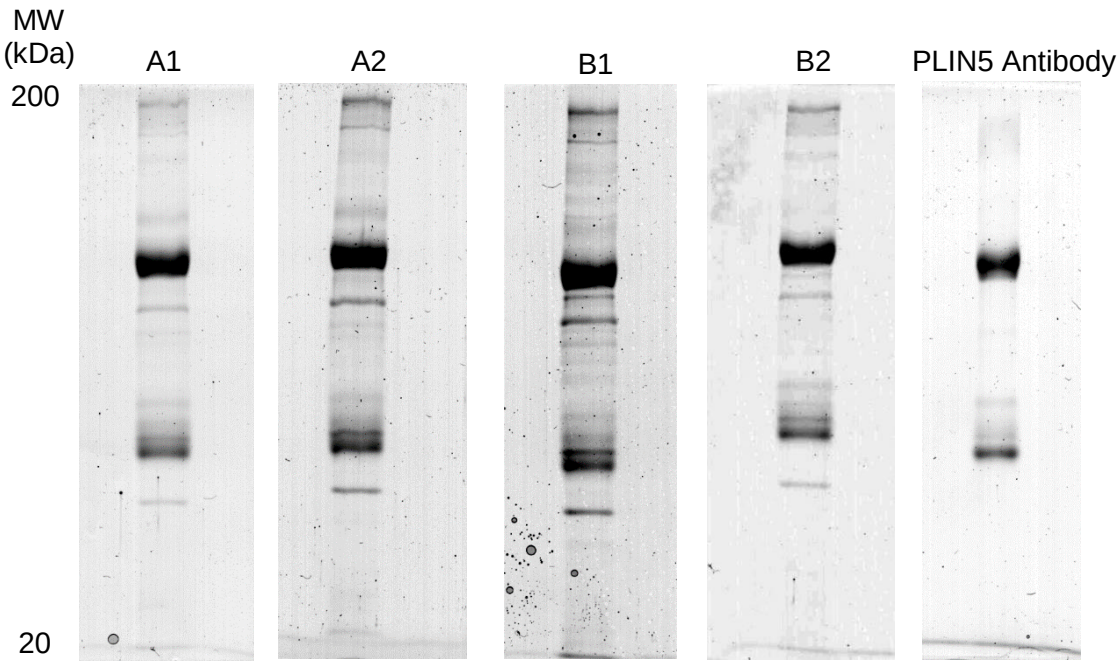

Figure 5.1. 1D SDS-PAGE of PLIN5-IP in *m. vastus lateralis* from lean healthy participants. 1D SDS-PAGE was performed twice following PLIN5-IP on two different pooled samples (A & B) from *m. vastus lateralis* of lean healthy participants. 1D SDS-PAGE also performed on Dynabeads-PLIN5 antibody combination without muscle tissue to highlight expected bands of Ig. MW, molecular weight; kDA, kilodaltons.

5.4.2 PLIN5-IP GeLC-MS/MS on *m. gluteus maximus* from obese and T2D *participants*

The PLIN5-IP GeLC-MS/MS protocol was performed three times each on pooled samples from *gluteus maximus* muscle of obese and T2D individuals (Figure 5.2). PLIN5 was only successfully immunoprecipitated once which occurred in muscle from T2D. (Table 5.2). The amount of Ig identified was notably lower compared to the PLIN5-IP GeLC-MS/MS performed on *m. vastus lateralis* from lean healthy participants. Comparisons revealed that at least 20 Ig proteins were absent from the PLIN5-IP GeLC-MS/MS that did not successfully immunoprecipitate PLIN5. The third replicate of T2D which successfully immunoprecipitated PLIN5 contained the immunoglobulin heavy variable 3-7 which was not present in the other obese or T2D replicates but was identified in all four of the *m. vastus lateralis* muscle sample. Importantly the variable domain of an antibody is the region responsible for specific antigen binding. The 1D SDS-PAGE of obese and T2D replicates lacked characterizable Ig bands that are observed when PLIN5 antibody is subject to 1D SDS-PAGE without incubation with muscle (Figure 5.2). Together this suggest that the PLIN5 antibody may become dissociated from the Dynabeads during incubation with the muscle. Due to the high number of proteins identified within this extract it is also possible that there was a high amount of non-specific binding of proteins to the Dynabead-antibody complex. If non-specific binding occurs from proteins that are of high abundance this can result in concealing peptides from lower abundance protein such as PLIN5 when analysed with LC-MS/MS. A more stringent wash protocol can remove non-specific binding of proteins. These results led us to test the PLIN5-IP GeLC-MS/MS protocol on different muscle from obese and T2D with different wash protocols.

Table 5.2 Number of proteins measured following PLIN5 IP GeLC-MS/MS of *gluteus maximus* muscle from obese and T2D participants

	Obese			T2D		
	1	2	3	1	2	3
Total no. proteins	236	253	176	413	532	445
Total no. of Ig	8	9	8	14	18	15
PLIN5 immunoprecipitated	X	X	X	X	X	√
No. Ig absent compared to lean healthy IP	24	24	24	20	24	19

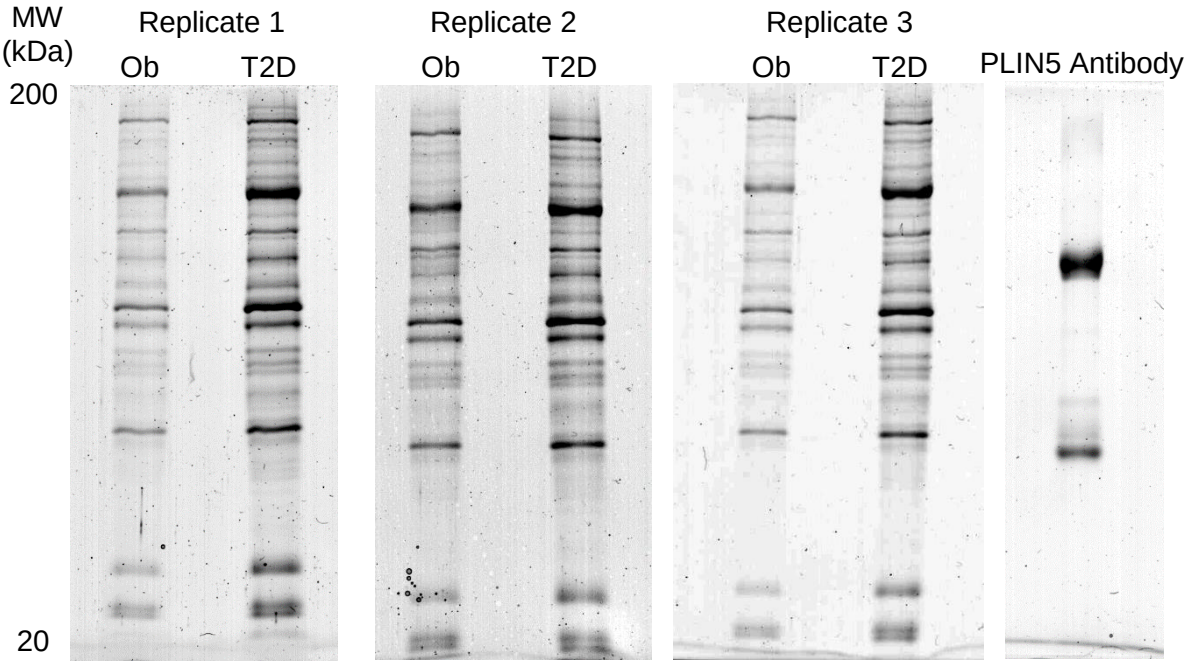

Figure 5.2. 1D SDS-PAGE of PLIN5-IP in *m. gluteus maximus* from obese and T2D participants. 1D SDS-PAGE was performed three times following PLIN5-IP on pooled samples of *m. gluteus maximus* from obese and T2D participants**.** 1D SDS-PAGE also performed on Dynabead-PLIN5 antibody combination without muscle tissue to highlight expected bands of Ig.

5.4.3 PLIN5-IP GeLC-MS/MS on *m. vastus lateralis* from obese and T2D participants

The PLIN5-IP GeLC-MS/MS protocol was performed twice on pooled samples from *m. vastus lateralis* from obese and T2D participants (Figure 5.3). The first samples consisted of the same wash technique as described in the methods (3 times in PBS-0.05 % Tween-20 by pipetting; washing protocol 1). The second samples were subject to washing protocol 2 which consisted of washing 5 times in wash buffer provided with the Dynabead kit (Invitrogen) by pipetting. On the last of the 5 washes the IP solution was placed on a hula-shaker for 1 min. All four PLIN5-IP GeLC-MS/MS successfully immunoprecipitated PLIN5. As anticipated, the more stringent wash protocol 2 reduced the amount of proteins identified in the samples (Table 5.3). Amongst the list of proteins identified was HSL, a known binding partner of PLIN5. Washing protocol 2 removed HSL from the list of proteins identified with the T2D muscle (Table 5.3). The bands from the 1D SDS-PAGE indicated successful elution of Igs comparable to when PLIN5-ab is subject to 1D SDS-PAGE without muscle incubation (Figure 5.3). The results from this part of the experiment demonstrate that the *gluteus maximus* muscle used previously may have disrupted the Dynabead-antibody-PLIN5 complex resulting in unsuccessful immunoprecipitation of PLIN5. Furthermore, although a stringent washing protocol decreased the total amount of protein identified and likely reduced non-specific binding of proteins this wash protocol also removed a known binding partner of PLIN5, HSL. The next part of the experiment aimed to apply the PLIN5-IP GeLC-MS/MS (washing protocol 1) technique to pooled m. vastus lateralis samples from; lean, obese and T2D participants. To control for the non-specific binding of proteins to the Dynabead-PLIN5-antibody complex a control IP GeLC-MS/MS was also performed.

Table 5.3 Number of proteins measured following PLIN5-IP GeLC-MS/MS of *vastus lateralis* muscle from obese and T2D.

	Obese		T2D	
	WP 1	WP2	WP1	WP2
Total no. proteins	558	467	484	293
Total no. Ig	41	39	8	11
PLIN5 immunoprecipitated	√	√	√	√
HSL co-immunoprecipitated	√	√	√	X

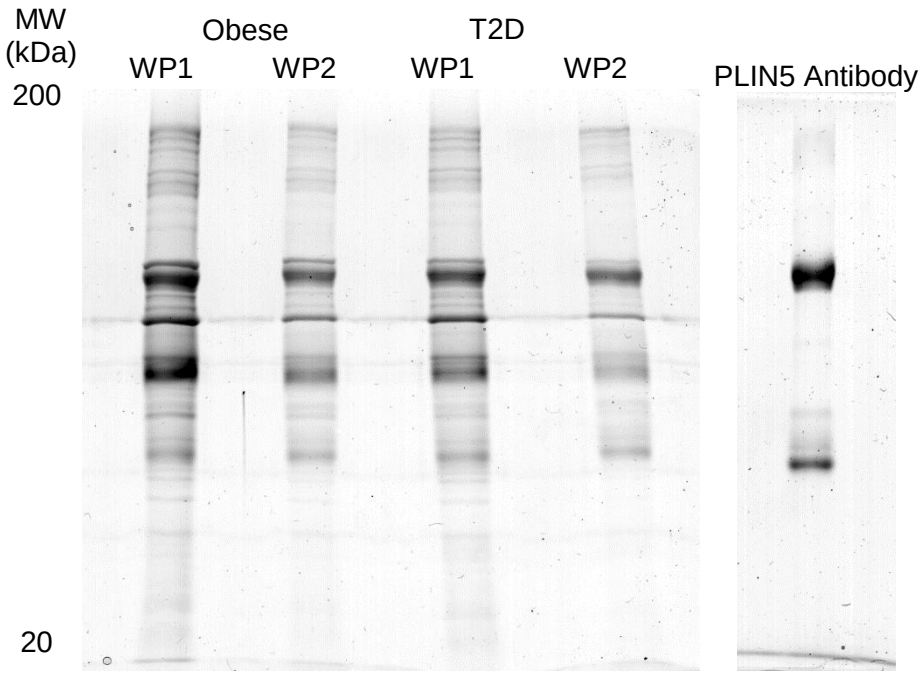

Figure 5.3. 1D SDS-PAGE of PLIN5-IP in *m. vastus lateralis* from obese and T2D participants with different wash protocols. 1D SDS-PAGE was performed twice following PLIN5-IP on pooled samples of *m.vastus lateralis* from obese and T2D participants**.** Washing protocol 1 (WP1) consisted of 3 washes with PBS- 0.05 % Tween-20 by pipetting. Washing protocol 2 consisted of 5 washes with wash buffer (Invitrogen) with last wash placed on hula-shaker for 1 min. 1D SDS-PAGE also performed on dynabead-PLIN5 antibody combination without muscle tissue to highlight expected bands of Ig.

5.4.4 PLIN5-IP GeLC-MS/MS on *m. vastus lateralis* from lean, obese and T2D sedentary participants.

The PLIN5-IP GeLC-MS/MS protocol was performed in replicates on pooled samples of *m. vastus lateralis* from lean (2 replicates), obese (3 replicates) and T2D (3 replicates) participants (Figure 5.4). A control-IP GeLC-MS/MS with an antibody against protein calicin was also performed 3 times in pooled samples of *m. vastus lateralis of* obese and T2D participants (Figure 5.4). All IPs combined identified a total of 1596 proteins. PLIN5 was identified in both PLIN5-IP lean replicates but only once in each of the obese and T2D PLIN5-IP replicates (Table 5.4). Expectantly PLIN5 was not present in the control-IP (Table 5.4). A total of 306 proteins were identified in both the lean PLIN5-IP replicates that successfully immunoprecipitated PLIN5. Due to there being insufficient *m. vastus lateralis* tissue from lean participants to run a control-IP , any proteins identified in replicates of the obese and T2D control-IP were subtracted from the lean PLIN5-IP resulting in a total of 62 proteins. Upon removal of known contaminants i.e. keratin, myosins, haemoglobin, and all Ig 52 proteins remained (see supplementary Table 2 in appendix for protein list). Upon removal of known suspected contaminants i.e. ribosomal proteins, ribonucleoproteins and tropomodulins (Trinkle-Mulcahy *et al.*, 2008), protein phospholipase A_2- group II, subgroup A (PA2GA) was the only protein remaining known to associate with LD, with no known mitochondrial proteins remaining. PA2GA therefore will be the focus of the discussion. Supplementary table 3 in appendix lists proteins identified from attempted PLIN5-IP and control-IP in *m.vastus lateralis* of obese and T2D participants.

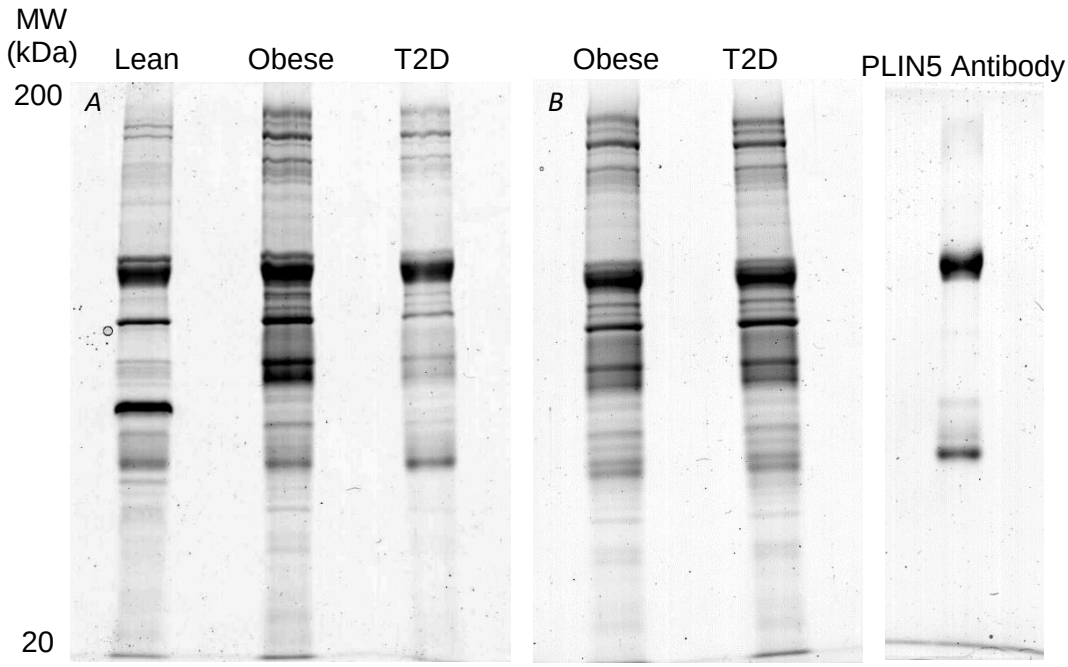

Figure 5.4. Representative 1D SDS-PAGE of PLIN5-IP (A) calicin-IP (B) in *vastus lateralis* muscle. 1D SDS-PAGE was performed following PLIN5-IP on pooled samples of *m. vastus lateralis* from lean, obese and T2D participants (A). 1D SDS-PAGE was then performed following calicin-IP (control) on pooled samples of *m. vastus lateralis* from obese and T2D participants (B). Due to insufficient *m. vastus lateralis* from lean participants a control IP could not be performed on this cohort. 1D SDS-PAGE was also performed on Dynabead-PLIN5 antibody combination without muscle tissue to highlight expected bands of Ig.

Table 5.4. Number of proteins identified from PLIN5-IP GeLC-MS/MS in *m. vastus lateralis* from lean, obese and T2D participants.

	Lean				Obese					T2D				
	1	2	Overlap	Total	1	2	3	Overlap	Total	1	2	3	Overlap	Total
Proteins	355	518	306	567	558	666	841	392	1014	484	616	541	321	812
Ig	36	40	33	43	41	35	37	27	48	35	41	32	26	47
PLIN5	√	√			√	X	X			√	X	X		

5.5 Discussion

The aim of this study was to develop an IP-mass spectrometry protocol that would capture PLIN5 and its associated proteins in human skeletal muscle in 3 different metabolic environments (lean sedentary, obese and T2D). PLIN5 was successfully and reproducibly immunoprecipitated in *m. vastus lateralis* from lean sedentary participants. This, however, was not replicated in *m. vastus lateralis* from obese and T2D participants. In the lean sedentary group PLIN5-IP extracted protein phospholipase A_2- group II, subgroup A which uniquely was not present in any of the control-IP and is not recognised as a known contaminant of Dynabead-antibody immunoprecipitation.

GeLC-MS/MS uses orthogonal separation to separate proteins by size (1D SDS-PAGE) and subsequent digested peptides by hydrophobicity during liquid chromatography (LC) allowing for a deeper insight into the muscle proteome and allowing lower abundance proteins to be recognised following immunoprecipitation. PLIN5 is a low abundance protein that is below the limit of detection when the GeLC-MS/MS protocol is performed directly in homogenates of soluble muscle proteins. The PLIN5-IP GeLC-MS/MS successfully and reproducibly immunoprecipitated PLIN5 in *m. vastus lateralis* from lean participants demonstrating enhanced sensitivity and selectivity when antibody immunoprecipitation is performed prior to mass spectrometry.

Due to the lack of *m. vastus lateralis* from lean sedentary participants, muscle the control IP GeLC-MS/MS was only conducted on *m. vastus lateralis* from obese and T2D participants. Proteins identified in either the obese or T2D control IP GeLC-MS/MS were subsequently extracted from proteins that appeared in both lean sedentary PLIN5-IP GeLC-MS/MS replicates, resulting in a list of proteins unique to a PLIN5-IP from *m. vastus lateralis* from lean sedentary participants. Although known contaminants such i.e. keratin, myosins, haemoglobin have been removed from this

list there are still a number of suspected contaminants i.e. ribosomal proteins, ribonucleoproteins and tropomodulins (Trinkle-Mulcahy *et al.*, 2008) . Within the unique set of proteins from the PLIN5-IP in the lean sedentary group phospholipase A_2 group II, subgroup A (PA2GA) was identified as a distinctive potential PLIN5 associated protein and will therefore be the focus of this discussion. Protein-protein interaction databases such as Struct2Net (Singh *et al.*, 2010)) and BioGRID 3.5 (Chatr-Aryamontri *et al.*, 2017) revealed at present there are no known interactions between PLIN5 and PA2GA.

PA2GA belongs to a family of phospholipase A_2s which can be found extracellularly, or membrane bound and are responsible for the hydrolysis of the *sn-2* position of glycerophospholipids producing FFA and lysophospholipids (Kramer *et al.*, 1989). PA2GA has been classified as a low molecular weight calcium dependent group II phospholipase A_2 (Dennis *et al.*, 2011) which can be secreted but importantly is also found in the cell (Guijas *et al.*, 2014). PA2GA in particular belongs to subgroup A of group II phospholipase A_2 which is also found in snake venom (Leiguez *et al.*, 2011). Isolated snake venom derived-PA2GA incubated in mice macrophages results in an increase in LD formation concomitant with an increased expression of PLIN2 and a recruitment of PLIN2 to the LD (Leiguez *et al.*, 2011). The exact role of every phospholipase A_2 has been made difficult by the fact that there are over 30 different variants and other enzymes that display related activity (Murakami *et al.*, 2011). Interestingly the key IMTG lipase, ATGL, also belongs to the Ca^{2+}-independent phospholipase A_2 group otherwise known as patatin-like phospholipase domain-containing lipases (Murakami *et al.*, 2011). It has previously been established that PLIN5 binds to ATGL and its co-activator CGI-58 (Wang *et al.*, 2011a). Research investigating the relationship between PLIN proteins and phospholipase A_2s is still in its infancy. The results from this chapter suggest that there may be an interaction between PLIN5 and PA2GA.

As anticipated there was a high degree of protein contaminants in all muscle samples however in the case of *m. vastus lateralis* from obese and T2D participants this may have increased the chances of PLIN5 being overshadowed and therefore not identified. A preclearing protocol prior to the PLIN5-IP may reduce protein contaminants and increase the chances of PLIN5 recognition. A pre-clearing step normally involves incubating the muscle with protein A/G Dynabeads and then discarding these Dynabeads thus removing any contaminant proteins that non-specifically bind to the protein A/G Dynabead complex. This presents a risk albeit low of removing proteins of interest that may have otherwise been bound to the target protein (i.e. PLIN5). Alternatively, a more stringent wash protocol can remove low non-specific binding to the Dynabead-antibody complex. A more stringent wash protocol was purposefully avoided in this protocol because during the development of the method we found removal of HSL (a known binding partner of PLIN5) occurred when a more thorough washing protocol (washing protocol 2) was used.

Interestingly PLIN1 was identified as a contaminant in *m. vastus lateralis* from lean sedentary, obese and T2D participants as it was identified not only in the attempted PLIN5-IP but also in the control-IP. PLIN1 has historically only been expressed in adipocytes and steroidogenic cells (Londos *et al.*, 1995). The conjecture that PLIN1 exists primarily in adipocytes exists because upon identification of the protein by Greenberg and colleagues (1991) they conducted western blots in various tissues including muscle with an antibody targeting PLIN1 and found it to be only expressed in adipocytes. Since this discovery research investigating PLIN proteins in skeletal muscle has focused on the remaining PLINs (PLIN2-5). This however has a potential to be an oversight. mRNA expression of PLINs demonstrated that PLIN1 was expressed in human skeletal muscle although to a lower extent than the other four PLINs (Gjelstad *et al.*, 2012). Additionally, deep proteomics of mouse skeletal muscle which quantified abundance of over 10,000 skeletal muscle proteins identified PLIN1

as the third most abundant PLIN protein (Deshmukh *et al.*, 2015b). Western blotting of human skeletal muscle has shown the presence of low PLIN1 levels (Hagstrom-Toft *et al.*, 2002) or none at all (Phillips *et al.*, 2005) which may be explained by antibody specificity or infiltration of extracellular adipocytes. Immunohistochemical staining of PLIN1 in porcine skeletal muscle showed localisation of PLIN1 surrounding muscle fibres (Gandolfi *et al.*, 2011) likely to be located on extracellular adipocyte depots. In this study PLIN1 was identified in *m. vastus lateralis* of lean sedentary, obese and T2D partiicpants but not in lean healthy participants used as part of the method development. The identification of PLIN1 from analysis of muscle samples may be a reflection of heightened extramyocellular lipids that is commonly observed in obesity (Hattori *et al.*, 2006)

In addition to PLIN1 adipocytes also highly express HSL (Hagstrom-Toft *et al.*, 2002), which together interact to stimulate lipolysis (Shen *et al.*, 2009). Considering the contamination of PLIN1 in the lean sedentary, obese and T2D participants it is plausible the HSL observed during the method development experiments was bound to PLIN1 in extramyocellular LD rather than PLIN5. PLIN5 is predominantly expressed in oxidative tissues such as skeletal muscle, heart muscle and liver (Wang & Sztalryd, 2011). Adipocytes, particularly from white adipose tissue have a lower oxidative capacity and therefore PLIN5 has often been undetectable in adipocytes from mice and rats (Wolins *et al.*, 2006; Ramos *et al.*, 2016). It is therefore unlikely that PLIN5 would be expressed highly in any extramyocellular LD. The presence of extramyocellular adipocytes in the muscle sample presents a new challenge when using immunoprecipitation-mass spectrometry to investigate lipid metabolism proteins in human skeletal muscle but also highlights the benefits of using a non-targeted mass spectrometry approach. For example, if a hypothesis driven approach was used to analyse this muscle such as PLIN5-IP followed by immunoblotting of HSL, the non-targeted PLIN1 discovery from mass spectrometry would not have been

identified and the potential contamination of adipocytes would have been unobserved. Through HSL bound to PLIN1 contamination, this may have misinformed us of a high abundance of HSL as a binding partner to PLIN5 in muscle from these cohorts. Together this highlights the benefits of using a non-targeted approach to detect PLIN5 associated proteins by critically evaluating proteins identified together from PLIN5-IP and control-IP.

To overcome the lack of detection of PLIN5 and associated proteins from muscle from obese and T2D participants in this PLIN5-IP GeLC-MS/MS protocol it may be more effective to use cultured muscle cells from these populations. This would remove contamination by extramyocellular adipocytes and allow the use of tag proteins (i.e. GFP) with SILAC. Whilst this would increase the likelihood of identifying PLIN5 binding partners it may sacrifice novel associated proteins that would only be detected *in vivo*. Notably, IMTG metabolism *in vivo* is subject to regulation from numerous factor such hormones, substrate levels and contraction (Donsmark *et al.*, 2003; Watt *et al.*, 2003c; Johnson *et al.*, 2004) cannot be accurately replicated *in vitro.* To preserve the *in vivo* environment, recent advancement in proteomics of mouse skeletal muscle have used peptide separation by isoelectric focusing which can identify up to a third more proteins in contrast to typical protein separation by gel electrophoresis (Hubner *et al.*, 2008). Improved sensitivity of detecting proteins can also be achieved by using an ion trap mass analyser (Deshmukh *et al.*, 2015b) allowing for deeper investigation into skeletal muscle proteome. The combination of peptide separation by isoelectric focusing combined with an ion trap analyser would increase the likelihood of PLIN5 and associated proteins being detected in muscle from obese and T2D participants *in vivo.*

Chapter 3 of this thesis highlighted PLIN5 is higher in oxidative type I muscle fibres in comparison to type II fibres in line with previous findings (Sollner, 2007; Shepherd *et al.*, 2013). Fibre type composition analysis has revealed a progressive shift from

type I fibres to type II fibres with increased insulin resistance (Marin *et al.*, 1994; Oberbach *et al.*, 2006; Stuart *et al.*, 2013; Albers *et al.*, 2015). It is anticipated in this study that the muscle from T2D and obese participants would therefore have a lower composition of type I fibres. The amount of PLIN5 that can be immunoprecipitated in muscle from obese and T2D participants may therefore be diluted by a lack of oxidative fibres which may have resulted in greater difficulty in the reproducibility of detecting PLIN5.

The aim of this study was to develop an immunoprecipitation-mass spectrometry protocol to pull-down PLIN5 and identify associated proteins in skeletal muscle with different metabolic environments. The PLIN5-IP GeLC-MS/MS protocol successfully immunoprecipitated PLIN5 and identified PA2GA as potential new protein interactor. Reverse immunoprecipitation of PA2GA would further validate this protein-protein interaction. Confocal immunofluorescence microscopy can be leveraged to investigate the colocalisation of these two proteins within skeletal muscle.. Obese and T2D muscle could not successfully replicate PLIN5-IP likely due to increased contaminants from extramyocellular adipocytes and/or decreased availability of PLIN5 due to known decreased composition of type I fibres. Future research needs to focus on optimising a protocol leveraging recent advancements in peptide separation by isoelectric focusing and high-resolution mass spectrometry (Hubner *et al.*, 2008; Deshmukh *et al.*, 2015b) to allow the investigation of PLIN5 associated proteins in muscle from obese and T2D participants.

Chapter 6. Discussion

6.1 Overview

Western lifestyle is characterised by reduced physical activity, increased sedentary time and over-consumption of energy dense foods. This has led to drastic increases in obesity and type 2 diabetes (T2D) (Diabetes UK, 2017; World Health Organisation, 2017) and an increased risk for cardiovascular disease (Laakso, 2010). Fat is considered to be very palatable yet very energy dense (Rolls, 2000) and readily available in western culture. Due to this, several studies have used high-fat high-calorie (HFHC) diets as a model to induce insulin resistance in humans and study the mechanisms behind this pathogenesis. Most of this research has been completed in cohorts of young healthy males and studies that did include females did not directly compare sexes. This is a considerable oversight considering pre-menopausal women with normal levels of the female hormones (oestrogen and progesterone) appear to be better protected against metabolic diseases compared to males.

Elevated intramuscular triglyceride (IMTG) content has been observed in insulin resistant individuals and endurance trained insulin sensitive individuals in a phenomenon called the athlete's paradox (Goodpaster *et al.*, 2001). A key discrepancy between endurance trained individuals and insulin resistant individuals is the higher capacity for turnover (i.e. deplete and resynthesise) of their IMTG stores (Perreault *et al.*, 2010) which is proposed to reduce the accumulation of lipid metabolites known to directly impair skeletal muscle insulin signalling. Research over the past two decades have explored the mechanisms behind IMTG re-synthesis and hydrolysis that help to regulate IMTG turnover. HFHC diets have also been shown to increase IMTG content. However, very few studies have investigated the mechanisms behind this increase in IMTG stores and how this relates to skeletal muscle insulin resistance. Perilipin (PLIN) proteins and synaptosomal-associated protein 23 (SNAP23) have been implicated in assisting the expansion of the IMTG stores following lipid excess (Bostrom *et al.*, 2007; Bosma *et al.*, 2012a; Bosma *et al.*,

2013; Shepherd *et al.*, 2017b). Furthermore, most research on the effects of HFHC diet on IMTG stores has been conducted on whole muscle homogenates (Gemmink *et al.*, 2016). This does not take into consideration that different fibre-types have different capacities to store and utilise IMTG (Shepherd *et al.*, 2013; Shepherd *et al.*, 2017b) or that larger lipid droplets (LD) storing IMTG located in subsarcolemmal region of muscle fibres are more associated with insulin resistance than intermyofibrillar LD (Crane *et al.*, 2010; Daemen *et al.*, 2018). The fibre-type and region-specific responses to a HFHC diet on IMTG content and proteins regulating IMTG stores have not yet been investigated.

IMTG is now recognised as an important energy source particularly during moderate-intensity exercise where maximal fat oxidation is elicited (van Loon *et al.*, 2001). Understanding the mechanisms behind IMTG hydrolysis in healthy insulin-sensitive individuals is important to understand how overall IMTG turnover is regulated. Hormone-sensitive lipase (HSL) and adipose triglyceride lipase (ATGL) are the main enzymes responsible for IMTG hydrolysis. LD associated with PLIN2 and PLIN5 are preferentially used during a 1 h bout of moderate intensity exercise (Shepherd *et al.*, 2012, 2013). PLIN2 and PLIN5 have been shown to interact or colocalise with HSL and ATGL (Prats *et al.*, 2006; Wang *et al.*, 2011a; MacPherson *et al.*, 2013a). Prior to this thesis little was known about the distribution and colocalisation of HSL and ATGL to LD and to PLIN proteins during a bout of moderate-intensity exercise in human skeletal muscle.

In recent years PLIN5 has emerged as an important PLIN in regulating IMTG hydrolysis (Wang *et al.*, 2011a; Shepherd *et al.*, 2013) and also provide metabolic linkage to mitochondria (Bosma *et al.*, 2012b). Hypothesis driven techniques such as PLIN5 immunoprecipitation (IP) followed by immunoblotting has confirmed that PLIN5 interacts with key lipolytic enzymes HSL (MacPherson *et al.*, 2013a), ATGL and its co-activator CGI-58 (Wang *et al.*, 2011a; MacPherson *et al.*, 2013a). Proteomic

analyses has revealed that over 300 proteins are associated with LD (Zhang *et al.*, 2011). As PLIN5 is a LD associated protein and is linked to mitochondria it is likely that PLIN5 is also associated to other proteins that have not yet been identified. Due to the differences in IMTG turnover between insulin sensitive and insulin resistant individuals (Perreault *et al.*, 2010) whether PLIN5 is associated to different proteins in different metabolic disease states needs investigation.

The overall aim of this thesis was to explore proteins that regulate skeletal muscle lipid metabolism in humans; focusing on the effects of a HFHC diet, an acute bout of moderate-intensity exercise and different metabolic disease states (lean, obese and T2D). Chapter 2 determined whether there were sex-specific differences in functional outcomes of cardio-metabolic health in response to 7 days HFHC diet. Chapter 3 investigated the fibre-type and region-specific changes in IMTG content and proteins (PLINs and SNAP23) regulating IMTG accumulation following a 7-day HFHC diet. Chapter 4 investigated colocalisation of key lipases HSL and ATGL to LD associated with PLIN2 and PLIN5 in response to a moderate-intensity exercise bout. Due to PLIN5 being identified as an important PLIN for regulating IMTG hydrolysis, Chapter 5 aimed to develop a novel immunoprecipitation mass-spectrometry protocol to identify PLIN5 associated proteins to investigate how these proteins change between different metabolic states (lean, obese and T2D).

6.2 High-fat high-calorie diets as a method to induce insulin resistance

Lipid-infusion studies have been extensively used to investigate lipid-induced insulin resistance particularly in skeletal muscle (Boden *et al.*, 1994; Shah *et al.*, 2002; Chow *et al.*, 2014). Results from the studies however may only provide an overview of acute responses to lipid excess rather than more chronic lipid overload observed in obesity and T2D. Consequently, many researches have used a more chronic lipid overload in the form of a HFHC diet to investigate lipid-induced insulin resistance (Brons *et al.*, 2009; Bakker *et al.*, 2014; Hulston *et al.*, 2015; Parry *et al.*, 2017). Although some

studies included female participants (Hulston *et al.*, 2015; Parry *et al.*, 2017), to date no study had directly compared sexes to clarify the sex-specific cardiovascular and metabolic responses to a short-term HFHC diet. The aim of chapter 2 was to determine sex-specific differences in functional outcomes of cardiovascular and metabolic health in response to 7 days HFHC diet. A wide range of metabolic and cardiovascular outcomes were measured including; metabolic flexibility and insulin sensitivity derived indexes from the oral glucose tolerance test, body composition from dual x-ray absorptiometry (DXA), arterial stiffness from aortic pulse wave velocity and blood lipid profile and liver enzymes from fasting blood samples. This gave a comprehensive overview of any detrimental effects of the HFHC diet on metabolic and cardiovascular health. The results showed there was no overall effect of the HFHC diet on any of the functional outcomes of cardiovascular or metabolic health in young healthy adults of either sex. This is in line with other studies which have also reported no effect of a HFHC diet on indices of insulin sensitivity (Adochio *et al.*, 2009; Brons *et al.*, 2009) and indicates that some individuals may be protected against these diets. Reduced physical activity with a HFHC diet has shown more clear reductions in insulin sensitivity (Knudsen *et al.*, 2012), whilst high cardio-respiratory fitness levels are protective against all-cause mortality (Blair *et al.*, 1989). It is noted that the participants in chapter 2 were all very physically active and had high levels of cardio-respiratory fitness and this may therefore have protected them against the detrimental effects of a HFHC diet. When the same HFHC diet was applied to a mixed cohort (n=13 males, n=2 females) in chapter 3 glucose tolerance from an oral glucose challenge was impaired and tracer-derived measurements showed a reduction in metabolic clearance rate. Together the data indicates a 7-day HFHC diet can impair insulin sensitivity in healthy adults but certain cohorts may be protected.

6.3 Fibre-type and region-specific changes in LD morphology following HFHC diet.

IMTG content increases following lipid infusion and/or after a high-fat diet (Bachmann *et al.*, 2001; Gemmink *et al.*, 2017a; Shepherd *et al.*, 2017b) (section 1.7). It is now accepted that type I fibres exhibit higher capacity to store IMTG (Shepherd *et al.*, 2013; Shepherd *et al.*, 2017b) and therefore fibre type specific approaches to investigate increases in IMTG need to be adopted. In addition to this transmission electron microscopy (TEM) has been able to identify larger LD located in the subsarcolemmal region are more associated with insulin resistance (Crane *et al.*, 2010; Daemen *et al.*, 2018) (section 1.6.2.3). Chapter 3 therefore used a fibre-type (type 1 *vs.* type IIa *vs.* type IIx) and region-specific (central *vs* peripheral) approach to investigate changes in IMTG content (LD number and morphology) following a 7-day HFHC diet. The results showed that following the HFHC diet increases in IMTG content were specific to type I fibres and occurred similarly between the peripheral and central region of type I muscle fibres. This fibre-type specific increase in IMTG is similar to that observed following 6 h of lipid infusion during a hyperinsulinaemic-euglycaemic clamp (Shepherd *et al.*, 2017b). This further highlights the importance of adopting fibre-type specific approaches to investigate changes in IMTG. Although IMTG content did not increase in type IIa or IIx fibres, there was an increase in IMTG content in the peripheral region of these muscle fibres due to an increase in LD size and number. Whilst overall IMTG content did not increase in the central region of type IIa or IIx fibres there was an increase in LD size. By leveraging a fibre-type and region-specific analysis of images obtained from confocal immunofluorescence microscopy chapter 3 was also to propose distinct patterns of IMTG accretion in human skeletal muscle, whereby lipid accumulates in type I fibres prior to type IIa or IIx fibres, changes in LD size precede an increase in LD density, and this occurs in the peripheral region of the cell before the central region. This preferable IMTG

accumulation in healthy individuals following a HFHC diet is distinct from that observed in insulin-resistant states which show IMTG accumulation in the subsarcolemmal region (Chee *et al.*, 2016), in type II fibres (Daemen *et al.*, 2018) and characterised by larger LD (Nielsen *et al.*, 2017). As there were no impairments in skeletal muscle insulin signalling following the 7-day HFHC diet (Chapter 3) it is proposed these increases in IMTG stores are a protective mechanism preventing the accumulation of lipid metabolites known to contribute to skeletal muscle insulin signalling.

6.4 The role of proteins in increasing IMTG content after HFHC diet.

Although IMTG increases following HFHC diet the mechanisms underpinning this increase are still unknown. Recently Gemmink et al., (2017a) showed that PLIN5 protein expression increased in whole muscle homogenates concomitant to an increase in IMTG. As previously explained type I fibres store higher IMTG content compared to type II fibres (Shepherd *et al.*, 2013; Shepherd *et al.*, 2017b) and therefore investigations of the mechanisms underpinning increased IMTG stores also need to be fibre type-specific. Chapter 3 demonstrated that PLIN3 was the only PLIN to increase in protein expression following a HFHC diet and this was exclusive to type I fibres. This did not however lead to an increase in PLIN3+ LD indicating that increases in PLIN3 are targeted to LD that already have PLIN3 associated suggesting that PLIN3 may support LD growth and stability.

Chapter 3 also showed there was an increase in the fraction of PLIN2 colocalising with LD resulting in an increase in PLIN2+ LD in type I fibres without an increase in PLIN2 protein expression following the HFHC diet. This is a similar finding to increase in PLIN2+ LD in type I fibres following 6 h lipid infusion without increases in PLIN2 protein expression (Shepherd *et al.*, 2017b). Colocalisation analysis from chapter 3 confirmed that only a fraction of PLIN2 (~0.4) is colocalised to LD however this is lower than previously reported findings (~0.60-0.65) (Shaw *et al.*, 2009; Shepherd *et*

al., 2013; Shepherd *et al.*, 2017b), but does indicate there is free PLIN2 within the muscle. Previous research from macrophages and adipocytes has indicated that PLIN2 has a role in supporting LD biogenesis (Brasaemle *et al.*, 1997; Robenek *et al.*, 2006), however is not associated with mature adipocytes (Brasaemle *et al.*, 1997). Newly-formed LD may therefore become associated with PLIN2 leading to an increase in PLIN2+ LD and it could be speculated that free PLIN2 within the muscle may indicate disassociation from the LD once they reach maturity. In chapter 3 colocalisation analysis also revealed that a fraction of PLIN3 and PLIN5 colocalise with LD in skeletal muscle and only a fraction of LD are colocalised to either PLIN2, PLIN3 or PLIN5 further confirming a heterogenous LD pool in human skeletal muscle (Shepherd *et al.*, 2013; Shepherd *et al.*, 2017b).

Chapter 3 also revealed that SNAP23 colocalisation to; the plasma membrane, LD and the mitochondria was not altered following the HFHC diet in either type I or type IIa fibres. Previous research in cardiomyocytes treated with oleic acid showed an increase in the LD-associated pool of SNAP23 with a concomitant reduction in SNAP23 at the plasma membrane (Bostrom *et al.*, 2007), leading to the hypothesis that LD 'hijack' SNAP23 from the plasma membrane to assist in LD fusion following lipid excess (Sollner, 2007). The lipid excess provided by a 7-day HFHC diet in chapter 3 did not stimulate any redistribution of SNAP23 in human skeletal muscle. There was an increase in LD size however and therefore it may be plausible that there was already sufficient SNAP23 colocalised to LD to regulate LD fusion. Research into SNAP23 regulation in human skeletal muscle is still very much in its infancy with only recently SNAP23 colocalisation to the plasma membrane, LD and mitochondria being investigated in human skeletal muscle (Strauss *et al.*, 2016). The evidence from chapter 3 further confirms the distribution of SNAP23 within skeletal muscle and in different fibre type which paves the way for future research investigating alterations in distribution as a result of metabolic changes such as T2D.

6.4.1. The use of confocal immunofluorescence microscopy in region specific analyses

Studies using TEM can accurately distinguish between the subsarcolemmal and intermyofibrillar regions of muscle fibres providing valuable information on LD size and density in these specific areas. Counterintuitively TEM can only exam small fragments of muscle and is limited in its ability to co-examine LD with multiple proteins of interest. In Chapter 3 confocal immunofluorescence microscopy was used to circumvent these problems; allowing full cross-sectional analysis of different fibre types and permitting colocalisation analyses to be performed. We identified 5μm from the cell border as the peripheral region and the remainder of the cell as the central region. Our aim was to identify these regions as one that was near the plasma membrane and close to insulin signalling cascades but also large enough area to be able to yield information regarding LD dynamics. The central region was then identified as an area distinguishably away from the plasma membrane and distant from insulin signalling cascades. This methodology consequently allowed for the benefits of confocal immunofluorescence microscopy to be deployed whilst gaining insights into region specific changes in lipid metabolism in different muscle fibres.

6.5 Distribution and colocalisation of lipases involved in IMTG hydrolysis

Evidence from isolated rat skeletal muscle demonstrated that HSL translocates to LD *ex vivo* from both adrenaline and electrically stimulated contraction (Prats *et al.*, 2006) (section 1.3.2.2) however whether this mechanism existed in human skeletal muscle *in vivo* was still unknown. Previously widefield microscopy was used to investigate the effects of moderate-intensity exercise on the localisation of ATGL to LD in human skeletal muscle (Mason *et al.*, 2014b) (section 1.3.2.2). This type of microscopy is limited by the refraction of light (compared to a laser) and the resolving power of the microscope. Chapter 4 used higher resolution confocal immunofluorescence microscopy to show that HSL preferentially redistributes to LD following 1 h moderate-

intensity exercise in human skeletal muscle. In contrast a proportion of ATGL was already colocalised to LD and this was unchanged following the exercise bout. PLIN proteins have also been implicated in IMTG hydrolysis (section 1.5.). Chapter 4 also showed that HSL preferentially redistributes to PLIN5+ LD in comparison to PLIN5- LD whereas PLIN2+ LD and PLIN2- LD had similar amounts of increased HSL colocalisation. These findings are consistent with a previous analysis of muscle samples used in chapter 4 showing that following endurance training PLIN5+ LD are preferentially used during 1 h of moderate-intensity exercise in human skeletal muscle compared to PLIN5-LD, whereas PLIN2+ LD and PLIN2- LD are used to a similar extent (Shepherd *et al.*, 2013). These results add to the current consensus that PLIN5 is the main PLIN involved in regulating IMTG hydrolysis. PLIN5 has also been shown to interact with ATGL and its co-activator CGI-58 (Wang *et al.*, 2011a) and recruits LD to the surface of mitochondria (Wang *et al.*, 2011b; Bosma *et al.*, 2012b). Together chapter 4 and recent evidence suggests that PLIN5 assists in IMTG hydrolysis by interacting with key enzymes HSL and ATGL and then assists in directing IMTG-derived FA to the mitochondria for subsequent β-oxidation.

6.5.1 Limitations of confocal immunofluorescence microscopy

Chapter 3 and 4 have generated novel data of LD dynamics using confocal immunofluorescence microscopy. Whilst these findings are important, it is crucial to appreciate the limitations of using this technique. The resolution of a confocal microscope is 200nm, whilst this is appreciably better than a widefield microscope it doesn't match the accuracy of a transmission electron microscope. When analysing colocalisation of a protein e.g. PLIN with a LD it is possible that a PLIN in close proximity to LD but not actually in contact would be counted as a PLIN+ LD due to this resolution power. Additionally due to microscope channel constraints PLIN+ LD analyses can only be conducted on a single PLIN protein with LD. We cannot exclude the possibility therefore that LD have multiple perilipin proteins colocalised to them. It

is also plausible that PLIN- LDs may also be newly formed LD that did not have sufficient PLIN associated to them to be detected by the lower detection limit of the microscope. The z plane of the confocal microscope is approximately 0.53 µm which means any LD within this Z field will be imaged by the microscope. PLIN proteins that are underneath but still associated to the LD and out of this depth will not however be imaged and included in the analysis. Nonetheless confocal immunofluorescence microscopy provides a higher resolution compared to widefield microscopy and still permits multiple labelling of proteins unlike TEM. Despite these limitations therefore confocal immunofluorescence microscopy remains a beneficial and suitable method for investigating skeletal muscle lipid metabolism.

6.6 A non-targeted approach to investigating PLIN5 associated proteins

Chapter 4 highlighted that PLIN5 is important for IMTG hydrolysis because HSL preferentially redistributes to PLIN5+ LD during a 1 h moderate-intensity exercise bout. PLIN5+ LD have also been shown to be preferentially used during 1 h of moderate-intensity exercise (Shepherd *et al.*, 2013) and PLIN5 also provides metabolic linkage to mitochondria (Bosma *et al.*, 2012b). Together the data suggests PLIN5 is important in regulating IMTG hydrolysis and directing IMTG-derived fatty acid to the mitochondria for subsequent β-oxidation. Chapter 5 aimed to develop a novel immunoprecipitation (IP)-mass spectrometry approach that would identify novel PLIN5 associated proteins in human skeletal muscle. By following PLIN5-IP with gel electrophoresis prior to high performance liquid chromatography tandem mass spectrometry (GeLC-MS/MS), a successful reproducible protocol was established that immunoprecipitated PLIN5 from the muscle of lean participants. Furthermore, a unique protein associated with PLIN5 was identified as phospholipase A_2- group II, subgroup A (PA2GA) from muscle lean sedentary participants. PA2GA has previously been linked to LD formation and recruitment of PLIN2 to LD in mice macrophages (Leiguez *et al.*, 2011). This finding generates the new hypothesis that PLIN5 and

PA2GA interact at the LD surface to regulate lipid metabolism in human skeletal muscle. However, the PLIN5-IP GeLC-MS/MS protocol developed in chapter 5 did not lead to a reproducible immunoprecipitation of PLIN5 from the muscles of inactive males and females with obesity and T2D undergoing elective orthopaedic surgery. Potential reasons for this were protein contaminations from extramyocellular adipocytes in these muscles and a low muscle PLIN5 content in these groups due to a reduced composition of type I fibres in insulin-resistant states. Chapter 5 was the first study to apply an IP-mass spectrometry technique to human skeletal muscle and these results highlight the complexity of using this technique particularly in diseased states such as obesity and T2D. Future work is certainly needed to develop a replicable IP- mass spectrometry protocol that can be applied to muscle from different metabolic conditions (lean, obese and T2D) and direct comparisons to be made. At present, investigations into skeletal muscle lipid metabolism can continue to occur with the use of confocal immunofluorescence microscopy, which can be effectively used in different diseased states to generate more robust conclusions.

6.7 Future research

6.7.1 Understanding what protects individuals from the detrimental effects of a HFHC diet on functional outcomes of cardiovascular and metabolic health.

The results from chapter 2 showed there were no impairments resulting from the HFHC diet on functional outcomes of cardiovascular and metabolic health. Whilst some studies investigating the effects of HFHC diets have shown reductions in measurements of whole-body insulin sensitivity (Hulston *et al.*, 2015; Parry *et al.*, 2017), others have shown no reduction in peripheral insulin sensitivity (Adochio *et al.*, 2009; Brons *et al.*, 2009), but have observed reductions in hepatic insulin sensitivity (Brons *et al.*, 2009). It is therefore apparent that some cohorts may be protected against the detrimental effects of a HFHC diet that clearly warrants further investigation. The participants in chapter 2 were all young, had high levels of physical

activity (PA) and had a good levels of cardio-respiratory fitness, all of which have the potential to be protective against cardiovascular and metabolic diseases.

High cardio-respiratory fitness reduces the risk of T2D and all-cause mortality (Blair *et al.*, 1989; Nojima *et al.*, 2017). In chapter 2 there were no detrimental effects observed following a 7-day HFHC diet in either sex and both males and females displayed good levels of cardio-respiratory fitness ($\dot{V}O_{2\ peak}$: 62.3 ± 8.7 and 58.2 ± 8.2 $ml.min^{-1}.kgFFM^{-1}$ for males and females respectively). A question therefore emerges of whether participants in chapter 2 were protected from the detrimental effects of a HFHC diet due to their elevated cardio-respiratory fitness. Studies using a similar duration HFHC diet protocol that have shown impairments in insulin sensitivity have not measured cardio-respiratory fitness prior to the dietary protocol (Hulston *et al.*, 2015; Parry *et al.*, 2017), making it difficult to ascertain whether cardio-respiratory fitness was a protecting factor. Future research should therefore investigate high cardio-respiratory fitness vs low cardio-respiratory fitness on the effects of HFHC diet on functional outcomes of cardiovascular and metabolic health. Importantly to determine whether cardio-respiratory fitness was the unique factor protecting these individuals, groups should be matched for sex and age and physical activity levels should be controlled for each group.

Notwithstanding, the differences in male and female responses to models that induce insulin resistance is still vastly understudied. It would therefore be pertinent to extend the findings of chapter 2 by using a more rigorous method of impairing functional outcomes of cardiovascular and metabolic health. This could occur in the form or combining a HFHC diet with reduced PA or by extending the duration of the HFHC diet to allow aberrations to occur. The understanding of how T2D develops in females still remains critical in our understanding of the pathology of this disease and how to develop interventions to combat it.

6.7.2. Quantification of lipid metabolites following a HFHC diet

Chapter 3 concluded that increases in IMTG following HFHC diet help to maintain the insulin signalling pathway likely by reducing the accumulation of lipid metabolites known to disrupt the insulin signalling pathway. Future research should confirm this hypothesis and quantify changes in lipid species following a HFHC diet when there are increases in IMTG. Previously lipid metabolite DAG was shown to impair skeletal muscle insulin signalling (Schmitz-Peiffer *et al.*, 1997; Itani *et al.*, 2002), however evidence has emerged that the subcellular location, saturation and FA positioning on the glycerol backbone are all influential factors in DAGs contribution to insulin resistance (Bergman *et al.*, 2010; Amati *et al.*, 2011). The identification of certain lipid species that increase following HFHC diet but do not result in disruption in skeletal muscle insulin signalling will be advantageous in recognising benign lipid stores that are not detrimental to skeletal muscle health. This will shed further light on the athlete's paradox by identifying which specific lipid moieties promote an insulin desensitizing effect.

6.7.3 The need for insulin signalling immunohistochemistry assays

In chapter 3 it was demonstrated that although whole body insulin sensitivity was reduced this was not due to impairments in skeletal muscle insulin signalling as quantified with western blot of whole muscle homogenates. The mechanisms behind this protective insulin signalling was investigated using fibre-type specific analyses of lipid metabolism. Here it was demonstrated that IMTG increased in type I fibres only, likely aided by a concurrent increase in PLIN3 protein expression and re-distribution of PLIN2 to existing LD stores. It would be useful to know if the maintenance of the insulin signalling pathway occurred across all fibre types or whether there was fibre-type or cell location specific changes. Glucose uptake from the muscle is also dependent on increased blood flow to microvascular units in the muscle (Keske *et al.*, 2016), allowing the effective delivery of glucose, insulin and other substrates. It is

also plausible that cell specific insulin signalling may be a result of perfusion to the cells from surrounding microvascular units. The development of immunohistochemistry assays that can measure cell-specific phosphorylation of insulin signalling intermediates would aid in answering these questions.

6.7.4. Is IMTG hydrolysis impaired after HFHC diet?

In chapter 3 it was concluded that increases in IMTG following a HFHC diet help to maintain the insulin signalling pathway likely by reducing the accumulation of lipid metabolites known to disrupt the insulin signalling pathway. Increases in IMTG are not correlated with decrements in skeletal muscle insulin sensitivity if an individual retains the capacity to turnover their IMTG stores (Perreault *et al.*, 2010), as is often observed in endurance trained individuals (van Loon, 2004). An increase in IMTG therefore also needs to be matched with an increased capability of IMTG turnover if skeletal muscle insulin sensitivity is to be maintained. Following HFHC diet induced increases in IMTG, future research should investigate whether the capacity to hydrolyse IMTG is impaired or not. Development of immunohistochemistry analyses have revealed unique mechanisms of how IMTG hydrolysis is regulated in human skeletal muscle. For example, during 1 h of moderate-intensity exercise, HSL preferentially redistributes to PLIN5+ LD (Chapter 4) and PLIN5+ LD are favourably used over PLIN5- LD (Shepherd *et al.*, 2013). Future research should specifically use these immunohistochemistry analyses to reveal whether these mechanisms in insulin-sensitive individuals are impaired or maintained following HFHC diets.

6.7.5. Does HSL redistribution change in endurance athletes or individuals with T2D?

Chapter 4 established that HSL preferentially redistributed to PLIN5+ LD in human skeletal muscle following moderate-intensity exercise. The study was conducted on lean healthy insulin sensitive individuals who typically display high IMTG turnover at rest (Kanaley *et al.*, 2009) and during submaximal exercise (Guo *et al.*, 2000).

Conversely, obese pre-diabetic individuals showed impaired IMTG turnover (Perreault *et al.*, 2010). Men diagnosed with type 2 diabetes have a lower skeletal muscle HSL protein content in comparison to normal glucose tolerant controls and their HSL activity shows signs of dysregulation at rest and following insulin-stimulation (Jocken *et al.*, 2013). Future research should investigate whether impairments in IMTG hydrolysis that exist in pre-diabetic and diabetic individuals is matched with impaired HSL distribution pre and post exercise. PLIN2+ LD are used during a moderate-intensity bout of exercise (Shepherd *et al.*, 2012). Following 6-weeks of endurance training or sprint interval training, healthy lean individuals preferentially utilised PLIN5+ LD in comparison to PLIN5- LD whereas both PLIN2+ LD and PLIN2 –LD were used to the same extent (Shepherd *et al.*, 2013) suggesting PLIN5 plays a pertinent role in increasing fat oxidation capacity in skeletal muscle. To add to the emerging field of PLIN research, it would be beneficial to know if HSL preferentially redistributes to PLIN5+ LD or whether this mechanism is diminished in obese or type 2 diabetic muscle. The participants in chapter 4 had undergone 6 weeks of endurance training prior to the experimental protocol but were not endurance athletes. Whether there is an increased distribution of HSL to PLIN5+ LD in muscle from endurance trained athletes that enhances their ability to utilise IMTG stores during exercise also warrants further investigation.

6.7.6 Advancing the use of proteomics to understand skeletal muscle lipid metabolism.

Recent developments in proteomics provide an unbiased comprehensive catalogue of the skeletal muscle proteome and represents an ideal analytical tool for high-throughput discovery of protein alterations in health and disease (Hochstrasser *et al.*, 2002). In 2015, state of the art mass spectrometry work flow was able to quantify abundance values of over 10,000 proteins in mouse skeletal muscle (Deshmukh *et al.*, 2015b). Mass-spectrometry based proteomics is a relatively new analytical

approach, developments in technology and refinements in protocols are now making it possible to; 1. quantify abundance values of the large data sets of the skeletal muscle proteome (Deshmukh *et al.*, 2015b), 2. recognise post-translational modifications to large protein data sets following acute contractions (Potts *et al.*, 2017) and 3. with the use of IP – mass spectrometry identify novel protein binding partners in different disease states (Yoon *et al.*, 2012). These advancements provide an exciting avenue to take a non-biased approach to explore regulation in skeletal muscle lipid metabolism. Chapter 5 developed an IP-mass spectrometry protocol to investigate proteins associated with PLIN5 and identified PA2GA as a unique protein associated to PLIN5 in muscle of lean sedentary participants. The difficulty of applying this technique to muscle of obese and T2D individuals was likely compromised by extramyocellular adipocytes and a potential reduction in PLIN5 protein expression from reduced composition of type I fibres. These difficulties can potentially be overcome by peptide separation by isoelectric focusing and high definition mass-spectrometry (Deshmukh *et al.*, 2015b). If achieved it be advantageous to investigate PLIN5 associated proteins in different diseases states. Given only a fraction of LD have a PLIN colocalised to them (Chapter 3 & 4) (Shaw *et al.*, 2012; Shepherd *et al.*, 2013; Shepherd *et al.*, 2017b), human skeletal muscle clearly has a heterogenous LD pool. Given the diverging roles of PLIN proteins it would be useful to take a non-targeted approach to detect proteins associated to other PLINs to further elucidate their role in human skeletal muscle.

6.8 Final conclusions

The work conducted in this thesis has produced novel information on proteins that regulate lipid metabolism in human skeletal muscle. Chapter 2 demonstrated that HFHC diet does not always impair functional measurements of cardiovascular and metabolic disease in young, healthy individuals with high levels of cardio-respiratory fitness. Chapter 3 provided novel evidence that 7-days HFHC diet induces fibre type

specific increases in IMTG stores primarily aided by an increase in PLIN3 protein expression and a redistribution of PLIN2 to LD. It is proposed that this increase in IMTG assisted by PLIN2 and PLIN3 help to minimise the accumulation of lipid metabolites known to contribute to skeletal muscle insulin resistance Chapter 4 demonstrated that HSL preferentially redistributed to PLIN5+ LD following 1 h of moderate-intensity exercise and thus added weight to the argument that PLIN5 is an important protein in regulating IMTG hydrolysis. Chapter 5 developed a PLIN5-IP mass spectrometry protocol that identified PA2GA is a unique PLIN5 associated protein in muscle from lean sedentary participants. Furthermore, methods and results generated from this thesis will assist in development of new hypotheses to investigate skeletal muscle lipid metabolism.

Chapter 7. References

Abdul-Ghani MA, Matsuda M, Balas B & DeFronzo RA. (2007). Muscle and liver insulin resistance indexes derived from the oral glucose tolerance test. *Diabetes Care* **30,** 89-94.

Abdullah A, Peeters A, de Courten M & Stoelwinder J. (2010). The magnitude of association between overweight and obesity and the risk of diabetes: a meta-analysis of prospective cohort studies. *Diabetes Res Clin Pract* **89,** 309-319.

Achten J & Jeukendrup AE. (2003). Maximal fat oxidation during exercise in trained men. *Int J Sports Med* **24,** 603-608.

Adams JM, 2nd, Pratipanawatr T, Berria R, Wang E, DeFronzo RA, Sullards MC & Mandarino LJ. (2004). Ceramide content is increased in skeletal muscle from obese insulin-resistant humans. *Diabetes* **53,** 25-31.

Adochio RL, Leitner JW, Gray K, Draznin B & Cornier MA. (2009). Early responses of insulin signaling to high-carbohydrate and high-fat overfeeding. *Nutr Metab (Lond)* **6,** 37.

Agarwal AK, Arioglu E, de Almeida S, Akkoc N, Taylor SI, Bowcock AM, Barnes RI & Garg A. (2002). AGPAT2 is mutated in congenital generalized lipodystrophy linked to chromosome 9q34. *Nat Genet* **31,** 21-23.

Aguer C, Mercier J, Man CY, Metz L, Bordenave S, Lambert K, Jean E, Lantier L, Bounoua L, Brun JF, Raynaud de Mauverger E, Andreelli F, Foretz M & Kitzmann M. (2010). Intramyocellular lipid accumulation is associated with permanent relocation ex vivo and in vitro of fatty acid translocase (FAT)/CD36 in obese patients. *Diabetologia* **53,** 1151-1163.

Albers PH, Pedersen AJ, Birk JB, Kristensen DE, Vind BF, Baba O, Nohr J, Hojlund K & Wojtaszewski JF. (2015). Human muscle fiber type-specific insulin signaling: impact of obesity and type 2 diabetes. *Diabetes* **64,** 485-497.

Alessi DR, Andjelkovic M, Caudwell B, Cron P, Morrice N, Cohen P & Hemmings BA. (1996). Mechanism of activation of protein kinase B by insulin and IGF-1. *Embo J* **15,** 6541-6551.

Alsted TJ, Nybo L, Schweiger M, Fledelius C, Jacobsen P, Zimmermann R, Zechner R & Kiens B. (2009). Adipose triglyceride lipase in human skeletal muscle is upregulated by exercise training. *Am J Physiol Endocrinol Metab* **296,** E445-453.

Alsted TJ, Ploug T, Prats C, Serup AK, Hoeg L, Schjerling P, Holm C, Zimmermann R, Fledelius C, Galbo H & Kiens B. (2013). Contraction-induced lipolysis is not impaired by inhibition of hormone-sensitive lipase in skeletal muscle. *J Physiol* **591,** 5141-5155.

Amati F, Dube JJ, Alvarez-Carnero E, Edreira MM, Chomentowski P, Coen PM, Switzer GE, Bickel PE, Stefanovic-Racic M, Toledo FG & Goodpaster BH. (2011). Skeletal muscle triglycerides, diacylglycerols, and ceramides in insulin resistance: another paradox in endurance-trained athletes? *Diabetes* **60,** 2588-2597.

American Diabetes A. (2015). (2) Classification and diagnosis of diabetes. *Diabetes Care* **38 Suppl,** S8-S16.

Anthonsen MW, Ronnstrand L, Wernstedt C, Degerman E & Holm C. (1998). Identification of novel phosphorylation sites in hormone-sensitive lipase that are phosphorylated in response to isoproterenol and govern activation properties in vitro. *J Biol Chem* **273,** 215-221.

Aon MA, Bhatt N & Cortassa SC. (2014). Mitochondrial and cellular mechanisms for managing lipid excess. *Front Physiol* **5,** 282.

Bachmann OP, Dahl DB, Brechtel K, Machann J, Haap M, Maier T, Loviscach M, Stumvoll M, Claussen CD, Schick F, Haring HU & Jacob S. (2001). Effects of intravenous and dietary lipid challenge on intramyocellular lipid content and the relation with insulin sensitivity in humans. *Diabetes* **50,** 2579-2584.

Badin PM, Louche K, Mairal A, Liebisch G, Schmitz G, Rustan AC, Smith SR, Langin D & Moro C. (2011). Altered skeletal muscle lipase expression and activity contribute to insulin resistance in humans. *Diabetes* **60,** 1734-1742.

Bakker LE, van Schinkel LD, Guigas B, Streefland TC, Jonker JT, van Klinken JB, van der Zon GC, Lamb HJ, Smit JW, Pijl H, Meinders AE & Jazet IM. (2014). A 5-day high-fat, high-calorie diet impairs insulin sensitivity in healthy, young South Asian men but not in Caucasian men. *Diabetes* **63,** 248-258.

Balkau B, Mhamdi L, Oppert JM, Nolan J, Golay A, Porcellati F, Laakso M, Ferrannini E & Group E-RS. (2008). Physical activity and insulin sensitivity: the RISC study. *Diabetes* **57,** 2613-2618.

Bao Y, Lopez JA, James DE & Hunziker W. (2008). Snapin interacts with the Exo70 subunit of the exocyst and modulates GLUT4 trafficking. *J Biol Chem* **283,** 324-331.

Baumann CA, Ribon V, Kanzaki M, Thurmond DC, Mora S, Shigematsu S, Bickel PE, Pessin JE & Saltiel AR. (2000). CAP defines a second signalling pathway required for insulin-stimulated glucose transport. *Nature* **407,** 202-207.

Berggard T, Linse S & James P. (2007). Methods for the detection and analysis of protein-protein interactions. *Proteomics* **7,** 2833-2842.

Bergman BC, Hunerdosse DM, Kerege A, Playdon MC & Perreault L. (2012). Localisation and composition of skeletal muscle diacylglycerol predicts insulin resistance in humans. *Diabetologia* **55,** 1140-1150.

Bergman BC, Perreault L, Hunerdosse DM, Koehler MC, Samek AM & Eckel RH. (2010). Increased intramuscular lipid synthesis and low saturation relate to insulin sensitivity in endurance-trained athletes. *J Appl Physiol (1985)* **108,** 1134-1141.

Bergman BC, Perreault L, Strauss A, Bacon S, Kerege A, Harrison K, Brozinick JT, Hunerdosse DM, Playdon MC, Holmes W, Bui HH, Sanders P, Siddall P, Wei T, Thomas MK, Kuo MS & Eckel RH. (2018). Intramuscular triglyceride synthesis: importance in muscle lipid partitioning in humans. *Am J Physiol Endocrinol Metab* **314,** E152-E164.

Bergstrom J. (1975). Percutaneous needle biopsy of skeletal muscle in physiological and clinical research. *Scand J Clin Lab Invest* **35,** 609-616.

Bergström J. (1975). Percutaneous needle biopsy of skeletal muscle in physiological and clinical research. *Scand J Clin Lab Invest* **35,** 609-616.

Bersuker K & Olzmann JA. (2017). Establishing the lipid droplet proteome: Mechanisms of lipid droplet protein targeting and degradation. *Biochim Biophys Acta* **1862,** 1166-1177.

Bhagavan NV & Ha C-E. (2011). Chapter 12 - Carbohydrate Metabolism I: Glycolysis and the Tricarboxylic Acid Cycle. In *Essentials of Medical Biochemistry*, ed. Bhagavan NV & Ha C-E, pp. 115-133. Academic Press, San Diego.

Bickerton AS, Roberts R, Fielding BA, Tornqvist H, Blaak EE, Wagenmakers AJ, Gilbert M, Humphreys SM, Karpe F & Frayn KN. (2008). Adipose tissue fatty acid metabolism in insulin-resistant men. *Diabetologia* **51,** 1466-1474.

Bingley CA, Gitau R & Lovegrove JA. (2008). Impact of menstrual cycle phase on insulin sensitivity measures and fasting lipids. *Horm Metab Res* **40,** 901-906.

Bjorndal B, Burri L, Staalesen V, Skorve J & Berge RK. (2011). Different adipose depots: their role in the development of metabolic syndrome and mitochondrial response to hypolipidemic agents. *J Obes* **2011,** 490650.

Blaak EE, Hul G, Verdich C, Stich V, Martinez A, Petersen M, Feskens EF, Patel K, Oppert JM, Barbe P, Toubro S, Anderson I, Polak J, Astrup A, Macdonald IA, Langin D, Holst C, Sorensen TI & Saris WH. (2006). Fat oxidation before and after a high fat load in the obese insulin-resistant state. *J Clin Endocrinol Metab* **91,** 1462-1469.

Blaak EE, Schiffelers SL, Saris WH, Mensink M & Kooi ME. (2004). Impaired beta-adrenergically mediated lipolysis in skeletal muscle of obese subjects. *Diabetologia* **47,** 1462-1468.

Blaak EE, van Aggel-Leijssen DP, Wagenmakers AJ, Saris WH & van Baak MA. (2000). Impaired oxidation of plasma-derived fatty acids in type 2 diabetic subjects during moderate-intensity exercise. *Diabetes* **49,** 2102-2107.

Blaak EE & Wagenmakers AJ. (2002). The fate of [U-(13)C]palmitate extracted by skeletal muscle in subjects with type 2 diabetes and control subjects. *Diabetes* **51,** 784-789.

Blair SN, Kohl HW, 3rd, Paffenbarger RS, Jr., Clark DG, Cooper KH & Gibbons LW. (1989). Physical fitness and all-cause mortality. A prospective study of healthy men and women. *JAMA* **262,** 2395-2401.

Blanco A & Blanco G. (2017). Chapter 19 - Integration and Regulation of Metabolism. In *Medical Biochemistry*, ed. Blanco A & Blanco G, pp. 425-445. Academic Press.

Boden G, Chen X, Ruiz J, White JV & Rossetti L. (1994). Mechanisms of fatty acid-induced inhibition of glucose uptake. *J Clin Invest* **93,** 2438-2446.

Boeszoermenyi A, Nagy HM, Arthanari H, Pillip CJ, Lindermuth H, Luna RE, Wagner G, Zechner R, Zangger K & Oberer M. (2015). Structure of a CGI-58 motif provides the molecular basis of lipid droplet anchoring. *J Biol Chem* **290,** 26361-26372.

Bonen A, Parolin ML, Steinberg GR, Calles-Escandon J, Tandon NN, Glatz JF, Luiken JJ, Heigenhauser GJ & Dyck DJ. (2004). Triacylglycerol accumulation in human obesity and type 2 diabetes is associated with increased rates of skeletal muscle fatty acid transport and increased sarcolemmal FAT/CD36. *Faseb J* **18,** 1144-1146.

Booth FW, Chakravarthy MV & Spangenburg EE. (2002). Exercise and gene expression: physiological regulation of the human genome through physical activity. *J Physiol* **543,** 399-411.

Borissova AM, Tankova T, Kirilov G & Koev D. (2005). Gender-dependent effect of ageing on peripheral insulin action. *Int J Clin Pract* **59,** 422-426.

Bosma M, Hesselink MK, Sparks LM, Timmers S, Ferraz MJ, Mattijssen F, van Beurden D, Schaart G, de Baets MH, Verheyen FK, Kersten S & Schrauwen P. (2012a). Perilipin 2 improves insulin sensitivity in skeletal muscle despite elevated intramuscular lipid levels. *Diabetes* **61,** 2679-2690.

Bosma M, Minnaard R, Sparks LM, Schaart G, Losen M, de Baets MH, Duimel H, Kersten S, Bickel PE, Schrauwen P & Hesselink MK. (2012b). The lipid droplet

coat protein perilipin 5 also localizes to muscle mitochondria. *Histochem Cell Biol* **137,** 205-216.

Bosma M, Sparks LM, Hooiveld GJ, Jorgensen JA, Houten SM, Schrauwen P, Kersten S & Hesselink MK. (2013). Overexpression of PLIN5 in skeletal muscle promotes oxidative gene expression and intramyocellular lipid content without compromising insulin sensitivity. *Biochim Biophys Acta* **1831,** 844-852.

Bostrom P, Andersson L, Rutberg M, Perman J, Lidberg U, Johansson BR, Fernandez-Rodriguez J, Ericson J, Nilsson T, Boren J & Olofsson SO. (2007). SNARE proteins mediate fusion between cytosolic lipid droplets and are implicated in insulin sensitivity. *Nat Cell Biol* **9,** 1286-1293.

Bostrom P, Rutberg M, Ericsson J, Holmdahl P, Andersson L, Frohman MA, Boren J & Olofsson SO. (2005). Cytosolic lipid droplets increase in size by microtubule-dependent complex formation. *Arterioscler Thromb Vasc Biol* **25,** 1945-1951.

Boura-Halfon S & Zick Y. (2009). Phosphorylation of IRS proteins, insulin action, and insulin resistance. *Am J Physiol Endocrinol Metab* **296,** E581-591.

Bradford MM. (1976). A rapid and sensitive method for the quantitation of microgram quantities of protein utilizing the principle of protein-dye binding. *Anal Biochem* **72,** 248-254.

Bradley H, Shaw CS, Bendtsen C, Worthington PL, Wilson OJ, Strauss JA, Wallis GA, Turner AM & Wagenmakers AJ. (2015). Visualization and quantitation of GLUT4 translocation in human skeletal muscle following glucose ingestion and exercise. *Physiol Rep* **3**.

Brasaemle DL, Barber T, Wolins NE, Serrero G, Blanchette-Mackie EJ & Londos C. (1997). Adipose differentiation-related protein is an ubiquitously expressed lipid storage droplet-associated protein. *J Lipid Res* **38,** 2249-2263.

Brasaemle DL, Levin DM, Adler-Wailes DC & Londos C. (2000). The lipolytic stimulation of 3T3-L1 adipocytes promotes the translocation of hormone-sensitive lipase to the surfaces of lipid storage droplets. *Biochim Biophys Acta* **1483,** 251-262.

British Heart Foundation. (2017). Physical Inactivity Report 2017. https://www.bhf.org.uk/informationsupport/publications/statistics/physical-inactivity-report-2017.

Brons C, Jacobsen S, Hiscock N, White A, Nilsson E, Dunger D, Astrup A, Quistorff B & Vaag A. (2012). Effects of high-fat overfeeding on mitochondrial function, glucose and fat metabolism, and adipokine levels in low-birth-weight subjects. *Am J Physiol Endocrinol Metab* **302,** E43-51.

Brons C, Jensen CB, Storgaard H, Hiscock NJ, White A, Appel JS, Jacobsen S, Nilsson E, Larsen CM, Astrup A, Quistorff B & Vaag A. (2009). Impact of short-term high-fat feeding on glucose and insulin metabolism in young healthy men. *J Physiol* **587,** 2387-2397.

Brook MS, Wilkinson DJ, Phillips BE, Perez-Schindler J, Philp A, Smith K & Atherton PJ. (2016). Skeletal muscle homeostasis and plasticity in youth and ageing: impact of nutrition and exercise. *Acta Physiol (Oxf)* **216,** 15-41.

Brouwers B, Schrauwen-Hinderling VB, Jelenik T, Gemmink A, Havekes B, Bruls Y, Dahlmans D, Roden M, Hesselink MKC & Schrauwen P. (2017). Metabolic disturbances of non-alcoholic fatty liver resemble the alterations typical for type 2 diabetes. *Clin Sci (Lond)* **131,** 1905-1917.

Bulankina AV, Deggerich A, Wenzel D, Mutenda K, Wittmann JG, Rudolph MG, Burger KNJ & Honing S. (2009). TIP47 functions in the biogenesis of lipid droplets. *Journal of Cell Biology* **185,** 641-655.

Burniston JG, Connolly J, Kainulainen H, Britton SL & Koch LG. (2014). Label-free profiling of skeletal muscle using high-definition mass spectrometry. *Proteomics* **14,** 2339-2344.

Bursten SL, Harris WE, Bomsztyk K & Lovett D. (1991). Interleukin-1 rapidly stimulates lysophosphatidate acyltransferase and phosphatidate phosphohydrolase activities in human mesangial cells. *J Biol Chem* **266,** 20732-20743.

Camera DM, Burniston JG, Pogson MA, Smiles WJ & Hawley JA. (2017). Dynamic proteome profiling of individual proteins in human skeletal muscle after a high-fat diet and resistance exercise. *Faseb J* **31,** 5478-5494.

Capaldo B, Gastaldelli A, Antoniello S, Auletta M, Pardo F, Ciociaro D, Guida R, Ferrannini E & Sacca L. (1999). Splanchnic and leg substrate exchange after ingestion of a natural mixed meal in humans. *Diabetes* **48,** 958-966.

Cases S, Smith SJ, Zheng YW, Myers HM, Lear SR, Sande E, Novak S, Collins C, Welch CB, Lusis AJ, Erickson SK & Farese RV. (1998). Identification of a gene encoding an acyl CoA : diacylglycerol acyltransferase, a key enzyme in triacylglycerol synthesis. *P Natl Acad Sci USA* **95,** 13018-13023.

Cases S, Stone SJ, Zhou P, Yen E, Tow B, Lardizabal KD, Voelker T & Farese RV. (2001). Cloning of DGAT2, a second mammalian diacylglycerol acyltransferase, and related family members. *Journal of Biological Chemistry* **276,** 38870-38876.

Chakravarthy MV & Booth FW. (2004). Eating, exercise, and "thrifty" genotypes: connecting the dots toward an evolutionary understanding of modern chronic diseases. *J Appl Physiol (1985)* **96,** 3-10.

Chatr-Aryamontri A, Oughtred R, Boucher L, Rust J, Chang C, Kolas NK, O'Donnell L, Oster S, Theesfeld C, Sellam A, Stark C, Breitkreutz BJ, Dolinski K & Tyers M. (2017). The BioGRID interaction database: 2017 update. *Nucleic Acids Res* **45,** D369-D379.

Chavez JA & Summers SA. (2012). A ceramide-centric view of insulin resistance. *Cell Metab* **15,** 585-594.

Cheatham B, Vlahos CJ, Cheatham L, Wang L, Blenis J & Kahn CR. (1994). Phosphatidylinositol 3-Kinase Activation Is Required for Insulin Stimulation of Pp70 S6 Kinase, DNA-Synthesis, and Glucose-Transporter Translocation. *Mol Cell Biol* **14,** 4902-4911.

Chee C, Shannon CE, Burns A, Selby AL, Wilkinson D, Smith K, Greenhaff PL & Stephens FB. (2016). Relative Contribution of Intramyocellular Lipid to Whole-Body Fat Oxidation Is Reduced With Age but Subsarcolemmal Lipid Accumulation and Insulin Resistance Are Only Associated With Overweight Individuals. *Diabetes* **65,** 840-850.

Chen W, Chang B, Wu X, Li L, Sleeman M & Chan L. (2013). Inactivation of Plin4 downregulates Plin5 and reduces cardiac lipid accumulation in mice. *Am J Physiol Endocrinol Metab* **304,** E770-779.

Choi CS, Savage DB, Kulkarni A, Yu XX, Liu ZX, Morino K, Kim S, Distefano A, Samuel VT, Neschen S, Zhang D, Wang A, Zhang XM, Kahn M, Cline GW, Pandey SK, Geisler JG, Bhanot S, Monia BP & Shulman GI. (2007). Suppression of diacylglycerol acyltransferase-2 (DGAT2), but not DGAT1, with antisense oligonucleotides reverses diet-induced hepatic steatosis and insulin resistance. *J Biol Chem* **282,** 22678-22688.

Chow LS, Mashek DG, Austin E, Eberly LE, Persson XM, Mashek MT, Seaquist ER & Jensen MD. (2014). Training status diverges muscle diacylglycerol accumulation during free fatty acid elevation. *Am J Physiol Endocrinol Metab* **307,** E124-131.

Clausen JO, Borch-Johnsen K, Ibsen H, Bergman RN, Hougaard P, Winther K & Pedersen O. (1996). Insulin sensitivity index, acute insulin response, and glucose effectiveness in a population-based sample of 380 young healthy Caucasians. Analysis of the impact of gender, body fat, physical fitness, and life-style factors. *J Clin Invest* **98,** 1195-1209.

Cocks M, Shaw CS, Shepherd SO, Fisher JP, Ranasinghe AM, Barker TA, Tipton KD & Wagenmakers AJ. (2013). Sprint interval and endurance training are equally effective in increasing muscle microvascular density and eNOS content in sedentary males. *J Physiol* **591,** 641-656.

Coen PM, Dube JJ, Amati F, Stefanovic-Racic M, Ferrell RE, Toledo FG & Goodpaster BH. (2010). Insulin resistance is associated with higher intramyocellular triglycerides in type I but not type II myocytes concomitant with higher ceramide content. *Diabetes* **59,** 80-88.

Coggan AR, Raguso CA, Gastaldelli A, Sidossis LS & Yeckel CW. (2000). Fat metabolism during high-intensity exercise in endurance-trained and untrained men. *Metabolism-Clinical and Experimental* **49,** 122-128.

Cohen P. (1999). The Croonian Lecture 1998. Identification of a protein kinase cascade of major importance in insulin signal transduction. *Philos T Roy Soc B* **354,** 485-495.

Colberg SR, Simoneau JA, Thaete FL & Kelley DE. (1995). Skeletal muscle utilization of free fatty acids in women with visceral obesity. *J Clin Invest* **95,** 1846-1853.

Coleman RA & Lee DP. (2004). Enzymes of triacylglycerol synthesis and their regulation. *Prog Lipid Res* **43,** 134-176.

Coleman RA, Lewin TM & Muoio DM. (2000). Physiological and nutritional regulation of enzymes of triacylglycerol synthesis. *Annu Rev Nutr* **20,** 77-103.

Compher C, Frankenfield D, Keim N, Roth-Yousey L & Evidence Analysis Working G. (2006). Best practice methods to apply to measurement of resting metabolic rate in adults: a systematic review. *J Am Diet Assoc* **106,** 881-903.

Coppack SW, Evans RD, Fisher RM, Frayn KN, Gibbons GF, Humphreys SM, Kirk ML, Potts JL & Hockaday TD. (1992). Adipose tissue metabolism in obesity: lipase action in vivo before and after a mixed meal. *Metabolism* **41,** 264-272.

Cornford AS, Hinko A, Nelson RK, Barkan AL & Horowitz JF. (2013). Rapid development of systemic insulin resistance with overeating is not accompanied by robust changes in skeletal muscle glucose and lipid metabolism. *Appl Physiol Nutr Metab* **38,** 512-519.

Corpeleijn E, Mensink M, Kooi ME, Roekaerts PM, Saris WH & Blaak EE. (2008). Impaired skeletal muscle substrate oxidation in glucose-intolerant men improves after weight loss. *Obesity (Silver Spring)* **16,** 1025-1032.

Corpeleijn E, Saris WH & Blaak EE. (2009). Metabolic flexibility in the development of insulin resistance and type 2 diabetes: effects of lifestyle. *Obes Rev* **10,** 178-193.

Covington JD, Galgani JE, Moro C, LaGrange JM, Zhang Z, Rustan AC, Ravussin E & Bajpeyi S. (2014). Skeletal muscle perilipin 3 and coatomer proteins are increased following exercise and are associated with fat oxidation. *Plos One* **9,** e91675.

Covington JD, Johannsen DL, Coen PM, Burk DH, Obanda DN, Ebenezer PJ, Tam CS, Goodpaster BH, Ravussin E & Bajpeyi S. (2017). Intramyocellular Lipid Droplet Size Rather Than Total Lipid Content is Related to Insulin Sensitivity After 8 Weeks of Overfeeding. *Obesity (Silver Spring)* **25,** 2079-2087.

Covington JD, Noland RC, Hebert RC, Masinter BS, Smith SR, Rustan AC, Ravussin E & Bajpeyi S. (2015). Perilipin 3 Differentially Regulates Skeletal Muscle Lipid Oxidation in Active, Sedentary, and Type 2 Diabetic Males. *J Clin Endocrinol Metab* **100,** 3683-3692.

Craig CL, Marshall AL, Sjostrom M, Bauman AE, Booth ML, Ainsworth BE, Pratt M, Ekelund U, Yngve A, Sallis JF & Oja P. (2003). International physical activity questionnaire: 12-country reliability and validity. *Med Sci Sports Exerc* **35,** 1381-1395.

Crane JD, Devries MC, Safdar A, Hamadeh MJ & Tarnopolsky MA. (2010). The effect of aging on human skeletal muscle mitochondrial and intramyocellular lipid ultrastructure. *J Gerontol A Biol Sci Med Sci* **65,** 119-128.

Currie E, Guo X, Christiano R, Chitraju C, Kory N, Harrison K, Haas J, Walther TC & Farese RV, Jr. (2014). High confidence proteomic analysis of yeast LDs identifies additional droplet proteins and reveals connections to dolichol synthesis and sterol acetylation. *J Lipid Res* **55,** 1465-1477.

Cushman SW & Wardzala LJ. (1980). Potential Mechanism of Insulin Action on Glucose-Transport in the Isolated Rat Adipose Cell - Apparent Translocation of Intracellular-Transport Systems to the Plasma-Membrane. *Journal of Biological Chemistry* **255,** 4758-4762.

Daemen S, Gemmink A, Brouwers B, Meex RCR, Huntjens PR, Schaart G, Moonen-Kornips E, Jorgensen J, Hoeks J, Schrauwen P & Hesselink MKC. (2018). Distinct lipid droplet characteristics and distribution unmask the apparent contradiction of the athlete's paradox. *Mol Metab*.

Dalen KT, Dahl T, Holter E, Arntsen B, Londos C, Sztalryd C & Nebb HI. (2007). LSDP5 is a PAT protein specifically expressed in fatty acid oxidizing tissues. *Biochim Biophys Acta* **1771,** 210-227.

De Bock K, Derave W, Eijnde BO, Hesselink MK, Koninckx E, Rose AJ, Schrauwen P, Bonen A, Richter EA & Hespel P. (2008). Effect of training in the fasted state on metabolic responses during exercise with carbohydrate intake. *J Appl Physiol (1985)* **104,** 1045-1055.

DeFronzo RA. (2004). Pathogenesis of type 2 diabetes mellitus. *Med Clin North Am* **88,** 787-835, ix.

DeFronzo RA, Gunnarsson R, Bjorkman O, Olsson M & Wahren J. (1985). Effects of insulin on peripheral and splanchnic glucose metabolism in noninsulin-dependent (type II) diabetes mellitus. *J Clin Invest* **76,** 149-155.

DeFronzo RA, Jacot E, Jequier E, Maeder E, Wahren J & Felber JP. (1981). The effect of insulin on the disposal of intravenous glucose. Results from indirect calorimetry and hepatic and femoral venous catheterization. *Diabetes* **30,** 1000-1007.

DeFronzo RA & Tripathy D. (2009). Skeletal muscle insulin resistance is the primary defect in type 2 diabetes. *Diabetes Care* **32 Suppl 2,** S157-163.

Dennis EA, Cao J, Hsu YH, Magrioti V & Kokotos G. (2011). Phospholipase A2 enzymes: physical structure, biological function, disease implication, chemical inhibition, and therapeutic intervention. *Chem Rev* **111,** 6130-6185.

Deshmukh AS, Murgia M, Nagaraj N, Treebak JT, Cox J & Mann M. (2015a). Deep proteomics of mouse skeletal muscle enables quantitation of protein isoforms, metabolic pathways, and transcription factors. *Mol Cell Proteomics* **14,** 841-853.

Deshmukh AS, Murgia M, Nagaraj N, Treebak JT, Cox J & Mann M. (2015b). Deep Proteomics of Mouse Skeletal Muscle Enables Quantitation of Protein Isoforms, Metabolic Pathways, and Transcription Factors. *Molecular & Cellular Proteomics* **14,** 841-853.

Devries MC, Samjoo IA, Hamadeh MJ, McCready C, Raha S, Watt MJ, Steinberg GR & Tarnopolsky MA. (2013). Endurance training modulates intramyocellular lipid compartmentalization and morphology in skeletal muscle of lean and obese women. *J Clin Endocrinol Metab* **98,** 4852-4862.

Diabetes UK. (2017). Diabetes Prevalence 2017. https://www.diabetes.org.uk/professionals/position-statements-reports/statistics/diabetes-prevalence-2017

Diamond J. (2003). The double puzzle of diabetes. *Nature* **423,** 599-602.

Dircks LK & Sul HS. (1997). Mammalian mitochondrial glycerol-3-phosphate acyltransferase. *Biochim Biophys Acta* **1348,** 17-26.

Donahue RP, Prineas RJ, DeCarlo Donahue R, Bean JA & Skyler JS. (1996). The female 'insulin advantage' in a biracial cohort: results from the Miami Community Health Study. *Int J Obes Relat Metab Disord* **20,** 76-82.

Donkor J, Sariahmetoglu M, Dewald J, Brindley DN & Reue K. (2007). Three mammalian lipins act as phosphatidate phosphatases with distinct tissue expression patterns. *Journal of Biological Chemistry* **282,** 3450-3457.

Donsmark M, Langfort J, Holm C, Ploug T & Galbo H. (2003). Contractions activate hormone-sensitive lipase in rat muscle by protein kinase C and mitogen-activated protein kinase. *J Physiol* **550,** 845-854.

Dresner A, Laurent D, Marcucci M, Griffin ME, Dufour S, Cline GW, Slezak LA, Andersen DK, Hundal RS, Rothman DL, Petersen KF & Shulman GI. (1999). Effects of free fatty acids on glucose transport and IRS-1-associated phosphatidylinositol 3-kinase activity. *J Clin Invest* **103,** 253-259.

Dries DR, Gallegos LL & Newton AC. (2007). A single residue in the C1 domain sensitizes novel protein kinase C isoforms to cellular diacylglycerol production. *Journal of Biological Chemistry* **282,** 826-830.

Dube JJ, Amati F, Toledo FG, Stefanovic-Racic M, Rossi A, Coen P & Goodpaster BH. (2011). Effects of weight loss and exercise on insulin resistance, and intramyocellular triacylglycerol, diacylglycerol and ceramide. *Diabetologia* **54,** 1147-1156.

Dube JJ, Sitnick MT, Schoiswohl G, Wills RC, Basantani MK, Cai L, Pulinilkunnil T & Kershaw EE. (2015). Adipose triglyceride lipase deletion from adipocytes, but not skeletal myocytes, impairs acute exercise performance in mice. *Am J Physiol Endocrinol Metab* **308,** E879-890.

Dyck DJ, Steinberg G & Bonen A. (2001). Insulin increases FA uptake and esterification but reduces lipid utilization in isolated contracting muscle. *Am J Physiol Endocrinol Metab* **281,** E600-607.

Eaton SB, Konner M & Shostak M. (1988). Stone agers in the fast lane: chronic degenerative diseases in evolutionary perspective. *Am J Med* **84,** 739-749.

Edgerton DS, Kraft G, Smith M, Farmer B, Williams PE, Coate KC, Printz RL, O'Brien RM & Cherrington AD. (2017). Insulin's direct hepatic effect explains the inhibition of glucose production caused by insulin secretion. *Jci Insight* **2**.

Egawa K, Maegawa H, Shi K, Nakamura T, Obata T, Yoshizaki T, Morino K, Shimizu S, Nishio Y, Suzuki E & Kashiwagi A. (2002). Membrane localization of 3-phosphoinositide-dependent protein kinase-1 stimulates activities of Akt and atypical protein kinase C but does not stimulate glucose transport and glycogen synthesis in 3T3-L1 adipocytes. *Journal of Biological Chemistry* **277,** 38863-38869.

Eichmann TO, Kumari M, Haas JT, Farese RV, Jr., Zimmermann R, Lass A & Zechner R. (2012). Studies on the substrate and stereo/regioselectivity of adipose triglyceride lipase, hormone-sensitive lipase, and diacylglycerol-O-acyltransferases. *J Biol Chem* **287,** 41446-41457.

Ellis BA, Poynten A, Lowy AJ, Furler SM, Chisholm DJ, Kraegen EW & Cooney GJ. (2000). Long-chain acyl-CoA esters as indicators of lipid metabolism and insulin sensitivity in rat and human muscle. *Am J Physiol Endocrinol Metab* **279,** E554-560.

Enevoldsen LH, Stallknecht B, Langfort J, Petersen LN, Holm C, Ploug T & Galbo H. (2001). The effect of exercise training on hormone-sensitive lipase in rat intra-abdominal adipose tissue and muscle. *J Physiol* **536,** 871-877.

Enoksson S, Degerman E, Hagstrom-Toft E, Large V & Arner P. (1998). Various phosphodiesterase subtypes mediate the in vivo antilipolytic effect of insulin on adipose tissue and skeletal muscle in man. *Diabetologia* **41,** 560-568.

Escalante Pulido JM & Alpizar Salazar M. (1999). Changes in insulin sensitivity, secretion and glucose effectiveness during menstrual cycle. *Arch Med Res* **30,** 19-22.

Esposito DL, Li YH, Cama A & Quon MJ. (2001). Tyr(612) and Tyr(632) in human insulin receptor substrate-1 are important for full activation of insulin-stimulated phosphatidylinositol 3-kinase activity and translocation of GLUT4 in adipose cells. *Endocrinology* **142,** 2833-2840.

Essen B, Jansson E, Henriksson J, Taylor AW & Saltin B. (1975). Metabolic characteristics of fibre types in human skeletal muscle. *Acta Physiol Scand* **95,** 153-165.

Faerch K & Vaag A. (2011). Metabolic inflexibility is a common feature of impaired fasting glycaemia and impaired glucose tolerance. *Acta Diabetol* **48,** 349-353.

Fazakerley DJ, Holman GD, Marley A, James DE, Stockli J & Coster AC. (2010). Kinetic evidence for unique regulation of GLUT4 trafficking by insulin and AMP-activated protein kinase activators in L6 myotubes. *J Biol Chem* **285,** 1653-1660.

Ferrannini E, Smith JD, Cobelli C, Toffolo G, Pilo A & DeFronzo RA. (1985). Effect of insulin on the distribution and disposition of glucose in man. *J Clin Invest* **76,** 357-364.

Festa A, Williams K, D'Agostino R, Jr., Wagenknecht LE & Haffner SM. (2006). The natural course of beta-cell function in nondiabetic and diabetic individuals: the Insulin Resistance Atherosclerosis Study. *Diabetes* **55,** 1114-1120.

Fletcher LM, Welsh GI, Oatey PB & Tavare JM. (2000). Role for the microtubule cytoskeleton in GLUT4 vesicle trafficking and in the regulation of insulin-stimulated glucose uptake. *Biochem J* **352,** 267-276.

Forouhi NG, Jenkinson G, Thomas EL, Mullick S, Mierisova S, Bhonsle U, McKeigue PM & Bell JD. (1999). Relation of triglyceride stores in skeletal muscle cells to

central obesity and insulin sensitivity in European and South Asian men. *Diabetologia* **42,** 932-935.

Foster LJ, Yaworsky K, Trimble WS & Klip A. (1999). SNAP23 promotes insulin-dependent glucose uptake in 3T3-L1 adipocytes: possible interaction with cytoskeleton. *Am J Physiol* **276,** C1108-1114.

Fowler MJ. (2008). Microvascular and Macrovascular Complications of Diabetes. *Clinical Diabetes* **26,** 77-82.

Frayn KN. (2000). Visceral fat and insulin resistance--causative or correlative? *Br J Nutr* **83 Suppl 1,** S71-77.

Frayn KN. (2002). Adipose tissue as a buffer for daily lipid flux. *Diabetologia* **45,** 1201-1210.

Fredrikson G, Stralfors P, Nilsson NO & Belfrage P. (1981a). Hormone-sensitive lipase from adipose tissue of rat. *Methods Enzymol* **71 Pt C,** 636-646.

Fredrikson G, Stralfors P, Nilsson NO & Belfrage P. (1981b). Hormone-sensitive lipase of rat adipose tissue. Purification and some properties. *J Biol Chem* **256,** 6311-6320.

Galgani JE, Heilbronn LK, Azuma K, Kelley DE, Albu JB, Pi-Sunyer X, Smith SR, Ravussin E & Look AARG. (2008a). Metabolic flexibility in response to glucose is not impaired in people with type 2 diabetes after controlling for glucose disposal rate. *Diabetes* **57,** 841-845.

Galgani JE, Moro C & Ravussin E. (2008b). Metabolic flexibility and insulin resistance. *Am J Physiol Endocrinol Metab* **295,** E1009-1017.

Ganda OP. (2000). Lipoatrophy, lipodystrophy, and insulin resistance. *Ann Intern Med* **133,** 304-306.

Gandolfi G, Mazzoni M, Zambonelli P, Lalatta-Costerbosa G, Tronca A, Russo V & Davoli R. (2011). Perilipin 1 and perilipin 2 protein localization and gene expression study in skeletal muscles of European cross-breed pigs with different intramuscular fat contents. *Meat Sci* **88,** 631-637.

Gavrilova O, Marcus-Samuels B, Graham D, Kim JK, Shulman GI, Castle AL, Vinson C, Eckhaus M & Reitman ML. (2000). Surgical implantation of adipose tissue reverses diabetes in lipoatrophic mice. *J Clin Invest* **105,** 271-278.

Gemmink A, Bakker LE, Guigas B, Kornips E, Schaart G, Meinders AE, Jazet IM & Hesselink MK. (2017a). Lipid droplet dynamics and insulin sensitivity upon a 5-day high-fat diet in Caucasians and South Asians. *Sci Rep* **7,** 42393.

Gemmink A, Bosma M, Kuijpers HJ, Hoeks J, Schaart G, van Zandvoort MA, Schrauwen P & Hesselink MK. (2016). Decoration of intramyocellular lipid droplets with PLIN5 modulates fasting-induced insulin resistance and lipotoxicity in humans. *Diabetologia* **59,** 1040-1048.

Gemmink A, Daemen S, Brouwers B, Huntjens PR, Schaart G, Moonen-Kornips E, Jorgensen J, Hoeks J, Schrauwen P & Hesselink MKC. (2018). Dissociation of intramyocellular lipid storage and insulin resistance in trained athletes and type 2 diabetes patients; involvement of perilipin 5? *J Physiol* **596,** 857-868.

Gemmink A, Goodpaster BH, Schrauwen P & Hesselink MKC. (2017b). Intramyocellular lipid droplets and insulin sensitivity, the human perspective. *Biochim Biophys Acta* **1862,** 1242-1249.

Gimeno RE & Cao J. (2008). Thematic review series: glycerolipids. Mammalian glycerol-3-phosphate acyltransferases: new genes for an old activity. *J Lipid Res* **49,** 2079-2088.

Giroux V, Saidj S, Simon C, Laville M, Segrestin B & Mathieu ME. (2018). Physical activity, energy expenditure and sedentary parameters in overfeeding studies - a systematic review. *BMC Public Health* **18,** 903.

Gjelstad IM, Haugen F, Gulseth HL, Norheim F, Jans A, Bakke SS, Raastad T, Tjonna AE, Wisloff U, Blaak EE, Riserus U, Gaster M, Roche HM, Birkeland KI & Drevon CA. (2012). Expression of perilipins in human skeletal muscle in vitro and in vivo in relation to diet, exercise and energy balance. *Arch Physiol Biochem* **118,** 22-30.

Gonzalez-Baro MR, Lewin TM & Coleman RA. (2007). Regulation of Triglyceride Metabolism. II. Function of mitochondrial GPAT1 in the regulation of triacylglycerol biosynthesis and insulin action. *Am J Physiol Gastrointest Liver Physiol* **292,** G1195-1199.

Goodpaster BH, He J, Watkins S & Kelley DE. (2001). Skeletal muscle lipid content and insulin resistance: evidence for a paradox in endurance-trained athletes. *J Clin Endocrinol Metab* **86,** 5755-5761.

Goodpaster BH, Thaete FL, Simoneau JA & Kelley DE. (1997). Subcutaneous abdominal fat and thigh muscle composition predict insulin sensitivity independently of visceral fat. *Diabetes* **46,** 1579-1585.

Goto T, Onuma T, Takebe K & Kral JG. (1995). The influence of fatty liver on insulin clearance and insulin resistance in non-diabetic Japanese subjects. *Int J Obes Relat Metab Disord* **19,** 841-845.

Granneman JG, Moore HP, Krishnamoorthy R & Rathod M. (2009). Perilipin controls lipolysis by regulating the interactions of AB-hydrolase containing 5 (Abhd5) and adipose triglyceride lipase (Atgl). *J Biol Chem* **284,** 34538-34544.

Granneman JG, Moore HP, Mottillo EP, Zhu Z & Zhou L. (2011). Interactions of perilipin-5 (Plin5) with adipose triglyceride lipase. *J Biol Chem* **286,** 5126-5135.

Greenberg AS, Coleman RA, Kraemer FB, McManaman JL, Obin MS, Puri V, Yan QW, Miyoshi H & Mashek DG. (2011). The role of lipid droplets in metabolic disease in rodents and humans. *J Clin Invest* **121,** 2102-2110.

Greenberg AS, Egan JJ, Wek SA, Garty NB, Blanchette-Mackie EJ & Londos C. (1991). Perilipin, a major hormonally regulated adipocyte-specific phosphoprotein associated with the periphery of lipid storage droplets. *J Biol Chem* **266,** 11341-11346.

Greenberg AS, Shen WJ, Muliro K, Patel S, Souza SC, Roth RA & Kraemer FB. (2001). Stimulation of lipolysis and hormone-sensitive lipase via the extracellular signal-regulated kinase pathway. *J Biol Chem* **276,** 45456-45461.

Groban L, Lindsey SH, Wang H & Alencar AK. (2016). Chapter 5 - Sex and Gender Differences in Cardiovascular Disease. In *Sex Differences in Physiology*, ed. Neigh GN & Mitzelfelt MM, pp. 61-87. Academic Press, Boston.

Gual P, Le Marchand-Brustel Y & Tanti JF. (2005). Positive and negative regulation of insulin signaling through IRS-1 phosphorylation. *Biochimie* **87,** 99-109.

Guijas C, Rodriguez JP, Rubio JM, Balboa MA & Balsinde J. (2014). Phospholipase A2 regulation of lipid droplet formation. *Biochim Biophys Acta* **1841,** 1661-1671.

Guo Y, Walther TC, Rao M, Stuurman N, Goshima G, Terayama K, Wong JS, Vale RD, Walter P & Farese RV. (2008). Functional genomic screen reveals genes involved in lipid-droplet formation and utilization. *Nature* **453,** 657-661.

Guo Z, Burguera B & Jensen MD. (2000). Kinetics of intramuscular triglyceride fatty acids in exercising humans. *J Appl Physiol (1985)* **89,** 2057-2064.

Gustavsson J, Parpal S, Karlsson M, Ramsing C, Thorn H, Borg M, Lindroth M, Peterson KH, Magnusson K & Stralfors P. (1999). Localization of the insulin receptor in caveolae of adipocyte plasma membrane. *Faseb J* **13,** 1961-1971.

Haemmerle G, Lass A, Zimmermann R, Gorkiewicz G, Meyer C, Rozman J, Heldmaier G, Maier R, Theussl C, Eder S, Kratky D, Wagner EF, Klingenspor M, Hoefler G & Zechner R. (2006). Defective lipolysis and altered energy metabolism in mice lacking adipose triglyceride lipase. *Science* **312,** 734-737.

Haemmerle G, Zimmermann R, Hayn M, Theussl C, Waeg G, Wagner E, Sattler W, Magin TM, Wagner EF & Zechner R. (2002a). Hormone-sensitive lipase deficiency in mice causes diglyceride accumulation in adipose tissue, muscle, and testis. *J Biol Chem* **277,** 4806-4815.

Haemmerle G, Zimmermann R, Strauss JG, Kratky D, Riederer M, Knipping G & Zechner R. (2002b). Hormone-sensitive lipase deficiency in mice changes the plasma lipid profile by affecting the tissue-specific expression pattern of lipoprotein lipase in adipose tissue and muscle. *J Biol Chem* **277,** 12946-12952.

Hagstrom-Toft E, Qvisth V, Nennesmo I, Ryden M, Bolinder H, Enoksson S, Bolinder J & Arner P. (2002). Marked heterogeneity of human skeletal muscle lipolysis at rest. *Diabetes* **51,** 3376-3383.

Hallakou S, Doare L, Foufelle F, Kergoat M, Guerre-Millo M, Berthault MF, Dugail I, Morin J, Auwerx J & Ferre P. (1997). Pioglitazone induces in vivo adipocyte differentiation in the obese Zucker fa/fa rat. *Diabetes* **46,** 1393-1399.

Hammond LE, Gallagher PA, Wang S, Hiller S, Kluckman KD, Posey-Marcos EL, Maeda N & Coleman RA. (2002). Mitochondrial glycerol-3-phosphate acyltransferase-deficient mice have reduced weight and liver triacylglycerol content and altered glycerolipid fatty acid composition. *Mol Cell Biol* **22,** 8204-8214.

Harris TE, Huffman TA, Chi A, Shabanowitz J, Hunt DF, Kumar A & Lawrence JC, Jr. (2007). Insulin controls subcellular localization and multisite phosphorylation of the phosphatidic acid phosphatase, lipin 1. *J Biol Chem* **282,** 277-286.

Hattori M, Nakagawa Y, Harada K, Banndo M & Okano G. (2006). Characteristics of intramyocellular lipid content in skeletal muscles of overweight men and endurance-trained athletes. *Jpn J Phys Fit Sport* **55,** 43-48.

Haupt A, Thamer C, Heni M, Machicao F, Machann J, Schick F, Stefan N, Fritsche A, Haring HU & Staiger H. (2010). Novel obesity risk loci do not determine distribution of body fat depots: a whole-body MRI/MRS study. *Obesity (Silver Spring)* **18,** 1212-1217.

He J, Goodpaster BH & Kelley DE. (2004). Effects of weight loss and physical activity on muscle lipid content and droplet size. *Obes Res* **12,** 761-769.

Helge JW, Biba TO, Galbo H, Gaster M & Donsmark M. (2006). Muscle triacylglycerol and hormone-sensitive lipase activity in untrained and trained human muscles. *Eur J Appl Physiol* **97,** 566-572.

Helge JW, Watt PW, Richter EA, Rennie MJ & Kiens B. (2001). Fat utilization during exercise: adaptation to a fat-rich diet increases utilization of plasma fatty acids

and very low density lipoprotein-triacylglycerol in humans. *J Physiol* **537,** 1009-1020.

Hesselink MKC, Daemen S, van Polanen N & Gemmink A. (2017). What are the benefits of being big? *J Physiol* **595,** 5409-5410.

Heymsfield SB, Gallagher D, Kotler DP, Wang Z, Allison DB & Heshka S. (2002). Body-size dependence of resting energy expenditure can be attributed to nonenergetic homogeneity of fat-free mass. *Am J Physiol Endocrinol Metab* **282,** E132-138.

Hickner RC, Racette SB, Binder EF, Fisher JS & Kohrt WM. (1999). Suppression of whole body and regional lipolysis by insulin: effects of obesity and exercise. *J Clin Endocrinol Metab* **84,** 3886-3895.

Hochstrasser DF, Sanchez JC & Appel RD. (2002). Proteomics and its trends facing nature's complexity. *Proteomics* **2,** 807-812.

Hoeg LD, Sjoberg KA, Jeppesen J, Jensen TE, Frosig C, Birk JB, Bisiani B, Hiscock N, Pilegaard H, Wojtaszewski JF, Richter EA & Kiens B. (2011). Lipid-induced insulin resistance affects women less than men and is not accompanied by inflammation or impaired proximal insulin signaling. *Diabetes* **60,** 64-73.

Hojlund K, Yi Z, Hwang H, Bowen B, Lefort N, Flynn CR, Langlais P, Weintraub ST & Mandarino LJ. (2008). Characterization of the human skeletal muscle proteome by one-dimensional gel electrophoresis and HPLC-ESI-MS/MS. *Mol Cell Proteomics* **7,** 257-267.

Holloway GP, Thrush AB, Heigenhauser GJ, Tandon NN, Dyck DJ, Bonen A & Spriet LL. (2007). Skeletal muscle mitochondrial FAT/CD36 content and palmitate oxidation are not decreased in obese women. *Am J Physiol Endocrinol Metab* **292,** E1782-1789.

Holloway KV, O'Gorman M, Woods P, Morton JP, Evans L, Cable NT, Goldspink DF & Burniston JG. (2009). Proteomic investigation of changes in human vastus lateralis muscle in response to interval-exercise training. *Proteomics* **9,** 5155-5174.

Hoppeler H. (2016). Molecular networks in skeletal muscle plasticity. *J Exp Biol* **219,** 205-213.

Hoppeler H, Billeter R, Horvath PJ, Leddy JJ & Pendergast DR. (1999). Muscle structure with low- and high-fat diets in well-trained male runners. *Int J Sports Med* **20,** 522-526.

Hu FB, Willett WC, Li T, Stampfer MJ, Colditz GA & Manson JE. (2004). Adiposity as compared with physical activity in predicting mortality among women. *New Engl J Med* **351,** 2694-2703.

Huang T, Qi Q, Zheng Y, Ley SH, Manson JE, Hu FB & Qi L. (2015). Genetic Predisposition to Central Obesity and Risk of Type 2 Diabetes: Two Independent Cohort Studies. *Diabetes Care* **38,** 1306-1311.

Hubner NC, Ren S & Mann M. (2008). Peptide separation with immobilized pI strips is an attractive alternative to in-gel protein digestion for proteome analysis. *Proteomics* **8,** 4862-4872.

Hulston CJ, Churnside AA & Venables MC. (2015). Probiotic supplementation prevents high-fat, overfeeding-induced insulin resistance in human subjects. *Br J Nutr* **113,** 596-602.

Hulston CJ, Woods RM, Dewhurst-Trigg R, Parry SA, Gagnon S, Baker L, James LJ, Markey O, Martin NRW, Ferguson RA & van Hall G. (2018). Resistance exercise stimulates mixed muscle protein synthesis in lean and obese young adults. *Physiological reports* **6,** e13799.

Hulver MW, Berggren JR, Cortright RN, Dudek RW, Thompson RP, Pories WJ, MacDonald KG, Cline GW, Shulman GI, Dohm GL & Houmard JA. (2003). Skeletal muscle lipid metabolism with obesity. *Am J Physiol Endocrinol Metab* **284,** E741-747.

Imamura M, Inoguchi T, Ikuyama S, Taniguchi S, Kobayashi K, Nakashima N & Nawata H. (2002). ADRP stimulates lipid accumulation and lipid droplet formation in murine fibroblasts. *Am J Physiol Endocrinol Metab* **283,** E775-783.

Itani SI, Pories WJ, Macdonald KG & Dohm GL. (2001). Increased protein kinase C theta in skeletal muscle of diabetic patients. *Metabolism* **50,** 553-557.

Itani SI, Ruderman NB, Schmieder F & Boden G. (2002). Lipid-induced insulin resistance in human muscle is associated with changes in diacylglycerol, protein kinase C, and IkappaB-alpha. *Diabetes* **51,** 2005-2011.

Itani SI, Zhou Q, Pories WJ, MacDonald KG & Dohm GL. (2000). Involvement of protein kinase C in human skeletal muscle insulin resistance and obesity. *Diabetes* **49,** 1353-1358.

Jacquier N, Choudhary V, Mari M, Toulmay A, Reggiori F & Schneiter R. (2011). Lipid droplets are functionally connected to the endoplasmic reticulum in Saccharomyces cerevisiae. *J Cell Sci* **124,** 2424-2437.

Jagerstrom S, Polesie S, Wickstrom Y, Johansson BR, Schroder HD, Hojlund K & Bostrom P. (2009). Lipid droplets interact with mitochondria using SNAP23. *Cell Biol Int* **33,** 934-940.

Jahn R & Scheller RH. (2006). SNAREs--engines for membrane fusion. *Nat Rev Mol Cell Biol* **7,** 631-643.

Janjic D. (1996). [Android-type obesity and gynecoid-type obesity]. *Praxis (Bern 1994)* **85,** 1578-1583.

Jensen J & Lai YC. (2009). Regulation of muscle glycogen synthase phosphorylation and kinetic properties by insulin, exercise, adrenaline and role in insulin resistance. *Arch Physiol Biochem* **115,** 13-21.

Jepson CA & Yeaman SJ. (1992). Inhibition of hormone-sensitive lipase by intermediary lipid metabolites. *FEBS Lett* **310,** 197-200.

Jewell JL, Oh E, Ramalingam L, Kalwat MA, Tagliabracci VS, Tackett L, Elmendorf JS & Thurmond DC. (2011). Munc18c phosphorylation by the insulin receptor links cell signaling directly to SNARE exocytosis. *J Cell Biol* **193,** 185-199.

Jiang W, Zhu J, Zhuang X, Zhang X, Luo T, Esser KA & Ren H. (2015). Lipin1 Regulates Skeletal Muscle Differentiation through Extracellular Signal-regulated Kinase (ERK) Activation and Cyclin D Complex-regulated Cell Cycle Withdrawal. *J Biol Chem* **290,** 23646-23655.

Jocken JW, Goossens GH, Boon H, Mason RR, Essers Y, Havekes B, Watt MJ, van Loon LJ & Blaak EE. (2013). Insulin-mediated suppression of lipolysis in adipose tissue and skeletal muscle of obese type 2 diabetic men and men with normal glucose tolerance. *Diabetologia* **56,** 2255-2265.

Jocken JW, Smit E, Goossens GH, Essers YP, van Baak MA, Mensink M, Saris WH & Blaak EE. (2008). Adipose triglyceride lipase (ATGL) expression in human skeletal muscle is type I (oxidative) fiber specific. *Histochem Cell Biol* **129,** 535-538.

Johnson NA, Stannard SR & Thompson MW. (2004). Muscle triglyceride and glycogen in endurance exercise: implications for performance. *Sports Med* **34,** 151-164.

Johnston MJ, ed. (1977). *Lipid metabolism in mammals* Plenum Press, New York.

Kaake RM, Wang X & Huang L. (2010). Profiling of protein interaction networks of protein complexes using affinity purification and quantitative mass spectrometry. *Mol Cell Proteomics* **9,** 1650-1665.

Kanaley JA, Shadid S, Sheehan MT, Guo Z & Jensen MD. (2009). Relationship between plasma free fatty acid, intramyocellular triglycerides and long-chain acylcarnitines in resting humans. *J Physiol* **587,** 5939-5950.

Kanzaki M. (2006). Insulin receptor signals regulating GLUT4 translocation and act in dynamics. *Endocr J* **53,** 267-293.

Karpe F, Dickmann JR & Frayn KN. (2011). Fatty acids, obesity, and insulin resistance: time for a reevaluation. *Diabetes* **60,** 2441-2449.

Kasuga M. (2006). Insulin resistance and pancreatic beta cell failure. *J Clin Invest* **116,** 1756-1760.

Katz LD, Glickman MG, Rapoport S, Ferrannini E & DeFronzo RA. (1983). Splanchnic and peripheral disposal of oral glucose in man. *Diabetes* **32,** 675-679.

Katzmarzyk PT. (2010). Physical activity, sedentary behavior, and health: paradigm paralysis or paradigm shift? *Diabetes* **59,** 2717-2725.

Kawanishi M, Tamori Y, Okazawa H, Araki S, Shinoda H & Kasuga M. (2000). Role of SNAP23 in insulin-induced translocation of GLUT4 in 3T3-L1 adipocytes. Mediation of complex formation between syntaxin4 and VAMP2. *J Biol Chem* **275,** 8240-8247.

Kearney J. (2010). Food consumption trends and drivers. *Philos Trans R Soc Lond B Biol Sci* **365,** 2793-2807.

Kelley DE, Goodpaster B, Wing RR & Simoneau JA. (1999). Skeletal muscle fatty acid metabolism in association with insulin resistance, obesity, and weight loss. *Am J Physiol* **277,** E1130-1141.

Kelley DE, He J, Menshikova EV & Ritov VB. (2002). Dysfunction of mitochondria in human skeletal muscle in type 2 diabetes. *Diabetes* **51,** 2944-2950.

Kelley DE & Mandarino LJ. (2000). Fuel selection in human skeletal muscle in insulin resistance: a reexamination. *Diabetes* **49,** 677-683.

Kelley DE & Simoneau JA. (1994). Impaired free fatty acid utilization by skeletal muscle in non-insulin-dependent diabetes mellitus. *J Clin Invest* **94,** 2349-2356.

Kelley DE, Thaete FL, Troost F, Huwe T & Goodpaster BH. (2000). Subdivisions of subcutaneous abdominal adipose tissue and insulin resistance. *Am J Physiol Endocrinol Metab* **278,** E941-948.

Kelley DE, Williams KV, Price JC, McKolanis TM, Goodpaster BH & Thaete FL. (2001). Plasma fatty acids, adiposity, and variance of skeletal muscle insulin resistance in type 2 diabetes mellitus. *J Clin Endocrinol Metab* **86,** 5412-5419.

Keske MA, Premilovac D, Bradley EA, Dwyer RM, Richards SM & Rattigan S. (2016). Muscle microvascular blood flow responses in insulin resistance and ageing. *J Physiol* **594,** 2223-2231.

Kiens B, Roemen TH & van der Vusse GJ. (1999). Muscular long-chain fatty acid content during graded exercise in humans. *Am J Physiol* **276,** E352-357.

Kim JK, Fillmore JJ, Sunshine MJ, Albrecht B, Higashimori T, Kim DW, Liu ZX, Soos TJ, Cline GW, O'Brien WR, Littman DR & Shulman GI. (2004). PKC-theta knockout mice are protected from fat-induced insulin resistance. *J Clin Invest* **114,** 823-827.

Kim JK, Gavrilova O, Chen Y, Reitman ML & Shulman GI. (2000a). Mechanism of insulin resistance in A-ZIP/F-1 fatless mice. *J Biol Chem* **275,** 8456-8460.

Kim JY, Hickner RC, Cortright RL, Dohm GL & Houmard JA. (2000b). Lipid oxidation is reduced in obese human skeletal muscle. *Am J Physiol Endocrinol Metab* **279,** E1039-1044.

Klein S, Coyle EF & Wolfe RR. (1994). Fat-Metabolism during Low-Intensity Exercise in Endurance-Trained and Untrained Men. *Am J Physiol-Endoc M* **267,** E934-E940.

Kleinert M, Parker BL, Chaudhuri R, Fazakerley DJ, Serup A, Thomas KC, Krycer JR, Sylow L, Fritzen AM, Hoffman NJ, Jeppesen J, Schjerling P, Ruegg MA, Kiens B, James DE & Richter EA. (2016). mTORC2 and AMPK differentially regulate muscle triglyceride content via Perilipin 3. *Mol Metab* **5,** 646-655.

Knudsen SH, Hansen LS, Pedersen M, Dejgaard T, Hansen J, Hall GV, Thomsen C, Solomon TP, Pedersen BK & Krogh-Madsen R. (2012). Changes in insulin sensitivity precede changes in body composition during 14 days of step reduction combined with overfeeding in healthy young men. *J Appl Physiol (1985)* **113,** 7-15.

Konrad D, Bilan PJ, Nawaz Z, Sweeney G, Niu WY, Liu Z, Antonescu CN, Rudich A & Klip A. (2002). Need for GLUT4 activation to reach maximum effect of insulin-mediated glucose uptake in brown adipocytes isolated from GLUT4myc-expressing mice. *Diabetes* **51,** 2719-2726.

Kory N, Farese RV, Jr. & Walther TC. (2016). Targeting Fat: Mechanisms of Protein Localization to Lipid Droplets. *Trends Cell Biol* **26,** 535-546.

Koves TR, Sparks LM, Kovalik JP, Mosedale M, Arumugam R, DeBalsi KL, Everingham K, Thorne L, Phielix E, Meex RC, Kien CL, Hesselink MK, Schrauwen P & Muoio DM. (2013). PPARgamma coactivator-1alpha contributes to exercise-induced regulation of intramuscular lipid droplet programming in mice and humans. *J Lipid Res* **54,** 522-534.

Koves TR, Ussher JR, Noland RC, Slentz D, Mosedale M, Ilkayeva O, Bain J, Stevens R, Dyck JR, Newgard CB, Lopaschuk GD & Muoio DM. (2008). Mitochondrial overload and incomplete fatty acid oxidation contribute to skeletal muscle insulin resistance. *Cell Metab* **7,** 45-56.

Krahmer N, Hilger M, Kory N, Wilfling F, Stoehr G, Mann M, Farese RV, Jr. & Walther TC. (2013). Protein correlation profiles identify lipid droplet proteins with high confidence. *Mol Cell Proteomics* **12,** 1115-1126.

Kramer RM, Hession C, Johansen B, Hayes G, McGray P, Chow EP, Tizard R & Pepinsky RB. (1989). Structure and properties of a human non-pancreatic phospholipase A2. *J Biol Chem* **264,** 5768-5775.

Kuhl J, Hilding A, Ostenson CG, Grill V, Efendic S & Bavenholm P. (2005). Characterisation of subjects with early abnormalities of glucose tolerance in the Stockholm Diabetes Prevention Programme: the impact of sex and type 2 diabetes heredity. *Diabetologia* **48,** 35-40.

Laakso M. (2010). Cardiovascular disease in type 2 diabetes from population to man to mechanisms: the Kelly West Award Lecture 2008. *Diabetes Care* **33,** 442-449.

Lachmanovich E, Shvartsman DE, Malka Y, Botvin C, Henis YI & Weiss AM. (2003). Co-localization analysis of complex formation among membrane proteins by computerized fluorescence microscopy: application to immunofluorescence co-patching studies. *J Microsc* **212,** 122-131.

Langfort J, Ploug T, Ihlemann J, Holm C & Galbo H. (2000). Stimulation of hormone-sensitive lipase activity by contractions in rat skeletal muscle. *Biochem J* **351,** 207-214.

Langfort J, Ploug T, Ihlemann J, Saldo M, Holm C & Galbo H. (1999). Expression of hormone-sensitive lipase and its regulation by adrenaline in skeletal muscle. *Biochem J* **340 (Pt 2),** 459-465.

Large V, Reynisdottir S, Langin D, Fredby K, Klannemark M, Holm C & Arner P. (1999). Decreased expression and function of adipocyte hormone-sensitive lipase in subcutaneous fat cells of obese subjects. *J Lipid Res* **40,** 2059-2066.

Lass A, Zimmermann R, Haemmerle G, Riederer M, Schoiswohl G, Schweiger M, Kienesberger P, Strauss JG, Gorkiewicz G & Zechner R. (2006). Adipose triglyceride lipase-mediated lipolysis of cellular fat stores is activated by CGI-58 and defective in Chanarin-Dorfman Syndrome. *Cell Metab* **3,** 309-319.

Lass A, Zimmermann R, Oberer M & Zechner R. (2011). Lipolysis - a highly regulated multi-enzyme complex mediates the catabolism of cellular fat stores. *Prog Lipid Res* **50,** 14-27.

Laurens C, Bourlier V, Mairal A, Louche K, Badin PM, Mouisel E, Montagner A, Marette A, Tremblay A, Weisnagel JS, Guillou H, Langin D, Joanisse DR & Moro C. (2016). Perilipin 5 fine-tunes lipid oxidation to metabolic demand and protects against lipotoxicity in skeletal muscle. *Sci Rep* **6,** 38310.

Lauritzen HPMM, Mug T, Prats C, Tavare JM & Galbo H. (2006). Imaging of insulin signaling in skeletal muscle of living mice shows major role of T-tubules. *Diabetes* **55,** 1300-1306.

Lee CD, Jackson AS & Blair SN. (1998). US weight guidelines: is it also important to consider cardiorespiratory fitness? *Int J Obes Relat Metab Disord* **22 Suppl 2,** S2-7.

Leiguez E, Zuliani JP, Cianciarullo AM, Fernandes CM, Gutierrez JM & Teixeira C. (2011). A group IIA-secreted phospholipase A2 from snake venom induces lipid body formation in macrophages: the roles of intracellular phospholipases A2 and distinct signaling pathways. *J Leukoc Biol* **90,** 155-166.

Lessard SJ, Rivas DA, Chen ZP, van Denderen BJ, Watt MJ, Koch LG, Britton SL, Kemp BE & Hawley JA. (2009). Impaired skeletal muscle beta-adrenergic activation and lipolysis are associated with whole-body insulin resistance in rats bred for low intrinsic exercise capacity. *Endocrinology* **150,** 4883-4891.

Levin MC, Monetti M, Watt MJ, Sajan MP, Stevens RD, Bain JR, Newgard CB, Farese RV, Sr. & Farese RV, Jr. (2007). Increased lipid accumulation and insulin resistance in transgenic mice expressing DGAT2 in glycolytic (type II) muscle. *Am J Physiol Endocrinol Metab* **293,** E1772-1781.

Lewin TM, Granger DA, Kim JH & Coleman RA. (2001). Regulation of mitochondrial sn-glycerol-3-phosphate acyltransferase activity: response to feeding status is unique in various rat tissues and is discordant with protein expression. *Arch Biochem Biophys* **396,** 119-127.

Li M, Paran C, Wolins NE & Horowitz JF. (2011). High muscle lipid content in obesity is not due to enhanced activation of key triglyceride esterification enzymes or the suppression of lipolytic proteins. *Am J Physiol Endocrinol Metab* **300,** E699-707.

Linden D, William-Olsson L, Ahnmark A, Ekroos K, Hallberg C, Sjogren HP, Becker B, Svensson L, Clapham JC, Oscarsson J & Schreyer S. (2006). Liver-directed overexpression of mitochondrial glycerol-3-phosphate acyltransferase results in hepatic steatosis, increased triacylglycerol secretion and reduced fatty acid oxidation. *Faseb J* **20,** 434-443.

Lipina C & Hundal HS. (2011). Sphingolipids: agents provocateurs in the pathogenesis of insulin resistance. *Diabetologia* **54,** 1596-1607.

Listenberger LL, Ostermeyer-Fay AG, Goldberg EB, Brown WJ & Brown DA. (2007). Adipocyte differentiation-related protein reduces the lipid droplet association of adipose triglyceride lipase and slows triacylglycerol turnover. *J Lipid Res* **48,** 2751-2761.

Liu KH, Chan YL, Chan JC, Chan WB & Kong WL. (2006a). Mesenteric fat thickness as an independent determinant of fatty liver. *Int J Obes (Lond)* **30,** 787-793.

Liu L, Zhang Y, Chen N, Shi X, Tsang B & Yu YH. (2007). Upregulation of myocellular DGAT1 augments triglyceride synthesis in skeletal muscle and protects against fat-induced insulin resistance. *J Clin Invest* **117,** 1679-1689.

Liu LZ, Zhao HL, Zuo J, Ho SKS, Chan JCN, Meng Y, Fang FD & Tong PCY. (2006b). Protein kinase C xi mediates insulin-induced glucose transport through actin remodeling in L6 muscle cells. *Molecular Biology of the Cell* **17,** 2322-2330.

Liu P, Ying Y, Zhao Y, Mundy DI, Zhu M & Anderson RG. (2004). Chinese hamster ovary K2 cell lipid droplets appear to be metabolic organelles involved in membrane traffic. *J Biol Chem* **279,** 3787-3792.

Londos C, Brasaemle DL, Gruia-Gray J, Servetnick DA, Schultz CJ, Levin DM & Kimmel AR. (1995). Perilipin: unique proteins associated with intracellular neutral lipid droplets in adipocytes and steroidogenic cells. *Biochem Soc Trans* **23,** 611-615.

Long AP, Manneschmidt AK, VerBrugge B, Dortch MR, Minkin SC, Prater KE, Biggerstaff JP, Dunlap JR & Dalhaimer P. (2012). Lipid droplet de novo formation and fission are linked to the cell cycle in fission yeast. *Traffic* **13,** 705-714.

Lopez JA, Burchfield JG, Blair DH, Mele K, Ng Y, Vallotton P, James DE & Hughes WE. (2009). Identification of a distal GLUT4 trafficking event controlled by actin polymerization. *Mol Biol Cell* **20,** 3918-3929.

Louche K, Badin PM, Montastier E, Laurens C, Bourlier V, de Glisezinski I, Thalamas C, Viguerie N, Langin D & Moro C. (2013). Endurance exercise training up-regulates lipolytic proteins and reduces triglyceride content in skeletal muscle of obese subjects. *J Clin Endocrinol Metab* **98,** 4863-4871.

Ludescher B, Najib A, Baar S, Machann J, Thamer C, Schick F, Buchkremer G, Claussen CD & Eschweiler GW. (2007). Gender specific correlations of adrenal gland size and body fat distribution: a whole body MRI study. *Horm Metab Res* **39,** 515-518.

MacPherson RE, Herbst EA, Reynolds EJ, Vandenboom R, Roy BD & Peters SJ. (2012). Subcellular localization of skeletal muscle lipid droplets and PLIN family proteins OXPAT and ADRP at rest and following contraction in rat soleus muscle. *Am J Physiol Regul Integr Comp Physiol* **302,** R29-36.

MacPherson RE, Ramos SV, Vandenboom R, Roy BD & Peters SJ. (2013a). Skeletal muscle PLIN proteins, ATGL and CGI-58, interactions at rest and following stimulated contraction. *Am J Physiol Regul Integr Comp Physiol* **304,** R644-650.

Macpherson RE, Vandenboom R, Roy BD & Peters SJ. (2013b). Skeletal muscle PLIN3 and PLIN5 are serine phosphorylated at rest and following lipolysis during adrenergic or contractile stimulation. *Physiol Rep* **1,** e00084.

Malik ZA, Cobley JN, Morton JP, Close GL, Edwards BJ, Koch LG, Britton SL & Burniston JG. (2013). Label-Free LC-MS Profiling of Skeletal Muscle Reveals Heart-Type Fatty Acid Binding Protein as a Candidate Biomarker of Aerobic Capacity. *Proteomes* **1,** 290-308.

Marin P, Andersson B, Krotkiewski M & Bjorntorp P. (1994). Muscle fiber composition and capillary density in women and men with NIDDM. *Diabetes Care* **17,** 382-386.

Martin A, Hales P & Brindley DN. (1987). A rapid assay for measuring the activity and the Mg2+ and Ca2+ requirements of phosphatidate phosphohydrolase in cytosolic and microsomal fractions of rat liver. *Biochem J* **245,** 347-355.

Mason RR, Meex RC, Lee-Young R, Canny BJ & Watt MJ. (2012). Phosphorylation of adipose triglyceride lipase Ser(404) is not related to 5'-AMPK activation during moderate-intensity exercise in humans. *Am J Physiol Endocrinol Metab* **303,** E534-541.

Mason RR, Meex RC, Russell AP, Canny BJ & Watt MJ. (2014a). Cellular localization and associations of the major lipolytic proteins in human skeletal muscle at rest and during exercise. *PLoS One* **9,** e103062.

Mason RR, Mokhtar R, Matzaris M, Selathurai A, Kowalski GM, Mokbel N, Meikle PJ, Bruce CR & Watt MJ. (2014b). PLIN5 deletion remodels intracellular lipid composition and causes insulin resistance in muscle. *Mol Metab* **3,** 652-663.

Masuda Y, Itabe H, Odaki M, Hama K, Fujimoto Y, Mori M, Sasabe N, Aoki J, Arai H & Takano T. (2006). ADRP/adipophilin is degraded through the proteasome-dependent pathway during regression of lipid-storing cells. *J Lipid Res* **47,** 87-98.

Matsuda M & DeFronzo RA. (1999). Insulin sensitivity indices obtained from oral glucose tolerance testing: comparison with the euglycemic insulin clamp. *Diabetes Care* **22,** 1462-1470.

Maughan DW, Henkin JA & Vigoreaux JO. (2005). Concentrations of glycolytic enzymes and other cytosolic proteins in the diffusible fraction of a vertebrate muscle proteome. *Mol Cell Proteomics* **4,** 1541-1549.

McQuaid SE, Hodson L, Neville MJ, Dennis AL, Cheeseman J, Humphreys SM, Ruge T, Gilbert M, Fielding BA, Frayn KN & Karpe F. (2011). Downregulation of adipose tissue fatty acid trafficking in obesity: a driver for ectopic fat deposition? *Diabetes* **60,** 47-55.

Meex RC, Hoy AJ, Mason RM, Martin SD, McGee SL, Bruce CR & Watt MJ. (2015). ATGL-mediated triglyceride turnover and the regulation of mitochondrial capacity in skeletal muscle. *Am J Physiol Endocrinol Metab* **308,** E960-970.

Menshikova EV, Ritov VB, Toledo FG, Ferrell RE, Goodpaster BH & Kelley DE. (2005). Effects of weight loss and physical activity on skeletal muscle mitochondrial function in obesity. *Am J Physiol Endocrinol Metab* **288,** E818-825.

Mensink M, Blaak EE, van Baak MA, Wagenmakers AJ & Saris WH. (2001). Plasma free Fatty Acid uptake and oxidation are already diminished in subjects at high risk for developing type 2 diabetes. *Diabetes* **50,** 2548-2554.

Mifflin MD, St Jeor ST, Hill LA, Scott BJ, Daugherty SA & Koh YO. (1990). A new predictive equation for resting energy expenditure in healthy individuals. *The American journal of clinical nutrition* **51,** 241-247.

Miinea CP, Sano H, Kane S, Sano E, Fukuda M, Peranen J, Lane WS & Lienhard GE. (2005). AS160, the Akt substrate regulating GLUT4 translocation, has a functional Rab GTPase-activating protein domain. *Biochem J* **391,** 87-93.

Montague CT & O'Rahilly S. (2000). The perils of portliness: causes and consequences of visceral adiposity. *Diabetes* **49,** 883-888.

Moran A, Jacobs DR, Jr., Steinberger J, Steffen LM, Pankow JS, Hong CP & Sinaiko AR. (2008). Changes in insulin resistance and cardiovascular risk during adolescence: establishment of differential risk in males and females. *Circulation* **117,** 2361-2368.

Morino K, Petersen KF & Shulman GI. (2006). Molecular mechanisms of insulin resistance in humans and their potential links with mitochondrial dysfunction. *Diabetes* **55 Suppl 2,** S9-S15.

Moro C, Bajpeyi S & Smith SR. (2008). Determinants of intramyocellular triglyceride turnover: implications for insulin sensitivity. *Am J Physiol Endocrinol Metab* **294,** E203-213.

Munguia-Miranda C, Sanchez-Barrera RG, Tuz K, Alonso-Garcia AL & Cruz M. (2009). [Impaired fasting glucose detection in blood donors population]. *Rev Med Inst Mex Seguro Soc* **47,** 17-24.

Muoio DM, Dohm GL, Tapscott EB & Coleman RA. (1999). Leptin opposes insulin's effects on fatty acid partitioning in muscles isolated from obese ob/ob mice. *Am J Physiol* **276,** E913-921.

Murakami M, Taketomi Y, Miki Y, Sato H, Hirabayashi T & Yamamoto K. (2011). Recent progress in phospholipase A(2) research: from cells to animals to humans. *Prog Lipid Res* **50,** 152-192.

Myers MG, Backer JM, Sun XJ, Shoelson S, Hu P, Schlessinger J, Yoakim M, Schaffhausen B & White MF. (1992). Irs-1 Activates Phosphatidylinositol 3'-Kinase by Associating with Src Homology-2 Domains of P85. *P Natl Acad Sci USA* **89,** 10350-10354.

Naja F, Hwalla N, Itani L, Karam S, Sibai AM & Nasreddine L. (2015). A Western dietary pattern is associated with overweight and obesity in a national sample of Lebanese adolescents (13-19 years): a cross-sectional study. *Br J Nutr* **114,** 1909-1919.

Neel JV. (1962). Diabetes mellitus: a "thrifty" genotype rendered detrimental by "progress"? *Am J Hum Genet* **14,** 353-362.

Neel JV. (1999). The "thrifty genotype" in 1998. *Nutr Rev* **57,** S2-9.

Newsom SA, Schenk S, Li M, Everett AC & Horowitz JF. (2011). High fatty acid availability after exercise alters the regulation of muscle lipid metabolism. *Metabolism* **60,** 852-859.

Nielsen J, Christensen AE, Nellemann B & Christensen B. (2017). Lipid droplet size and location in human skeletal muscle fibers are associated with insulin sensitivity. *Am J Physiol Endocrinol Metab* **313,** E721-E730.

Nielsen S, Guo Z, Johnson CM, Hensrud DD & Jensen MD. (2004). Splanchnic lipolysis in human obesity. *J Clin Invest* **113,** 1582-1588.

Nojima H, Yoneda M, Watanabe H, Yamane K, Kitahara Y, Sekikawa K, Yamamoto H, Yokoyama A, Hattori N, Kohno N & Stud HUHP. (2017). Association between aerobic capacity and the improvement in glycemic control after the exercise training in type 2 diabetes. *Diabetol Metab Syndr* **9**.

Nuutila P, Knuuti MJ, Maki M, Laine H, Ruotsalainen U, Teras M, Haaparanta M, Solin O & Yki-Jarvinen H. (1995). Gender and insulin sensitivity in the heart and in skeletal muscles. Studies using positron emission tomography. *Diabetes* **44,** 31-36.

Oakes ND, Bell KS, Furler SM, Camilleri S, Saha AK, Ruderman NB, Chisholm DJ & Kraegen EW. (1997a). Diet-induced muscle insulin resistance in rats is ameliorated by acute dietary lipid withdrawal or a single bout of exercise:

parallel relationship between insulin stimulation of glucose uptake and suppression of long-chain fatty acyl-CoA. *Diabetes* **46,** 2022-2028.

Oakes ND, Cooney GJ, Camilleri S, Chisholm DJ & Kraegen EW. (1997b). Mechanisms of liver and muscle insulin resistance induced by chronic high-fat feeding. *Diabetes* **46,** 1768-1774.

Oberbach A, Bossenz Y, Lehmann S, Niebauer J, Adams V, Paschke R, Schon MR, Bluher M & Punkt K. (2006). Altered fiber distribution and fiber-specific glycolytic and oxidative enzyme activity in skeletal muscle of patients with type 2 diabetes. *Diabetes Care* **29,** 895-900.

Okada T, Kawano Y, Sakakibara T, Hazeki O & Ui M. (1994). Essential role of phosphatidylinositol 3-kinase in insulin-induced glucose transport and antilipolysis in rat adipocytes. Studies with a selective inhibitor wortmannin. *J Biol Chem* **269,** 3568-3573.

Okuno A, Tamemoto H, Tobe K, Ueki K, Mori Y, Iwamoto K, Umesono K, Akanuma Y, Fujiwara T, Horikoshi H, Yazaki Y & Kadowaki T. (1998). Troglitazone increases the number of small adipocytes without the change of white adipose tissue mass in obese Zucker rats. *J Clin Invest* **101,** 1354-1361.

Olefsky JM. (1977). Insensitivity of large rat adipocytes to the antilipolytic effects of insulin. *J Lipid Res* **18,** 459-464.

Ong JM & Kern PA. (1989). Effect of feeding and obesity on lipoprotein lipase activity, immunoreactive protein, and messenger RNA levels in human adipose tissue. *J Clin Invest* **84,** 305-311.

Ostman J, Arner P, Engfeldt P & Kager L. (1979). Regional differences in the control of lipolysis in human adipose tissue. *Metabolism* **28,** 1198-1205.

Oti M, Snel B, Huynen MA & Brunner HG. (2006). Predicting disease genes using protein-protein interactions. *J Med Genet* **43**.

Pagnon J, Matzaris M, Stark R, Meex RC, Macaulay SL, Brown W, O'Brien PE, Tiganis T & Watt MJ. (2012). Identification and functional characterization of protein kinase A phosphorylation sites in the major lipolytic protein, adipose triglyceride lipase. *Endocrinology* **153,** 4278-4289.

Pan DA, Lillioja S, Kriketos AD, Milner MR, Baur LA, Bogardus C, Jenkins AB & Storlien LH. (1997). Skeletal muscle triglyceride levels are inversely related to insulin action. *Diabetes* **46,** 983-988.

Pan JJ & Fallon MB. (2014). Gender and racial differences in nonalcoholic fatty liver disease. *World Journal of Hepatology* **6,** 274-283.

Paolisso G, Gambardella A, Amato L, Tortoriello R, D'Amore A, Varricchio M & D'Onofrio F. (1995). Opposite effects of short- and long-term fatty acid infusion on insulin secretion in healthy subjects. *Diabetologia* **38,** 1295-1299.

Parry SA, Smith JR, Corbett TRB, Woods RM & Hulston CJ. (2017). Short-term, high-fat overfeeding impairs glycaemic control but does not alter gut hormone responses to a mixed meal tolerance test in healthy, normal-weight individuals. *Brit J Nutr* **117,** 48-55.

Pelsers MM, Tsintzas K, Boon H, Jewell K, Norton L, Luiken JJ, Glatz JF & van Loon LJ. (2007). Skeletal muscle fatty acid transporter protein expression in type 2 diabetes patients compared with overweight, sedentary men and age-matched, endurance-trained cyclists. *Acta Physiol (Oxf)* **190,** 209-219.

Perreault L, Bergman BC, Hunerdosse DM & Eckel RH. (2010). Altered intramuscular lipid metabolism relates to diminished insulin action in men, but not women, in progression to diabetes. *Obesity (Silver Spring)* **18,** 2093-2100.

Perry RJ, Samuel VT, Petersen KF & Shulman GI. (2014). The role of hepatic lipids in hepatic insulin resistance and type 2 diabetes. *Nature* **510,** 84-91.

Pessin JE & Saltiel AR. (2000). Signaling pathways in insulin action: molecular targets of insulin resistance. *J Clin Invest* **106,** 165-169.

Peters SJ, Samjoo IA, Devries MC, Stevic I, Robertshaw HA & Tarnopolsky MA. (2012). Perilipin family (PLIN) proteins in human skeletal muscle: the effect of sex, obesity, and endurance training. *Appl Physiol Nutr Metab* **37,** 724-735.

Petersen KF, Dufour S, Savage DB, Bilz S, Solomon G, Yonemitsu S, Cline GW, Befroy D, Zemany L, Kahn BB, Papademetris X, Rothman DL & Shulman GI. (2007). The role of skeletal muscle insulin resistance in the pathogenesis of the metabolic syndrome. *Proc Natl Acad Sci U S A* **104,** 12587-12594.

Phan J, Peterfy M & Reue K. (2004). Lipin expression preceding peroxisome proliferator-activated receptor-gamma is critical for adipogenesis in vivo and in vitro. *Journal of Biological Chemistry* **279,** 29558-29564.

Phillips SA, Choe CC, Ciaraldi TP, Greenberg AS, Kong AP, Baxi SC, Christiansen L, Mudaliar SR & Henry RR. (2005). Adipocyte differentiation-related protein in human skeletal muscle: relationship to insulin sensitivity. *Obes Res* **13,** 1321-1329.

Phillips SM, Green HJ, Tarnopolsky MA, Heigenhauser GF, Hill RE & Grant SM. (1996). Effects of training duration on substrate turnover and oxidation during exercise. *J Appl Physiol (1985)* **81,** 2182-2191.

Phizicky EM & Fields S. (1995). Protein-protein interactions: methods for detection and analysis. *Microbiol Rev* **59,** 94-123.

Polotsky HN & Polotsky AJ. (2010). Metabolic implications of menopause. *Semin Reprod Med* **28,** 426-434.

Potts GK, McNally RM, Blanco R, You JS, Hebert AS, Westphall MS, Coon JJ & Hornberger TA. (2017). A map of the phosphoproteomic alterations that occur after a bout of maximal-intensity contractions. *J Physiol-London* **595,** 5209-5226.

Pourteymour S, Lee S, Langleite TM, Eckardt K, Hjorth M, Bindesboll C, Dalen KT, Birkeland KI, Drevon CA, Holen T & Norheim F. (2015). Perilipin 4 in human skeletal muscle: localization and effect of physical activity. *Physiol Rep* **3**.

Powell DJ, Hajduch E, Kular G & Hundal HS. (2003). Ceramide disables 3-phosphoinositide binding to the pleckstrin homology domain of protein kinase B (PKB)/Akt by a PKCzeta-dependent mechanism. *Mol Cell Biol* **23,** 7794-7808.

Prats C, Donsmark M, Qvortrup K, Londos C, Sztalryd C, Holm C, Galbo H & Ploug T. (2006). Decrease in intramuscular lipid droplets and translocation of HSL in response to muscle contraction and epinephrine. *J Lipid Res* **47,** 2392-2399.

Racette SB, Evans EM, Weiss EP, Hagberg JM & Holloszy JO. (2006). Abdominal adiposity is a stronger predictor of insulin resistance than fitness among 50-95 year olds. *Diabetes Care* **29,** 673-678.

Ramos SV, MacPherson RE, Turnbull PC, Bott KN, LeBlanc P, Ward WE & Peters SJ. (2014). Higher PLIN5 but not PLIN3 content in isolated skeletal muscle mitochondria following acute in vivo contraction in rat hindlimb. *Physiol Rep* **2**.

Ramos SV, Turnbull PC & MacPherson RE. (2016). Adipose tissue depot specific differences of PLIN protein content in endurance trained rats. *Adipocyte* **5,** 212-223.

Ramos SV, Turnbull PC, MacPherson RE, LeBlanc PJ, Ward WE & Peters SJ. (2015). Changes in mitochondrial perilipin 3 and perilipin 5 protein content in rat skeletal muscle following endurance training and acute stimulated contraction. *Exp Physiol* **100,** 450-462.

Randle PJ, Garland PB, Hales CN & Newsholme EA. (1963). The glucose fatty-acid cycle. Its role in insulin sensitivity and the metabolic disturbances of diabetes mellitus. *Lancet* **1,** 785-789.

Rando RR & Young N. (1984). The Stereospecific Activation of Protein Kinase-C. *Biochem Bioph Res Co* **122,** 818-823.

Rattarasarn C, Leelawattana R, Soonthornpun S, Setasuban W & Thamprasit A. (2004). Gender differences of regional abdominal fat distribution and their relationships with insulin sensitivity in healthy and glucose-intolerant Thais. *J Clin Endocrinol Metab* **89,** 6266-6270.

Ravichandran V, Chawla A & Roche PA. (1996). Identification of a novel syntaxin- and synaptobrevin/VAMP-binding protein, SNAP-23, expressed in non-neuronal tissues. *J Biol Chem* **271,** 13300-13303.

Remuzzi G, Schieppati A & Ruggenenti P. (2002). Clinical practice. Nephropathy in patients with type 2 diabetes. *N Engl J Med* **346,** 1145-1151.

Ritov VB, Menshikova EV, He J, Ferrell RE, Goodpaster BH & Kelley DE. (2005). Deficiency of subsarcolemmal mitochondria in obesity and type 2 diabetes. *Diabetes* **54,** 8-14.

Robenek H, Hofnagel O, Buers I, Robenek MJ, Troyer D & Severs NJ. (2006). Adipophilin-enriched domains in the ER membrane are sites of lipid droplet biogenesis. *J Cell Sci* **119,** 4215-4224.

Roden M, Price TB, Perseghin G, Petersen KF, Cline GW, Rothman DL & Shulman GI. (1996). Mechanism of free fatty acid induced insulin resistance in humans. *Diabetes* **45,** 33-33.

Roden M, Stingl H, Chandramouli V, Schumann WC, Hofer A, Landau BR, Nowotny P, Waldhausl W & Shulman GI. (2000). Effects of free fatty acid elevation on postabsorptive endogenous glucose production and gluconeogenesis in humans. *Diabetes* **49,** 701-707.

Roepstorff C, Vistisen B, Donsmark M, Nielsen JN, Galbo H, Green KA, Hardie DG, Wojtaszewski JF, Richter EA & Kiens B. (2004). Regulation of hormone-sensitive lipase activity and Ser563 and Ser565 phosphorylation in human skeletal muscle during exercise. *J Physiol* **560,** 551-562.

Rolls BJ. (2000). The role of energy density in the overconsumption of fat. *J Nutr* **130,** 268S-271S.

Romijn JA, Coyle EF, Sidossis LS, Gastaldelli A, Horowitz JF, Endert E & Wolfe RR. (1993). Regulation of endogenous fat and carbohydrate metabolism in relation to exercise intensity and duration. *Am J Physiol* **265,** E380-391.

Rowe ER, Mimmack ML, Barbosa AD, Haider A, Isaac I, Ouberai MM, Thiam AR, Patel S, Saudek V, Siniossoglou S & Savage DB. (2016). Conserved Amphipathic Helices Mediate Lipid Droplet Targeting of Perilipins 1-3. *J Biol Chem* **291,** 6664-6678.

Ruan H & Pownall HJ. (2001). Overexpression of 1-acyl-glycerol-3-phosphate acyltransferase-alpha enhances lipid storage in cellular models of adipose tissue and skeletal muscle. *Diabetes* **50,** 233-240.

Russell AP. (2004). Lipotoxicity: the obese and endurance-trained paradox. *Int J Obes Relat Metab Disord* **28 Suppl 4,** S66-71.

Russell AP, Gastaldi G, Bobbioni-Harsch E, Arboit P, Gobelet C, Deriaz O, Golay A, Witztum JL & Giacobino JP. (2003). Lipid peroxidation in skeletal muscle of obese as compared to endurance-trained humans: a case of good vs. bad lipids? *FEBS Lett* **551,** 104-106.

Ryysy L, Hakkinen AM, Goto T, Vehkavaara S, Westerbacka J, Halavaara J & Yki-Jarvinen H. (2000). Hepatic fat content and insulin action on free fatty acids and glucose metabolism rather than insulin absorption are associated with insulin requirements during insulin therapy in type 2 diabetic patients. *Diabetes* **49,** 749-758.

Sacchetti M, Saltin B, Olsen DB & van Hall G. (2004). High triacylglycerol turnover rate in human skeletal muscle. *J Physiol-London* **561,** 883-891.

Sadur CN, Yost TJ & Eckel RH. (1984). Insulin responsiveness of adipose tissue lipoprotein lipase is delayed but preserved in obesity. *J Clin Endocrinol Metab* **59,** 1176-1182.

Samocha-Bonet D, Campbell LV, Viardot A, Freund J, Tam CS, Greenfield JR & Heilbronn LK. (2010). A family history of type 2 diabetes increases risk factors associated with overfeeding. *Diabetologia* **53,** 1700-1708.

Samuel VT, Petersen KF & Shulman GI. (2010). Lipid-induced insulin resistance: unravelling the mechanism. *Lancet* **375,** 2267-2277.

Sanyal D, Mukherjee P, Raychaudhuri M, Ghosh S, Mukherjee S & Chowdhury S. (2015). Profile of liver enzymes in non-alcoholic fatty liver disease in patients with impaired glucose tolerance and newly detected untreated type 2 diabetes. *Indian J Endocrinol Metab* **19,** 597-601.

Schenk S & Horowitz JF. (2007). Acute exercise increases triglyceride synthesis in skeletal muscle and prevents fatty acid-induced insulin resistance. *J Clin Invest* **117,** 1690-1698.

Schmitt B, Fluck M, Decombaz J, Kreis R, Boesch C, Wittwer M, Graber F, Vogt M, Howald H & Hoppeler H. (2003). Transcriptional adaptations of lipid metabolism in tibialis anterior muscle of endurance-trained athletes. *Physiol Genomics* **15,** 148-157.

Schmitz-Peiffer C, Browne CL, Oakes ND, Watkinson A, Chisholm DJ, Kraegen EW & Biden TJ. (1997). Alterations in the expression and cellular localization of

protein kinase C isozymes epsilon and theta are associated with insulin resistance in skeletal muscle of the high-fat-fed rat. *Diabetes* **46,** 169-178.

Schrauwen-Hinderling VB, Kooi ME, Hesselink MK, Moonen-Kornips E, Schaart G, Mustard KJ, Hardie DG, Saris WH, Nicolay K & Schrauwen P. (2005). Intramyocellular lipid content and molecular adaptations in response to a 1-week high-fat diet. *Obes Res* **13,** 2088-2094.

Schrauwen P, van Aggel-Leijssen DP, Hul G, Wagenmakers AJ, Vidal H, Saris WH & van Baak MA. (2002). The effect of a 3-month low-intensity endurance training program on fat oxidation and acetyl-CoA carboxylase-2 expression. *Diabetes* **51,** 2220-2226.

Schulze PC. (2009). Myocardial lipid accumulation and lipotoxicity in heart failure. *J Lipid Res* **50,** 2137-2138.

Shah P, Vella A, Basu A, Basu R, Adkins A, Schwenk WF, Johnson CM, Nair KS, Jensen MD & Rizza RA. (2002). Effects of free fatty acids and glycerol on splanchnic glucose metabolism and insulin extraction in nondiabetic humans. *Diabetes* **51,** 301-310.

Shaw CS, Jones DA & Wagenmakers AJ. (2008). Network distribution of mitochondria and lipid droplets in human muscle fibres. *Histochem Cell Biol* **129,** 65-72.

Shaw CS, Shepherd SO, Wagenmakers AJM, Hansen D, Dendale P & van Loon LJC. (2012). Prolonged exercise training increases intramuscular lipid content and perilipin 2 expression in type I muscle fibers of patients with type 2 diabetes. *Am J Physiol-Endoc M* **303,** E1158-E1165.

Shaw CS, Sherlock M, Stewart PM & Wagenmakers AJ. (2009). Adipophilin distribution and colocalization with lipid droplets in skeletal muscle. *Histochem Cell Biol* **131,** 575-581.

Shen WJ, Patel S, Miyoshi H, Greenberg AS & Kraemer FB. (2009). Functional interaction of hormone-sensitive lipase and perilipin in lipolysis. *J Lipid Res* **50,** 2306-2313.

Shepherd SO, Cocks M, Meikle PJ, Mellett NA, Ranasinghe AM, Barker TA, Wagenmakers AJM & Shaw CS. (2017a). Lipid droplet remodelling and reduced muscle ceramides following sprint interval and moderate-intensity continuous exercise training in obese males. *Int J Obes (Lond)* **41,** 1745-1754.

Shepherd SO, Cocks M, Tipton KD, Ranasinghe AM, Barker TA, Burniston JG, Wagenmakers AJ & Shaw CS. (2012). Preferential utilization of perilipin 2-associated intramuscular triglycerides during 1 h of moderate-intensity endurance-type exercise. *Exp Physiol* **97,** 970-980.

Shepherd SO, Cocks M, Tipton KD, Ranasinghe AM, Barker TA, Burniston JG, Wagenmakers AJ & Shaw CS. (2013). Sprint interval and traditional endurance training increase net intramuscular triglyceride breakdown and expression of perilipin 2 and 5. *J Physiol* **591,** 657-675.

Shepherd SO, Cocks M, Tipton KD, Witard OC, Ranasinghe AM, Barker TA, Wagenmakers AJ & Shaw CS. (2014). Resistance training increases skeletal muscle oxidative capacity and net intramuscular triglyceride breakdown in type I and II fibres of sedentary males. *Exp Physiol* **99,** 894-908.

Shepherd SO, Strauss JA, Wang Q, Dube JJ, Goodpaster B, Mashek DG & Chow LS. (2017b). Training alters the distribution of perilipin proteins in muscle following acute free fatty acid exposure. *J Physiol* **595,** 5587-5601.

Shin DH, Paulauskis JD, Moustaid N & Sul HS. (1991). Transcriptional regulation of p90 with sequence homology to Escherichia coli glycerol-3-phosphate acyltransferase. *J Biol Chem* **266,** 23834-23839.

Singh R, Park D, Xu J, Hosur R & Berger B. (2010). Struct2Net: a web service to predict protein-protein interactions using a structure-based approach. *Nucleic Acids Res* **38,** W508-515.

Smith SJ, Cases S, Jensen DR, Chen HC, Sande E, Tow B, Sanan DA, Raber J, Eckel RH & Farese RV, Jr. (2000). Obesity resistance and multiple mechanisms of triglyceride synthesis in mice lacking Dgat. *Nat Genet* **25,** 87-90.

Sollner T, Whitehart SW, Brunner M, Erdjumentbromage H, Geromanos S, Tempst P & Rothman JE. (1993). Snap Receptors Implicated in Vesicle Targeting and Fusion. *Nature* **362,** 318-324.

Sollner TH. (2007). Lipid droplets highjack SNAREs. *Nat Cell Biol* **9,** 1219-1220.

Staiano AE & Katzmarzyk PT. (2012). Ethnic and sex differences in body fat and visceral and subcutaneous adiposity in children and adolescents. *Int J Obes (Lond)* **36,** 1261-1269.

Stehouwer CDA. (2018). Microvascular Dysfunction and Hyperglycemia: A Vicious Cycle With Widespread Consequences. *Diabetes* **67,** 1729-1741.

Stettler R, Boesch C, Ith M, Tappy L, Acheson KJ, Binnert C & Decombaz J. (2005). Interaction between dietary lipids and physical inactivity on insulin sensitivity and on intramyocellular lipids in healthy men. *Diabetes Care* **28,** 1404-1409.

Stevens J, Cai JW, Evenson KR & Thomas R. (2002). Fitness and fatness as predictors of mortality from all causes and from cardiovascular disease in men and women in the Lipid Research Clinics Study. *American Journal of Epidemiology* **156,** 832-841.

Stone SJ, Levin MC & Farese RV, Jr. (2006). Membrane topology and identification of key functional amino acid residues of murine acyl-CoA:diacylglycerol acyltransferase-2. *J Biol Chem* **281,** 40273-40282.

Stone SJ, Levin MC, Zhou P, Han J, Walther TC & Farese RV, Jr. (2009). The endoplasmic reticulum enzyme DGAT2 is found in mitochondria-associated membranes and has a mitochondrial targeting signal that promotes its association with mitochondria. *J Biol Chem* **284,** 5352-5361.

Straczkowski M, Kowalska I, Baranowski M, Nikolajuk A, Otziomek E, Zabielski P, Adamska A, Blachnio A, Gorski J & Gorska M. (2007). Increased skeletal muscle ceramide level in men at risk of developing type 2 diabetes. *Diabetologia* **50,** 2366-2373.

Straczkowski M, Kowalska I, Nikolajuk A, Dzienis-Straczkowska S, Kinalska I, Baranowski M, Zendzian-Piotrowska M, Brzezinska Z & Gorski J. (2004). Relationship between insulin sensitivity and sphingomyelin signaling pathway in human skeletal muscle. *Diabetes* **53,** 1215-1221.

Stratford S, Hoehn KL, Liu F & Summers SA. (2004). Regulation of insulin action by ceramide - Dual mechanisms linking ceramide accumulation to the inhibition of Akt/protein kinase B. *Journal of Biological Chemistry* **279,** 36608-36615.

Strauss JA, Shaw CS, Bradley H, Wilson OJ, Dorval T, Pilling J & Wagenmakers AJ. (2016). Immunofluorescence microscopy of SNAP23 in human skeletal muscle reveals colocalization with plasma membrane, lipid droplets, and mitochondria. *Physiol Rep* **4**.

Stuart CA, McCurry MP, Marino A, South MA, Howell ME, Layne AS, Ramsey MW & Stone MH. (2013). Slow-twitch fiber proportion in skeletal muscle correlates with insulin responsiveness. *J Clin Endocrinol Metab* **98,** 2027-2036.

Su CL, Sztalryd C, Contreras JA, Holm C, Kimmel AR & Londos C. (2003). Mutational analysis of the hormone-sensitive lipase translocation reaction in adipocytes. *J Biol Chem* **278,** 43615-43619.

Summers SA & Nelson DH. (2005). A role for sphingolipids in producing the common features of type 2 diabetes, metabolic syndrome X, and Cushing's syndrome. *Diabetes* **54,** 591-602.

Szendroedi J, Yoshimura T, Phielix E, Koliaki C, Marcucci M, Zhang DY, Jelenik T, Muller J, Herder C, Nowotny P, Shulman GI & Roden M. (2014). Role of diacylglycerol activation of PKC theta in lipid-induced muscle insulin resistance in humans. *P Natl Acad Sci USA* **111,** 9597-9602.

Sztalryd C, Xu G, Dorward H, Tansey JT, Contreras JA, Kimmel AR & Londos C. (2003). Perilipin A is essential for the translocation of hormone-sensitive lipase during lipolytic activation. *J Cell Biol* **161,** 1093-1103.

Takeuchi K & Reue K. (2009). Biochemistry, physiology, and genetics of GPAT, AGPAT, and lipin enzymes in triglyceride synthesis. *Am J Physiol Endocrinol Metab* **296,** E1195-1209.

Tarnopolsky MA, Rennie CD, Robertshaw HA, Fedak-Tarnopolsky SN, Devries MC & Hamadeh MJ. (2007). Influence of endurance exercise training and sex on intramyocellular lipid and mitochondrial ultrastructure, substrate use, and mitochondrial enzyme activity. *Am J Physiol Regul Integr Comp Physiol* **292,** R1271-1278.

Taschler U, Radner FP, Heier C, Schreiber R, Schweiger M, Schoiswohl G, Preiss-Landl K, Jaeger D, Reiter B, Koefeler HC, Wojciechowski J, Theussl C, Penninger JM, Lass A, Haemmerle G, Zechner R & Zimmermann R. (2011). Monoglyceride lipase deficiency in mice impairs lipolysis and attenuates diet-induced insulin resistance. *J Biol Chem* **286,** 17467-17477.

Teodoro BG, Sampaio IH, Bomfim LH, Queiroz AL, Silveira LR, Souza AO, Fernandes AM, Eberlin MN, Huang TY, Zheng D, Neufer PD, Cortright RN & Alberici LC. (2017). Long-chain acyl-CoA synthetase 6 regulates lipid synthesis and mitochondrial oxidative capacity in human and rat skeletal muscle. *J Physiol* **595,** 677-693.

Thompson AL & Cooney GJ. (2000). Acyl-CoA inhibition of hexokinase in rat and human skeletal muscle is a potential mechanism of lipid-induced insulin resistance. *Diabetes* **49,** 1761-1765.

Thrush AB, Brindley DN, Chabowski A, Heigenhauser GJ & Dyck DJ. (2009). Skeletal muscle lipogenic protein expression is not different between lean and obese individuals: a potential factor in ceramide accumulation. *J Clin Endocrinol Metab* **94,** 5053-5061.

Townsend N, Bhatnagar P, Wickramasinghe K, Scarborough P, Foster C & Rayner M. (2012). Physical activity

statistics 2012. *British Heart Foundation: London*.

Trinkle-Mulcahy L, Boulon S, Lam YW, Urcia R, Boisvert FM, Vandermoere F, Morrice NA, Swift S, Rothbauer U, Leonhardt H & Lamond A. (2008). Identifying specific protein interaction partners using quantitative mass spectrometry and bead proteomes. *J Cell Biol* **183,** 223-239.

Tuomilehto J, Lindstrom J, Eriksson JG, Valle TT, Hamalainen H, Ilanne-Parikka P, Keinanen-Kiukaanniemi S, Laakso M, Louheranta A, Rastas M, Salminen V, Uusitupa M & Finnish Diabetes Prevention Study G. (2001). Prevention of type

2 diabetes mellitus by changes in lifestyle among subjects with impaired glucose tolerance. *N Engl J Med* **344,** 1343-1350.

Ukropcova B, Sereda O, de Jonge L, Bogacka I, Nguyen T, Xie H, Bray GA & Smith SR. (2007). Family history of diabetes links impaired substrate switching and reduced mitochondrial content in skeletal muscle. *Diabetes* **56,** 720-727.

Uranga AP, Levine J & Jensen M. (2005). Isotope tracer measures of meal fatty acid metabolism: reproducibility and effects of the menstrual cycle. *Am J Physiol Endocrinol Metab* **288,** E547-555.

Ureta T. (1982). The comparative isozymology of vertebrate hexokinases. *Comp Biochem Physiol B* **71,** 549-555.

Valdes CT & Elkind-Hirsch KE. (1991). Intravenous glucose tolerance test-derived insulin sensitivity changes during the menstrual cycle. *J Clin Endocrinol Metab* **72,** 642-646.

van Loon LJ. (2004). Use of intramuscular triacylglycerol as a substrate source during exercise in humans. *J Appl Physiol (1985)* **97,** 1170-1187.

van Loon LJ, Greenhaff PL, Constantin-Teodosiu D, Saris WH & Wagenmakers AJ. (2001). The effects of increasing exercise intensity on muscle fuel utilisation in humans. *J Physiol* **536,** 295-304.

van Loon LJ, Koopman R, Manders R, van der Weegen W, van Kranenburg GP & Keizer HA. (2004). Intramyocellular lipid content in type 2 diabetes patients compared with overweight sedentary men and highly trained endurance athletes. *Am J Physiol Endocrinol Metab* **287,** E558-565.

van Loon LJ, Koopman R, Stegen JH, Wagenmakers AJ, Keizer HA & Saris WH. (2003a). Intramyocellular lipids form an important substrate source during moderate intensity exercise in endurance-trained males in a fasted state. *J Physiol* **553,** 611-625.

van Loon LJ, Manders RJ, Koopman R, Kaastra B, Stegen JH, Gijsen AP, Saris WH & Keizer HA. (2005a). Inhibition of adipose tissue lipolysis increases intramuscular lipid use in type 2 diabetic patients. *Diabetologia* **48,** 2097-2107.

van Loon LJ, Schrauwen-Hinderling VB, Koopman R, Wagenmakers AJ, Hesselink MK, Schaart G, Kooi ME & Saris WH. (2003b). Influence of prolonged endurance cycling and recovery diet on intramuscular triglyceride content in trained males. *Am J Physiol Endocrinol Metab* **285,** E804-811.

van Loon LJ, Thomason-Hughes M, Constantin-Teodosiu D, Koopman R, Greenhaff PL, Hardie DG, Keizer HA, Saris WH & Wagenmakers AJ. (2005b). Inhibition of adipose tissue lipolysis increases intramuscular lipid and glycogen use in vivo in humans. *Am J Physiol Endocrinol Metab* **289,** E482-493.

Van Pelt RE, Gozansky WS, Schwartz RS & Kohrt WM. (2003). Intravenous estrogens increase insulin clearance and action in postmenopausal women. *Am J Physiol Endocrinol Metab* **285,** E311-317.

Van Proeyen K, Szlufcik K, Nielens H, Deldicque L, Van Dyck R, Ramaekers M & Hespel P. (2011a). High-fat diet overrules the effects of training on fiber-specific intramyocellular lipid utilization during exercise. *J Appl Physiol (1985)* **111,** 108-116.

Van Proeyen K, Szlufcik K, Nielens H, Ramaekers M & Hespel P. (2011b). Beneficial metabolic adaptations due to endurance exercise training in the fasted state. *J Appl Physiol* **110,** 236-245.

Vancura A & Haldar D. (1994). Purification and characterization of glycerophosphate acyltransferase from rat liver mitochondria. *J Biol Chem* **269,** 27209-27215.

Villena JA, Roy S, Sarkadi-Nagy E, Kim KH & Sul HS. (2004). Desnutrin, an adipocyte gene encoding a novel patatin domain-containing protein, is induced by fasting and glucocorticoids: ectopic expression of desnutrin increases triglyceride hydrolysis. *J Biol Chem* **279,** 47066-47075.

Vogt M, Puntschart A, Howald H, Mueller B, Mannhart C, Gfeller-Tuescher L, Mullis P & Hoppeler H. (2003). Effects of dietary fat on muscle substrates, metabolism, and performance in athletes. *Med Sci Sports Exerc* **35,** 952-960.

Wagenmakers AJ, Strauss JA, Shepherd SO, Keske MA & Cocks M. (2016). Increased muscle blood supply and transendothelial nutrient and insulin transport induced by food intake and exercise: effect of obesity and ageing. *J Physiol* **594,** 2207-2222.

Wajchenberg BL, Giannella-Neto D, da Silva ME & Santos RF. (2002). Depot-specific hormonal characteristics of subcutaneous and visceral adipose tissue and their relation to the metabolic syndrome. *Horm Metab Res* **34,** 616-621.

Walhin JP, Richardson JD, Betts JA & Thompson D. (2013). Exercise counteracts the effects of short-term overfeeding and reduced physical activity independent of energy imbalance in healthy young men. *J Physiol-London* **591,** 6231-6243.

Walther TC & Farese RV, Jr. (2009). The life of lipid droplets. *Biochim Biophys Acta* **1791,** 459-466.

Wang H, Bell M, Sreenivasan U, Hu H, Liu J, Dalen K, Londos C, Yamaguchi T, Rizzo MA, Coleman R, Gong D, Brasaemle D & Sztalryd C. (2011a). Unique regulation of adipose triglyceride lipase (ATGL) by perilipin 5, a lipid droplet-associated protein. *J Biol Chem* **286,** 15707-15715.

Wang H, Hu L, Dalen K, Dorward H, Marcinkiewicz A, Russell D, Gong D, Londos C, Yamaguchi T, Holm C, Rizzo MA, Brasaemle D & Sztalryd C. (2009). Activation of hormone-sensitive lipase requires two steps, protein phosphorylation and binding to the PAT-1 domain of lipid droplet coat proteins. *J Biol Chem* **284,** 32116-32125.

Wang H, Sreenivasan U, Hu H, Saladino A, Polster BM, Lund LM, Gong DW, Stanley WC & Sztalryd C. (2011b). Perilipin 5, a lipid droplet-associated protein, provides physical and metabolic linkage to mitochondria. *J Lipid Res* **52,** 2159-2168.

Wang H & Sztalryd C. (2011). Oxidative tissue: perilipin 5 links storage with the furnace. *Trends Endocrinol Metab* **22,** 197-203.

Watkins PJ. (2003). ABC of diabetes - Retinopathy. *Brit Med J* **326,** 924-926.

Watson RT, Kanzaki M & Pessin JE. (2004). Regulated membrane trafficking of the insulin-responsive glucose transporter 4 in adipocytes. *Endocr Rev* **25,** 177-204.

Watt MJ & Cheng Y. (2017). Triglyceride metabolism in exercising muscle. *Biochim Biophys Acta* **1862,** 1250-1259.

Watt MJ, Heigenhauser GJ, O'Neill M & Spriet LL. (2003a). Hormone-sensitive lipase activity and fatty acyl-CoA content in human skeletal muscle during prolonged exercise. *J Appl Physiol (1985)* **95,** 314-321.

Watt MJ, Heigenhauser GJ & Spriet LL. (2002). Intramuscular triacylglycerol utilization in human skeletal muscle during exercise: is there a controversy? *J Appl Physiol (1985)* **93,** 1185-1195.

Watt MJ, Heigenhauser GJ & Spriet LL. (2003b). Effects of dynamic exercise intensity on the activation of hormone-sensitive lipase in human skeletal muscle. *J Physiol* **547,** 301-308.

Watt MJ, Holmes AG, Pinnamaneni SK, Garnham AP, Steinberg GR, Kemp BE & Febbraio MA. (2006). Regulation of HSL serine phosphorylation in skeletal muscle and adipose tissue. *Am J Physiol Endocrinol Metab* **290,** E500-508.

Watt MJ, Steinberg GR, Chan S, Garnham A, Kemp BE & Febbraio MA. (2004). Beta-adrenergic stimulation of skeletal muscle HSL can be overridden by AMPK signaling. *Faseb J* **18,** 1445-1446.

Watt MJ, Stellingwerff T, Heigenhauser GJ & Spriet LL. (2003c). Effects of plasma adrenaline on hormone-sensitive lipase at rest and during moderate exercise in human skeletal muscle. *J Physiol* **550,** 325-332.

Wegener G & Krause U. (2002). Different modes of activating phosphofructokinase, a key regulatory enzyme of glycolysis, in working vertebrate muscle. *Biochem Soc Trans* **30,** 264-270.

Weir JB. (1949). New methods for calculating metabolic rate with special reference to protein metabolism. *J Physiol* **109,** 1-9.

Welte MA. (2009). Fat on the move: intracellular motion of lipid droplets. *Biochem Soc Trans* **37,** 991-996.

Weyer C, Foley JE, Bogardus C, Tataranni PA & Pratley RE. (2000). Enlarged subcutaneous abdominal adipocyte size, but not obesity itself, predicts type II diabetes independent of insulin resistance. *Diabetologia* **43,** 1498-1506.

White MF & Kahn CR. (1994a). The insulin signaling system. *Journal of Biological Chemistry* **269,** 1-4.

White MF & Kahn CR. (1994b). The insulin signaling system. *J Biol Chem* **269,** 1-4.

Whytock KL, Shepherd SO, Wagenmakers AJM & Strauss JA. (2018). Hormone-sensitive lipase preferentially redistributes to lipid droplets associated with perilipin-5 in human skeletal muscle during moderate-intensity exercise. *J Physiol*.

Wilcox G. (2005). Insulin and insulin resistance. *Clin Biochem Rev* **26,** 19-39.

Wild S, Roglic G, Green A, Sicree R & King H. (2004). Global prevalence of diabetes: estimates for the year 2000 and projections for 2030. *Diabetes Care* **27,** 1047-1053.

Wilfling F, Wang H, Haas JT, Krahmer N, Gould TJ, Uchida A, Cheng JX, Graham M, Christiano R, Frohlich F, Liu X, Buhman KK, Coleman RA, Bewersdorf J, Farese RV, Jr. & Walther TC. (2013). Triacylglycerol synthesis enzymes mediate lipid droplet growth by relocalizing from the ER to lipid droplets. *Dev Cell* **24,** 384-399.

Wohl P, Wohl P, Girman P & Pelikanova T. (2004). Inflexibility of energy substrate oxidation in type 1 diabetic patients. *Metabolism* **53,** 655-659.

Wolins NE, Quaynor BK, Skinner JR, Schoenfish MJ, Tzekov A & Bickel PE. (2005). S3-12, Adipophilin, and TIP47 package lipid in adipocytes. *J Biol Chem* **280,** 19146-19155.

Wolins NE, Quaynor BK, Skinner JR, Tzekov A, Croce MA, Gropler MC, Varma V, Yao-Borengasser A, Rasouli N, Kern PA, Finck BN & Bickel PE. (2006). OXPAT/PAT-1 is a PPAR-induced lipid droplet protein that promotes fatty acid utilization. *Diabetes* **55,** 3418-3428.

World Health Organisation. (2017). Obesity and Overweight factsheet. http://new.who.int/news-room/fact-sheets/detail/obesity-and-overweight.

Wulan SN, Westerterp KR & Plasqui G. (2014). Metabolic profile before and after short-term overfeeding with a high-fat diet: a comparison between South Asian and White men. *Br J Nutr* **111,** 1853-1861.

Xie X, Langlais P, Zhang X, Heckmann BL, Saarinen AM, Mandarino LJ & Liu J. (2014). Identification of a novel phosphorylation site in adipose triglyceride lipase as a regulator of lipid droplet localization. *Am J Physiol Endocrinol Metab* **306,** E1449-1459.

Xu GH, Sztalryd C, Lu XY, Tansey JT, Gan JW, Dorward H, Kimmel AR & Londos C. (2005). Post-translational regulation of adipose differentiation-related protein by the ubiquitin/proteasome pathway. *Journal of Biological Chemistry* **280,** 42841-42847.

Yamaguchi T, Omatsu N, Matsushita S & Osumi T. (2004). CGI-58 interacts with perilipin and is localized to lipid droplets. Possible involvement of CGI-58 mislocalization in Chanarin-Dorfman syndrome. *J Biol Chem* **279,** 30490-30497.

Yamashita A, Hayashi Y, Matsumoto N, Nemoto-Sasaki Y, Oka S, Tanikawa T & Sugiura T. (2014). Glycerophosphate/Acylglycerophosphate acyltransferases. *Biology (Basel)* **3,** 801-830.

Yang F, Wei Z, Ding X, Liu X, Ge X, Song G, Li G & Guo H. (2013). Upregulation of triglyceride synthesis in skeletal muscle overexpressing DGAT1. *Lipids Health Dis* **12,** 63.

Yang X, Lu X, Lombes M, Rha GB, Chi YI, Guerin TM, Smart EJ & Liu J. (2010). The G(0)/G(1) switch gene 2 regulates adipose lipolysis through association with adipose triglyceride lipase. *Cell Metab* **11,** 194-205.

Yen CL & Farese RV, Jr. (2003). MGAT2, a monoacylglycerol acyltransferase expressed in the small intestine. *J Biol Chem* **278,** 18532-18537.

Yki-Jarvinen H. (1984). Sex and insulin sensitivity. *Metabolism* **33,** 1011-1015.

Yoon JH, Johnson E, Xu R, Martin LT, Martin PT & Montanaro F. (2012). Comparative proteomic profiling of dystroglycan-associated proteins in wild type, mdx, and Galgt2 transgenic mouse skeletal muscle. *J Proteome Res* **11,** 4413-4424.

Yu CL, Chen Y, Cline GW, Zhang DY, Zong HH, Wang YL, Bergeron R, Kim JK, Cushman SW, Cooney GJ, Atcheson B, White MF, Kraegen EW & Shulman GI. (2002a). Mechanism by which fatty acids inhibit insulin activation of insulin

receptor substrate-1 (IRS-1)-associated phosphatidylinositol 3-kinase activity in muscle. *Journal of Biological Chemistry* **277,** 50230-50236.

Yu J, Li Y, Zou F, Xu S & Liu P. (2015). Phosphorylation and function of DGAT1 in skeletal muscle cells. *Biophys Rep* **1,** 41-50.

Yu YH, Zhang Y, Oelkers P, Sturley SL, Rader DJ & Ginsberg HN. (2002b). Posttranscriptional control of the expression and function of diacylglycerol acyltransferase-1 in mouse adipocytes. *J Biol Chem* **277,** 50876-50884.

Yudkin JS. (2007). Inflammation, obesity, and the metabolic syndrome. *Horm Metab Res* **39,** 707-709.

Zderic TW, Davidson CJ, Schenk S, Byerley LO & Coyle EF. (2004). High-fat diet elevates resting intramuscular triglyceride concentration and whole body lipolysis during exercise. *Am J Physiol Endocrinol Metab* **286,** E217-225.

Zechner R, Kienesberger PC, Haemmerle G, Zimmermann R & Lass A. (2009). Adipose triglyceride lipase and the lipolytic catabolism of cellular fat stores. *J Lipid Res* **50,** 3-21.

Zhang H, Wang Y, Li J, Yu J, Pu J, Li L, Zhang H, Zhang S, Peng G, Yang F & Liu P. (2011). Proteome of skeletal muscle lipid droplet reveals association with mitochondria and apolipoprotein a-I. *J Proteome Res* **10,** 4757-4768.

Zhang P, Verity MA & Reue K. (2014). Lipin-1 regulates autophagy clearance and intersects with statin drug effects in skeletal muscle. *Cell Metab* **20,** 267-279.

Zhou YP & Grill V. (1995). Long term exposure to fatty acids and ketones inhibits B-cell functions in human pancreatic islets of Langerhans. *J Clin Endocrinol Metab* **80,** 1584-1590.

Zimmermann R, Strauss JG, Haemmerle G, Schoiswohl G, Birner-Gruenberger R, Riederer M, Lass A, Neuberger G, Eisenhaber F, Hermetter A & Zechner R. (2004). Fat mobilization in adipose tissue is promoted by adipose triglyceride lipase. *Science* **306,** 1383-1386.

Chapter 8. Appendix

Supplementary Material 1. Anti-HSL antibody validation

Basic Local Alignment Search Tool (BLAST) search confirmed the target immunogen for anti-HSL antibody was 100% specific to human HSL.

Western blot method. Snap frozen muscle was powdered in liquid nitrogen before being transferred to Eppendorf tubes that contained lysis buffer (1x RIPA buffer, Cell Signalling, including 1 complete mini protease inhibitor tablet, Roche Diagnostics, Germany) and mixed on ice for 2 h. Samples were then homogenized on ice for ~30 sec at slow speed (Polytron), before being centrifuged for 20 min at 4°C and 10,000 g. The supernatant was removed and a small portion was extracted to assess protein concentration (Pierce BCA assay kit; Pierce, Rockford, IL, USA). Samples were then diluted to a concentration of 3 µgµl-1, using a homogenization buffer and Laemmli sample buffer (Sigma, Gillingham, UK). Samples were subsequently boiled for 5 minutes in 5 µg.µl-1 reducing buffer (Sigma Gillingham, UK) and loaded 50 µg per lane in pre-cast gels in a MiniVe (GE Healthcare, Amersham, UK) electrophoresis tank. Electrophoresis was performed on pre-cast gels at 80 V for 20 min and at 140 V for 40 min in order to separate equal quantities of protein. Samples were subsequently transferred to nitrocellulose membrane at 25 V for 2 h in transfer buffer. Transfer efficacy was assessed using Ponceau S staining and subsequently imaged on ChemiDoc XRS+ system (Bio-Rad, Hemel Hempstead, UK), in order to quantify the total protein stain of each line. Membranes were subsequently destained in sodium hydroxide 0.1 M, before being blocked for 1 hour in 5% Non-fat dried milk (NFDM) in phosphate-buffered saline with 0.1% Tween (PBS-Tw) and incubated overnight at room temperature with anti-HSL (Abcam, Cambridge, UK) primary antibody diluted in 1% NFDM in PBS-Tw. The membranes were washed three times for 5 min in PBS-Tw and subsequently blocked in 5% NFDM in PBS-Tw for 1 h at room temperature before being incubated with appropriate horseradish peroxidase-conjugated IgG secondary antibodies diluted in 1% NFDM in PBS-Tw for 1 h and 30

min. Membranes were washed in PBS-Tw a further two times for 5 min and once for 15 min before being incubated with ECL Prime Reagent for 5 min in the dark. Antibody binding was detected using enhanced chemiluminescence HRP detection reagent (GE Healthcare). Following this imaging and band quantification was performed using ChemiDoc XRS+ system (Bio-Rad, Hemel Hempstead, UK) (Supplementary figure 1A).

Immunofluorescence staining. Sections were fixed for 1 h in 3.7% formaldehyde, rinsed 3 x 30 s in doubly distilled water (dd H_2O) and permeabilised in 0.5% Triton X-100 for 5 min, before being washed 3 x 5 min in Phosphate Buffered Saline (PBS, 137mM sodium chloride, 3 mM potassium chloride, 8 mM sodium phosphate dibasic and 3mM potassium phosphate monobasic, pH of 7.4). Subsequently, slides were incubated with rabbit polyclonal anti-HSL overnight (supplementary figure 1B) of PBS control (supplementary figure 1C) before being washed again 3 x 5 min in PBS. Sections were then incubated with Alexa Fluor goat anti-rabbit IgG 546 (Invitrogen, Paisley, UK) for 30 min, followed by a further 3 x 5 min PBS washes. After the final wash, coverslips were mounted with Vectashield (H-1000, Vector Laboratories, Burlingame, CA, USA) and sealed.

An inverted confocal microscope (Zeiss LSM710; Oberkochen, Germany) was used to obtain digital images of cross-sectionally orientated muscle sections. A helium-neon laser excited the Alexa Fluor 546 fluorophores. Images were acquired with a 40x 0.7 NA oil immersion objective to examine the cellular distribution of HSL (supplementary figure 1B) and confirm omission of staining with PBS control (supplementary figure 1C).

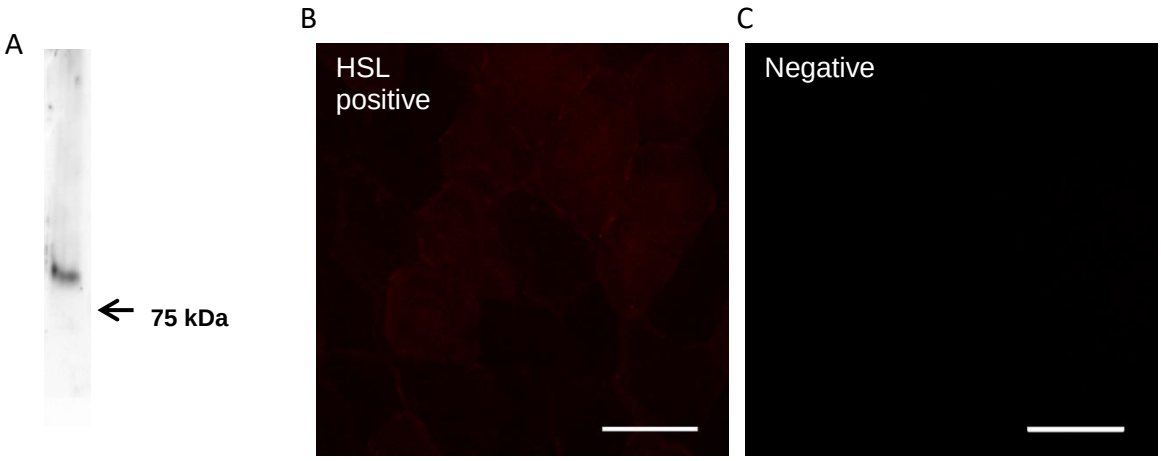

Supplementary Figure 1. Antibody validation. Immunoblot using anti-HSL (Abcam) of human skeletal muscle from a lean male. Results show single molecular weight band above 75 kDa. Expected molecular weight of HSL is 84 kDa (A). Immunofluorescence staining of HSL reveals expected distribution pattern (B). HSL antibody omitted from staining protocol to confirm antibody specificity for immunohistochemistry. Results confirmed no positive staining following omission of antibody (C). Scale bars 50 µm.

Supplementary table 1. List of proteins identified from PLIN5 IP GeLC-MS/MS of lean healthy male participants

Accession	Protein name	MW (Da)	MOWSE score	Sequence coverage (%)
1433E	14-3-3 protein epsilon	29326	230 ± 68	(20.4 - 51.0)
1433G	14-3-3 protein gamma	28456	137 ± 10	(17.0 - 21.1)
ACADM	Medium-chain specific acyl-CoA dehydrogenase, mitochondrial	47015	60 ± 11	(13.3 - 29.5)
ACSL1	Long-chain-fatty-acid--CoA ligase 1	78919	181 ± 47	(11.6 - 36.4)
ACTB	Actin, cytoplasmic 1	42052	441 ± 102	(36.3 - 49.9)
ACTS	Actin, alpha skeletal muscle	42366	828 ± 118	(56.0 - 61.8)
ADT1	ADP/ATP translocase 1	33271	117 ± 13	(33.2 - 38.3)
ARHL1	[Protein ADP-ribosylarginine] hydrolase-like protein 1	40649	111 ± 21	(12.4 - 28.0)
AT2A1	Sarcoplasmic/endoplasmic reticulum calcium ATPase 1	111550	1742 ± 333	(34.4 - 48.9)
AT2A2	Sarcoplasmic/endoplasmic reticulum calcium ATPase 2	116336	1104 ± 224	(23.2 - 45.2)
ATPA	ATP synthase subunit alpha, mitochondrial	59828	666 ± 153	(40.7 - 54.8)
ATPB	ATP synthase subunit beta, mitochondrial	56525	640 ± 129	(39.5 - 67.1)
ATPG	ATP synthase subunit gamma, mitochondrial	33032	71 ± 7	(13.1 - 18.5)
CASQ1	Calsequestrin-1	45132	195 ± 36	(16.4 - 21.7)
CMC1	Calcium-binding mitochondrial carrier protein Aralar1	75114	98 ± 40	(13.1- 40.9)
CRYAB	Alpha-crystallin B chain	20146	194 ± 28	(34.3 - 65.7)
ECHA	Trifunctional enzyme subunit alpha, mitochondrial	83688	252 ± 100	(15.2 - 42.9)
ECHB	Trifunctional enzyme subunit beta, mitochondrial	51547	162 ± 53	(17.1 - 38.2)
ENOB	Beta-enolase	47299	668 ± 223	(31.1- 60.1)

Accession	Protein name	MW (Da)	MOWSE score	Sequence coverage (%)
G3P	Glyceraldehyde-3-phosphate dehydrogenase	36201	175 ± 71	(16.0 - 41.2)
HS90B	Heat shock protein HSP 90-beta	83554	292 ± 92	(8.3 - 36.9)
HSPB1	Heat shock protein beta-1	22826	619 ± 117	(53.7 - 80.0)
IDH3A	Isocitrate dehydrogenase [NAD] subunit alpha, mitochondrial	40022	100 ± 22	(12.6 - 34.4)
IL25	Interleukin-25	20887	41 ± 2	(5.6 - 10.7)
KCRM	Creatine kinase M-type	43302	160 ± 63	(11.5 - 44.6)
KLH41	Kelch-like protein 41	68792	54 ± 7	(4.8 - 23.9)
LDHA	L-lactate dehydrogenase A chain	36950	77 ± 19	(12.7 - 29.2)
LMCD1	LIM and cysteine-rich domains protein 1	42004	95 ± 47	(5.2 - 44.9)
MPCP	Phosphate carrier protein, mitochondrial	40525	45 ± 5	(8.0 - 13.0)
NB5R1	NADH-cytochrome b5 reductase 1	34244	41 ± 4	(6.2 - 21.3)
PANK4	Pantothenate kinase 4	86621	45 ± 3	(1.8 - 12.7)
PHKG1	Phosphorylase b kinase gamma catalytic chain, skeletal muscle/heart isoform	45280	221 ± 63	(20.4 - 64.6)
PLIN5	Perilipin-5	51444	73 ± 21	(12.3 - 27.2)
POTEE	POTE ankyrin domain family member E	122882	295 ± 89	(8.0 - 15.2)
QCR2	Cytochrome b-c1 complex subunit 2, mitochondrial	48584	70 ± 11	(3.5 - 22.1)
SRCA	Sarcalumenin	101069	201 ± 82	(8.5 - 25.0)
TBA4A	Tubulin alpha-4A chain	50634	160 ± 49	(12.3 - 40.8)
TBB4B	Tubulin beta-4B chain	50255	236 ± 45	(24.5 - 44.9)

Accession	Protein name	MW (Da)	MOWSE score	Sequence coverage (%)
TBB5	Tubulin beta chain	50095	254 ± 54	(20.7 - 45.5)
THIL	Acetyl-CoA acetyltransferase, mitochondrial	45456	256 ± 107	(23.9 - 55.0)
TRI72	Tripartite motif-containing protein 72	53609	85 ± 20	(5.0 - 29.8)

MOWSE score presented as means ± SEM. Sequence coverage (%) presented as (min-max) from the 4 replicates. MW, molecular weight; Da, daltons.

Supplementary table 2. List of proteins identified from PLIN5 IP GeLC-MS/MS from *vastus lateralis of* lean sedentary participants

Accession	Protein name	Mass (Da)	MOWSE score	Sequence coverage (%)
41	Protein 4.1	97528	226 ± 25	(25.5 - 25.9)
ABLM2	Actin-binding LIM protein 2	69479	148 ± 46	(30.8 - 36)
ACTG	Actin, cytoplasmic 2	42108	1356 ± 1260	(72.8 - 22.4)
AINX	Alpha-internexin	55528	49 ± 8	(10.4 - 3.8)
AP2A1	AP-2 complex subunit alpha-1	108561	122 ± 59	(15 - 21.6)
AP2A2	AP-2 complex subunit alpha-2	104807	68 ± 5	(11.4 - 15.5)
BAF	Barrier-to-autointegration factor	10280	63 ± 18	(48.3 - 50.6)
C4BPA	C4b-binding protein alpha chain	69042	48 ± 8	(10.1 - 3.4)
CAPZB	F-actin-capping protein subunit beta	31616	74 ± 28	(15.2 - 26.4)
CENPE	Centromere-associated protein E	317588	38 ± 0	(5.8 - 6)
DDX1	ATP-dependent RNA helicase DDX1	83349	133 ± 73	(18.5 - 25.7)
DZIP1	Zinc finger protein DZIP1	99286	37 ± 2	(5.8 - 3.8)
FLNC	Filamin-C	293407	306 ± 220	(8.6 - 18.9)
FXR1	Fragile X mental retardation syndrome-related protein 1	70020	55 ± 1	(6.9 - 6.3)
H2A1B	Histone H2A type 1-B/E	14127	89 ± 33	(4 - 26.9)
H2B1C	Histone H2B type 1-C/E/F/G/I	13898	92 ± 43	(26.2 - 26.2)
HNRPC	Heterogeneous nuclear ribonucleoproteins C1/C2	33707	115 ± 23	(27.1 - 27.1)
HNRPM	Heterogeneous nuclear ribonucleoprotein M	77749	150 ± 7	(19 - 28.9)
HNRPQ	Heterogeneous nuclear ribonucleoprotein Q	69788	80 ± 2	(10.6 - 11.9)

Accession	Protein name	Mass (Da)	MOWSE score	Sequence coverage (%)
HSPB8	Heat shock protein beta-8	21762	46 ± 8	(10.7 - 10.7)
KCC2D	Calcium/calmodulin-dependent protein kinase type II subunit delta	56961	120 ± 52	(12.6 - 20.4)
MFAP5	Microfibrillar-associated protein 5	20055	45 ± 2	(17.9 - 6.9)
NEXN	Nexilin	80837	63 ± 10	(7.1 - 5.9)
NID1	Nidogen-1	139142	105 ± 64	(2.5 - 11.4)
OPTN	Optineurin	66279	132 ± 5	(8.7 - 15.4)
PA2GA	Phospholipase A2, membrane associated	16870	53 ± 3	(12.5 - 17.4)
PABP1	Polyadenylate-binding protein 1	70854	101 ± 4	(12.4 - 13.5)
PABP3	Polyadenylate-binding protein 3	70215	51 ± 13	(9.8 - 8.4)
PABP4	Polyadenylate-binding protein 4	71080	166 ± 12	(32.8 - 29.5)
PGM5	Phosphoglucomutase-like protein 5	62756	149 ± 50	(11.6 - 29.8)
PHKG1	Phosphorylase b kinase gamma catalytic chain, skeletal muscle/heart isoform	45280	66 ± 15	(8.5 - 19.1)
PLEC	Plectin	533462	38 ± 0	(6.7 - 4.1)
PLIN5	Perilipin-5	51444	103 ± 23	(24 - 17.3)
PURA	Transcriptional activator protein Pur-alpha	35003	122 ± 20	(17.1 - 12.4)
RL11	60S ribosomal protein L11	20468	55 ± 2	(19.7 - 20.2)
RL18A	60S ribosomal protein L18a	21034	49 ± 2	(21 - 15.3)
RL30	60S ribosomal protein L30	12947	91 ± 2	(24.3 - 24.3)
RL31	60S ribosomal protein L31	14454	65 ± 5	(18.4 - 18.4)

Accession	Protein name	Mass (Da)	MOWSE score	Sequence coverage (%)
RLA0	60S acidic ribosomal protein P0	34423	73 ± 10	(25.2 - 16.7)
ROA2	Heterogeneous nuclear ribonucleoproteins A2/B1	37464	74 ± 5	(21.2 - 24.6)
RS11	40S ribosomal protein S11	18590	47 ± 6	(40.5 - 41.8)
RT22	28S ribosomal protein S22, mitochondrial	41425	40 ± 2	(6.1 - 11.7)
RTRAF	RNA transcription, translation and transport factor protein	28165	88 ± 2	(19.7 - 24.6)
SGCD	Delta-sarcoglycan	32393	60 ± 14	(9 - 12.1)
SGCG	Gamma-sarcoglycan	32815	67 ± 31	(4.8 - 17.2)
SYNCI	Syncoilin	55494	54 ± 1	(8.5 - 21.8)
TAF1	Transcription initiation factor TFIID subunit 1	213969	37 ± 1	(2.1 - 2.6)
TBA4B	Putative tubulin-like protein alpha-4B	27819	88 ± 23	(17.8 - 30.7)
TGM2	Protein-glutamine gamma-glutamyltransferase 2	78420	109 ± 63	(15.9 - 25.9)
TMOD1	Tropomodulin-1	40658	70 ± 32	(32.9 - 27.6)
TMOD4	Tropomodulin-4	39653	155 ± 10	(23.2 - 23.2)
YBOX3	Y-box-binding protein 3	40066	53 ± 8	(18.8 - 17.2)

MOWSE score presented as means ± SEM. Sequence coverage (%) presented as (min-max) from the 2 replicates. MW, molecular weight; Da, daltons.

Supplementary Table 3. Proteins identified from 3 replicates of PLIN5-IP and control-IP in obese and T2D *vastus lateralis* muscle

Accession	Protein	Obese PLIN5-IP	T2D PLIN5-IP	Obese control-IP	T2D control-IP
1433B	14-3-3 protein beta/alpha	√	√	√	√
1433E	14-3-3 protein epsilon	√	√	√	√
1433F	14-3-3 protein eta	√	√	√	√
1433G	14-3-3 protein gamma	√	√	√	√
1433T	14-3-3 protein theta	X	X	√	X
1433Z	14-3-3 protein zeta/delta	√	√	√	√
2AAA	Serine/threonine-protein phosphatase 2A 65 kDa regulatory subunit A alpha isoform	√	√	√	√
2ABA	Serine/threonine-protein phosphatase 2A 55 kDa regulatory subunit B alpha isoform	√	√	√	√
41	Protein 4.1	X	√	X	X
5NT1A	Cytosolic 5~-nucleotidase 1A	X	√	√	√
5NT3A	Cytosolic 5~-nucleotidase 3A	X	X	X	√
A1AT	Alpha-1-antitrypsin	√	X	√	√
AAMDC	Mth938 domain-containing protein	√	√	√	√
AATM	Aspartate aminotransferase, mitochondrial	√	√	√	√
ABEC2	C->U-editing enzyme APOBEC-2	X	X	√	√
ABHEB	Protein ABHD14B	X	√	√	√
ACADM	Medium-chain specific acyl-CoA dehydrogenase, mitochondrial	√	√	√	√
ACADS	Short-chain specific acyl-CoA dehydrogenase, mitochondrial	X	X	√	√
ACADV	Very long-chain specific acyl-CoA dehydrogenase, mitochondrial	√	√	√	√
ACDSB	Short/branched chain specific acyl-CoA dehydrogenase, mitochondrial	X	X	√	X
ACO13	Acyl-coenzyme A thioesterase 13	X	X	√	√
ACOC	Cytoplasmic aconitate hydratase	X	X	√	√
ACON	Aconitate hydratase, mitochondrial	√	√	√	√
ACOT1	Acyl-coenzyme A thioesterase 1	X	X	√	√
ACSL1	Long-chain-fatty-acid--CoA ligase 1	√	√	√	√

Accession	Protein	Obese PLIN5-IP	T2D PLIN5-IP	Obese control-IP	T2D control-IP
ACSL3	Long-chain-fatty-acid--CoA ligase 3	√	X	√	√
ACTA	Actin, aortic smooth muscle	√	√	√	√
ACTB	Actin, cytoplasmic 1	√	√	√	√
ACTBL	Beta-actin-like protein 2	√	√	√	√
ACTBM	Putative beta-actin-like protein 3	X	√	X	X
ACTC	Actin, alpha cardiac muscle 1	√	√	√	√
ACTN1	Alpha-actinin-1	√	X	√	√
ACTN2	Alpha-actinin-2	√	√	√	√
ACTN3	Alpha-actinin-3	√	X	√	√
ACTN4	Alpha-actinin-4	√	X	√	X
ACTS	Actin, alpha skeletal muscle	√	√	√	√
ACTY	Beta-centractin	X	X	X	√
ACTZ	Alpha-centractin	√	√	√	√
ACY1	Aminoacylase-1	X	X	X	√
ADH1B	Alcohol dehydrogenase 1B	√	√	√	√
ADH1G	Alcohol dehydrogenase 1C	X	X	X	√
ADT1	ADP/ATP translocase 1	√	√	√	√
ADT2	ADP/ATP translocase 2	√	√	√	√
ADT3	ADP/ATP translocase 3	√	√	√	√
AFG32	AFG3-like protein 2	√	X	X	X
AHNK2	Protein AHNAK2	X	√	X	√
AIFM1	Apoptosis-inducing factor 1, mitochondrial	√	√	√	√
AIMP2	Aminoacyl tRNA synthase complex-interacting multifunctional protein 2	√	X	√	X
AINX	Alpha-internexin	√	X	X	X
AK1C1	Aldo-keto reductase family 1 member C1	X	X	√	X

Accession	Protein	Obese PLIN5-IP	T2D PLIN5-IP	Obese control-IP	T2D control-IP
AL3A2	Fatty aldehyde dehydrogenase	√	X	X	X
AL4A1	Delta-1-pyrroline-5-carboxylate dehydrogenase, mitochondrial	X	X	√	X
ALBU	Serum albumin	√	√	√	√
ALDH2	Aldehyde dehydrogenase, mitochondrial	√	√	√	√
ALDOA	Fructose-bisphosphate aldolase A	√	√	√	√
AMPD1	AMP deaminase 1	√	√	√	√
AN32A	Acidic leucine-rich nuclear phosphoprotein 32 family member A	√	√	√	√
AN32B	Acidic leucine-rich nuclear phosphoprotein 32 family member B	√	X	X	X
ANM5	Protein arginine N-methyltransferase 5	X	X	√	X
ANXA2	Annexin A2	X	X	√	√
ANXA7	Annexin A7	X	X	√	X
AOFA	Amine oxidase [flavin-containing] A	√	√	√	√
AOFB	Amine oxidase [flavin-containing] B	√	X	X	X
AP2B1	AP-2 complex subunit beta	X	X	X	√
ARF1	ADP-ribosylation factor 1	X	√	√	√
ARF4	ADP-ribosylation factor 4	√	√	√	√
ARF5	ADP-ribosylation factor 5	X	X	√	√
ARF6	ADP-ribosylation factor 6	X	X	√	√
ARHL1	[Protein ADP-ribosylarginine] hydrolase-like protein 1	√	√	√	√
ARL1	ADP-ribosylation factor-like protein 1	X	X	√	X
ARL8B	ADP-ribosylation factor-like protein 8B	X	X	√	X
ASAP2	Arf-GAP with SH3 domain, ANK repeat and PH domain-containing protein 2	√	X	√	√
ASPN	Asporin	√	√	√	√
ASPP2	Apoptosis-stimulating of p53 protein 2	√	X	X	√
AT1A2	Sodium/potassium-transporting ATPase subunit alpha-2	√	X	√	√

Accession	Protein	Obese PLIN5-IP	T2D PLIN5-IP	Obese control-IP	T2D control-IP
AT2A1	Sarcoplasmic/endoplasmic reticulum calcium ATPase 1	√	√	√	√
AT2A2	Sarcoplasmic/endoplasmic reticulum calcium ATPase 2	√	√	√	√
AT5F1	ATP synthase F(0) complex subunit B1, mitochondrial	√	√	√	√
ATP5H	ATP synthase subunit d, mitochondrial	√	√	√	√
ATP5I	ATP synthase subunit e, mitochondrial	√	√	√	√
ATP5L	ATP synthase subunit g, mitochondrial	√	√	√	√
ATP6	ATP synthase subunit a	√	√	√	X
ATPA	ATP synthase subunit alpha, mitochondrial	√	√	√	√
ATPB	ATP synthase subunit beta, mitochondrial	√	√	√	√
ATPD	ATP synthase subunit delta, mitochondrial	√	X	√	X
ATPG	ATP synthase subunit gamma, mitochondrial	√	√	√	√
ATPK	ATP synthase subunit f, mitochondrial	√	√	√	√
ATPO	ATP synthase subunit O, mitochondrial	√	√	√	√
B3AT	Band 3 anion transport protein	√	√	√	√
BAF	Barrier-to-autointegration factor	X	√	X	X
BGH3	Transforming growth factor-beta-induced protein ig-h3	√	√	√	√
C1QB	Complement C1q subcomponent subunit B	X	X	√	√
C1S	Complement C1s subcomponent	X	X	√	X
C1TC	C-1-tetrahydrofolate synthase, cytoplasmic	√	X	√	√
CAH3	Carbonic anhydrase 3	√	√	√	√
CALM1	Calmodulin-1	X	X	X	√
CALR	Calreticulin	X	X	X	√
CALU	Calumenin	√	X	X	X
CAN1	Calpain-1 catalytic subunit	√	√	√	√
CAN2	Calpain-2 catalytic subunit	X	X	√	√
CAN3	Calpain-3	√	X	√	√

Accession	Protein	Obese PLIN5-IP	T2D PLIN5-IP	Obese control-IP	T2D control-IP
CANB1	Calcineurin subunit B type 1	X	X	√	X
CARM1	Histone-arginine methyltransferase CARM1	X	X	√	√
CASQ1	Calsequestrin-1	√	√	√	√
CASQ2	Calsequestrin-2	√	√	√	√
CAV1	Caveolin-1	√	√	X	X
CAVN1	Caveolae-associated protein 1	√	√	√	√
CAVN2	Caveolae-associated protein 2	√	√	√	√
CAVN3	Caveolae-associated protein 3	√	√	√	√
CAVN4	Caveolae-associated protein 4	√	√	√	√
CAZA2	F-actin-capping protein subunit alpha-2	√	X	√	√
CBPA3	Mast cell carboxypeptidase A	√	X	X	X
CD5L	CD5 antigen-like	√	X	√	X
CH60	60 kDa heat shock protein, mitochondrial	√	√	√	√
CHIP	E3 ubiquitin-protein ligase CHIP	X	X	√	X
CISD1	CDGSH iron-sulfur domain-containing protein 1	X	X	√	√
CISY	Citrate synthase, mitochondrial	X	X	X	√
CLIC1	Chloride intracellular channel protein 1	X	X	√	√
CLUS	Clusterin	√	√	√	√
CMBL	Carboxymethylenebutenolidase homolog	X	X	X	√
CMC1	Calcium-binding mitochondrial carrier protein Aralar1	√	√	√	√
CNTRL	Centriolin	X	√	X	X
CO3	Complement C3	X	X	√	X
CO6A1	Collagen alpha-1(VI) chain	√	X	√	√
CO6A2	Collagen alpha-2(VI) chain	√	X	X	√
CO6A3	Collagen alpha-3(VI) chain	√	√	√	√

Accession	Protein	Obese PLIN5-IP	T2D PLIN5-IP	Obese control-IP	T2D control-IP
COF1	Cofilin-1	X	√	√	√
COF2	Cofilin-2	√	√	√	√
COMP	Cartilage oligomeric matrix protein	√	√	√	√
COPD	Coatomer subunit delta	X	X	X	√
COQ5	2-methoxy-6-polyprenyl-1,4-benzoquinol methylase, mitochondrial	√	X	√	√
COQ6	Ubiquinone biosynthesis monooxygenase COQ6, mitochondrial	X	X	√	√
COQ8A	Atypical kinase COQ8A, mitochondrial	√	√	√	√
COX2	Cytochrome c oxidase subunit 2	√	√	√	√
CPNS1	Calpain small subunit 1	√	X	√	X
CPT1B	Carnitine O-palmitoyltransferase 1, muscle isoform	√	√	√	√
CRIP2	Cysteine-rich protein 2	X	X	√	X
CRYAB	Alpha-crystallin B chain	√	√	√	√
CSN1	COP9 signalosome complex subunit 1	X	X	√	X
CSN4	COP9 signalosome complex subunit 4	X	X	√	√
CSN8	COP9 signalosome complex subunit 8	X	X	√	X
CSRP1	Cysteine and glycine-rich protein 1	√	X	√	X
CSRP3	Cysteine and glycine-rich protein 3	√	√	√	√
CUL5	Cullin-5	√	√	√	√
CWC22	Pre-mRNA-splicing factor CWC22 homolog	X	X	√	X
CX7A1	Cytochrome c oxidase subunit 7A1, mitochondrial	X	√	√	√
CY1	Cytochrome c1, heme protein, mitochondrial	√	√	√	√
DCD	Dermcidin	X	X	X	√
DCTN2	Dynactin subunit 2	√	√	√	√
DCTN3	Dynactin subunit 3	√	√	√	X
DCTN4	Dynactin subunit 4	√	X	X	X

Accession	Protein	Obese PLIN5-IP	T2D PLIN5-IP	Obese control-IP	T2D control-IP
DCXR	L-xylulose reductase	X	X	√	X
DECR	2,4-dienoyl-CoA reductase, mitochondrial	√	X	√	√
DERM	Dermatopontin	√	X	√	√
DESM	Desmin	√	√	√	√
DEST	Destrin	√	X	√	√
DHB12	Very-long-chain 3-oxoacyl-CoA reductase	√	√	√	√
DHRS7	Dehydrogenase/reductase SDR family member 7	√	X	√	√
DLDH	Dihydrolipoyl dehydrogenase, mitochondrial	√	√	√	√
DMXL2	DmX-like protein 2	X	X	X	√
DNM1L	Dynamin-1-like protein	X	X	√	√
DPYL2	Dihydropyrimidinase-related protein 2	X	X	√	√
DPYL3	Dihydropyrimidinase-related protein 3	X	X	√	√
DRS7B	Dehydrogenase/reductase SDR family member 7B	√	X	√	X
DRS7C	Dehydrogenase/reductase SDR family member 7C	√	X	√	√
DTNA	Dystrobrevin alpha	√	X	√	X
DUPD1	Dual specificity phosphatase DUPD1	X	X	X	√
DUS23	Dual specificity protein phosphatase 23	√	X	√	X
DUS3	Dual specificity protein phosphatase 3	√	X	√	X
DX39B	Spliceosome RNA helicase DDX39B	X	X	√	X
ECHA	Trifunctional enzyme subunit alpha, mitochondrial	√	√	√	√
ECHB	Trifunctional enzyme subunit beta, mitochondrial	√	√	√	√
ECHM	Enoyl-CoA hydratase, mitochondrial	√	√	√	√
ECI1	Enoyl-CoA delta isomerase 1, mitochondrial	X	X	√	√
EF1A1	Elongation factor 1-alpha 1	√	√	√	√
EF1A2	Elongation factor 1-alpha 2	√	√	√	√

Accession	Protein	Obese PLIN5-IP	T2D PLIN5-IP	Obese control-IP	T2D control-IP
EF1D	Elongation factor 1-delta	X	X	√	X
EF1G	Elongation factor 1-gamma	√	X	√	√
EF2	Elongation factor 2	√	√	√	√
EFTU	Elongation factor Tu, mitochondrial	√	√	√	√
EHD1	EH domain-containing protein 1	√	X	√	√
EHD2	EH domain-containing protein 2	√	√	√	√
EHD3	EH domain-containing protein 3	√	X	X	X
EHD4	EH domain-containing protein 4	√	√	√	√
EI2BD	Translation initiation factor eIF-2B subunit delta	√	X	X	X
EIF3D	Eukaryotic translation initiation factor 3 subunit D	X	X	X	√
EIF3L	Eukaryotic translation initiation factor 3 subunit L	X	√	√	X
ENDD1	Endonuclease domain-containing 1 protein	X	X	X	√
ENOA	Alpha-enolase	√	√	√	√
ENOB	Beta-enolase	√	√	√	√
ENPL	Endoplasmin	X	X	√	√
EPB42	Erythrocyte membrane protein band 4.2	X	√	√	√
ERAP1	Endoplasmic reticulum aminopeptidase 1	√	X	X	√
ERLN2	Erlin-2	√	√	√	√
ETFA	Electron transfer flavoprotein subunit alpha, mitochondrial	X	X	√	√
ETFB	Electron transfer flavoprotein subunit beta	X	X	√	X
ETFD	Electron transfer flavoprotein-ubiquinone oxidoreductase, mitochondrial	X	X	√	X
EVPL	Envoplakin	X	X	X	√
F13A	Coagulation factor XIII A chain	√	√	√	√
F16P1	Fructose-1,6-bisphosphatase 1	X	X	X	X
F16P2	Fructose-1,6-bisphosphatase isozyme 2	X	X	√	X

Accession	Protein	Obese PLIN5-IP	T2D PLIN5-IP	Obese control-IP	T2D control-IP
FERM2	Fermitin family homolog 2	X	X	√	√
FHL1	Four and a half LIM domains protein 1	√	√	√	√
FHL3	Four and a half LIM domains protein 3	√	√	√	√
FIBA	Fibrinogen alpha chain	√	√	√	√
FIBB	Fibrinogen beta chain	√	√	√	√
FIBG	Fibrinogen gamma chain	√	√	√	√
FITM1	Fat storage-inducing transmembrane protein 1	√	X	X	X
FKB1A	Peptidyl-prolyl cis-trans isomerase FKBP1A	X	√	X	X
G3P	Glyceraldehyde-3-phosphate dehydrogenase	√	√	√	√
GALK1	Galactokinase	√	X	√	X
GAMT	Guanidinoacetate N-methyltransferase	X	X	√	√
GANAB	Neutral alpha-glucosidase AB	X	X	X	√
GBB1	Guanine nucleotide-binding protein G(I)/G(S)/G(T) subunit beta-1	X	X	√	√
GELS	Gelsolin	√	√	√	√
GLUCM	D-glutamate cyclase, mitochondrial	√	√	√	√
GNAI2	Guanine nucleotide-binding protein G(i) subunit alpha-2	X	X	√	√
GNAS1	Guanine nucleotide-binding protein G(s) subunit alpha isoforms XLas	X	X	X	√
GPD1L	Glycerol-3-phosphate dehydrogenase 1-like protein	√	√	√	√
GPDA	Glycerol-3-phosphate dehydrogenase [NAD(+)], cytoplasmic	√	√	√	√
GPX1	Glutathione peroxidase 1	X	X	√	X
GRHPR	Glyoxylate reductase/hydroxypyruvate reductase	X	X	X	√
GRP75	Stress-70 protein, mitochondrial	√	√	√	X
GRP78	78 kDa glucose-regulated protein	X	√	√	X
GSH0	Glutamate--cysteine ligase regulatory subunit	X	X	√	√
GSTK1	Glutathione S-transferase kappa 1	X	X	√	√

Accession	Protein	Obese PLIN5-IP	T2D PLIN5-IP	Obese control-IP	T2D control-IP
GSTM1	Glutathione S-transferase Mu 1	X	X	X	√
GSTM2	Glutathione S-transferase Mu 2	X	X	√	√
GSTM3	Glutathione S-transferase Mu 3	X	X	√	X
GSTO1	Glutathione S-transferase omega-1	X	X	√	X
GSTP1	Glutathione S-transferase P	X	X	√	√
GSTT1	Glutathione S-transferase theta-1	X	X	√	√
GYS1	Glycogen [starch] synthase, muscle	√	√	√	√
H2A1B	Histone H2A type 1-B/E	√	√	X	X
H2B1B	Histone H2B type 1-B	X	X	√	√
H2B1C	Histone H2B type 1-C/E/F/G/I	√	X	X	X
H31T	Histone H3.1t	X	X	√	X
H4	Histone H4	√	√	√	√
HBA	Hemoglobin subunit alpha	X	√	√	√
HBB	Hemoglobin subunit beta	√	√	√	√
HCDH	Hydroxyacyl-coenzyme A dehydrogenase, mitochondrial	X	X	√	√
HDHD5	Haloacid dehalogenase-like hydrolase domain-containing 5	X	X	√	√
HNRPK	Heterogeneous nuclear ribonucleoprotein K	√	√	X	√
HNRPU	Heterogeneous nuclear ribonucleoprotein U	√	X	X	√
HS12A	Heat shock 70 kDa protein 12A	X	X	√	X
HS71A	Heat shock 70 kDa protein 1A	√	√	√	√
HS90A	Heat shock protein HSP 90-alpha	√	√	√	√
HS90B	Heat shock protein HSP 90-beta	√	√	√	√
HSDL2	Hydroxysteroid dehydrogenase-like protein 2	X	X	√	√
HSP72	Heat shock-related 70 kDa protein 2	√	√	√	√
HSP7C	Heat shock cognate 71 kDa protein	√	√	√	√

Accession	Protein	Obese PLIN5-IP	T2D PLIN5-IP	Obese control-IP	T2D control-IP
HSPB1	Heat shock protein beta-1	√	√	√	√
HSPB2	Heat shock protein beta-2	√	√	√	√
HSPB3	Heat shock protein beta-3	X	X	√	√
HSPB6	Heat shock protein beta-6	√	X	√	√
HV307	Immunoglobulin heavy variable 3-7	√	√	X	X
HV315	Immunoglobulin heavy variable 3-15	√	√	√	√
HV323	Immunoglobulin heavy variable 3-23	√	√	√	√
HV349	Immunoglobulin heavy variable 3-49	√	√	X	√
HV364	Immunoglobulin heavy variable 3-64	√	√	X	X
HV372	Immunoglobulin heavy variable 3-72	X	√	√	X
HV43D	Immunoglobulin heavy variable 3-43D	√	X	√	X
HV64D	Immunoglobulin heavy variable 3-64D	√	√	√	√
HV69D	Immunoglobulin heavy variable 1-69D	X	√	X	√
HVC33	Immunoglobulin heavy variable 3-30-3	√	√	√	√
HXK1	Hexokinase-1	√	X	√	√
ICLN	Methylosome subunit pICln	X	X	X	√
ICT1	Peptidyl-tRNA hydrolase ICT1, mitochondrial	√	X	X	X
IDH3A	Isocitrate dehydrogenase [NAD] subunit alpha, mitochondrial	√	X	√	√
IDH3B	Isocitrate dehydrogenase [NAD] subunit beta, mitochondrial	√	X	√	√
IDHC	Isocitrate dehydrogenase [NADP] cytoplasmic	X	X	√	√
IDHP	Isocitrate dehydrogenase [NADP], mitochondrial	√	√	√	√
IF2A	Eukaryotic translation initiation factor 2 subunit 1	X	X	X	√
IF4A1	Eukaryotic initiation factor 4A-I	√	X	√	√
IFIT2	Interferon-induced protein with tetratricopeptide repeats 2	√	√	√	√
IGA2	Immunoglobulin alpha-2 heavy chain	√	√	√	√

Accession	Protein	Obese PLIN5-IP	T2D PLIN5-IP	Obese control-IP	T2D control-IP
IGG1	Immunoglobulin gamma-1 heavy chain	√	√	√	√
IGHA1	Immunoglobulin heavy constant alpha 1	√	√	√	√
IGHG2	Immunoglobulin heavy constant gamma 2	√	√	√	√
IGHG3	Immunoglobulin heavy constant gamma 3	√	√	√	√
IGHG4	Immunoglobulin heavy constant gamma 4	√	√	√	√
IGHM	Immunoglobulin heavy constant mu	√	√	√	√
IGJ	Immunoglobulin J chain	X	X	√	X
IGK	Immunoglobulin kappa light chain	√	√	√	√
IGKC	Immunoglobulin kappa constant	√	√	√	√
IGL1	Immunoglobulin lambda-1 light chain	√	X	X	X
IGLC2	Immunoglobulin lambda constant 2	√	√	√	√
IGLC7	Immunoglobulin lambda constant 7	√	X	X	X
IGLL5	Immunoglobulin lambda-like polypeptide 5	√	X	X	√
IL25	Interleukin-25	√	√	√	√
ILK	Integrin-linked protein kinase	X	X	√	X
IMA4	Importin subunit alpha-4	X	X	√	X
IMA5	Importin subunit alpha-5	√	X	X	√
IMA7	Importin subunit alpha-7	√	X	X	X
IMB1	Importin subunit beta-1	X	X	√	√
IMDH2	Inosine-5~-monophosphate dehydrogenase 2	√	√	√	X
IMPA1	Inositol monophosphatase 1	X	X	√	X
IMPA2	Inositol monophosphatase 2	√	√	√	√
IPYR2	Inorganic pyrophosphatase 2, mitochondrial	X	X	√	√
K1614	Uncharacterized protein KIAA1614	X	X	X	√
K1C10	Keratin, type I cytoskeletal 10	√	√	√	√

Accession	Protein	Obese PLIN5-IP	T2D PLIN5-IP	Obese control-IP	T2D control-IP
K1C13	Keratin, type I cytoskeletal 13	√	√	√	√
K1C14	Keratin, type I cytoskeletal 14	√	√	√	√
K1C16	Keratin, type I cytoskeletal 16	√	√	√	√
K1C17	Keratin, type I cytoskeletal 17	X	X	√	X
K1C20	Keratin, type I cytoskeletal 20	X	X	√	X
K1C24	Keratin, type I cytoskeletal 24	X	X	√	X
K1C9	Keratin, type I cytoskeletal 9	√	√	√	√
K1H1	Keratin, type I cuticular Ha1	X	X	√	X
K22E	Keratin, type II cytoskeletal 2 epidermal	√	√	√	√
K22O	Keratin, type II cytoskeletal 2 oral	X	X	√	X
K2C1	Keratin, type II cytoskeletal 1	√	√	√	√
K2C1B	Keratin, type II cytoskeletal 1b	√	X	√	X
K2C4	Keratin, type II cytoskeletal 4	X	X	√	√
K2C5	Keratin, type II cytoskeletal 5	√	√	√	√
K2C6A	Keratin, type II cytoskeletal 6A	√	√	√	√
K2C6B	Keratin, type II cytoskeletal 6B	√	√	√	√
K2C73	Keratin, type II cytoskeletal 73	X	X	√	X
K2C75	Keratin, type II cytoskeletal 75	X	√	X	X
K2C79	Keratin, type II cytoskeletal 79	X	X	√	X
K2C8	Keratin, type II cytoskeletal 8	√	X	√	X
K2C80	Keratin, type II cytoskeletal 80	X	X	X	√
KAD1	Adenylate kinase isoenzyme 1	X	√	√	√
KAP2	cAMP-dependent protein kinase type II-alpha regulatory subunit	X	X	√	√
KAPCA	cAMP-dependent protein kinase catalytic subunit alpha	X	X	√	√
KCC2A	Calcium/calmodulin-dependent protein kinase type II subunit alpha	√	√	√	√

Accession	Protein	Obese PLIN5-IP	T2D PLIN5-IP	Obese control-IP	T2D control-IP
KCRM	Creatine kinase M-type	√	√	√	√
KCRS	Creatine kinase S-type, mitochondrial	X	√	√	√
KGP1	cGMP-dependent protein kinase 1	√	√	√	√
KLH40	Kelch-like protein 40	X	X	√	√
KLH41	Kelch-like protein 41	√	√	√	√
KPBB	Phosphorylase b kinase regulatory subunit beta	√	X	X	√
KPYM	Pyruvate kinase PKM	√	√	√	√
KRT34	Keratin, type I cuticular Ha4	X	X	√	X
KRT85	Keratin, type II cuticular Hb5	X	X	√	X
KRT86	Keratin, type II cuticular Hb6	X	X	√	X
KS6A3	Ribosomal protein S6 kinase alpha-3	X	X	√	X
KV108	Immunoglobulin kappa variable 1-8	X	X	√	√
KV224	Immunoglobulin kappa variable 2-24	X	X	√	√
KV315	Immunoglobulin kappa variable 3-15	√	X	X	X
KV320	Immunoglobulin kappa variable 3-20	√	√	√	√
KV401	Immunoglobulin kappa variable 4-1	√	X	√	X
KVD07	Immunoglobulin kappa variable 3D-7	X	X	√	X
KVD11	Immunoglobulin kappa variable 3D-11	X	√	X	X
KVD13	Immunoglobulin kappa variable 1D-13	X	X	√	√
KVD20	Immunoglobulin kappa variable 3D-20	√	√	√	√
KVD26	Immunoglobulin kappa variable 2D-26	√	√	√	√
KVD33	Immunoglobulin kappa variable 1D-33	√	X	√	X
KVD39	Immunoglobulin kappa variable 1D-39	X	√	X	X
L2HDH	L-2-hydroxyglutarate dehydrogenase, mitochondrial	X	X	X	√
LAMA2	Laminin subunit alpha-2	√	X	√	X

Accession	Protein	Obese PLIN5-IP	T2D PLIN5-IP	Obese control-IP	T2D control-IP
LDB3	LIM domain-binding protein 3	√	√	√	√
LDHA	L-lactate dehydrogenase A chain	√	√	√	√
LDHB	L-lactate dehydrogenase B chain	X	√	√	√
LEG1	Galectin-1	√	√	√	√
LIPS	Hormone-sensitive lipase	√	√	√	√
LKHA4	Leukotriene A-4 hydrolase	X	X	√	√
LMCD1	LIM and cysteine-rich domains protein 1	√	√	√	√
LMNA	Prelamin-A/C	√	√	√	X
LONM	Lon protease homolog, mitochondrial	X	X	√	√
LRC47	Leucine-rich repeat-containing protein 47	X	X	X	√
LUM	Lumican	√	√	√	√
LV147	Immunoglobulin lambda variable 1-47	X	√	√	√
LV39	Immunoglobulin lambda variable 3-9	X	√	√	√
M2OM	Mitochondrial 2-oxoglutarate/malate carrier protein	√	√	√	√
MACD1	O-acetyl-ADP-ribose deacetylase MACROD1	X	X	√	√
MCCA	Methylcrotonoyl-CoA carboxylase subunit alpha, mitochondrial	√	X	√	X
MCCB	Methylcrotonoyl-CoA carboxylase beta chain, mitochondrial	X	X	√	X
MCU	Calcium uniporter protein, mitochondrial	X	X	√	√
MDHM	Malate dehydrogenase, mitochondrial	√	√	√	√
MEIOC	Meiosis-specific coiled-coil domain-containing protein MEIOC	X	X	X	√
MELT	Ventricular zone-expressed PH domain-containing protein homolog 1	X	X	√	X
MET7A	Methyltransferase-like protein 7A	√	√	√	√
MFAP4	Microfibril-associated glycoprotein 4	X	X	√	X
MFAP5	Microfibrillar-associated protein 5	√	X	X	X
MGST1	Microsomal glutathione S-transferase 1	X	X	X	√

Accession	Protein	Obese PLIN5-IP	T2D PLIN5-IP	Obese control-IP	T2D control-IP
MGST2	Microsomal glutathione S-transferase 2	X	X	√	X
MGST3	Microsomal glutathione S-transferase 3	√	√	√	√
MIC19	MICOS complex subunit MIC19	√	√	√	√
MIC27	MICOS complex subunit MIC27	√	√	√	√
MIC60	MICOS complex subunit MIC60	√	√	√	√
MIME	Mimecan	√	X	√	X
ML12A	Myosin regulatory light chain 12A	√	√	√	X
MLRS	Myosin regulatory light chain 2, skeletal muscle isoform	√	√	√	√
MLRV	Myosin regulatory light chain 2, ventricular/cardiac muscle isoform	√	√	√	√
MMSA	Methylmalonate-semialdehyde dehydrogenase [acylating], mitochondrial	X	X	√	X
MP2K1	Dual specificity mitogen-activated protein kinase kinase 1	X	X	X	√
MPC2	Mitochondrial pyruvate carrier 2	X	X	X	√
MPCP	Phosphate carrier protein, mitochondrial	√	√	√	√
MYG	Myoglobin	√	√	√	√
MYH1	Myosin-1	√	√	√	√
MYH13	Myosin-13	√	X	X	√
MYH2	Myosin-2	√	√	√	√
MYH3	Myosin-3	X	√	X	X
MYH4	Myosin-4	√	X	X	√
MYH6	Myosin-6	√	√	√	√
MYH7	Myosin-7	√	√	√	√
MYH8	Myosin-8	√	√	√	√
MYL1	Myosin light chain 1/3, skeletal muscle isoform	√	√	√	√
MYL3	Myosin light chain 3	√	√	√	√
MYL6	Myosin light polypeptide 6	√	√	√	√

Accession	Protein	Obese PLIN5-IP	T2D PLIN5-IP	Obese control-IP	T2D control-IP
MYL6B	Myosin light chain 6B	X	√	√	√
MYL9	Myosin regulatory light polypeptide 9	√	√	√	X
MYLK2	Myosin light chain kinase 2, skeletal/cardiac muscle	X	X	√	X
MYOC	Myocilin	√	√	√	√
MYOM2	Myomesin-2	X	X	X	√
MYOTI	Myotilin	√	√	X	√
MYOZ1	Myozenin-1	√	√	√	√
MYP0	Myelin protein P0	√	X	√	X
NB5R1	NADH-cytochrome b5 reductase 1	√	X	√	√
NDUA2	NADH dehydrogenase [ubiquinone] 1 alpha subcomplex subunit 2	X	√	√	√
NDUA4	Cytochrome c oxidase subunit NDUFA4	X	√	√	√
NDUA5	NADH dehydrogenase [ubiquinone] 1 alpha subcomplex subunit 5	X	X	√	√
NDUA6	NADH dehydrogenase [ubiquinone] 1 alpha subcomplex subunit 6	X	X	√	√
NDUA7	NADH dehydrogenase [ubiquinone] 1 alpha subcomplex subunit 7	X	X	√	√
NDUA8	NADH dehydrogenase [ubiquinone] 1 alpha subcomplex subunit 8	X	√	X	√
NDUA9	NADH dehydrogenase [ubiquinone] 1 alpha subcomplex subunit 9, mitochondrial	√	√	√	√
NDUAA	NADH dehydrogenase [ubiquinone] 1 alpha subcomplex subunit 10, mitochondrial	√	X	√	√
NDUAB	NADH dehydrogenase [ubiquinone] 1 alpha subcomplex subunit 11	X	X	√	√
NDUAC	NADH dehydrogenase [ubiquinone] 1 alpha subcomplex subunit 12	X	√	√	√
NDUAD	NADH dehydrogenase [ubiquinone] 1 alpha subcomplex subunit 13	√	√	√	√
NDUB4	NADH dehydrogenase [ubiquinone] 1 beta subcomplex subunit 4	√	√	√	√
NDUS1	NADH-ubiquinone oxidoreductase 75 kDa subunit, mitochondrial	√	√	√	√
NDUS2	NADH dehydrogenase [ubiquinone] iron-sulfur protein 2, mitochondrial	√	√	√	√
NDUS3	NADH dehydrogenase [ubiquinone] iron-sulfur protein 3, mitochondrial	√	√	√	√
NDUS4	NADH dehydrogenase [ubiquinone] iron-sulfur protein 4, mitochondrial	X	X	√	X

Accession	Protein	Obese PLIN5-IP	T2D PLIN5-IP	Obese control-IP	T2D control-IP
NDUS5	NADH dehydrogenase [ubiquinone] iron-sulfur protein 5	√	√	√	√
NDUS6	NADH dehydrogenase [ubiquinone] iron-sulfur protein 6, mitochondrial	X	√	√	√
NDUS7	NADH dehydrogenase [ubiquinone] iron-sulfur protein 7, mitochondrial	√	√	√	√
NDUS8	NADH dehydrogenase [ubiquinone] iron-sulfur protein 8, mitochondrial	√	√	√	√
NDUV1	NADH dehydrogenase [ubiquinone] flavoprotein 1, mitochondrial	√	√	√	√
NDUV2	NADH dehydrogenase [ubiquinone] flavoprotein 2, mitochondrial	√	√	√	√
NEST	Nestin	X	X	√	X
NFH	Neurofilament heavy polypeptide	√	√	√	√
NID1	Nidogen-1	√	X	X	X
NIPS2	Protein NipSnap homolog 2	X	√	√	√
NLRC4	NLR family CARD domain-containing protein 4	X	X	X	√
NLRX1	NLR family member X1	X	X	X	√
NNTM	NAD(P) transhydrogenase, mitochondrial	X	X	X	√
NP1L4	Nucleosome assembly protein 1-like 4	X	X	√	X
NPL4	Nuclear protein localization protein 4 homolog	X	X	√	X
NSF	Vesicle-fusing ATPase	X	X	√	√
NUCL	Nucleolin	√	X	X	X
NXN	Nucleoredoxin	X	X	X	√
ODO1	2-oxoglutarate dehydrogenase, mitochondrial	√	X	√	√
ODO2	Dihydrolipoyllysine-residue succinyltransferase component of 2-oxoglutarate dehydrogenase complex, mitochondrial	X	X	√	√
ODP2	Dihydrolipoyllysine-residue acetyltransferase component of pyruvate dehydrogenase complex, mitochondrial	√	√	√	√
ODPA	Pyruvate dehydrogenase E1 component subunit alpha, somatic form, mitochondrial	√	√	√	√
ODPB	Pyruvate dehydrogenase E1 component subunit beta, mitochondrial	√	√	√	√
ODPX	Pyruvate dehydrogenase protein X component, mitochondrial	X	X	√	X
OLA1	Obg-like ATPase 1	X	√	X	X

Accession	Protein	Obese PLIN5-IP	T2D PLIN5-IP	Obese control-IP	T2D control-IP
OST48	Dolichyl-diphosphooligosaccharide--protein glycosyltransferase 48 kDa subunit	X	X	√	X
OTUB1	Ubiquitin thioesterase OTUB1	X	X	√	X
PABP4	Polyadenylate-binding protein 4	√	X	X	X
PADI2	Protein-arginine deiminase type-2	√	√	√	√
PANK4	Pantothenate kinase 4	√	√	√	√
PBIP1	Pre-B-cell leukemia transcription factor-interacting protein 1	√	X	X	√
PCBP1	Poly(rC)-binding protein 1	√	√	√	√
PCBP2	Poly(rC)-binding protein 2	X	X	√	X
PDC6I	Programmed cell death 6-interacting protein	X	X	√	√
PDIA6	Protein disulfide-isomerase A6	√	√	√	√
PDLI3	PDZ and LIM domain protein 3	√	√	√	√
PDLI5	PDZ and LIM domain protein 5	√	X	X	√
PERI	Peripherin	√	X	X	√
PFKAL	ATP-dependent 6-phosphofructokinase, liver type	√	X	√	√
PFKAM	ATP-dependent 6-phosphofructokinase, muscle type	√	√	√	√
PFKAP	ATP-dependent 6-phosphofructokinase, platelet type	X	X	√	√
PGAM2	Phosphoglycerate mutase 2	X	√	X	X
PGM1	Phosphoglucomutase-1	X	√	√	√
PGM2L	Glucose 1,6-bisphosphate synthase	X	X	√	√
PGP	Glycerol-3-phosphate phosphatase	√	√	√	√
PGS1	Biglycan	√	√	√	√
PGS2	Decorin	√	√	√	√
PHB	Prohibitin	√	√	√	√
PHB2	Prohibitin-2	√	√	√	√
PHKG1	Phosphorylase b kinase gamma catalytic chain, skeletal muscle/heart isoform	√	√	X	X

Accession	Protein	Obese PLIN5-IP	T2D PLIN5-IP	Obese control-IP	T2D control-IP
PIMT	Protein-L-isoaspartate(D-aspartate) O-methyltransferase	X	√	√	√
PLAP	Phospholipase A-2-activating protein	X	X	√	√
PLIN1	Perilipin-1	√	√	√	√
POTEE	POTE ankyrin domain family member E	√	X	√	√
POTEF	POTE ankyrin domain family member F	X	X	√	X
POTEI	POTE ankyrin domain family member I	√	√	X	√
POTEJ	POTE ankyrin domain family member J	X	X	X	X
PP1B	Serine/threonine-protein phosphatase PP1-beta catalytic subunit	√	√	√	X
PPAC	Low molecular weight phosphotyrosine protein phosphatase	√	√	√	√
PPCE	Prolyl endopeptidase	X	X	√	√
PRDX1	Peroxiredoxin-1	√	√	√	√
PRDX2	Peroxiredoxin-2	√	√	√	√
PRDX3	Thioredoxin-dependent peroxide reductase, mitochondrial	X	X	√	X
PRDX5	Peroxiredoxin-5, mitochondrial	X	X	X	X
PRDX6	Peroxiredoxin-6	√	√	√	√
PRELP	Prolargin	√	√	√	√
PROF1	Profilin-1	X	X	X	√
PROF2	Profilin-2	√	X	√	√
PRPS1	Ribose-phosphate pyrophosphokinase 1	X	X	√	√
PRS4	26S proteasome regulatory subunit 4	X	X	√	X
PRS7	26S proteasome regulatory subunit 7	X	X	√	X
PSA	Puromycin-sensitive aminopeptidase	√	√	√	√
PSB5	Proteasome subunit beta type-5	X	√	X	X
PSD11	26S proteasome non-ATPase regulatory subunit 11	X	X	√	√

Accession	Protein	Obese PLIN5-IP	T2D PLIN5-IP	Obese control-IP	T2D control-IP
PSMD2	26S proteasome non-ATPase regulatory subunit 2	X	X	√	√
PSMD3	26S proteasome non-ATPase regulatory subunit 3	√	X	√	√
PUR8	Adenylosuccinate lyase	X	X	√	√
PYGB	Glycogen phosphorylase, brain form	X	X	√	√
PYGL	Glycogen phosphorylase, liver form	X	X	√	√
PYGM	Glycogen phosphorylase, muscle form	√	√	√	√
QCR1	Cytochrome b-c1 complex subunit 1, mitochondrial	√	√	√	√
QCR2	Cytochrome b-c1 complex subunit 2, mitochondrial	√	√	√	√
QCR6	Cytochrome b-c1 complex subunit 6, mitochondrial	X	√	X	X
QCR8	Cytochrome b-c1 complex subunit 8	X	√	√	X
QCR9	Cytochrome b-c1 complex subunit 9	X	√	√	√
RAB10	Ras-related protein Rab-10	X	X	X	√
RAB14	Ras-related protein Rab-14	X	X	√	√
RAB1B	Ras-related protein Rab-1B	X	√	√	√
RACK1	Receptor of activated protein C kinase 1	X	X	√	√
RAN	GTP-binding nuclear protein Ran	√	√	√	√
RETST	All-trans-retinol 13,14-reductase	√	X	√	√
RHOA	Transforming protein RhoA	X	X	√	X
RINI	Ribonuclease inhibitor	√	√	√	√
RL12	60S ribosomal protein L12	X	X	√	X
RL14	60S ribosomal protein L14	√	X	√	X
RL15	60S ribosomal protein L15	X	X	√	X
RL18	60S ribosomal protein L18	√	X	X	X
RL22	60S ribosomal protein L22	√	√	X	√
RL27	60S ribosomal protein L27	√	X	X	X

Accession	Protein	Obese PLIN5-IP	T2D PLIN5-IP	Obese control-IP	T2D control-IP
RL27A	60S ribosomal protein L27a	X	X	X	√
RL31	60S ribosomal protein L31	√	X	X	X
RL40	Ubiquitin-60S ribosomal protein L40	X	X	X	√
RL7	60S ribosomal protein L7	√	X	√	√
RL7A	60S ribosomal protein L7a	√	X	X	X
RLA0	60S acidic ribosomal protein P0	√	X	X	X
RM49	39S ribosomal protein L49, mitochondrial	√	X	X	X
RO60	60 kDa SS-A/Ro ribonucleoprotein	X	√	√	X
RPN1	Dolichyl-diphosphooligosaccharide--protein glycosyltransferase subunit 1	√	√	√	√
RPN2	Dolichyl-diphosphooligosaccharide--protein glycosyltransferase subunit 2	X	X	√	√
RS13	40S ribosomal protein S13	√	√	X	X
RS14	40S ribosomal protein S14	√	√	√	√
RS15A	40S ribosomal protein S15a	√	X	X	X
RS16	40S ribosomal protein S16	√	X	√	X
RS18	40S ribosomal protein S18	√	√	√	X
RS2	40S ribosomal protein S2	√	√	√	√
RS23	40S ribosomal protein S23	√	X	√	X
RS25	40S ribosomal protein S25	X	X	√	√
RS27A	Ubiquitin-40S ribosomal protein S27a	X	X	√	√
RS3	40S ribosomal protein S3	√	X	√	√
RS4X	40S ribosomal protein S4, X isoform	X	X	√	√
RS5	40S ribosomal protein S5	√	X	X	X
RS8	40S ribosomal protein S8	√	√	√	√
RTN2	Reticulon-2	√	√	√	√
S10A8	Protein S100-A8	X	X	√	X

Accession	Protein	Obese PLIN5-IP	T2D PLIN5-IP	Obese control-IP	T2D control-IP
S27A1	Long-chain fatty acid transport protein 1	√	X	√	√
SAHH	Adenosylhomocysteinase	X	X	√	√
SAM50	Sorting and assembly machinery component 50 homolog	X	√	√	X
SAMH1	Deoxynucleoside triphosphate triphosphohydrolase SAMHD1	√	X	√	X
SAMP	Serum amyloid P-component	√	√	√	√
SC22B	Vesicle-trafficking protein SEC22b	√	X	√	X
SCFD1	Sec1 family domain-containing protein 1	X	X	√	X
SDHA	Succinate dehydrogenase [ubiquinone] flavoprotein subunit, mitochondrial	√	√	√	√
SDHB	Succinate dehydrogenase [ubiquinone] iron-sulfur subunit, mitochondrial	X	√	√	√
SERA	D-3-phosphoglycerate dehydrogenase	X	X	√	X
SESN1	Sestrin-1	X	X	√	X
SET	Protein SET	X	X	√	X
SH3BG	SH3 domain-binding glutamic acid-rich protein	√	√	√	√
SMD3	Small nuclear ribonucleoprotein Sm D3	√	√	√	√
SNTA1	Alpha-1-syntrophin	√	√	√	√
SNTB1	Beta-1-syntrophin	√	X	X	X
SNTB2	Beta-2-syntrophin	√	X	X	X
SQSTM	Sequestosome-1	X	X	X	√
SRCA	Sarcalumenin	√	√	√	√
SRCH	Sarcoplasmic reticulum histidine-rich calcium-binding protein	√	√	X	√
STAT1	Signal transducer and activator of transcription 1-alpha/beta	X	X	√	X
STAT3	Signal transducer and activator of transcription 3	√	X	√	√
STML2	Stomatin-like protein 2, mitochondrial	√	X	X	√
STOM	Erythrocyte band 7 integral membrane protein	√	√	√	√
SUCA	Succinate--CoA ligase [ADP/GDP-forming] subunit alpha, mitochondrial	X	X	√	√

Accession	Protein	Obese PLIN5-IP	T2D PLIN5-IP	Obese control-IP	T2D control-IP
SUCB1	Succinate--CoA ligase [ADP-forming] subunit beta, mitochondrial	√	X	√	√
SYDC	Aspartate--tRNA ligase, cytoplasmic	X	√	√	√
SYFB	Phenylalanine--tRNA ligase beta subunit	X	X	X	X
SYIM	Isoleucine--tRNA ligase, mitochondrial	√	X	X	√
SYNC	Asparagine--tRNA ligase, cytoplasmic	X	X	√	√
SYPL2	Synaptophysin-like protein 2	√	√	√	√
SYQ	Glutamine--tRNA ligase	√	√	√	√
SYRC	Arginine--tRNA ligase, cytoplasmic	√	X	√	√
TBA1A	Tubulin alpha-1A chain	√	√	√	√
TBA1B	Tubulin alpha-1B chain	√	√	√	√
TBA4A	Tubulin alpha-4A chain	√	√	√	√
TBA8	Tubulin alpha-8 chain	√	√	√	√
TBAL3	Tubulin alpha chain-like 3	√	X	√	√
TBB2A	Tubulin beta-2A chain	√	√	√	√
TBB3	Tubulin beta-3 chain	√	X	√	√
TBB4A	Tubulin beta-4A chain	√	X	X	X
TBB4B	Tubulin beta-4B chain	√	√	√	√
TBB5	Tubulin beta chain	√	√	√	√
TBB6	Tubulin beta-6 chain	√	X	√	X
TBC17	TBC1 domain family member 17	X	√	√	X
TCPA	T-complex protein 1 subunit alpha	√	√	√	√
TCPD	T-complex protein 1 subunit delta	√	√	√	√
TCPE	T-complex protein 1 subunit epsilon	√	X	√	√
TCPG	T-complex protein 1 subunit gamma	√	√	√	√
TCPH	T-complex protein 1 subunit eta	X	X	√	√

Accession	Protein	Obese PLIN5-IP	T2D PLIN5-IP	Obese control-IP	T2D control-IP
TCPQ	T-complex protein 1 subunit theta	√	X	√	√
TCPZ	T-complex protein 1 subunit zeta	√	X	X	√
TELT	Telethonin	X	X	√	√
TERA	Transitional endoplasmic reticulum ATPase	√	√	√	√
TFR1	Transferrin receptor protein 1	X	X	X	√
THIL	Acetyl-CoA acetyltransferase, mitochondrial	√	√	√	√
THIM	3-ketoacyl-CoA thiolase, mitochondrial	√	√	√	√
TITIN	Titin	√	√	√	√
TM109	Transmembrane protein 109	√	X	√	X
TM143	Transmembrane protein 143	X	X	X	√
TM38A	Trimeric intracellular cation channel type A	√	√	√	√
TM38B	Trimeric intracellular cation channel type B	X	X	√	X
TMM33	Transmembrane protein 33	X	X	√	X
TNNC1	Troponin C, slow skeletal and cardiac muscles	√	√	√	√
TNNC2	Troponin C, skeletal muscle	√	√	√	√
TNNI1	Troponin I, slow skeletal muscle	√	√	√	√
TNNI2	Troponin I, fast skeletal muscle	√	√	√	√
TNNT1	Troponin T, slow skeletal muscle	√	√	√	√
TNNT3	Troponin T, fast skeletal muscle	√	√	√	√
TPIS	Triosephosphate isomerase	X	√	√	√
TPM1	Tropomyosin alpha-1 chain	√	√	√	√
TPM2	Tropomyosin beta chain	√	√	√	√
TPM3	Tropomyosin alpha-3 chain	√	√	√	√
TPM4	Tropomyosin alpha-4 chain	√	X	√	√
TRAP1	Heat shock protein 75 kDa, mitochondrial	X	X	√	√

Accession	Protein	Obese PLIN5-IP	T2D PLIN5-IP	Obese control-IP	T2D control-IP
TRI72	Tripartite motif-containing protein 72	√	√	√	√
TRY1	Trypsin-1	X	X	√	√
TRY3	Trypsin-3	√	√	√	√
TRY6	Putative trypsin-6	√	X	√	√
TRYD	Tryptase delta	X	X	X	√
TSP4	Thrombospondin-4	√	X	√	√
TTBK1	Tau-tubulin kinase 1	X	X	X	X
TTHY	Transthyretin	X	X	√	√
UB2D1	Ubiquitin-conjugating enzyme E2 D1	√	X	X	√
UBE2N	Ubiquitin-conjugating enzyme E2 N	X	X	√	X
UBE3A	Ubiquitin-protein ligase E3A	X	X	√	X
UBP14	Ubiquitin carboxyl-terminal hydrolase 14	X	X	√	X
UBP5	Ubiquitin carboxyl-terminal hydrolase 5	X	X	√	X
UCRI	Cytochrome b-c1 complex subunit Rieske, mitochondrial	√	√	√	√
UGDH	UDP-glucose 6-dehydrogenase	X	X	√	X
UN45B	Protein unc-45 homolog B	√	X	√	√
USMG5	Up-regulated during skeletal muscle growth protein 5	X	√	√	√
USO1	General vesicular transport factor p115	√	X	X	√
VDAC1	Voltage-dependent anion-selective channel protein 1	√	X	√	√
VDAC3	Voltage-dependent anion-selective channel protein 3	√	√	√	√
VIME	Vimentin	√	√	√	√
VPS35	Vacuolar protein sorting-associated protein 35	X	√	√	√
VTNC	Vitronectin	X	√	√	√
WDR1	WD repeat-containing protein 1	X	X	√	√
XPO1	Exportin-1	X	X	X	√

Accession	Protein	Obese PLIN5-IP	T2D PLIN5-IP	Obese control-IP	T2D control-IP
XPO2	Exportin-2	X	X	X	√
XRCC5	X-ray repair cross-complementing protein 5	X	X	√	√
XRCC6	X-ray repair cross-complementing protein 6	X	√	√	√
Z804A	Zinc finger protein 804A	X	X	√	X